Imperial College London

A versatile platform for intracellular delivery of various macromolecules using a pH-responsive, biomimetic polymer

Michal Tomasz Kopytynski

Thesis submitted in accordance with the requirements of

Imperial College London for the degree of

DOCTOR OF PHILOSOPHY

Department of Chemical Engineering

Imperial College London

September 2018

Declaration

This thesis is submitted for the degree of Doctor of Philosophy at Imperial College London.

The research reported herein was carried out under the supervision of Dr Rongjun Chen between October 2014 and September 2018.

I can confirm the research presented within this thesis is the result of my own work. Any results obtained in collaboration are specifically indicated and acknowledged within the text.

This thesis does not contain material that has been previously accepted for the award of any qualification at Imperial College London or any other educational institution.

This thesis contains 75 figures, 7 tables, and 51,973 words in length excluding the bibliography and appendix.

Sections of this work have been presented at MedImmune UK Science Fair (2018), MedImmune PhD Symposium (2017), 44th Annual meeting and Exposition of the Controlled Release Society (2017), The SoftComp Network Annual Meeting (2016), CLSS-UK Annual Meeting (2016), IChemE BESIG Young Researchers Meeting (2016), The SNAL Network Annual Meeting (2015), Imperial College Chemical Engineering PhD Symposium (2015- 2018).

Parts of this work are to be presented in the following publications:

Michal Kopytynski, Sandrine Legg, Ralph Minter and Rongjun Chen, A versatile polymer based platform for intracellular delivery of macromolecules, in preparation.

Michal Kopytynski, Sandrine Legg, Ralph Minter and Rongjun Chen, Intracellular delivery of macromolecules by conjugation to a pH-responsive, biomimetic polymer (working title), in preparation.

Michal Kopytynski

September 2018

The copyright of this thesis rests with the author and is made available under a Creative Commons Attribution Non-Commercial No Derivatives licence. Researchers are free to copy, distribute or transmit the thesis on the condition that they attribute it, that they do not use it for commercial purposes and that they do not alter, transform or build upon it. For any reuse or redistribution, researchers must make clear to others the license terms of this work.

To my family and friends

“There is scarcely any passion without struggle”

- Albert Camus

Acknowledgments

It is hard to express my gratitude to all the amazing people who have played a part in supporting me during my time as a PhD student at Imperial College and MedImmune. Thank you all so much, I would not have made it so far without you.

First and foremost, I would like to express my gratitude to my supervisor, Dr Rongjun Chen, for the opportunity to join his group at Imperial College and his continued guidance, advice, constructive criticism and support. I am grateful for everything that I have learned in the past 4 years while working on my PhD project and the professional and personal growth I have undergone.

I owe my deepest thanks to Dr Sandrine Legg and to Dr Ralph Minter, who warmly welcomed me into the Minter Team at MedImmune and provided constant support, guidance and (sometimes much needed) encouragement.

I am extremely grateful to Dr Fabien Garcon for his enthusiasm and invaluable help with setting-up, design and supervision of the *in vivo* experiments. My thanks to Jen Spooner, who performed the HPSEC and endotoxin analysis and to Dr Susan Fowler, for her advice and kind help with peptide separation. I would like to thank Dr Christina Schindler for sharing her expertise and donating EVs. I want to thank Dr Ron Jackson and the entire Minter Team and others at MedImmune who kindly offered their help, including Guglielmo, Carl, Elina, Chris, John, Aidan, Tom, Andrea, Jatinder, Natalie, Matt, Alan, Paulina, Sophie, Kelli, Jeff, Cathy, Grace, Shannon, James, Tomek, Tuomas.

I wish to express my gratitude to Stephen Rothery, David Gaboriau, Jane Srivastava and Jess Rowley of Imperial College for training and help with confocal microscopy and flow cytometry. Thank you to Dr Spencer Crowder for providing hMSCs, plasmids and useful discussion. I am grateful to the support and administrative staff at the Department of Chemical Engineering, Imperial College.

I am lucky to have worked with my wonderful colleagues at Imperial College: Shiqi Wang, Siyuan Chen and Marie Bachelet, “The Oldies”. I will never forget their camaraderie, patience and support during long hours spent in the lab and the pleasant times outside. I am grateful to Deborah Roebuck for passing on her knowledge and motivation when it was much needed. Thank you to Isabel Neto, Anna Sofia Tascini and Ruijiao Dong. I would also like to thank Sophia Berry and Camilla Trevor for making me feel welcome in Cambridge, their friendship, support (in and out of lab) and the booth lunches.

I am extremely grateful to my dear parents, Lucyna and Aleksander, and my brother Piotr for their understanding, support and cheering me on. Thank you to all my lovely friends, housemates and people who have come into my life in the past 4 years and helped me, in many various ways, on the way towards completing my PhD.

I am grateful to Roger and Barbara Jones who kindly provided a perfect home in the middle of busy Fulham during much of my studies.

I also own appreciation to Imperial College Trust and the Old Centralians' Trust for providing travel funding to support my attendance at conferences.

I am very thankful to BBSRC and to MedImmune for their financial support over the past 4 years via the iCASE PhD scholarship.

Thank you all so very much

Abstract

The physical barrier posed by the plasma membrane greatly restricts the potential of intracellular delivery of macromolecules. Currently available delivery methods suffer from various limitations, including low delivery efficiency or high cytotoxicity. To overcome these issues, stimuli-responsive polymers such as the bio-inspired, pH-responsive PP50 polymer, comprising a poly-L-lysine isophthalamide backbone with hydrophobic L-phenylalanine grafts can be used. In mildly acidic environments, PP50 can permeabilise the cell membrane overcoming the problem of payload entrapment in the endosomes and allowing for efficient delivery of molecules into the cell interior.

The work presented herein demonstrates that PP50 is capable of delivering various macromolecular payloads *in vitro*, such as different-sized dextrans, green fluorescent protein and the apoptotic peptide Bim by simple co-incubation with the desired cargo at pH 6.5. The delivery process was fast, non-toxic and compatible with multiple cell lines tested, including adherent and suspension cell lines, primary human mesenchymal stem cells as well as cells grown as spheroids. In addition, peptide delivery by co-incubation with PP50 was at least 3 times more effective than delivery using other common delivery methods, including poly(ethyleneimine), cell penetrating peptides and electroporation.

In addition, novel conjugates of PP50 and different model and functional payloads were developed using a cleavable crosslinker to enable *in vivo* delivery and release. Model fluorescent payloads such as a peptide-sized PEG and green fluorescent protein were delivered to HeLa cells following conjugation with PP50. Finally, Bim conjugated to PP50 was shown to retain its apoptotic effect *in vitro* and was demonstrated to be non-immunogenic and well tolerated in a mouse model and exhibited preferential tumour accumulation.

Our findings suggest that PP50-mediated payload delivery is a versatile method allowing delivery of various payloads to many different cell lines and can find many potential uses both *in vitro* and *in vivo*.

Table of Contents

Chapter 1 - Introduction.....32

1.1 Introduction – stimulus-responsive polymers as delivery agents 32

1.2 Challenges for intracellular delivery 35

1.2.1 Extracellular barriers.....36

1.2.2 Cellular barriers and membrane permeabilisation strategies.....39

1.3 Delivery strategies 44

1.3.1 Physical methods.....45

1.3.2 Chemical and biological delivery agents.....48

1.4 Therapeutic payloads and methods of their delivery using anionic polymers 60

1.4.1 Different-sized payloads in modern drug therapies 60

1.4.2 Cargo delivery methods using PP polymers 61

1.5 Polymer delivery agents with cleavable crosslinkers 62

1.5.1 PP-polymers and PDPH crosslinker 63

1.6 Aims of the project 65

Chapter 2 - Materials and Methods.....67

2.1 Materials 67

2.2 PLP Synthesis..... 69

2.3 PP50 Synthesis: grafting of PLP with L-phenylalanine 70

2.4 Labelling of PP50 with fluorescent dyes – Rhodamine110 and Cy5..... 71

2.5 Haemolysis 72

2.6 Cell culture..... 73

2.7 Laser scanning confocal microscopy 74
2.8 Flow cytometry 75
2.9 AlamarBlue cell survival assay 76
2. 10 CellTiterGlo 2.0 cell survival assay 76
2.11 Dynamic Light Scattering (DLS) and Zeta Potential 77
2.12 Spheroids 77
2.13 Caspase activation assays 77
2.14 IncuCyte® ZOOM 78
2.15 Delivery method comparison 78
2.16 EVs – production and loading 79
2.17 EVs - analysis using NanoSight 79
2.18 EVs – analysis using flow cytometry 80
2.19 PDPH grafting 80
2.20 PDPH characterisation 81
2.21 2-mercaptopyridine release kinetics 81
2.22 Conjugation of PEG-FITC 81
2.23 Conjugation of Proteins 82
2.24 Conjugation of Bim and scrBim 83
2.25 Bim-Cy7 and scrBim-Cy7 removal by dialysis - analysis 84
2.26 High Pressure Size Exclusion Chromatography (HPSEC) 84
2.27 Endotoxin quantification 85
2.28 IL-6 and TNFα ELISAs 85
2.29 In vivo study 87
2.30 Statistical analysis 88

Chapter 3 - Payload delivery by co-incubation with PP50: mechanism and delivery characterisation 89

3.1 Introduction 89

3.2 Results and Discussion 91

3.2.1 pH-responsive interaction with biological membranes 91

3.2.2 Formation of ghost cells 95

3.2.3 Delivery of FITC-Dextran to erythrocyte ghosts 97

3.2.4 Interaction between PP50 and nucleated mammalian cells 98

3.2.5 PP50 mediated delivery of FITC-Dextran to HeLa cells 101

3.2.6 The effect of temperature on the PP50-mediated delivery 106

3.2.7 The importance of endosomal acidifaction on PP50-mediated deliviery 108

3.2.8 The effect of payload concentration 109

3.2.9 The effect of polymer concentration 110

3.2.10 The effect of treatment time 112

3.2.11 The effect of extracellular pH 114

3.2.12 Cytotoxicity of PP50-mediated delivery 115

3.2.13 The interaction between PP50 and model payload 117

3.3 Conclusions 119

Chapter 4 - Delivery by co-incubation – technology versatility and investigation of possible uses 120

4.1 Introduction 120

4.2 Results and Discussion 121

4.2.1 Delivery to different cell lines 121

4.2.2. Delivery to multicellular A549 spheroids 126

4.2.3 Delivery of different-sized FITC-Dextran....128
4.2.4 Delivery of green fluorescent protein....132
4.2.5 Delivery in the presence of serum....133
4.2.6 Strength of intracellular fluorescence over time and topping-up....135
4.2.7 Antibody delivery....138
4.2.8 Plasmid delivery....139
4.2.9 Delivery of Bim....140
4.2.10 Delivery to extracellular vesicles....150
4.3 Conclusions....153

Chapter 5 - Payload delivery by conjugation with PP50....155
5.1 Introduction....155
5.2 Results and Discussion....156
5.2.1 PDPH grafting....156
5.2.2 Membrane disruptive ability of PP50-PDPH vs PP50....158
5.2.3 Release of 2-mercaptpyridine – a small molecule drug model....159
5.2.4 Conjugation and delivery of PEG-FITC....164
5.2.5 Conjugation and delivery of proteins....171
5.3 Conclusions....179

Chapter 6 - Development and in vivo delivery of PP50-Bim conjugates..181
6.1 Introduction....181
6.2 Results and Discussion....183
6.2.1 Conjugation of Bim and scrBim to PP50....183

6.2.2 Apoptotic effect of PP50-Bim and PP50-scrBim 183

6.2.3 Conjugation of Bim-Cy7 and scrBim-Cy7 to PP50 and peptide purification 185

6.2.4 Apoptotic effect of PP50-Bim-Cy7 and PP50-scrBim-Cy7 188

6.2.5 Apoptotic effect of PP50-Bim-Cy7 and PP50-scrBim-Cy7 – Incucyte analysis 189

6.2.6 Immunogenicity of PP50-Bim 192

6.2.7 Tolerability studies 194

6.2.8 Biodistribution 198

6.3 Conclusions 202

Chapter 7 – Conclusions and Future Work 204

7.1 Research summary and project novelties 204

7.2 Future work 207

7.2.1 Delivery to EVs 207

7.2.2 Delivery of nucleic acids 207

7.2.3 Delivery of large proteins by conjugation 208

7.2.4 Tumour growth inhibition effect in vivo 208

7.3 Closing remarks 209

8. Bibliography 210

9. Appendix 229

Appendix A 229

Appendix B 230

Appendix C 231

Appendix D 232
Appendix E 233
Appendix F 234

List of Figures

Figure 1-1. The mechanism of controlled drug delivery using pH responsive polymers. The polymer-drug conjugate (or mix) is internalised by endocytosis. Acidification of early endosomes leads to change of hydrophobic/hydrophilic balance of the polymer, enabling it to become membrane disruptive. This leads to release of the drug into the cytosol and its further diffusion to the site of action (e.g. the nucleus). Membrane disruption of early endosomes prevents their maturation to late endosomes and fusion with lysosomes, where the engulfed cargo would have been degraded by hydrolytic enzymes. Based on (Plank et al., 1998). 35

Figure 1-2. Different types of endocytosis**.** Source: (Mayor and Pagano, 2007). 41

Figure 1-3. The "proton sponge" effect. (A) Entrapment of cationic polymers in endosomes. (B) Polymers become protonated during endosome maturation and resist further acidification of endosomes. More protons are pumped to lower the pH. (C) Passive influx of chloride ions increases ionic concentration and encourages water influx. High ionic pressure causes endosome swelling and rupture. Modified from (Wanling and Jenny, 2012). 54

Figure 1-4. Poly(L-lysine isophthalamide) grafted with L-phenylalanine (PP polymers), where a certain percentage of OH at position R is replaced with L-phenylalanine..... 58

Figure 1-5. Molecular structure of PDPH. The disulphide bond is highlighted in yellow. The amine group available for formation of amide bonds with pendant carboxyl groups present on polymer backbone is highlighted in green. 64

Figure 3-1. (A) Haemolysis of ovine erythrocytes after incubation with PP50 (100 μg mL^{-1}) for 1 h in a shaking water bath at 37^{o}C in 7 different pH environments in the range of pH 4.5-7.4. (B) Delivery of TexasRed dye (0.62 kDa, 1 μM) to ovine erythrocytes by co-incubation with PP50 (50 μg mL^{-1}) at pH 6.0, 6.5, 7.0 and 7.4, as analysed by confocal microscopy. Scale bar = 20 μm. 92

Figure 3-2. Delivery of TexasRed (1 μM) to ovine erythrocytes by co-incubation with PP50 (50 μg mL^{-1}) at pH 6.5 for 30 min in a shaking water bath (37^{o}C), compared to polymer-free control sample, as analysed by confocal microscopy. Red channel represents TexasRed. Differential interference contrast (DIC) is also shown. Scale bar = 20 μm. 95

Figure 3-3. Binding of PP50 labelled with fluorescent dye Rhodamine110 (Ex 498/ Em 521 nm) on the membrane of ovine erythrocytes following a 3-minute treatment at 37^{o}C with the polymer at the concertation of 50 μg mL^{-1}. Analysed by confocal microscopy. Scale bar = 20 μm. 96

Figure 3-4. Delivery of 10 and 150 kDa FITC-Dextran (10 μM) to ovine erythrocytes following a 30-minute co-incubation with PP50 (100 μg mL^{-1}) at pH 6.5. Analysed by confocal microscopy. Scale bar = 10 μm. 98

Figure 3-5. Polymer uptake by HeLa cells: (A) Uptake of PP50-Cy5 (0.5 mg mL^{-1}) over a period of 50 minutes after the addition of the polymer at extracellular pH 6.5, visualised by confocal microscopy. Scale bar = 20 μm. (B) Uptake of PP50-Cy5 (1 mg mL^{-1}) following a 1 h treatment at pH 6.5 or pH 7.4 and a further 30 min incubation period in serum-supplemented DMEM following a wash with PBS. Scale bar = 10 μm. 100

Figure 3-6. Delivery of 150 kDa FITC-Dextran (10 μM) to HeLa cells following co-incubation with Cy5-labelled PP50 (1 mg mL^{-1}) for 1 h at pH 6.5, visualised by confocal microscopy. Scale bar = 20 μm..... 102

Figure 3-7. (A) Intracellular delivery of 150 kDa FITC-Dextran (10 μM) to HeLa cells by co-incubation with PP50 (0.5 mg mL^{-1}) at pH 7.4 and pH 6.5 for a period of 30 minutes and corresponding polymer-free negative controls (FITC-Dextran only) visualised by confocal microscopy (scale bar = 10 μm) and (B) fluorescence intensity profiles in the cross-sectional area indicated by the yellow lines in the green, red and blue channels, created using ImageJ. 103

Figure 3-8. Flow cytometry analysis of HeLa cells illustrating fluorescence intensity of intracellular FITC after delivery of FITC-Dextran (5 μM) to HeLa cells by co-incubation with PP50 (0.5 mg mL^{-1}) at pH 6.5 and pH 7.4 for 30 minutes. Results are based on a minimum of 10,000 events analysed..... 104

Figure 3-9. 3D projection created using Z-stack obtained via confocal microscopy illustrating the diffused nature of the fluorescent signal throughout the cytosol and the nucleus and the co-localisation of the green signal with blue DNA stain Hoechst following the intracellular delivery of 150 kDa FITC-Dextran (10 μM) to HeLa cells by co-incubation with PP50 (0.5 mg mL^{-1}) at pH 6.5 for 30 minutes. 105

Figure 3-10. (A) Delivery of 150 kDa FITC-Dextran (10 μM) to HeLa cells by co-incubation with PP50-Cy5 (1 mg mL^{-1}) at pH 6.5 for 30 minutes on ice, visualised by confocal microscopy. Scale bar = 10 μm. (B) Haemolysis of ovine erythrocytes following a 1 h incubation with PP50 (100 μg mL^{-1}) at 37°C (water bath), room temperature (20°C, benchtop) as well as on ice. Mean ± standard deviation (SD), n = 3. 106

Figure 3-11. Delviery of FITC-Dextran (10 μM) to HeLa cells by co-incubation with PP50 (1 mg mL^{-1}) in 1 h treatment at pH 6.5 and pH 7.4 and with- or without blocking the endosomal acidification by addition of 10 μM NH_4Cl 1 h prior to the treatment, during the treatment, and subsequent to the treatment duirng analysis. The cells were visualised by confocal microscopy. Scale bar = 20 μm..... 108

Figure 3-12. Relative median cell fluorescence, analysed by flow cytometry, following a treatment with 150 kDa FITC-Dextran at various concentrations using a fixed concentration of PP50 (0.5 mg mL^{-1}) and a treatment time of 30 minutes. Delivery at pH 6.5 and 7.4, as well as corresponding polymer-free controls, are compared. Mean ± SD, n = 3. Statistical comparison between cells treated with FITC-Dextran and PP50 at pH 7.4 and pH 6.5 at the set payload concentrations was performed using two-tailed unpaired Student's t-test. 110

Figure 3-13. Relative median cell fluorescence, analysed by flow cytometry, following a 30-minute treatment with a fixed concentration of FITC-Dextran (10 μM) and PP50 concentration within the range of 50-2000 μg mL^{-1}. Delivery at pH 6.5 and 7.4 is compared. Mean ± SD, n = 3. 111

Figure 3-14. Intracellular fluorescence visualised by confocal microscopy, following treatment with a mixture of PP50 (0.5 μg mL^{-}) and 150 kDa FITC-Dextran (2.5 μM) at pH 6.5 for different time periods within the range of 15-180 minutes, compared to polymer-free samples. Scale bar = 10 μm. (B) Relative median cell fluorescence, analysed by flow cytometry, following delivery of 150 kDa FITC-Dextran at pH 6.5 using PP50 (0.5 μg mL^{-1}) and different treatment times. Mean ± SD, n = 3. 113

Figure 3-15. Relative median cell fluorescence, analysed by flow cytometry, following delivery of 150 kDa FITC-Dextran (5 μM) using PP50 (0.5 mg mL^{-1}) in different pH environments ranging from pH 5.5 to 7.4. Polymer-containing and polymer-free samples are compared. Mean ± SD, n = 3..... 114

Figure 3-16. (A) Cell survival after a 24 h treatment of HeLa cells with different concentrations of PP50 in DMEM (neutral pH), analysed with AlamarBlue assay (B) Cytotoxicity of the delivery process of 150 kDa Dextran (10 μM) after incubation with PP50 (different concentrations used) for 30 minutes (PBS, pH 6.5 and pH 7.4), determined using AlamarBlue assay and (C) cytotoxicity of the delivery process determined using AlamarBlue assay after incubation with PP50 (1 mg mL^{-1}) and 150 kDa Dextran (10 μM) at pH 6.5 and 7.4, comparing different treatment times (PBS, pH 6.5 and pH 7.4). Mean ± SD, n = 3..... 116

Figure 3-17. Hydrodynamic particle size of FITC-Dextran (150 kDa), PP50 and FITC-Dextran + PP50 mixture at pH 6.5, determined via dynamic light scattering. PP50 concentration was 0.5 mg mL^{-1} and FITC-Dextran concentration was 10 μM..... 117

Figure 4-1. Delivery of 150 kDa FITC-Dextran (10 μM) to 9 different cell types using PP50 (1 mg mL^{-1}) using a 1 h treatment (HeLa, A549, MC 3t3, SU-DHL-8, CHO, hMSCs) or the same-sized FITC-Dextran at the concentration equal to 5 μM in 0.5 h treatment using the same polymer concentration (RAW 264.7, MES-SA, MES-SA/Dx5) at pH 6.5. FITC-Dextran and Lysotracker are presented in greyscale. The merged images depict green (FITC-Dextran), red (Lysotracker) and blue (Hoechst) channels. Scale bar = 20 μm. 123

Figure 4-2. Fluorescence intensity of the 9 different cell types after delivery of 10 μM FITC-Dextran using PP50 at the concentration of 1 mg mL^{-1} in 1h treatment. Cells were treated in the absence or presence of polymer at pH 7.4 ("pH 7.4-" and "pH 7.4+", respectively) and at pH 6.5 ("pH 6.5-" and "pH 6.5+", respectively). Mean ± SD, n = 3. One-way ANOVA and Tukey's tests were performed to compare different treatments. Different letters represent statistically significant difference with p-values < 0.5. 125

Figure 4-3. Cytotoxicity of the delivery process of 10 μM Dextran using PP50 (1 mg mL^{-1}) to different cell types at pH 7.4 and pH 6.5 following a 1 h treatment as analysed by AlamarBlue assay. Mean ± SD, n = 3. 126

Figure 4-4. Z-stack projections obtained using confocal microscopy illustrating delivery of 150 kDa FITC-Dextran (10 μM) to the A549 spheroids by co-incubation with PP50 (0.5 mg mL^{-1}) for a period of 2 h. Delivery at pH 6.5 and pH 7.4 were compared, in addition to corresponding polymer-free controls. The 3D projections were shown from the top and were a merge of green channel (FITC-Dextran) and red channel (PI stain of dead cells). The insets show bright field images of the corresponding spheroid. Scale bar = 200 μm. 128

Figure 4-5. Confocal microscopy illustrating delivery of 10, 70, 150 and 2000 kDa FITC-Dextran (0.15 mg mL^{-1}) using PP50 (0.5 mg mL^{-1}) at pH 6.5 in a 30-minute treatment. The merged pictures combine green (FITC-Dextran), red (Lysotracker) and blue (Hoechst) channels. Scale bar = 10 μm. 131

Figure 4-6. Strength of the fluorescent signal of cells as analysed by flow cytometry following a treatment with PP50 (0.5 mg mL^{-1}) and FITC-Dex (0.15 mg mL^{-1}). Treatment time was equal to 1 h. Mean ± SD, n = 3. 131

Figure 4-7. Delivery of GFP (2 μM) to HeLa cells using PP50 (0.25 mg mL^{-1}) at pH 6.5 and pH 7.4 following 1 h of treatment. Scale bar = 20 μm. 132

Figure 4-8. Delivery of 150 kDa FITC-Dextran (10 μM) to HeLa cells by co-incubation with PP50 (0.5 mg mL^{-1}) in a 3 h treatment, analysed by confocal microscopy. The merged pictures combine green (FITC-Dextran), red (Lysotracker) and blue (Hoechst) channels. Scale bar = 20 μm. 134

Figure 4-9. Flow cytometry of HeLa cells following a 4 h treatment with PP50 and 150 kDa FITC-Dextran (5 μM) at pH 6.5 with or without FBS at 10% v/v. Mean ± SD, n = 3. 135

Figure 4-10. Cytosolic fluorescence of HeLa cells delivered with 150 kDa FITC-Dextran (10 μM) in a 30-minutes treatment with PP50 (0.5 mg mL^{-1}) in PBS at pH 6.5 and pH 7.4. (A) Analysed by confocal microscopy at 0.5, 6 and 24 h post-treatment, scale bar = 10 μm, and analysed by flow cytometry at the same time points and

expressed as (B) Median fluorescence intensity of the cells and (C), percentage of fluorescent cells compared to a negative control. Mean ± SD, n = 3. 137

Figure 4-11. Multiple dosing of 150 kDa FITC-Dextran (10 μM) in HeLa cells by repeated delivery with PP50 (0.5 mg $mL^{-1)}$ in a 30-minute treatment at pH 6.5, compared to a polymer-free control, analysed by flow cytometry. Mean ± SD, n = 3. 138

Figure 4-12. Delivery of Anti-non-muscle Myosin IIA antibody (Alexa Fluor® 647) to A549 cells: comparison of PP50-mediated delivery (0.5 mg mL^{-1}) of the antibody (50 μg mL^{-1}or 333 nM) in a 1 h treatment at pH 6.5 against passive delivery to fixed and permeabilised cells of the same antibody concentration in 1 h treatment. Scale bar = 10 μm. 139

Figure 4-13. Delivery of dsRED (1 μg mL^{-1}) to HeLa cells by co-incubation with PP50 (0.5 mg mL^{-1}) at pH 6.5. Treatment time was equal to 2 h. Scale bar = 10 μm..... 140

Figure 4-14. Caspase activation after delivery of Bim (20 μM) by co-incubation with PP50 (1 mg mL^{-1}) for a period of 3 h at pH 6.5 and pH 7.4, as compared to controls: PP50 mediated delivery of scrambled Bim, and cells incubated with Bim, PP50 or PBS alone, analysed using (A) Caspase 9 Glo and (B) Caspase 3/7 Glo assays. Membrane permeable small molecule Bim mimetic, ABT-737 (20 μM), was used as a positive control. Mean ± SD, n = 3. Two-way ANOVA and Tukey's tests were performed to compare the cells treated with the different materials to PBS-treated cells. 142

Figure 4-15. Survival of cells after delivery of Bim (20 μM) by co-incubation with PP50 (1 mg mL^{-1}) for a period of 3 h at pH 6.5 and pH 7.4 following a further incubation period of 24 h, analysed using AlamarBlue assay. Mean ± SD, n = 3. Two-way ANOVA and Tukey's test was performed to compare the cells treated with the different materials to PBS-treated cells. 142

Figure 4-16. Cell morphology and death followed by delivery of Bim (20 μM) by co-incubation with PP50 (1 mg mL^{-1}) at pH 6.5 in a 4 h treatment compared to cell death caused by continuous treatment with ABT-737 (20 μM), analysed in IncuCyte® using Caspase-3/7 Green Apoptosis Assay. 144

Figure 4-17. Number of apoptotic cells following delivery of Bim (20 μM) by co-incubation with PP50 (1 mg mL^{-1}) at pH 6.5 in a 4 h treatment compared to cell death caused by continuous treatment with ABT-737 (20 μM), analysed in IncuCyte® using Caspase-3/7 Green Apoptosis Assay over a 20 h period. Mean ± SD, n = 3..... 144

Figure 4-18. Caspase 3/7 activation following a treatment with PP50 (0.5 mg mL^{-1}) and either Bim or scrBim in the concentration range of 0.1-20 μM at pH 6.5. Treatment time was equal to 3 h, followed by a wash and 4 h of further incubation and analysis using the Caspase 3/7 Glo Assay. Mean ± SD, n = 3. 146

Figure 4-19. Survival of cells following a treatment with PP50 (0.5 mg mL^{-1}) and either Bim or scrBim in the concentration range of 0.1-20 μM at pH 6.5 or treatment with ABT-737 in the same concentration range. Treatment time was equal to 3 h, followed by a wash and analysis using AlamarBlue assay 24 h post-treatment. Mean ± SD, n = 3. 146

Figure 4-20. Flow cytometry of A549 cells following a 1 h treatment with PP50 (1 mg mL^{-1}) and either Bim-Cy7 or scrBim-Cy7 (10 μM) at pH 6.5. Corresponding polymer-free controls were used for comparison. 147

Figure 4-21. Comparison of cell death caused by the delivery of 15 μM Bim(Cy7) using different delivery methods. For the chemical delivery agents, the treatment time was equal to 4h. Cell survival was quantified using CellTiter-Glo 2.0 assay 24 h after the end of the treatment. Mean ± SD, n = 3. Statistical comparison between PP50-mediated delivery of Bim-Cy7 and scrBim-Cy7, as well as between PP50 and PEI 25 kDa (delivery of Bim-Cy7) was performed using two-tailed unpaired Student's t-test. 149

Figure 4-22. (A) concentration and (B) means size of EVs following loading of Bim-Cy7 (20 μM) by co-incubation with PP50 (1 mg mL^{-1}) at pH 6.5 for 1.5 h and EV isolation by ultracentrifugation, compared to the original EV concentration and size, analysed by NanoSight. Mean ± SD, n = 3. One-way ANOVA and Tukey's tests were performed for comparison. Different letters represent statistically significant difference with p-values < 0.5. 152

Figure 4-23. Fluorescence of EVs concentrated on magnetic beads following loading of Bim-Cy7 (20 μM) by co-incubation with PP50 (1 mg mL^{-1}) at pH 6.5 for 1.5 h and EV isolation by ultracentrifugation, analysed by flow cytometry. Flow cytometry of EVs was performed by Christina Schindler (MedImmune). 152

Figure 4-24. Survival of A549 cells treated with EVs loaded with Bim-Cy7 using PP50 at pH 6.5, following a continous treatment over 24 h, analysed using CellTiterGlo 2.0 Assay. Mean ± SD, n = 3. P-values were calculated using unpaired Student's t-test.153

Figure 5-1. Relative haemolysis of red blood cells using PP50 and PP50-PDPH at 100 μg mL^{-1}. Incubation time = 1 h, temperature = 37°C. Mean ± SD, n = 3. 159

Figure 5-2. Structure of PDPH with 2-mercaptopyridine highlighted. 160

Figure 5-3. Release of 2-mercaptopyrine from PP50-PDPH using the cytosol (0.5 and/or 10 mM) and plasma (2 μM) concentrations of GSH (A) over a period of 2 h and (B) 24 h from the start of the reaction. Mean ± SD, n = 3. 162

Figure 5-4. Release of 2-mercaptopyrine from PP50-PDPH using the cytosol (100 μM) and plasma (20 μM) concentrations of cysteine (A) over a period of 2 h and (B) 24 h from the start of the reaction. Mean ± SD, n = 3. 163

Figure 5-5. Structure of PEG-FITC 164

Figure 5-6. Kinetics of the conjugation of FITC-PEG-Thiol onto PP50-PDPH in PBS (pH 7.4) at 0.5:1, 1:1 and 2:1 molar ratios of payload to PDPH over 2.5 hours at room temperature. Mean ± SD, n = 3. 165

Figure 5-7. Kinetics of the conjugation of FITC-PEG-Thiol on PP50-PDPH in PBS (pH 7.4) at 0.5:1, 1:1 and 2:1 molar ratios of the payload to PDPH over 22 hours at room temperature. Mean ± SD, n = 3. 166

Figure 5-8. The efficiency of the conjugation reaction between PEG-FITC and PP50-PDPH in different reaction environments at a 1:1 molar ratio of the payload to the crosslinker, measured by quantifying the release of 2-mercaptopyridine by UV-Vis spectroscopy. The conjugation was performed at room temperature, t = 5 h. PP50-PDPH concentration = 1 mg mL^{-1}. Mean ± SD, n = 3. 167

Figure 5-9. Relative haemolysis of PP50 and PP50-PEG (PEG size equal to 2 or 6 kDa, one PEG payload conjugated per 1 polymer chain). Polymer concentration was equal to 100 µg mL^{-1} (2.2 µM) and conjugate concentration was 2.2 µM. The incubation time was 1 h. The treatment was performed at 37^{o}C in a shaking water bath. Mean ± SD, n = 3. 168

Figure 5-10. Survival of HeLa cells, determined by AlamarBlue assay, following a 24 h treatment with various concentrations of PP50, PP50-PDPH and PP50-PEG2k (1.3 PEG molecules per 1 polymer chain) at equivalent PP50 concentrations. Mean ± SD, n = 3. 169

Figure 5-11. Delivery of PP50-PEG-FITC (11 µM) to HeLa, as analysed by confocal microscopy. 2 PEG-FTIC molecules were conjugation via the PDPH crosslinker per each one PP50 chain. Cells were treated in the absence or presence of polymer at pH 7.4 ("pH 7.4 PP50-" and "pH 7.4 PP50+", respectively) and at pH 6.5 ("pH 6.5 PP50-" and "pH 6.5 PP50+", respectively) for 1 h, which was followed by cell washing and 3 h of further incubation in serum-supplemented DMEM. Channels: Red = LysoTracker, Blue = Hoechst33342, Green = FITC-PEG. Scale bar = 10 µm. 171

Figure 5-12. The structure of Albumin with free cysteine highlighted. Modified from Kim and Lee (2012). 172

Figure 5-13. The efficiency of BSA conjugation to PDPH-modified PP50, analysed by the 2-mercaptopyridine release assay: (A) Conjugation of BSA to PP50-PDPH at 0.5, 1:1 and 2:1 molar ratios of BSA to PDPH. Concentration of PP50-PDPH = 1 mg mL^{-1}. (B) Conjugation of BSA to PP50-PDPH at 1:1 protein to PDPH molar ratio. Concentration of PP50-PDPH = 1, 2 and 5 mg mL^{-1}. (C) Conjugation efficiency of PP50-PDPH to SATA-modified BSA compared to conjugation of unmodified BSA in PBS. Concentration of PP50-PDPH = 1 mg mL^{-1} (D) Conjugation efficiency of PP50-

PDPH to SATA-modified BSA in PBS compared to conjugation of unmodified SATA in 50%DMSO/50% PBS. Concentration of PP50-PDPH = 1 mg mL^{-1}. All reactions were performed at room temperature. Reaction time was equal to 24 hours. Mean ± SD, n = 3. 174

Figure 5-14. Delivery of GFP to HeLa cells following conjugation to PDPH-modified PP50, analysed by confocal microscopy. GFP was conjugated to PP50-PDPH at 1.1 protein per 1 polymer chain (PP50-GFP concentration = 24 μM) and compared to delivery of GFP alone (4.6 μM). The materials were applied in serum-free DMEM for 1 h, followed by cell washing and 6 h of further incubation in serum-complemented DMEM. Channels: Green = GFP; Merge = Green channel + Red (LysoTrackerRED) and Blue (Hoechst33342). Scale bar = 10 μm..... 176

Figure 5-15. Relative haemolysis of PP50-IgG (0.27 μM, 4 polymer chains per IgG) and IgG mixed with PP50 (IgG concentration was equal to 0.27 μM, PP50 concentration was 50 μg mL^{-1} or 1.1 μM). Mean ± SD, n = 3..... 177

Figure 5-16. Delivery of IgG-FITC to HeLa cells following conjugation to PP50-PDPH, analysed by confocal microscopy. IgG-FITC was conjugated to PP50-PDPH at 4 polymer chains per 1 IgG molecule (PP50-IgG-FITC concentration was equal to 5.4 μM) and compared to delivery of IgG-FITC mixed with PP50 (polymer conc. = 1 mg mL^{-1} or 22 μM, IgG-FITC conc. = 4.8 μM). The materials were applied in serum-free DMEM for 1 h, followed by cell washing and 6 h of further incubation in serum-supplemented DMEM. Channels: Green = GFP, Red = LysoTrackerRED, Blue = Hoechst33342. Scale bar = 10 μm. 178

Figure 6-1. Caspase 3/7 activation in A549 cells following delivery of Bim and scrBim conjugated to PP50 polymer (one PDPH crosslinker per polymer chain). Concentrations of PP50, PP50-Bim and PP50-scrBim used in the experiment were equal to 22, 12 and 17 μM, respectively. The treatment time was equal to 1.5 h, followed by wash with PBS, replacement of DMEM and a 3 h period of further incubation. Mean ± SD, n = 3. 184

Figure 6-2. Qualitative analysis of the dialysis efficiency performed by exciting aliquots from the dialysate, sample undergoing dialysis and negative control (buffer only) at 800 nm using Odyssey. 186

Figure 6-3. Size spectra of Bim-Cy7, PP50 and PP50-Bim-Cy7 obtained by High Performance Size Exclusion Chromatography. HPSEC was performed by Jen Spooner (MedImmune). 187

Figure 6-4. Caspase 3/7 activation in A549 cells following delivery of Bim-Cy7 and scrBim-Cy7 conjugated to PP50 via PDPH (one crosslinker per polymer chain) and a mixture of the conjugates and free PP50. PP50-Bim-Cy7 and PP50-scrBim-Cy7 concentrations of 3, 6 and 12.5 μM were used. Delivery of conjugates at 3 μM was compared to the delivery of the same amount of conjugates supplement with free PP50

at 0.5 mg mL^{-1} (or 11 μM). The treatment was performed at pH 6.5 for 3 h, followed by a wash with PBS, replacement of DMEM and a 3 h period of further incubation. Mean ± SD, n = 3. One-way ANOVA and Tukey's tests were performed for comparison of samples within the PP50-scrBim-Cy7 and PP50-Bim-Cy7 groups. Different letters represent statistically significant difference with P-values < 0.5. 189

Figure 6-5. Images of A549 cells following treatment with 35 μM PP50-Bim-Cy7- or PP50-scrBim-Cy7. The IncuCyte® Caspase-3/7 Green Apoptosis reagent present in the growth medium was excited at 488 nm to indicate apoptotic cells. 191

Figure 6-6. Number of apoptotic A549 cells following treatment with different concentrations of PP50 conjugated with Bim-Cy7 or scrBim-Cy7 at pH 6.5 (A) or pH 7.4 (B) over a 24 h period post-treatment. n = 1. 192

Figure 6-7. In vitro stimulation of the immune response by PP50-Bim-Cy7 and PP50-scrBim-Cy7 following incubation of human PBMCs, determined by ELISA. Expression of two immunity markers was analysed: TNFα (A) and (B) as well as IL-6 (C) and (D). Cells were treated following concentrations of materials: PP50 = 11 μM (or 0.5 mg mL^{-1}), Bim-Cy7 and scrBim-Cy7 = 27 μM, PP50-Bim-Cy7 and PP50-scrBim-Cy7 = 8 μM in (A) and (C) as well as PP50 = 2.2 μM (or 0.1 mg mL^{-1}), Bim-Cy7 and scrBim-Cy7 = 5.4 μM, PP50-Bim-Cy7 and PP50-scrBim-Cy7 = 1.6 μM in (B) and (D). Mean ± SD, n = 3. 194

Figure 6-8. Body weight of mice measured 7 days post-injection with PP50. Mean ± SD, n = 3. 195

Figure 6-9. Recovery of Bim-Cy7 and scrBim-Cy7 dissolved in 6 buffers with different compositions. Measurement of peptide absorbance at 220 nm followed centrifugation and filtration to ensure removal of any precipitates and was compared to the initial absorbance to calculate the percentage of peptide recovery. n = 1. 196

Figure 6-10. Body weight of mice measured for 7 days following a single injection with PP50-Bim-Cy7 and PP50-scrBim-Cy7 at 17.5 μM. Mean ± SD, n = 6. 197

Figure 6-11. Body weight of mice following two injections with PP50-Bim-Cy7 and PP50-scrBim-Cy7 at 17.5 μM. The first injection was performed on day 0, followed by the second injection on day 2. Mean ± SD, n= 6. 198

Figure 6-12. Distribution of the Cy7 fluorescent signal in tumour-bearing CD-1 nude mice (lateral view) 1 h after intravenous injection of PP50-Bim-Cy7 at 17.5 μM. The bright yellow and orange areas correspond to a stronger fluorescent signal. The composite image shows the tissue autofluorescence in green and the Cy7 specific signal in blue, indicating preferential accumulation of the conjugate in the tumours. The minimum and maximum recorded fluorescence values are presented in the insets for each image. 201

Figure 6-13. Distribution of the Cy7 signal in internal organs of two CD-1 mice dosed with PP50-Bim-Cy7 at 17.5 μM. The organs were harvested and screened following the imaging of whole animals at t = 1 h post-injection. 201

List of Tables

Table 1-1. Tumour barriers for drug delivery. 38

Table 1-2. Novel and commonly used physical methods for intracellular delivery. Modified from (Stewart et al., 2016b). 44

Table 1-3. Novel and commonly used biochemical methods for intracellular delivery. Modified from (Stewart et al., 2016b). 45

Table 3-1. Summary of data by analysis of FITC-Dextran (150 kDa) and PP50 using dynamic light scattering and Zeta potential. PP50 concentration was 0.5 mg mL^{-1} and FITC-Dextran concentration was 10 µM. 117

Table 4-1. Cells types used for PP50-mediated delivery of FITC-Dextran and their details. 122

Table 4-2. Delivery techniques used in the comparison study. 148

Table 6-1. Compositions of the buffer formulations tested for the in vivo study 196

Abbreviations

A	
ATP	Adenosine 5'-triphosphate
B	
Bcl-2	B-cell lymphoma/leukemia-2 gene
Bcl-xl	B-cell lymphoma-extra large
C	
CHO	Chinese hamster ovary derivedcells
CPP	Cell penetrating peptide
Cys	Cysteine
D	
Da	Dalton
DARPin	Designed ankyrin repeat protein
DCC	N,N'-dicyclohexylcarbodiimide
DLS	Dynamic light scattering
DMAP	dimethylaminopyridine
DMEM	Dulbecco's modified Eagle's medium
DMF	N,N-dimethylformamide
DMSO	Dimethyl sulfoxide
DNA	Deoxyribonucleic acid
DOTAP	N-[1-(2,3-Dioleoyloxy)propyl]-N,N,N-trimethylammonium methyl-sulfate
DTT	Dithiothreitol
D-PBS	Dulbecco's phosphate buffered saline
E	
EDTA	Ethylenediaminetetraacetic acid
ELISA	Enzyme-linked immunosorbent assay
EPC	Enhanced permeability and retention

F

FBS	Foetal bovine serum
FITC	Fluorescein
FITC-Dextran	Fluorescein isothiocyanate–dextran

G

GSH	Glutathione

H

HeLa	Henrietta Lacks cell line
Her2	Human epidermal growth factor receptor 2
hMSC	Human mesenchymal stem cells

I

IC_{50}	Half inhibition concentration
IgG	Immunoglobulin G

M

MFI	Mean fluorescence intensity
M_n	number average molecular weight
M_w	molecular weight

N

NMR	Nuclear Magnetic Resonance

P

PDPH	3-[2-Pyridyldithio]propionyl hydrazide
PEG	poly(ethylene glycol)
PEI	Poly(ethyleneimine)
pKa	Acid dissosciation constant
PLL	Poly(L-lysine)
PLP	poly(L-lysine isophthalamide)
PP50	PLP grafted with L-phenylalanine at stoichiometric ratio of 50%

PP75	PLP grafted with L-phenylalanine at stoichiometric ratio of 50%
R	
RBCs	Red blood cells
S	
Scr	Scrambled (non-active)
siRNA	small interfering RNA
T	
TAT	HIV-1 Trans-activator gene product

Thesis outline

The work presented within this thesis is divided into seven chapters which are outlined below:

Chapter 1 discusses the challenges and opportunities for intracellular delivery of macromolecules. Different delivery strategies are described, including physical methods as well as biological and chemical delivery agents. The bioinspired, pH-responsive PP-family polymers are introduced and proposed as delivery agents

Chapter 2 describes the materials and methods used in the subsequent chapters. Synthesis and modification of the PP50 as well as conjugation of the polymer to a number of model and functional payloads is presented. The methodology behind both, the cell-based and *in vivo* studies aiming to illustrate the versatility of PP50-mediated delivery are described.

Chapter 3 aims to discuss the mechanisms underlying PP50-mediated delivery to mammalian cell using the co-incubation strategy. The interaction between the polymer and the membranes of ovine erythrocytes, which serve as simplified models of more complex cells, is first studied. This is followed by the analysis of the intracellular fate of the polymer in HeLa cells and of the PP50-mediated delivery of a large, fluorescent dextran to these cells. In addition, the delivery process is characterised as a function of various parameters, including treatment time, payload and polymer concentration and the environmental pH.

Chapter 4 describes the investigation into the versatility of PP50-mediated delivery by co-incubation with the payload. Different cell types and payload with different molecular weight and properties are used. Delivery to 3D multicellular spheroids is also examined. Finally, PP50-mediataed delivery of an apoptotic peptide is compared to the delivery using other common delivery methods.

Chapter 5 discusses the grafting of the cleavable crosslinker PDPH onto PP50, followed by conjugation of payloads of various size. PP50-mediated delivery of a short polymer, green fluorescent protein and antibody to HeLa cells conjugated onto the polymer is investigated.

Chapter 6 describes the conjugation of the apoptotic peptide Bim to PP50, followed by *in vitro* testing of the conjugate potency at tumour-like pH. The conjugates are also tested for potential immunogenicity *in vitro* and tolerability in a mouse model, followed by visualisation of their biodistribution.

Chapter 7 summarises the findings of this thesis and presents potential future work opportunities

Chapter 1 - Introduction

1.1 Introduction – stimulus-responsive polymers as delivery agents

Intracellular delivery of exogenous molecules, particularly macromolecules, remains a challenge (Khalil et al., 2006; Stewart et al., 2016b). This is because of the difficulty of overcoming the barrier posed by the plasma membrane, which completely inhibits or greatly limits the ability of large molecules to traverse to the cell interior. There exists, therefore, a large number of potential applications for a novel method which would enable intracellular delivery of macromolecular cargo, including both *in vitro*/*ex vivo* as well as *in vivo* settings.

Successful *in vitro* and *ex vivo* delivery of macromolecular cargo, such as peptides, proteins, nucleic acids and nanoparticles, to the cytosol and the nucleus of various cell types, including hard-to-transfect immune system and stem cells, would enable many potential uses in various fields. These include (i) modulation of gene expression and gene editing by delivery of nucleic acids, transcription factors or Cas9, (ii) screening of protein and peptide libraries without the necessity for DNA transfection, (iii) labelling of proteins and organelles using intracellular probes (iv) modelling of disease mechanisms and phenotypic analysis, (v) delivery of antibodies or antibody fragments with intracellular targets, (vi) production of pluripotent stem cells and (vii) cell-based therapy, among others (Kim et al., 2009a; Rajendran et al., 2010; Yoo et al., 2011; Marschall et al., 2014; Kollmannsperger et al., 2016; Stewart et al., 2016b).

In addition, intracellular delivery *in vivo* has an enormous therapeutic potential, especially in the field of cancer. Cancer is one of the leading causes of morbidity and mortality worldwide, with people living in developed countries having a 40% chance of developing some form of cancer in their lifetime (Sasieni et al., 2011). Despite the wide prevalence of cancer, its treatment and survivability still remains unsatisfactory (Siegel et al., 2017). The most prevalent forms of cancer

therapy include invasive surgery, radiotherapy and chemotherapy. Small molecule drugs used in chemotherapy are well known for their side effects arising from their cytotoxicity as well as inefficient and non-specific distribution in the bloodstream (Speth et al., 1988; Imai and Takaoka, 2006; Zhang et al., 2009; Pérez-Herrero and Fernández-Medarde, 2015). In order to increase the effectiveness of cancer therapy and to counteract the invasiveness and toxicity of the currently used methods, a group of novel, biologically derived and highly specific therapeutic macromolecules have been developed. Such biopharmaceuticals include proteins (antibodies, antibody fragments, hormones, enzymes) as well as nucleic acids (DNA, therapeutic RNA, siRNA) (Dincer et al., 2005; Jozala et al., 2016; Moorkens et al., 2017). Despite their impressive therapeutic potential and effectiveness in targeting extracellular sites, biomacromolecules have very limited clinical use as modulators of intracellular pathways due to the difficulty of their transport across the plasma membrane (Guillard et al., 2015). Therefore, there is an urgent need for a drug delivery agent capable of transporting different sized therapeutic payloads to desired intracellular sites in *in vivo* settings, ensuring their stability as well as precise targeting, release and accumulation in diseased tissues.

Stimuli-responsive, “smart”, polymers are capable of sensing and responding to an external stimulus by undergoing a change in their structure and/or properties (Wei et al., 2017). Such stimuli include a wide number of physical and chemical conditions, such as temperature, pH, ionic strength, and light, and may lead to alteration of the polymer conformation, phase, hydrophobicity and other properties. Stimuli responsive polymers are a promising drug delivery agent and have received a lot of attention in the field of nanomedicine research (Schmaljohann, 2006; Hrubý et al., 2015; Baudis et al., 2014; Wei et al., 2017) The wide variety and plasticity of polymers offers a number of potential uses and applications, including as dissolved free polymers, hydrogels, micelles, polymers grafted or adsorbed to other structures and polymers conjugated to various therapeutic molecules (Hoffman, 2013).

One of the most promising groups of smart polymers are pH responsive polymers, which have been designed to take advantage of the pH gradients present in the cell as well as in the microenvironment of tumours, and could

significantly improve delivery of biomacromolecules to the cell interior (Eccleston et al., 2000). Of particular interest are pH gradients associated with internalisation of extracellular particles, including therapeutic molecules, via the endosomal pathway. The process of maturation of endosomal vesicles, following uptake of foreign molecules, is associated with progressive acidification of the endosome interior, ultimately leading to fusion with lysosomes and degradation of the engulfed cargo (Eccleston et al., 2005).

pH-responsive polymers are capable of overcoming intracellular delivery barriers and facilitating endosomal escape and intracellular delivery of macromolecules. These polymers contain ionisable groups which cause the polymer to undergo a conformation change in decreasing pH conditions (Dincer et al., 2005; Chen et al., 2009c). Non-active at physiological pH, these polymers gain membrane disruptive abilities as environmental pH drops, due to a change in the hydrophobic/hydrophilic balance and polymer structure. This reversible shift allows for permeabilisation of endosome membrane and release of the endocytosed material to the cytosol (Figure 1-1) (Eccleston et al., 2005). Additionally, the acidic extracellular microenvironments of tumours, ranging between pH 6.5-7.2 (compared to physiological pH 7.4) might also be exploited to aid membrane permeabilisation and controlled drug delivery (Vaupel et al., 1989; Junttila and de Sauvage, 2013; Kanamala et al., 2016). The mildly acidic tumour environment can be also mimicked *in vitro* to activate pH-responsive polymers in the extracellular space and promote membrane permeabilisation (Lynch et al., 2011), which could be used for *in vitro* and *ex vivo* cell modification and engineering via delivery of various macromolecular payloads.

The aim of this chapter is to provide an overview of approaches to delivery of macromolecular payloads using various methods. Extracellular and intracellular barriers to successful delivery of payloads are discussed, and the potential mechanisms of translocation through the plasma membrane are explored in more detail. Various physical and chemical/biochemical delivery methods are mentioned, with a special focus given to anionic, pH responsive polymers, such as the PP-polymers (Chen et al., 2009a). Finally, specific methodology of payload delivery using PP-polymers is described.

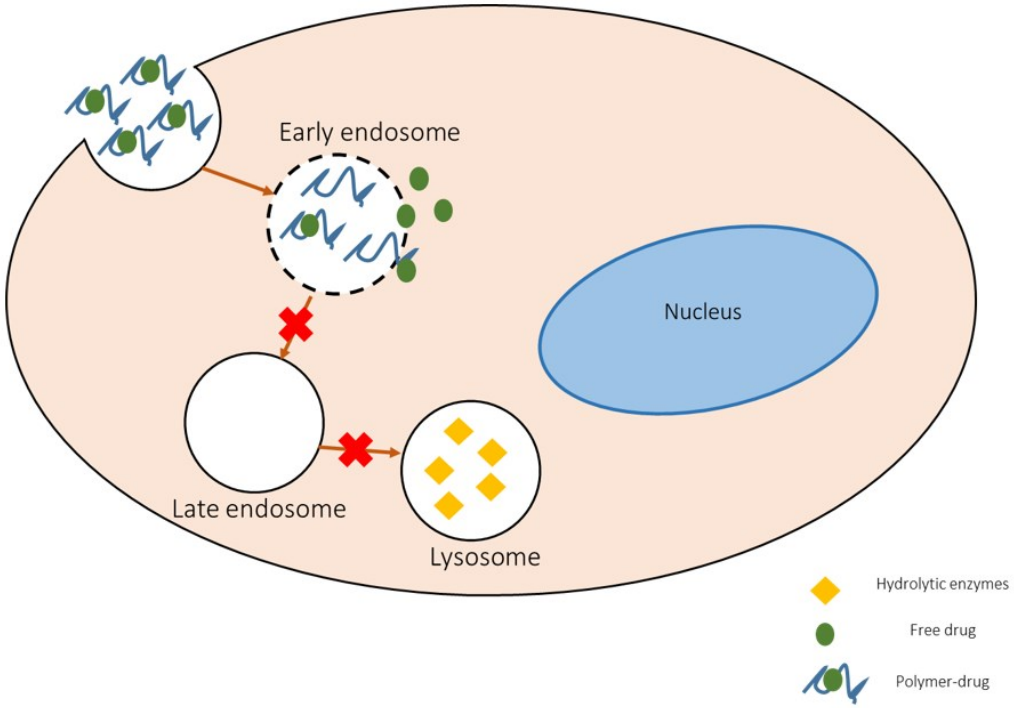


Figure 1-1. The mechanism of controlled drug delivery using pH responsive polymers. The polymer-drug conjugate (or mix) is internalised by endocytosis. Acidification of early endosomes leads to change of hydrophobic/hydrophilic balance of the polymer, enabling it to become membrane disruptive. This leads to release of the drug into the cytosol and its further diffusion to the site of action (e.g. the nucleus). Membrane disruption of early endosomes prevents their maturation to late endosomes and fusion with lysosomes, where the engulfed cargo would have been degraded by hydrolytic enzymes. Based on (Plank et al., 1998).

1.2 Challenges for intracellular delivery

Delivery of therapeutic, membrane-impermeable substances to the desired sites is a complex process involving the need to overcome a number of barriers, both extra- and intracellular. Depending on the application, this can involve transportation to the targeted organ or tissue, passing through the plasma membrane, and trafficking to the appropriate intracellular compartment.

1.2.1 Extracellular barriers

1.2.1.1 Systemic barriers and targeted delivery

One of the main problems facing delivery of drugs and use of delivery agents *in vivo* is their rapid clearance from the body. This can be caused by renal elimination and/or the immune system (including Mononuclear Phagocyte System or MPS):

- Glomerular filtration in the kidneys might lead to removal of drugs and drug carriers from the bloodstream. In order to avoid premature renal clearance, the molecular weight of the delivery agents should be higher than the molecular weight cut-off for renal filtration, i.e. 30-50 kDa (Harris and Chess, 2003; Duncan, 2006; Yu and Zheng, 2015).
- MPS consists mostly of macrophages, whose role is elimination of foreign particles from the body, such as drug delivery agents. Foreign materials can be removed from circulation by organs such as liver and spleen. In order to avoid elimination by MPS, drug delivery agents should be hydrophilic and smaller than 100 nm (Adams et al., 2003; Brannon-Peppas and Blanchette, 2004; Owens and Peppas, 2006; García et al., 2014; Liu et al., 2017b).

In addition, low stability of the therapeutic substances and delivery agents might lead to loss of functionality (Pack et al., 2005). These potential issues need to be addressed during early development and investigation of pharmacokinetics and dynamics, in order to ensure sufficient levels of distribution and accumulation at the target site. One phenomenon which might facilitate passive targeting of tumour sites is the Enhanced Permeability and Retention (EPR) effect, which relies on the fact that hypervascularisation and aberrant vascular architecture of solid tumours leads to an enhanced permeability to various micro and macromolecules (Maeda et al., 2009; Greish, 2010; Nakamura et al., 2016; Nel et al., 2017).

Another strategy which can aid localisation of the drugs and delivery agent to the tumour site and prevent their passive diffusion in the blood stream is the use of targeted delivery. A number of potential molecules with high affinity for extracellular targets on cancer cells could be used, including biomolecules such

as immunoglobulin antibodies as well as antibody fragments and mimetics, including fragment antigen-binding (Fab'), designed ankyrin repeat proteins (DARPin) and single-chain variable fragments (scFv) (Nelson, 2010; Zahnd et al., 2010; Kikuchi et al., 2017; Fiedler et al., 2018). Conjugation of high affinity targeting ligands to delivery agents could stimulate active targeting via enhanced membrane binding or receptor-mediated endocytosis. One of the most studied and promising target for high affinity ligands is the transmembrane receptor tyrosine-protein kinase erbB-2, encoded by human epidermal growth factor 2 (*HER2*) gene, which is over-expressed in up to 30% of invasive breast carcinomas (Slamon et al., 1989; Scott et al., 1993). This biomarker, associated with aggressive metastasis, is targeted by the monoclonal antibody Trastuzumab (Herceptin), developed by Genentech and widely used in the clinical settings (Garnock-Jones et al., 2010). HER2-positive cancers could also be targeted by special DARPins, generated to target this receptor and allowing specific delivery of drugs (Stumpp et al., 2008; Siegler et al., 2017). Compared to full size antibodies and other antibody fragments, DARPins are especially good candidates for this task due to their high stability and small size (14 or 18 kDa), which reduces the risk of altering membrane properties of delivery agents, which could be the case if larger targeting ligands were used. Another potential antigen which could be used for targeting is the folate receptor, which is overexpressed in some ovarian, breast and lung cancers (Cheung et al., 2016).

Ligand-attached macromolecules display a number of advantages, such as high specificity for cancer cells and improved cellular uptake. However, the "binding site barrier" effect has been described, whereby delivery agents possessing ligands actively targeting receptors on tumour cells bind to the tumour periphery only due to strong receptor-ligand interactions, preventing further tumour penetration (Saga et al., 1995). In addition, receptors can been expressed in a heteregoneous manner between different individuals, tumour types or even different stages of the same tumour, which is another difficulty for ligand-assisted active targeting (Chen et al., 2017).

1.2.1.2 Tumour microenvironment barriers

The penetration of the tumour tissue poses another barrier for drug delivery. The tumour microenvironment possesses a number of characteristics which can prevent efficient diffusion of drugs and delivery agents to deep tissue and thus need to be considered when designing cancer therapeutics (Hatakeyama et al., 2006; Chen et al., 2017). The main types of such barriers and ways to address them are described in Table 1-1.

Table 1-1. Tumour barriers for drug delivery.

Barrier	Possible strategy to overcome it / use it to the advantage of drug delivery
Extracellular matrix – dense matrix can inhibit particle diffusion in the tumour (Kuppen et al., 2001)	Treatment with collagenase (Kuhn et al., 2006) Co-infusion with hypertonic buffer (Neeves et al., 2007)
Abnormal angiogenesis – leads to uneven vasculature and blood flow and the high interstitial fluid pressure (IFP) effect (Jain, 2001; Junttila and de Sauvage, 2013)	Angiogenesis therapy targeting the vascular endothelial growth factor (VEGF) (Tong et al., 2004; Zarrabi et al., 2017)
Mildly acidic extracellular pH – arises due to the "Warburg effect", can affect drug permeability by causing increased polarity or charge (Gerweck et al., 1999; Mahoney et al., 2003; Vander Heiden et al., 2009)	Encapsulation into pH-sensitive nanoparticles (Koren et al., 2012) Use of pH-responsive drug delivery agents (Sawant et al., 2012; Khormaee et al., 2013)
Hypoxic core - due to insufficient oxygen supply in areas which are distant from blood vessels; can impart partial resistance to therapies and immune system evasion (Cairns et al., 2006; Facciabene et al., 2011; Wilson and Hay, 2011)	Hypoxia-specific targeting Use of hypoxia-sensitive prodrugs (Harada et al., 2005; Thambi et al., 2016)

Upregulation of extracellular enzymes - such a metalloproteinases, peptidases and lipases, which degrade the extracellular matrix and promote metastasis (Egeblad and Werb, 2002; Chen et al., 2017)	Downregulation of enzyme expression (Chetty et al., 2008) Use of enzyme-sensitive delivery systems (Zhu et al., 2012; Wei et al., 2016)

Various drug delivery systems have been developed which aim to take advantage of the listed unique characteristics of the tumour microenvironment and use them as a stimulus to enable drug delivery either at the site of the tumour or directly into the interior of tumour cells (Kim et al., 2010; Thambi et al., 2014; Chen et al., 2017). Of main interest to the current work are pH-sensitive delivery agents. These include pH-sensing peptides and polymers relying on a pronation/deprotonation mechanism for plasma membrane destabilisation and internalisation, use of acid-labile crosslinkers for conjugation of drugs and delivery agents as well as drug masking, shielding or encapsulation in pH-sensitive complexes (He et al., 2013; Kanamala et al., 2016).

Despite a number of proposed solutions for utilising the mildly acidic extracellular tumour pH as the trigger to facilitate drug delivery, the focus has been on delivery of small molecule anticancer drugs, such as Doxorubicin and Paclitaxel, and progress remains to be made in the area of delivery of mac

romolecular payloads (He et al., 2013; Jain et al., 2015; Wang et al., 2017).

1.2.2 Cellular barriers and membrane permeabilisation strategies

Intracellular delivery of therapeutic agents both *in vitro* and *in vivo* requires overcoming the barrier posed by the presence of a bilayer lipid membrane in all cells. Endocytosis is the most common cellular mechanism for internalisation of nanomaterials and large payloads (Iversen et al., 2011; Oh and Park, 2014) . There exist two major types of endocytosis: phagocytosis and pinocytosis, consisting of two general steps: encapsulation of an extracellular particle into a

membrane-derived intracellular vesicle (i.e. the endosome) and further trafficking of the endosome within the cell, leading to the ultimate degradation of its content in the lysosome (Christie and Grainger, 2003; Blanco et al., 2015). Since phagocytosis involves encapsulation of relatively large particles, such as pathogenic micro-organisms, it is not directly applicable to drug delivery (Swanson, 2008; Sarantis and Grinstein, 2012).

Pinocytosis is the other general category of endocytosis, which is utilised by the cell to internalise solutes and fluids, including proteins and lipids, with the aim of digesting and recycling them in the biosynthesis processes (Duncan and Richardson, 2012). Pinocytosis can be divided into, clathrin-dependant endocytosis, caveolin-dependant endocytosis, clathirn- and caveoiln-independent endocytosis as well as macropinocytosis, which is used primarily for non-selective uptake of fluids (Mukherjee et al., 1997; Mayor and Pagano, 2007; Mayor et al., 2014; Kaksonen and Roux, 2018). The different endocytosis pathways are illustrated in Figure 1-2.

Clathrin-dependant endocytosis is a pinocytic pathway which relies on formation of pits in the plasma membrane coated with clathrin, enabling internalisation of extracellular molecules, such as growth factors and transferrin. In order to initiate the assembly of clathrin on the cytosol side, activation of appropriate transmembrane receptors present at specialised sites on the plasma membrane must take place. Following invagination and detachment from the plasma membrane, clathrin-coated vesicles uncoat and fuse to form early endosomes (Wendland, 2002; Mousavi et al., 2004; Mettlen et al., 2018).

Caveolin-dependant endocytosis relies on formation of caveolae (flask-shaped pits utilising caveolin proteins) in the plasma membrane after appropriate ligand activation, which, similarly to clathrin-dependant endocytosis, is followed by invagination, detachment from the plasma membrane and migration into the cytosol to form the early endosome (Parton and Simons, 2007; Chaudhary et al., 2014).

The process of endosome maturation is characterised by rapid and progressive acidification, from pH 7.4 (physiological) to pH 6.8-6.0 (early endosomes), followed by a further influx of protons via ATP-dependant proton pumps, causing

the pH level to drop to 6.0-5.0, which is characteristic of late stage endosomes. Normally, late endosomes fuse with lysosomes, where low pH (5.5-4.5) stimulates and promotes the action of lytic proteases leading to degradation of the endocytosed cargo (Authier et al., 1996; Mellman, 1996; Pack et al., 2005; Oh and Park, 2014). Alternatively, trafficking to other organelles, such as the Golgi apparatus, can also take place (Mukherjee et al., 1997; Hu et al., 2015; Xue et al., 2017).

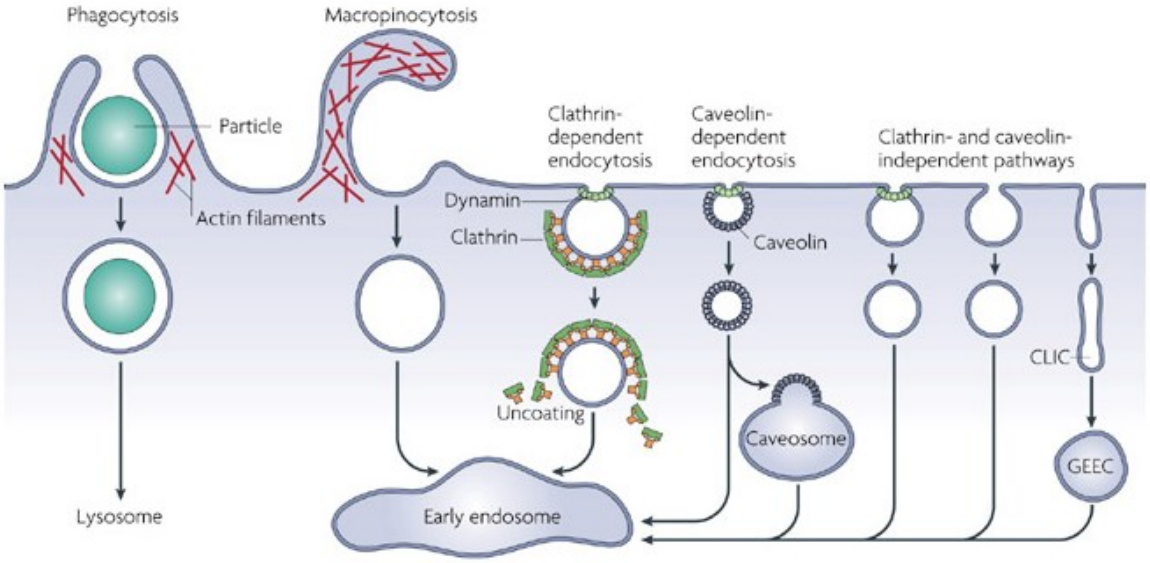


Figure 1-2. Different types of endocytosis**.** Source: Mayor and Pagano (2007).

Entrapment and accumulation of therapeutic payloads in maturing endosomes, leading to their enzymatic degradation in lysosomes, would greatly reduce the efficiency of many biopharmeceutical-based courses of treatment. Thus, the escape of internalised payloads from endosomal space and their release into the cytosol are necessary (Varkouhi et al., 2011; El-Sayed et al., 2005; Stewart et al., 2016a). An exception to this are some antibody-small molecule drug conjugates, which rely on lysosomal degradation of the carrier antibody for drug release (Chalouni and Doll, 2018).

To solve the problem of endosomal entrapment, several strategies can be adopted, including (Plank et al., 1998):

- Disruption of early endosomal membrane resulting in release of the endocytosed material to the cytosol. The idea of “hijacking” the endocytosis pathway for cellular delivery was first proposed by de Duve et al. (1974). A more novel concept involves usage of pH responsive polymers capable of disrupting endosomal membrane prior to the lysosomal degradation of the engulfed cargo. As a result, payloads are delivered to the cytosol where they can interact with various intracellular molecules. One issue associated with this approach is that while some of the endocytosis pathways described above are present in all cells, others are specific to certain cell types or tissues (Duncan and Richardson, 2012). For example, caveolin-mediated endocytosis might be more common in endothelial cells and smooth-muscle cells (Parton and Simons, 2007). This could lead to a decreased delivery efficiency if the delivery agent used relies mostly on this type of endocytosis for internalisation. For this reason, endocytosis should be studied in a number of different cell lines when developing new drug carriers in order to obtain a good understanding and control of membrane permeabilisation by endocytosis. This can be achieved by e.g. blocking specific endocytotic pathways (Vercauteren et al., 2010; Dutta and Donaldson, 2012; Elkin et al., 2016). Endosomal escape using pH responsive cargo delivery agents will be discussed in more detail later.

- Direct plasma membrane penetration, in which the endosomal-lysosomal pathway is bypassed, is another mechanism which could be of interest for intercellular delivery of macromolecules. Direct membrane permeabilisation by formation of pores can be achieved by a large number of physical methods, which will be described later. Chemical, biochemical and biologically-derived delivery agents have also been used for cargo delivery using this approach. Normally, direct penetration achieved by such agents has been only viable for delivery of small molecules and macromolecules not exceeding a couple of nanometers in size, as they do not lead to detrimental and irreversible disruption of membrane integrity (Goda et al., 2010). An exception to this are phospholipid based polymers, which mimic the chemical composition of phospholipids in the plasma membrane. As reported by Goda et al. (2010), those synthetic polymers with average size of 10 nm can pass through the plasma membrane even when the energy dependant endocytosis mechanisms are blocked. Another group of

molecules possessing the ability to pass the plasma membrane directly are arginine rich cell penetrating peptides (CPPs) (Hirose et al., 2012; Brock, 2014).

The precise mechanism by which such peptides penetrate the plasma membrane remains unknown and could vary depending on various parameters, however, it might involve formation of multivesicular structures on the membrane, leading to its topical inversion and peptide translocation into the cytosol. The efficiency of this process might be increased by conjugation of hydrophobic residues onto the peptides (Hirose et al., 2012).

Direct membrane penetration can also be achieved by fusion of delivery agents (such as liposomes) with plasma membrane, leading to cargo release directly into the cytosol. Alternatively, transient plasma membrane permeabilisation using electroporation can be used, but is impractical for organism-wide drug delivery (Plank et al., 1998; Venslauskas and Satkauskas, 2015).

1.3 Delivery strategies

A large number of intracellular delivery strategies have been developed to overcome the barriers outlined above in both *in vitro and in vivo* scenarios. The delivery methods which are employed currently are often divided into physical and chemical/biochemical as shown in Table 1-2 and Table 1-3.

Table 1-2. Novel and commonly used physical methods for intracellular delivery. Modified from (Stewart et al., 2016b).

Type	Method	Reference
Mechanical	Fluid shear	(Hallow et al., 2008)
	Squeezing	(Kollmannsperger et al., 2016)
	Cavitation	(Prentice et al., 2005)
	Osmotic	(Borle and Snowdowne, 1982)
	Impact and scraping	(McNeil, 1988)
	Nanoneedles	(Timothy et al., 2003)
	Microinjection	(Capecchi, 1980)
	Ballistic particles	(Klein et al., 1987)
	Sonoporation	(Tomizawa et al., 2013)
Other	Optoporation	(Tsukakoshi et al., 1984)
	Thermal	(He et al., 2006)
	Electroporation	(Chen et al., 2006)

Table 1-3. Novel and commonly used biochemical methods for intracellular delivery. Modified from (Stewart et al., 2016b).

Type	Method	Reference
Bioinspired	Pore forming agents and detergents	(Gurtovenko et al., 2010; Bischofberger et al., 2012)
	Ghost cells	(Schoen and Machluf, 2016)
	Viral vectors	(Thomas et al., 2003)
	Ligand conjugates	(Yoo et al., 2011)
	Cell penetrating peptides	(Guidotti et al., 2017)
	Extracellular vesicles	(Vader et al., 2016)
Nanotechnology	Nanotubes	(Heller et al., 2005)
	Lipid nanocarriers	(Gilleron et al., 2013; Chatin et al., 2015)
	Inorganic nanocarriers	(Derfus et al., 2004)
	Polymer nanocarriers	(Yoo et al., 2011)

1.3.1 Physical methods

Physical delivery methods rely on temporary membrane disruption using physical factors, such as mechanical contact, squeezing, microfluidic stress, electric field, laser beam, cavitation or thermal heat (Stewart et al., 2016b).

Membrane disruption must be impactful enough to allow the delivery of the payload of interest but not significant enough to prevent the cell from repairing itself post-treatment – a balance which can prove difficult to achieve and often resulting in high cell death as a side effect of cargo delivery using physical methods. Due to their nature, most physical methods are currently limited for *in vitro* delivery only. Payload delivery by electroporation, sonoporation and microfluidics-aided cell squeezing, which are some of the most successful or promising physical delivery methods, are described in more detail below.

1.3.1.1 Electroporation

Electroporation is a method of permeabilising the plasma membrane using an electric field (Chen et al., 2006). The method relies on the application of very short (micro – to millisecond) electric pulses to a sample containing cells mixed with the desired payload. This has an effect of producing a high transient trans-membrane potential which in turns leads to the rearrangement of the membrane structure induced by penetration by water molecules and formation of pores. The pore formation enhances ionic and molecular trafficking through the plasma membrane.

Electroporation has been extensively used for many years enabling, among others, efficient intracellular delivery of nucleic acids into a wide range of cells (Young and Dean, 2015), CRISPR/Cas9 delivery to mouse zygotes (Teixeira et al., 2018) and protein delivery to mammalian cells grown in adherent culture (Deora et al., 2007).

Electroporation, however, is often associated with high cell death as a side effect of the harsh treatment with the electric field which can lead to irreversible damage to the membrane (Yarmush et al., 2014). In addition, electroporation has limited uses for delivery to organs and tissues, due to the difficulty of application of the electric fields via invasive methods and the fact that cells of different shape or type within tissues would be affected by the applied electric field nonhomogenously, which can lead to uneven or incomplete transfection (Miklavcic et al., 2000; Ayuni et al., 2010; Kotnik et al., 2015).

1.3.1.2 Sonoporation

Sonoporation for intracellular delivery applications relies on using ultrasound to permeabilise the plasma membrane (Tomizawa et al., 2013; Shapiro et al., 2016). Payload delivery by sonoporation is often enhanced by usage of microbubbles consisting of a gas core and a shell composed of polymers, proteins or lipids with stabilising properties. Microbubble movement combined with oscillating fluctuations induced by low acoustic pressure and ultrasonic radiation can induce interaction with the membrane leading to endocytosis (Lu

et al., 2003; Watanabe et al., 2010; De Cock et al., 2015; Shapiro et al., 2016). High acoustic pressure amplitudes, in contrast, can lead to microbubble collapse, which causes shear stress and the induction of spatiotemporal pores in the plasma membrane, which is thought to be another mechanism enabling payload delivery using this approach. Microbubble-enhanced sonoporation has been shown to aid delivery of naked DNA resulting in efficient gene transduction (Lu et al., 2003)

Microbubbles can be functionalised to target a specific population of cells and to carry a payload (Kaufmann and Lindner, 2007). Along with the ability to control and localise ultrasound, this allows for systemic application of microbubbles and their activation in the region of interest, including deep tissues, with no evidence of tissue damage. This, therefore, has potential applications in the fields of diagnostics or *in vivo* gene therapy (Shapiro et al., 2016).

1.3.1.3 Microfluidics-aided cell squeezing

Microfluidics is a relatively new method of payload delivery which utilises controlled flow through microchannels to cause temporary membrane disruption induced by shear stress (Hallow et al., 2008) or by passing the cell through narrow constrictions (squeezing) (Sharei et al., 2013). Delivery by microfluidics-aided cell squeezing in particular has received a lot of attention lately (Szeto et al., 2015; Li et al., 2017). In this method cells are mechanically deformed while they move through channels which are 30 to 80% more narrow than the cell diameter, which results in rapid membrane deformation and formation of transient pores in the plasma membrane, enabling diffusion of payloads present in the buffer at the time of the procedure.

Microfluidics-aided cell squeezing has been used to deliver payloads within the size range of 3 to 2,000 kDa, including proteins, nucleic acids and nanoparticles such as quantum dots and carbon nanotubes (Saung et al., 2016). In addition, cell squeezing was used to deliver imaging probes for protein labelling in live cells at nanomolar concentrations of the payload, allowing for precise super-resolution imaging (Kollmannsperger et al., 2016).

Membrane disruption using microfluidic methods can also be combined with electroporation (Ding et al., 2017). In this approach, cell suspension containing plasmid DNA is squeezed through narrow constrictions leading to membrane permeabilisation, followed by a treatment with electric field, which was shown to disrupt the nuclear envelope and allow cytosolic and nuclear delivery of the cargo. The throughput for cell transfection using this method was up to millions of cells per minute.

All intracellular delivery methods which rely on pore formation have a potential of inducing cell death due to their enabling of bidirectional movement of molecules across the plasma membrane which can cause an irreparable loss of cellular haemostasis. In the case of cell squeezing, the time required for membrane healing post-permeabilisation was between 30s to 5 minutes (Kollmannsperger et al., 2016). The resulting cell viability appeared to vary between cell and payload type, reaching 90% for delivery of dextran to HeLa cells but only 56% for delivery of antibody to T cells. In addition, repeated delivery was shown to result in significant loss of viability (Sharei et al., 2013; Sharei et al., 2014). Other associated problems include clogging, which limits throughput, scalability issues, potential high initial cost and the inability to deliver to cells grown as adherent cultures or as 3D multicellular spheroids.

1.3.2 Chemical and biological delivery agents

Chemical, biological or bio-inspired compounds can be used as drug delivery agents. A successful drug delivery agent needs to be soluble in aqueous solutions as well as non-toxic and non-immunogenic. In therapeutic applications, it would ideally be able to improve drug efficacy and stability, enabling precise and targeted delivery. Furthermore, following drug release, the agent needs to be safely degraded or excreted from the cell or the body to avoid potentially harmful accumulation.

Different types of commonly used chemical, biological and bio-inspired delivery agents include viral vectors, liposomes, exosomes, cell penetrating peptides (CPPs) and polymers (Torchilin, 2014). They are discussed below.

1.3.2.1 Viral vectors

Viral vectors and virus-like particles have been extensively studied for applications in delivery of nucleic acids in gene therapy as they excel at efficient intracellular and nuclear delivery of genetic material (Davidson and Breakefield, 2003; Yoo et al., 2011). The most commonly used viruses for transduction include adenoviruses, adeno-associated viruses, retroviruses and lentiviruses, which are derived from human viral pathogens and can infect a wide spectrum of cell types (David and Doherty, 2017). Despite this, the clinical usefulness of viral-based delivery systems remains low. This is due to the potential safety issues associated with the immunogenicity and genotoxicity of viral vectors which can arise due to insertional mutagenesis, promoter activation and upregulation of cellular proto-oncogenes (Knight et al., 2013; David and Doherty, 2017).

1.3.2.2 Lipid-based drug delivery agents

Liposomes are self-assembled, closed spherical vesicles, composed of concentric lipid layers. The lipid bilayer of liposomes is made up of either synthetic or natural phospholipids (Allen and Cullis, 2013). The liposome interior as well as the space between the lipid bilayer is aqueous and hydrophilic. The amphiphilic nature of liposomes enables entrapment of both hydrophilic and hydrophobic drugs – the former encapsulated within the interior of the vesicle, and the latter loaded in the lipid bilayer membrane (Torchilin, 2005; Benvegnu et al., 2009; Alavi et al., 2017).

Liposomes have a number of advantages. Since they can be prepared using natural lipids, liposomes are biocompatible and exhibit low toxicity to tissues. Furthermore, they can adsorb onto or fuse with the cell or endosomal membrane, releasing the trapped payload directly into the cytosol (Watson et al., 2012).

Additionally, liposomes are modifiable. Their size, charge and surface properties can be adjusted by altering lipid composition or preparation method. It is also possible to design liposomes with lipid components mimicking those found in viruses, stimulating liposome-membrane interaction and improving endocytosis

efficiency (Torchilin, 2005). The disadvantages of liposomes, such as their potential instability and high chance of being removed by the immune system can be remediated by modification with poly-(ethylene glycol) (PEG) and targeting ligands, leading to an improved circulation profile and targeting, resulting in higher accumulation at the desired site (Milla et al., 2012). These properties make liposomes a promising drug delivery agent, with a number of clinical trials currently taking place (Chang and Yeh, 2012; Lamichhane et al., 2018).

Like liposomes, extracellular vesicles, including exosomes, are another potential lipid-based membranous cargo carrier, which have received a lot of attention in the past decade (Vader et al., 2016; Yim et al., 2016). In contrast to liposomes, extracellular vesicles are derived directly from cells and the composition of their membrane closely resembles the original plasma membrane. However, their preparation techniques can be challenging and laborious. In addition, extra steps are required for encapsulation of the desired payload into exosomes. Extracellular vesicles are described in more detail in Chapter 4.

1.3.2.3 Peptide based drug delivery agents

Another potential solution to overcome the problem of endosomal entrapment is the use of cell penetrating peptides (CPPs) for *in vitro* and *in vivo* delivery for intracellular cargo delivery. Cell penetrating peptides are a group of short (less than 30 amino acids), arginine and lysine rich peptides, which can penetrate the plasma membrane and hold a potential of being used for delivery of various macromolecular payloads into the cell interior (Torchilin, 2008; Bolhassani, 2011; Copolovici et al., 2014; Ruoslahti, 2017; Guidotti et al., 2017).The precise mechanisms of membrane translocation remains unknown, with both endocytosis and non-endocytosis dependant penetration reported, dependant on the cell line, payload type and peptide concentration used (Jiao et al., 2009).

CPPs are biodegradable and biocompatible, showing moderate levels of cytotoxicity. The most studied CPP is TAT, derived from HIV-1. It has been used to study intracellular delivery of various payloads, including small molecules,

nucleic acids, peptides and proteins (Brooks et al., 2005; Rizzuti et al., 2015). CPPs can be simply mixed with macromolecular cargo to enable cytosolic delivery (Heitz et al., 2009; Lee et al., 2010; Erazo-Oliveras et al., 2014). Herce and Garcia (2007) proposed that the mechanisms responsible for membrane translocation of TAT peptides depends on their interactions with phosphate groups on both sides of the lipid bilayer, leading to insertion of the charged peptide residues and formation of transient pores in the plasma membrane CPPs, however, offer a relatively low delivery efficiency via endosomal escape and have poor scalability due to high production cost.

1.3.2.4 Synthetic polymers as drug delivery agents

One of the most promising group of non-viral drug delivery agents are synthetic polymers. Use of polymers as agents facilitating delivery of macromolecules offers many advantages over using therapeutic substances alone, such as an improvement in drug stability, solubility and biocompatibility (Eccleston et al., 2005; Schmaljohann, 2006; Jaimes-Aguirre et al., 2016).

One approach to drug delivery is usage of stimuli-responsive polymers, which are able to undergo some form of a change as a reaction to a change in the environment, such as temperature, pH, light, ionic strength or mechanical stress. The response can vary from change in shape or conformation, degradation, dissolution or precipitation and drug release (Schmaljohann, 2006; Cheng et al., 2014). As described before, the human body possesses a wide range of pH environments, which can be taken advantage of while designing drug carriers. The following review focuses on pH-responsive polymers, which can be divided into cationic and anionic. Both utilise environmental pH as the trigger, which is the measure of the hydrogen ion concentration in the given solution and can be calculated using the following equation:

$$\mathrm{pH} = -\log_{10}[\mathrm{H}+]$$

Where [H+] is the total molar hydrogen ion (proton) concentration and depends on the concentration and identity of the compounds in solution.

A helpful characteristic used to describe ionisable compounds, such as pH-responsive polymer, is pK_a, or the negative log of the acid dissociation constant as calculated using the following equation:

$$pK_a = -\log_{10} K_a$$

The relationship between pH and pK_a is described by the Henderson–Hasselbalch equation:

$$pH = pK_a + \log_{10}\left(\frac{[A-]}{[HA]}\right)$$

Where [A-] is the molar concentration of ions dissociated with protons, and [HA] is the molar concentration of ions associated with protons. The equation illustrates that when pH = pK_a exactly half of the ionisable groups in the solution are protonated and half are in the non-associated state.

1.3.2.5 Cationic synthetic polymers

Positively charged cationic polymers (polycations) are capable of forming complexes with negatively charged nucleic acids, making them a good candidate for gene transfection, and have therefore been investigated as potential intracellular drug delivery agents (Kim et al., 2009b).

The membrane-lytic properties of synthetic cationic polymers are activated at low pH and depend on the presence of ionisable amine groups in the polymer structure. Polycations are thought to mediate disruption of the endosomal membrane via the so-called “proton-sponge” effect (Erbacher et al., 2004; Pack et al., 2005; Lale et al., 2015). This mechanism relies on the polymer acting as a buffer (or a sponge) whereby its unprotonated amines bind protons which are pumped into the endosome via ATPase proton pumps during the process of endosome maturation (Figure 1-3). This results in a further increase of proton influx into the endosome, followed by an influx of negatively charged ions and water molecules, which aim to counteract the increasing positive charge (Boussif et al., 1995; Sonawane et al., 2003). The described phenomenon leads to an increase in osmotic pressure within, resulting in endosomal swelling and

bursting, with its content released into the cytosol (Behr, 1997; Kircheis et al., 2001; Miele et al., 2012)

Examples of cationic polymers include poly(ethyleneimine) (PEI), poly(L-lysine) (PLL), poly(L-histidine) and poly(2-(dimethylamino)ethyl methacrylate) (PDMAEMA) (Schmaljohann, 2006; Hoffman, 2013). The most commonly used of those is PEI, which has been shown to condense and form homogenous, spherical particles with DNA (Ogris et al., 1999; Hou et al., 2011). This is followed by plasma membrane binding, endosomal uptake and escape resulting in gene expression (Godbey et al., 1999b; Taranejoo et al., 2015). PEI-mediated transfection has been demonstrated to be a versatile gene delivery platform and become a “gold standard” for polymer-mediated nucleic acid delivery (Boussif et al., 1995; Morille et al., 2008). Another commonly used cationic delivery agent is PLL, which has peptide-based structure and is therefore biodegradable. However, in contrast to PEI, PLL cannot form blood-stable complexes with DNA and offers a weaker transfection efficiency (Merdan et al., 2002; Morille et al., 2008).

Despite their potential for gene delivery, cationic polymers suffer from a number of limitations, such as their cytotoxicity and immunogenicity (Fischer et al., 1999). The cytotoxicity of polycations can arise from their strong electrostatic attraction to the negatively charged lipid membrane, leading to cytotoxic polymer adsorption on cell surface. Indeed, some polycations have been proposed as antimicrobial agents thanks to their cytotoxic effect (Vaidyanathan et al., 2015; Kostritskii et al., 2016).

Furthermore, polycations show a high potential for non-specific interactions and binding to negatively charged proteins present in the serum, limiting polymer circulation and availability (Suh et al., 1994; Murthy et al., 2003; Alexander, 2006). Conjugation with PEG has been shown to increase the circulation time of polycations and reduce their cytotoxicity, but can also result in a lower transfection efficiency as the trade-off (Wang et al., 2012b). In addition, the efficiency of transfection achieved by cationic polymers is lower than viral vector-mediated gene transfer (Zhang et al., 2007).

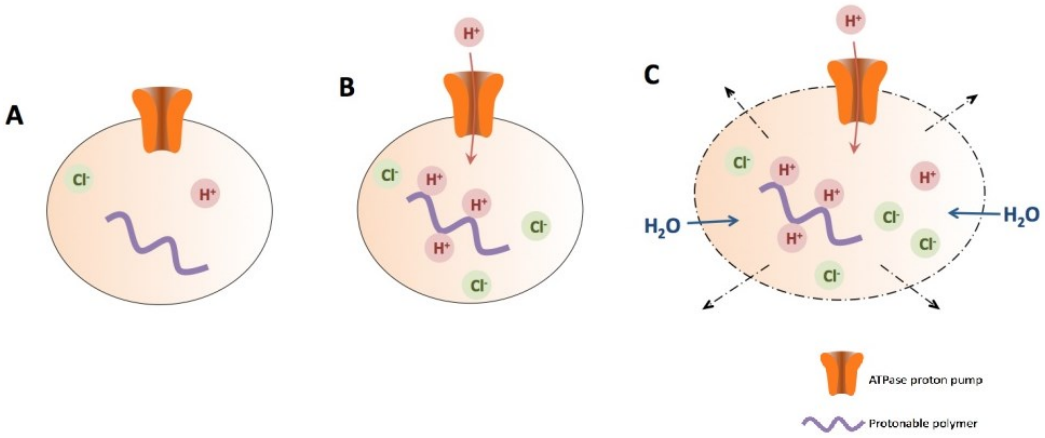


Figure 1-3. The "proton sponge" effect. (A) Entrapment of cationic polymers in endosomes. (B) Polymers become protonated during endosome maturation and resist further acidification of endosomes. More protons are pumped to lower the pH. (C) Passive influx of chloride ions increases ionic concentration and encourages water influx. High ionic pressure causes endosome swelling and rupture. Modified from (Wanling and Jenny, 2012).

1.3.2.6 Anionic synthetic polymers

Membrane disruptive anionic polymers are an alternative to cationic polymers and offer lower cytotoxicity and higher stability during circulation with reduced renal clearance, most likely due to a lower level of unwanted interactions with positively-charged serum proteins and off-site membrane interactions (Yessine and Leroux, 2004). Anionic polymers are often designed to contain ionisable carboxyl groups, which enables the sensing of environmental pH and pH-induced functionalities in combination with hydrophobic side-chine moieties to promote membrane anchorage and permeabilisation via hydrophobic-hydrophilic interactions (Hoffman, 2013; Fleige et al., 2012).

Synthetic anionic polymers have been specially designed to mimic naturally occurring pH-responsive viral fusogenic proteins in order to employ a similar strategy for cytosol entry as the one used by viruses (Chen et al., 2009a; Soliman et al., 2012). The mechanisms responsible for propagation of viruses such as influenza, adenovirus and picornaviruses relies on receptor mediated endocytosis of viral particles. In the case of influenza virus, protonation of the

amphipathic HA2 subunit of haemagglutinin (HA) peptide during endosomal acidification leads to its activation by conformational change to a membrane-active α-helix. Activated fusogenic peptide then insert into the endosome membrane causing endosome disruption and release of the endocytosed viruses into the cytosol, allowing insertion of virus nucleic acid into the cell genome and further virus replication (Plank et al., 1998; Cheng et al., 2016).

In a manner similar to viral fusogenic proteins, anionic polymers are capable of undergoing conformation changes and gaining the ability to interact with endosomal membranes, causing release of endocytosed materials (Chen et al., 2009a). Anionic polymers are amphiphilic due to presence of both hydrophobic alkyl groups and weak, ionisable polyacids. The pH inside the endosome dictates the behaviour of anionic polymers. At physiological pH, anionic polymers remain hydrophilic. Increasing acidification of maturing endosomes leads to ionisation of weakly charged polyacids (such as carboxyl groups) increasing the hydrophobicity of the polymer backbone (Yessine and Leroux, 2004). Such alteration of the hydrophobic/hydrophilic balance, caused by interacting electrostatic forces between carboxyl groups, leads to a coil-to-globule conformation change - extended polymer coils (hydrophilic) collapse into compact globular structures, which are maintained by hydrophobic forces (other forces such as Van der Waals forces and hydrogen bonds might also play a role) (Chen et al., 2009a). As a result of hydrophobic interactions, the condensed polymer destabilises the endosome membrane, causing its disruption and allowing payload delivery into the cytosol (Plank et al., 1994; Murthy et al., 2003; Blanco et al., 2015). Increasing acidification (e.g. to the values occurring inside lysosomes) leads to an increase in polymer hydrophobicity and polymer precipitation, rendering it inactive. Thus, the most effective membrane disruption behaviour is obtained in the pH range between the start of coil-to-globule transition and polymer precipitation (specific values depend on polymer used) (Chen et al., 2005; Chen et al., 2009a).

Due to this advantageous property, a number of pH-responsive polyanions have been developed as potential delivery agents of therapeutic substances. They include non-biodegradable polymers based on vinyls as well as biodegradable poly(amino acids) and pseudo peptides, such as poly(L-lysine isophthalamide)

(PLP) and its derivative, PP75 (Eccleston et al., 1999; Al-Muallem et al., 2002; Chen et al., 2009a).

1.3.2.7 Non-biodegradable anionic polymers

Vinyl polymers, such as poly(α-methylacrylic acid) (PMAA) and poly(α-ethylacrylic acid) (PEAA), have been investigated as potential drug delivery agents and were reported to disrupt biological membranes at acidic pH (Seki and Tirrell, 1984; Thomas et al., 1996). Further investigation of this family of polymers inspired the synthesis of poly(propylacrylic acid) (PPAA) and poly(butylacrylic acid) (PBAA) with longer hydrophobic α-alkyl side-groups (Murthy et al., 1999; Murthy et al., 2001)

The modification of PEAA to PPAA relied on the addition of just one methyelne group onto the side chains of the polymer and resulted in a 15-fold increased membrane disruptive ability, with the optimal pH value equal to 6.3 (compared to pH 5.0 for PEAA) (Murthy et al., 1999). Further increase in the number of methylene groups on the side chains was used to produce PBAA and resulted in a highly membrane active polymer, causing 100% haemolysis of red blood cells at pH 7.4 (Murthy, Robichaud, Tirrell, et al., 1999). Thus, the ratio of carboxylic to hydrophobic groups is of critical importance and a key factor controlling the pH-induced conformational change of anionic polymers and their membrane destablisiation capabilities and can be exploited to design polymers with specific properties (El-Sayed et al., 2005)

PPAA was used for intracellular protein and antibody delivery by conjugation and via the simple mixing strategy (Lackey et al., 2002; El-Sayed et al., 2005). The polymer was also investigated for gene delivery applications and was shown to enhance transfection of plasmid DNA into NIH-3T3 fibroblasts as well as in TPS2-null knockout mice when administered in a mixture with the cationic lipid N-[1-(2,3-Dioleoyloxy)propyl]-N,N,N-trimethylammonium methyl-sulfate (DOTAP) (Cheung, Murthy, Stayton, et al., 2001).

However, poly(vinyl)-based polymers suffer from limitations arising from the inability to degrade their carbon-carbon backbones in biological settings. The use of this family of polymers is therefore limited by their size as they need to

remain below the renal exclusion threshold to ensure systemic clearance and to prevent harmful accumulation (Duncan, 2006).

1.3.2.8 Biodegradable anionic polymers - PLP and PP-family

In order to solve the problems associated with potential systemic accumulation, novel polymers can be designed containing hydrolytically or enzymatically degradable linkers in their backbone, such as amides, anhydrides or esters (Eccleston *et al.* 1999). One group of such polymers are the biodegradable, anionic poly(amino acids)s, such as poly(aspartic acid) (PAA), poly(glutamic acid) (PGA) and their derivatives (Mallakpour and Dinari, 2011). These biocompatible polymers have been shown to be capable of efficient gene delivery using receptor-mediated energy-dependent transport processes with low toxicity, as well as protein delivery for vaccination applications (Kurosaki et al., 2009; Kurosaki et al., 2012).

Another group of biodegradable anionic polymers is composed of poly(L-lysine isophthalamide) (PLP) and its derivatives. PLP is an anionic, pH-responsive polymer which was developed by the group of Eccleston et al. (1999). PLP is synthesised by using L-lysine methyl ester dihydrochloride and isophthaloyl chloride in a polycondensation reaction to obtain a metabolically derived, biodegradable and non-cytotoxic polymer possessing a hydrophobic backbone and pendant carboxyl groups (Eccleston et al., 2005).

Eccleston et al. (2000) demonstrated that the membrane lytic ability of PLP is most efficient in the pH range of 4.6-5.0, characteristic of lysosomes. The polymer also exhibited relatively low levels of overall membrane disruption (~15% haemolysis) (Chen et al., 2005; Chen et al., 2008). The above properties limit the clinical usefulness of PLP as a drug delivery agent, as ideally the polymer would cause much higher levels of membrane lysis at pH corresponding to early endosomal environments (pH range of 6.0-6.8), in order to avoid lysosomal degradation of the desired payloads.

The described limitations of PLP were overcome by (Chen et al., 2009b) who grafted hydrophobic amino acids (including L-valine, L-leucine and L-phenylalanine) on the pendant carboxyl groups of PLP via amide bonds. This

was done in order to enhance polymer amphiphilicity and to make it more representative of viral peptides, which possess pendant hydrophobic alkyl groups. This reaction successfully increased the threshold pH value for initiation of conformational change of the polymer, thus demonstrating that it is possible to fine-tune the properties and pH-responsiveness of the PLP-derived polymers towards desired effects (Chen et al., 2009c).

Specifically, it was discovered that grafting poly(L-lysine isophthalamide) with L-phenylalanine (PP polymers) greatly increased membrane disrupting ability. PP75 (M_w 49kDa, M_n 24.9 kDa, polydispersity 1.99), which was obtained by grafting with L-phenylalanine at a stoichiometric ratio of 75% relative to the pendant carboxylic acid groups on the PLP backbone (Figure 1-4) (actual degree of grafting = 63%, as confirmed by ^{1}H-NMR), showed 35 times the lytic activity of melittin, which is a highly membrane disruptive bee-sting peptide, used for comparison (Chen et al., 2009c; Zhang et al., 2011). This suggested that high membrane destabilising capacity of the polymer resulted from hydrophobic modification of the side chain due to the presence of the aromatic ring in each L-phenylalanine, making PP75 a functional and potent mimic of membrane disruptive, phenylalanine rich viral fusogenic peptides (Chen et al., 2009c).

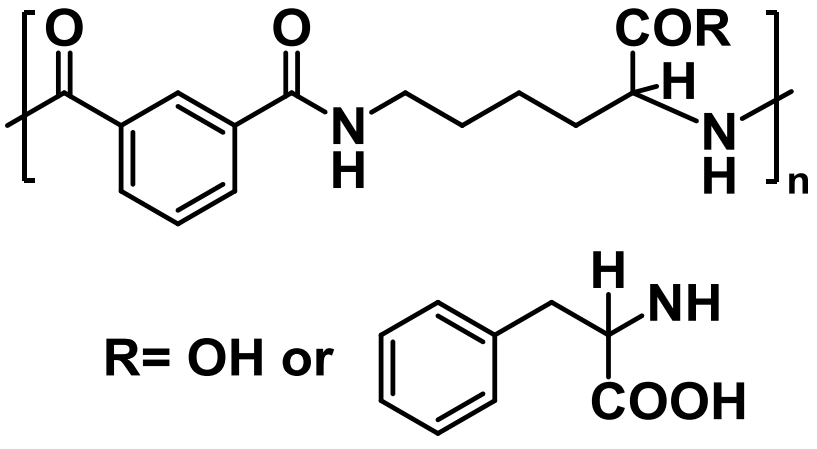


Figure 1-4. Poly(L-lysine isophthalamide) grafted with L-phenylalanine (PP polymers), where a certain percentage of OH at position R is replaced with L-phenylalanine.

The optimum level of haemolysis of sheep red blood cells (RBCs), equal to 90%, was recorded at pH 6.0-7.0 after 1h incubation with PP75 at a low concentration of 0.025 mg mL^{-1} (0.5 μM). No functional lytic activity was recorded at physiological pH of 7.4. This observed pH-dependant lytic profile of PP75 is therefore a desirable enhancement of the behaviour of the parental polymer, PLP. The activation and conformational change of PP75 occurs at the pH range characteristic to early endosomes, with highest level of membrane disruption level occurring well before lysosomal fusion, enabling payload release into the cytosol while avoiding its degradation. Furthermore, the recorded high level of haemolysis proves that the negative charge associated with PP75 is not an obstacle for successful disruption of negatively charged biological membranes, suggesting that the hydrophobic forces outweigh electrostatic repulsion between the two components (Chen et al., 2009a; Chen et al., 2009c). In addition, the negative charge of the polymer might prevent aggregation *in vivo*, which is normally caused by binding with negatively charged serum proteins and leads to carrier inactivation (Whitehead et al., 2009).

The novel pseudopeptidic polymer PP75 was demonstrated to have promising potential for drug delivery applications. PP75 has been used for delivery of small and large payloads to a variety of cells (Chen et al., 2009c; Liechty et al., 2009). In addition, PP75 enabled delivery of small molecule model drug to cells in 3D multicellular spheroids by efficient spheroid penetration and endosomal disruption (Ho et al., 2011). PP75 was also demonstrated to be capable of stathmin siRNA delivery by conjugation using a cleavable disulphide linker, which resulted in silencing of stathmin expression and, combined with carmustine, inhibited tumour growth following intra-tumoral injection (Khormaee et al., 2013).

Another PLP derivative which might be of potential interest as a drug delivery agent is PP50. PP50 is obtained by grafting PLP with L-phenylalanine at a stoichiometric ratio of 50% relative to the pendant carboxylic acid groups. PP50 was successfully used to permeabilise the membrane of ovine erythrocytes as well as osteosarcoma cells and mediate non-toxic delivery of the small molecule cryoprotectant trehalolse to the cell interior, resulting in increased cryosurvival (Mercado and Slater, 2016b; Lynch et al., 2011).

1.4 Therapeutic payloads and methods of their delivery using anionic polymers

1.4.1 Different-sized payloads in modern drug therapies

The size and properties of therapeutic agents are of crucial importance when it comes to the process of their efficient delivery. Many traditional “small molecule” drug agents with molecular weights of <500 Da have good oral bioavailability and translocate through the plasma membrane using passive or facilitated diffusion. Small molecule drugs are well defined, stable and easy to manufacture and characterise. On the other hand, due to their small size, conventional drugs have low target selectivity which can lead to off-site targeting and system-wide side effects (Craik et al., 2013). In addition, they are often substrates for efflux pumps present in the plasma membrane, which can decrease their efficiency and cause resistance to the treatment (Moitra et al., 2011). For this reason, the attention in the pharmaceutical industry is shifting towards alternative novel therapy options (Agyei et al., 2017; de la Torre and Albericio, 2018). Nevertheless, improvement of specificity of small molecule drugs used in chemotherapy, such as Doxorubicin and Paclitaxel, leading to lower off-target interaction, remains an interesting area of research.

Macromolecules such as peptides, proteins and nucleic acid are a novel group of biologically-derived therapeutic agents capable of targeting intracellular targets and modulating intracellular protein-protein interactions and thus viable for treatment of a wide range of cancers and other diseases (Elvin et al., 2013; Guillard et al., 2015). The so-called “biologics” have a wide range of size and molecular weight, typically above 3-5 kDa (peptides), and up to 150 kDa (IgG antibodies). Biologics are complex, difficult to characterise and, with exclusion of peptides which can be synthesised chemically, need to be produced using living cells, which makes the manufacturing process challenging and expensive. However, the high specificity and efficiency of biologics makes them a highly researched area, with a number of macromolecular drugs targeting extracellular sites already available on the market (Agyei et al., 2017).

In contrast to small molecules, the large size and polarity of most novel biotherapeutics prevents them from entering the cell via passive diffusion (Christie and Grainger, 2003). In addition, biologics can be unstable, immunogenic and sensitive to external conditions. This has prevented the usage of macromolecules as drugs targeting intracellular pathways; however, researchers are now trying to extend the application of therapeutic proteins to intracellular sites (Guillard et al., 2015). The described issues could potentially be remediated by usage of drug delivery agents, such as the anionic PP-polymers.

1.4.2 Cargo delivery methods using PP polymers

The PP-family polymers are trigger-responsive, bio-inspired and biodegradable group of polymers which have been shown to possess a promising drug delivery potential (Chen et al., 2009c). PP polymers offer low cellular toxicity and reduce the risk of unwanted interactions with negatively charged serum proteins due to their anionic nature. Furthermore, PP polymers can be easily chemically modified or used to create conjugate constructs with desired payloads. For those reasons, this group of polymers were chosen as the subject of the studies presented in this thesis. In particular, PP50, which was shown to offer superior degree of membrane permeabilisation and payload loading to human erythrocytes, compared to other PP polymers (Liechty et al., 2009) and can be reproducibly synthesised with low batch-to-batch variability in terms of the precise stoichiometric ratio of L-phenylalanine grafting.

Two possible methods of payload delivery using PP polymers include:

- Simply mixing the two components - The efficiency of PP50- and PP75-mediated payload delivery into mammalian cells has already been demonstrated. The polymer was used to deliver Apoptin, a potent protein capable of inducing apoptosis, into human osteogenic sarcoma Saos-2 cells (Liechty et al., 2009). PP75 was found to facilitate both efficient cellular uptake and endosomal escape of calcein (Chen et al., 2009a). Furthermore, Lynch et al (2010) used PP50 to successfully permeabilise the plasma membrane of sheep erythrocytes, facilitating intracellular delivery of trehalose, which is a

bioprotectant dissacahride, mixed with the polymer. This allowed for an improved cryosurvival of erythrocytes, which was ca. 20% better compared to erythrocytes not loaded with trehalose. Simple mixing of the payload with the delivery agent, such as PP polymers, is suited predominantly for *in vitro* and *ex vivo* applications as *in vivo* delivery using this strategy would be difficult due to the separation of the two components in the bloodstream and off-site targeting. Potential payloads can include both therapeutic cargos and molecules with other biological functions such as molecular probes, enzymes and transcription factors.

- Conjugation of payloads to PP polymers - Conjugation of payloads to water soluble polymers by a cleavable linker was first proposed by Ringsdorf (1975). Cargo conjugation to polymers is possible due to the adaptable nature of polymer chemistry, allowing covalent binding of various groups (including crosslinkers) onto pendant groups present on the polymer backbone. One disadvantage of this approach is possible alteration of the original polymer properties following cargo attachment (such as hydrophobic/hydrophilic balance), which could affect membrane disruption ability as well as pharmacokinetics and dynamics (Kopeček et al., 2000). Functionality of newly obtained polymer-drug conjugates would need to be studied in each case.

  Conjugation of therapeutic biologics to polymeric carriers could result in their enhanced solubility and extended circulation time. In addition, addition of targeting ligands onto the polymer could increase specific targeting of diseased cells and tissues (Haag and Kratz, 2006).

1.5 Polymer delivery agents with cleavable crosslinkers

A suitable crosslinker between a polymeric delivery agent and payload should ensure the stability of the construct during application and circulation in the bloodstream, while also enabling payload release after successful uptake into the cytosol (Wang et al., 2012a). Many types of cleavable linkages have been developed, including those sensitive to pH, light, enzymatic hydrolysis and

reducing environment (Haag and Kratz, 2006; Ramachandran and Urban, 2011).

Reduction sensitive crosslinkers containing a disulphide bond are a promising option for drug delivery. Disulphide bonds are formed between 2 thiol (SH) groups and are present in some proteins where they maintain the 3D structure. Disulphide bonds are susceptible to reversible cleavage after being exposed to reducing agents, such as dithiothreitol (DTT) or naturally occurring glutathione (GSH) (Leriche et al., 2012). Due to the large difference in intracellular and plasma concentration of GSH, constructs containing disulphide bonds can be cleaved after entering the highly reducing cytosol environment (Saito et al., 2003). Since tumour cells can exhibit GSH concentrations at least 4 times higher than cells in healthy tissues, reduction-sensitive crosslinkers are a promising option for controlled intracellular drug release (Kuppusamy et al., 2002).

1.5.1 PP-polymers and PDPH crosslinker

3-[2-Pyridyldithio]propionyl hydrazide (PDPH) (Figure 1-5) is a commercially available, bifunctional crosslinker with molecular weight equal to 229.32 g mol^{-1}. It contains a carboxyl-reactive amine group as well as a thiol-reactive pyridyldithiol group, which can react with free thiols present in many biological payloads to form disulphide bonds. PDPH has previously been successfully used in a number of thiol exchange-based conjugation reactions (Pain and Surolia, 1981; Greenfield et al., 1990; Friden et al., 1993). The reaction of thiol exchange results in release of the protective 2-mercaptopyridine, which can be easily detected using UV-Vis Spectrophotometry to analyse reaction efficiency. Furthermore, the amine group of the crosslinker can be used in a DCC/DMAP coupling reaction to bond with carboxyl groups present on PP polymers via amide bonds. For these reasons, PDPH is a promising candidate for the crosslinker of choice in the process of developing PP polymer-payload conjugates.

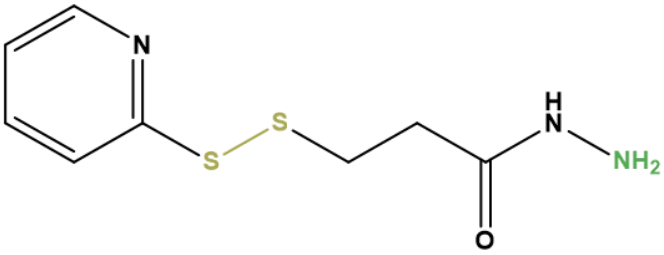


Figure 1-5. Molecular structure of PDPH. The disulphide bond is highlighted in yellow. The amine group available for formation of amide bonds with pendant carboxyl groups present on polymer backbone is highlighted in green.

1.6 Aims of the project

The aim of this project is to expand the understanding and potential scope of polymer-mediated intracellular delivery of macromolecules using the pH responsive, membrane permeabilising polymer PP50. The ultimate goal of this work would be to develop a new platform technology based on PP50 with a wide range of applications, both *in vitro* and *in vivo*. The main objectives of the work presented herein include the following areas:

1) **Systematic study and analysis of the mechanism and crucial parameters influencing cargo delivery into the cell interior by co-incubation with the pseudopeptidic polymer PP50 and optimisation of the delivery process**

   The work presented in this thesis aims to expand the potential scope of PP50-mediated cargo delivery, specifically to include various types of macromolecules for cell engineering and therapeutic applications. To achieve a better understanding of the delivery process and the intracellular fate of the polymer, the interaction between the polymer and ovine erythrocytes as well as HeLa cells will be studied. In addition, delivery of large fluorescent model payloads will be attempted and analysed and a number of different parameters important for delivery efficiency, such as the concentrations of the components and delivery time will be explored and optimised. Payload delivery by PP50 at physiological and mildly acidic, tumour-like pH will be compared.

2) **Extensive exploration of the potential applications of PP50-mediated cargo delivery *in vitro***

   Limited payload or cell type compatibility, low delivery efficiency due to endosomal entrapment and high toxicity remain problematic issues for many *in vitro* and *ex vivo* delivery agents. This work will further explore the capabilities and limitations of intracellular macromolecule delivery by co-incubation with PP50. Model payloads with a wide size range will be used along with 9 different cell lines in order to investigate the versatility

of this delivery technique. Payload delivery to cells grown as 3D spheroids will also be analysed. Cytotoxicity of the delivery process *in vitro* will be quantified in various cell types. Finally, delivery of a potential macromolecular drug – an apoptotic peptide – using PP50 will be compared to delivery using other commonly used delivery methods, including chemical and physical approaches.

3) **Development of novel polymer-payload conjugates and exploration of their delivery potential *in vitro***

Conjugation approaches can increase payload stability and circulation time as well to decrease any potential cytotoxicity to off-target tissues. This project aims to develop novel conjugates of PP50 with different-sized macromolecules, including peptide- and protein-sized model payloads. Key parameters affecting the efficiency of the conjugation reaction will be studied, along with the membrane permeabilisation potential and intracellular delivery of the newly synthesised constructs.

4) **Development of novel polymer-macromolecular drug conjugates and utilisation of tumour-like pH to enhance payload delivery**

Conjugates of the polymer with a functional peptidic apoptotic payload will be developed and analysed for their potency and safety *in vitro*, followed by an *in vivo* study using the mouse model which will include assessment of tolerability and biodistribution. The potential to utilise mildly acidic, tumour-like extracellular pH to enhance the delivery efficiency of such conjugates will be analysed and verified.

Chapter 2 - Materials and Methods

2.1 Materials

3-[2-Pyridyldithio]propionyl hydrazide (PDPH), dimethyl sulfoxide (DMSO), N,N-dimethylformamide (DMF), dimethylaminopyridine (DMAP), sodium bicarbonate ($NaHCO_3$), sodium chloride (NaCl), Hoechst 33342, AlamarBlue, TexasRed® hydrazide, potassium chloride (KCl), LysoTracker® red DND-99, disodium phosphate (Na_2HPO_4), N-succinimidyl S-acetylthioacetate (SATA), ACK Red Blood Cell Lysing Buffer, monopotassium phosphate (KH_2PO_4), Rhodamine110 chloride, Accutase, polyethyleneimine (PEI) 0.6 kDa, branched and 25 kDa linear, 5,5'-dithio-bis-[2-nitrobenzoic acid] (DTNB, Ellman's reagent), Nunc® MaxiSorp™ black 96-well plates were purchased from Fisher Scientific (Loughborough, UK).

Fluorescein isothiocyanate–dextran (FITC-dextran, average Mw 10, 70, 150, 500 and 2000 kDa), Dulbecco's modified Eagle's medium (DMEM), MEM non-essential amino acid solution (100x), foetal bovine serum (FBS), penicillin, phosphate buffer saline (D-PBS), Melittin (GIGAVLKVLTTGLPALISWIKRKRQQ) (cat. no. M2272-5MG), Tat (YGRKKRRQRRR) (cat. no. H0292-1MG), BioPORTER® (cat. no. BPQ24-1KT), penicillin, alpha-moddified MEM, glutathione, cysteine, 2-mercaptopyridine, dithiothreitol (DTT*),* Ficoll, Amicon Ultra 0.5 mL centrifugal filters, hydroxylamine, bovine serum albumin (BSA), lipopolysaccharides (cat. no. L2630-10MG) and TWEEN®20 were purchased from Sigma-Aldrich (Gillingham, UK).

Diethyl ether, hydrochloric acid, potassium carbonate, sodium hydroxide, triethylamine, sodium citrate dihydrate, sodium phosphate were purchased from VWR (Lutterworth, UK).

Glass-bottom cell culture dishes (35 mm) (cat. no. P35G-1.5-14-C) were purchased from MatTek, (Ashland, MA, USA).

L-phenylalanine methyl ester hydrochloride, L-lysine methyl ester dihydrochloride, *N*,*N'*-dicyclohexylcarbodiimide (DCC), triton® X-100 were purchased from Alfa Aesar (Heysham, UK).

Defibrinated sheep blood (cat. no. SB054) was ordered form TCS Biosciences (Buckingham, UK).

FITC-PEG-thiol (3.4 kDa) (cat. no. PG2-FCTH-3k) was purchased from Nanocs, Inc. (New York, USA).

Anti-non-muscle Myosin IIA antibody (Alexa Fluor® 647) (cat. no. ab204676) and Goat Anti-Human IgG (biotin) (cat. no. ab97223) were purchased from abcam (Cambridge, UK).

BD CellFIX (cat. no. 340181) was purchased from BD Biosciences UK (Wokingham, Berkshire, UK).

ABT-737 (cat. no. S1002-SEL) was purchased from Stratech Scientific (Ely, UK)

Human leukocyte cones were obtained from Addenbrookes Hospital, Cambridge, UK, in full compliance with regulations of Human Tissue Act 2004.

IncuCyte® Caspase-3/7 Green Apoptosis Assay was purchased from Essen BioScience (Welwyn Garden City, UK).

Cyanine5 amide (cat. no. 130C0) was purchased from Lumiprobe (Hannover, Germany)

Anhydrous ethanol, acetone, hydrochloric acid, sodium hydroxide and PULSin® (cat. no. 501-01) were obtained from VWR (Lutterworth, UK).

Caspase-Glo® 3/7 Assay and CellTiter-Glo® 2.0 Assay were purchased from Promega (Southampton, UK).

Penetratin (RQIKIWFQNRRMKWKKGG) (cat. no. AS-64885) was purchased from Tebu-Bio (Peterborough, UK).

Electroporation kit Cell Line Nucleofector® Kit T (cat. no. VCA-1002) was purchased from Lonza (Slough, UK).

dsRed plasmid (4200 bp) was kindly donated by Dr Spencer Crowder (Department of Materials, Imperial College London).

Sulfocyanine7 (Cy7)-labelled Bim and scrBim peptides with the sequences shown below were synthesised and purchased from Cambridge Research Biochemicals (Billingham, UK).

Bim(Cy7):[Sulfocyanine7]-RPEI-W-IAQELRRIGDEFNAYYAR-Ahx-Cys-amide

scrBim(Cy7):[Sulfocyanine7]-DLERRGIANFEQAI-W-RAYYIEPR-Ahx-Cys-amide.

2.2 PLP Synthesis

PP50 is derived from poly(L-lysine isophthalamide) (PLP). Both polymers were synthesised in-house at Imperial College London.

Polycondensation

PLP is synthesised in a single-phase polymerisation reaction as described by Eccleston (Eccleston et al., 1999; Eccleston et al., 2000). Briefly, L-lysine methyl ester·2 HCl (0.15 mol) and potassium carbonate (0.60 mol, 4 times molar excess over L-lysine) were dissolved in 750 mL dH_2O and stirred in an ice bath. Anhydrous iso-phthaloyl chloride (0.2 M) dissolved in dried acetone (750 mL) pre-cooled overnight at -20^oC was rapidly poured into the aqueous reaction mixture and stirred rapidly. The reaction was allowed to proceed until visible observation of the precipitation of poly(L-lysine methyl ester *iso*-phthalamide) (PLP methyl ester). The polymer was recovered from the solvent solution and thoroughly washed with dH_2O to remove the solvent, followed by being stretched and torn into smaller fragments and dried overnight in an oven at 70^oC. The drier polymer was subsequently blended into white powder using an electric blender.

Ester hydrolysis

Sodium hydroxide (2.5 molar equivalents to PLP methyl ester) was dissolved in anhydrous ethanol to a final concentration of 5 wt% and added in multiple portions to PLP methyl ester dissolved in dry DMSO (0.5M). The hydrolysed product, PLP, precipitated out within 10 minutes and was collected out by vacuum filtration and re-dissolved in dH_2O.

Purification

Several purification steps were necessary to ensure complete removal of residual organic solvents, salts and low molecular weight PLP oligomers.

First, 0.2M HCl was added dropwise to the PLP solution in deionized water (dH_2O) in order to precipitate the polymer. The precipitated polymer collected by vacuum filtration and dissolved again in deionized water with 0.2 M NaOH. The process of precipitation with HCL, filtration and re-dissolution was repeated at least 2 more times.

Following the last dissolution step, a dialysis step was performed. The crude PLP solution was placed in Visking tubing membrane (Medicell, MWCO 12-14 kDa), cut to appropriate size, and dialysed against dH_2O for up to one week. The water was changed frequently to provide a strong concentration gradient. Dialysed PLP solution was adjusted to pH 7.4 using NaOH (0.2 M), frozen and lyophilized to produce PLP in the salt sodium form (fluffy, white powder). In order to prepare the solvent-soluble, neutral PLP (acidic form) used in the side chain modification reactions, a solution of the sodium salt form PLP was acidified to pH 3.0 with concentrated HCl (added dropwise), and the precipitating polymer was collected by vacuum filtration and washed with dH_2O, frozen and lyophilized again to produce a fine, white powder.

2.3 PP50 Synthesis: grafting of PLP with L-phenylalanine

PP50 was synthesised as outlined by Chen et al. (2009a) by grafting of PLP with L-phenylalanine via DCC/DMAP coupling. In the case of PP50, the stochiometric ratio of L-phenylalanine to the carboxylic acid groups on the PLP backbone is 50%.

Acid form of PLP (3.0 g, 11 mmol), L-phenylalanine methyl ester hydrochloride (1.17g, 5.3 mmol), triethylamine (2.4 molar equivalents to L-phenylalanine) and DMAP (0.6g) were dissolved in a mixture of anhydrous DMSO and DMF (1:3 v/v, 60mL) and stirred. DCC (2-3 molar equivalents to L-phenylalanine) was dissolved in 20 mL anhydrous DMF and added drop-wise to the reaction mixture

while stirring at room temperature. The reaction was allowed to proceed with continuous, rapid stirring at room temperature for ca. 60h.

Solid impurities and the dicyclohexylurea (DCU) side product were removed by vacuum filtration after 60 h. Sodium hydroxide (5 wt%, 28 mL) was dissolved in anhydrous ethanol and added to the polymer solution and stirred at room temperature to allow hydrolysis. Five volumes of diethyl ether were added to the hydrolysed polymer solution which resulted in polymer precipitation. The precipitant was collected by vacuum filtration and re-dissolved in dH_2O. Dialysis was performed to purify the solution, as described before. PP50 sodium salt and acidic forms were obtained following pH adjustment and lyophilisation, as described before.

2.4 Labelling of PP50 with fluorescent dyes – Rhodamine110 and Cy5

Fluorescently-labelled PP50 was prepared by grafting Rhodamine110 chloride or Cyanine5 (Cy5) amine to the pendant carboxylic acid groups on PP50 via DCC/DMAP coupling. Fluorescent dye (3% mol stoichiometric ratio to PP50's [COOH]), PP50 (100 mg; 0.28 mmol [COOH]) and DMAP (20 mg, 20% wt of PP50) were dissolved in anhydrous DMF (400 µL) in a flat bottom, disposable glass tube (5 mL). DCC (3 molar equivalents to Rhodamine110 or Cy5) in anhydrous DMF (40 µL) was added to the polymer solution while stirring at room temperature. The tube was tightly sealed with parafilm and the reaction was left to proceed at room temperature for 24 h, using magnetic stirring to facilitate mixing. Centrifugation at 9,500 g was used to spin down DCU. The supernatant was collected using a pipette and subsequently rapidly poured into 5 volumes of diethyl ether, where precipitation of fluorescently-labelled PP50 occurred. The precipitate was collected using vacuum filtration and re-dissolved in sodium bicarbonate (0.1 M). Dialysis was performed in order to remove remaining inorganic salts, solvents and ungrafted dye using 12-14 kDa MWCO Visking tube membrane (Medicell) against deionised water. The water was changed frequently to maintain the concentration gradient up until no obvious coloration of the dialysate was observed, suggesting thorough dye removal. The polymer

solution was then frozen and freeze dried to produce blue (Cy5) or yellowish (Rhodamine110) powder

2.5 Haemolysis

Sheep RBCs are used as a whole cell model in order to analyse the interaction between PP50 and their plasma membrane, which can inform about interactions between the polymer and the endosomal and plasma membrane of nucleated cells (Chen et al., 2009c).

100 mM citrate buffers were prepared in the pH range of 4.5-5.0 and 100 mM phosphate buffer in the pH range of 5.5-7.4. They were isosmotic to the intracellular environment of RBCs to ensure negligible levels of membrane disruption. The studied substances (PP50, PP50-PDPH, polymer-payload conjugates) were dissolved in the buffers at specific pH and concentration.

Defibrinated sheep RBCs were centrifuged for 4 min at 1,500 g, and the supernatant was replaced with an equivalent volume of 150 mM NaCl solution. The cells were then resuspended and the procedure was repeated until the supernatant was clear (3 times). The number of cells present in the sample was extrapolated from RBCs counting performed using an Inverso TC100 Inverted Biological Microscope (Medline Scientific, UK) and a haemocytometer. RBCs were then added to polymer buffer solutions so that each sample contained ca. 1.5×10^8 RBCs mL^{-1} (Chen et al., 2005; Chen et al., 2009c). The samples were subsequently incubated at 37^{o}C for 1 h using a shaking water bath and spun down at 1,500 g for 4 min. The supernatant from each sample was transferred to disposable plastic cuvettes, and the absorbance of released haemoglobin was analysed using the GENESYS 10S UV/Vis Spectrophotometer (Thermo Fisher Scientific, USA), at 540 nm. The negative control was prepared by addition of RBCs to buffer alone while the positive control by addition of RBCs to deionised water. The testing was performed in triplicates with number of samples for each data point equal to n = 3. The percentage of haemolysis was analysed using the following equation:

$$\text{Relative hemolysis (\%)} = \frac{\text{(Test sample absorbance) - (negative control absorbance)}}{\text{(Positive control absorbance)}} \times 100$$

2.6 Cell culture

All of the cell cultures were maintained in a humidified incubator at 37 ^{o}C with 5% CO_2.

HeLa (human cervical cancer), A549 (human lung carcinoma) and RAW 264.7 (murine macrophages) were grown in Dulbecco's modified Eagle's medium (DMEM) supplemented with 10% (v/v) FBS, 100 U mL^{-1} penicillin and 100 µg mL^{-1} streptomycin. CHO (Chinese hamster ovary) cells were cultured in DMEM supplemented with 1% non-essential amino acids, 10% (v/v) FBS, 100 U mL^{-1} penicillin and 100 µg mL^{-1} streptomycin.

SU-DHL-8 (human lymph node B lymphocytes) were grown in suspension in Roswell Park Memorial Institute (RPMI-1640) medium supplemented with 10% (v/v) FBS, 100 U mL^{-1} penicillin and 100 µg mL^{-1} streptomycin.

Human mesenchymal stem cells (hMSCs) and MC 3t3 (murine osteoblast precursor) cells were grown in alpha-modified MEM culture medium supplemented with 10% (v/v) hMSC-grade FBS, 100 U mL^{-1} penicillin and 100 µg mL^{-1} streptomycin. hMSCs were donated by Dr Spencer Crowder.

MES-SA (human uterus cells) and the Dox-resistant version of this cell line, MES-SA/Dx5 (The European Collection of Authenticated Cell Cultures) (Angelini et al., 2010), were grown in McCoy's 5A culture medium supplemented with 10% (v/v) FBS, 100 U mL^{-1} penicillin and 100 µg mL^{-1} streptomycin.

HeLa, A549, CHO and hMSC cells were detached using Trypsin-EDTA for passaging. MES-SA and MES-SA/Dx5 were detached using EDTA solution for passaging (0.8 mM disodium EDTA, 68.5 mM NaCl, 6.7 mM sodium bicarbonate, 5.6 mM glucose and 5.4 mM KCl). RAW 264.7 cells were detached by scraping using cell culture scrapers. SU-DHL-8 cells were passaged by aliquoting.

2.7 Laser scanning confocal microscopy

The laser scanning confocal microscopy data show representative images from at least 2 separate experiments.

Confocal microscopy of ovine erythrocytes and ghost cell formation

The formation of ghost cells (plasma membrane shells obtained following cell permeabilisation and haemoglobin leakage) and payload delivery to ovine erythrocytes following treatment with PP50 was analysed using laser scanning confocal microscopy. Ovine erythrocytes were prepared by washing 3 times with 150 mM NaCl by centrifugation and resuspended in pH-adjusted buffers containing a specified concentration of PP50 (or Rhodamine110-labelled PP50), FITC-Dextran and/or 1 μM TexasRed® hydrazide. Ca. 10^7 erythrocytes were used in each sample of 1 mL. The solutions were transferred to glass-bottom dishes (35 mm, MatTek, USA) and analysed using inverted LSM-510 microscope (Zeiss, Germany). The samples were kept at 37°C within the microscope's heating chamber. FITC (FITC-Dextran) and TexasRed were excited at 488 nm and 543 nm, respectively. The images were analysed using ImageJ 1.51n.

Time-dependant uptake of PP50-Cy5

The intracellular fate of PP50 labelled with Cy5 was investigated. Glass bottom MatTek dishes containing live HeLa cells seeded at 1 x 10^5 cells per dish 24 h prior the analysis were placed on the inverted Zeiss LSM-510 microscope (heated chamber, 37°C). DMEM was replaced with a PP50-Cy5 solution at 0.5 mg mL^{-1} (1 mL). Images were then captured every 10 minutes, starting at t = 5 minutes post-addition, by exciting Cy5 at 633nm. The images were analysed using ImageJ 1.51n.

Intracellular delivery of various fluorescent payloads

Delivery of many different fluorescent materials was tested to assess the versatility of the PP50 delivery platform. Those included fluorescent dextrans (FITC-Dextran) of various size (10 – 2,000 kDa), green fluorescent protein (GFP), FITC-PEG (3.4 kDa) and FITC-IgG (150 kDa). The general protocol for

analysis of payload delivery by laser scanning confocal microscopy is presented here. Appropriate cell lines were seeded in collagen coated, glass-bottom dishes (MatTek) at 1 x 10^5 cells per dish and cultured in an incubator with 5% CO_2 at 37 ^oC for 24 h. The cells were then treated with magnesium and calcium-containing D-PBS with a specific concentration of PP50 and the desired payload, whose pH had been adjusted to 6.5 or 7.4 and sterile-filtered using 0.22 µm syringe filters. After treatment for a specific period of time in an incubator, the cells were washed three times with D-PBS to remove extracellular payload and polymer and were stained with LysoTracker® red DND-99 (50 nM) and Hoechst 33342 (1 µg mL^{-1}). 1 mL of growth medium was then added to each dish and the cells were analysed using LSM-510 laser scanning inverted confocal microscope (Zeiss, Germany). For FITC-containing payload, excitation at 488 nm was used. The images were analysed using ImageJ 1.51n.

Antibody delivery and cell fixing

A549 cells were seeded in transparent-bottom, black wall 96 well-plates at 1 x 10^4 cells per well and cultured in an incubator with 5% CO_2 at 37 ^oC for 24 h. A portion of the cells were then fixed with BD CellFIX and permeabilised with 1% Triton-X. Anti non-muscle Myosin IIA antibody (Alexa Fluor 647) (333 nM) was added to the fixed/permeabilised cells as well as live cells in a mixture with PP50 at 0.5 mg mL^{-1} (pH 6.5) and incubated for 1 h. Following a wash with PBS and staining with Hoechst, the delivery of the antibody was compared by confocal microscopy by Alexa Fluor647 at 650 nm. The images were analysed using ImageJ 1.51n.

2.8 Flow cytometry

1 mL of HeLa cells (3 x 10^5 cells mL^{-1}) were cultured in 6-well plates for 24 h followed by treatment with a PBS solution containing a desired concentration of PP50 and FITC-Dextran adjusted to the desired pH. After the treatment, the cells were washed three times with D-PBS. After cell detachment using 0.5 mL of Trypsin-EDTA (EDTA in case of MES-SA and MES-SA/Dx5 cells, cell scraping in case of RAW 264.7 cells) 0.5 mL of serum-free DMEM was added to each well and the samples were centrifuged in 2 mL Eppenderf tubes for 5

minutes at 950 g. The supernatant was discarded and replaced with 0.5 mL of serum-free DMEM.

The samples were filtered using Flowmi™ cell strainers (40 µm) and analysed in 5 mL Falcon plastic tubes using a BD LSRFortessa cytometer (BD Biosciences, USA). The samples were excited at 488 nm and the emission was collected in the 570 - 585/42 nm band. The results were analysed using FlowJo v10.

2.9 AlamarBlue cell survival assay

AlamarBlue assay allows to quantify cell viability by using resazurin – a cell permeable compound which is turned over to highly fluorescent resorufin upon entry to healthy cells. Cells were seeded on black, flat, transparent-bottom 96-well plate (Corning, USA) at 1 x 10^4 cells per well in 0.1 mL culture medium and incubated for 24 h. The spent medium was replaced with sterile-filtered D-PBS containing PP50 or PP50 mixed with Dextran and incubated for a specific period of time. The polymer solutions were replaced with DMEM containing 10% (v/v) alamarBlue® reagent and further incubated for 4 h, as per the manufacturer's protocol. The fluorescence was measured using a spectrofluorometer (GloMax®-Multi Detection System, Promega) at emission wavelength of 580-640 nm with excitation wavelength of 525 nm. The cytotoxic effect was determined by comparison to an untreated control sample.

2.10 CellTiterGlo 2.0 cell survival assay

CellTiterGlo 2.0 Assay enables detection of ATP present in solution allowing for quantification of metabolically active cells, which is useful in determining the cytotoxic effect of different treatment regiments. Cells were seeded at 1 x 10^4 cells per well (0.1 mL) in black, flat, transparent-bottom 96-well plate (Corning, USA) and incubated for 24 h. The spent medium was replaced with sterile-filtered D-PBS containing materials whose cytotoxicity was being tested, such as PP50 and Bim and PP50 and scrBim. Following a specified treatment time inside a humidified incubator with 5% CO_2 at 37 ^oC, the polymer solutions were replaced with FBS and penicllin/streptomycin supplemented DMEM and were

cultured for another 24 h. 40 µL of the CellTiterGlo 2.0 reagent was added to each well and the luminescence was analysed using an Envision 2100-series plate reader (PerkinElmer, USA). The cytotoxic effect was determined by comparison to an untreated control sample.

2.11 Dynamic Light Scattering (DLS) and Zeta Potential

Zetasizer Nano ZS (Malvern, UK) instrument was used to characterise the hydrodynamic size and zeta potential of PP50 (0.5 mg mL^{-1}), 150 kDa FITC-Dextran (10 µM) and the two components mixed together. PP50 and FITC-Dextran were dissolved in PBS at pH 6.5. The hydrodynamic radius was measured in 10 mm-wide disposable cuvettes with 173^{o} backscatter angle and repeated 3 times for each sample. Zeta potential was analysed in disposable capillary cells and repeated 3 times for each sample.

2.12 Spheroids

A549 cells were seeded at 2.5 x 10^3 cells per well in DMEM in Corning® 96 Well Ultra Low Attachment Spheroid Microplates and cultured in an incubator (5% CO_2 at 37 ^{o}C) for 2 days. The spheroids formed at the bottom of the wells were treated with 10µM FITC-Dextran at pH 6.5 and 7.4 for 2 h with or without PP50 (0.5 mg mL^{-1}). The spheroids were subsequently washed 3 times by submerging in 10 mL of D-PBS and stained with propidium iodide (1 µg mL^{-1}), after which they were characterised using Z-stack imaging with a Zeiss LSM-510 laser scanning confocal microscope. The depth of images was 65-90 µm and the thickness of individual focal slices was equal to 2 µm. The image analysis was performed using Volocity Version 6.3.0.

2.13 Caspase activation assays

A549 cells were seeded on white, flat-bottom, opaque 96-well plate (Corning, USA) at 0.5 x 10^4 cells per well in 0.1 mL culture medium and incubated for 24 h. The spent medium was replaced with sterile-filtered D-PBS containing PP50 and Bim and incubated for 3 h. The solutions were replaced with DMEM

and further incubated for 4 h, after which the growth medium was removed and replaced with 20 µL of serum free DMEM. 20 µL of Caspase-Glo® 3/7 Assay reagent was added to each of the wells and incubated on a plate shaker for 1 h at room temperature. The luminescence was measured using a spectrofluorometer (GloMax®-Multi Detection System, Promega). The cytotoxic effect was determined by comparison to appropriate control samples. Corresponding AlamarBlue assays were performed as described above.

2.14 IncuCyte® ZOOM

IncuCyte® ZOOM is an automated fluorescent microscope system which allows the imaging of cells growing at 37°C and 5% CO_2 over time, enabling collection of physiologically relevant data as well as the study of kinetics of various biological processes. A549 cells were seeded in black, flat, transparent-bottom 96-well plates (Corning, USA) at 1 x 10^4 cells per well in 0.1 mL DMEM and incubated for 24 h, followed by the addition of PP50, Bim-Cy7, scrBim-Cy7, ABT-737, PP50-Bim-Cy7 or PP50-scrBim-Cy7 at a specific concentration and incubated for a specific period of time. The solutions containing the tested substances was replaced with 100 µL FBS- and penicillin/streptomycin-supplemented DMEM containing 5 µM IncuCyte® Caspase-3/7 Green Apoptosis Assay Reagent, placed within the incubator chamber of the IncuCyte® ZOOM (Welwyn Garden City, Hertfordshire) and imaged every 2 h by exciting at 488 nm. The images were analysed using the integrated IncuCyte Zoom software v. 2016B.

2.15 Delivery method comparison

A549 cells were cultured in 96 well plates at 2 x 10^4 cells per well as described above. Bim and scrBim (15 µM) was added to the cells with the following delivery agents: PP50 (22 µM), PLP (29 µM), PEI 0.6 kDa (1.7 mM), PEI 25 kDa (2 µM), Melittin (1 µM), Tat (20 µM) and Penetratin (20 µM). These concentrations were determined using literature and experimental optimisation. Peptide delivery using BioPORTER®, PULSin® and electroporation was performed using manufacturer's instructions. Treatment time was equal to 4 h in either PBS pH

6.5 (PP50 and PLP) or serum free DMEM (remaining chemical agents). Cell survival was assessed using CellTiter-Glo® 2.0 by adding 40 µL of the assay reagent to each of the wells 24 h after the end of the treatment, and the luminescence was analysed using Envision 2100-series plate reader (PerkinElmer, USA) and compared to corresponding controls with untreated cells.

2.16 EVs – production and loading

Extracellular vesicles were derived from human embryonic kidney cells 293 (HEK-293) by Christina Schindler (MedImmune) following a sequential three-step filtration protocol described by Heinemann and Vykoukal (2017). EVs at the concentration of 2.0 x 10^{12} particles mL^{-1} obtained thus were placed in PBS, pH 6.5, for the final aliquot volume equal to 80 µL, and frozen.

For PP50-mediated peptide loading of EVs, the samples were thawed at room temperature and spun for 1 min using a benchtop centrifuge. The EVs were then mixed with 10 µL of PP50 stock solution (10 mg mL^{-1}) and 10 µL of Bim stock (200 µM) to produce samples with the final volume of 100 µL containing 1 mg mL^{-1} and 20 µM of polymer and peptide, respectively. Appropriate polymer-free control as well as peptide-free controls were used. The loading was performed at 37^{o}C (incubator) for 1.5 h. This treatment was followed by partial peptide removal by spinning down the samples using a benchtop centrifuge (13.3k g, 15 minutes). Bim-Cy7 which is not very stable in aqueous solutions formed a pellet at the bottom of the tubes. The second purification step relied on using ultracentrifugation to spin the samples at 100k g for 1 h 15 min in thick-walled ultracentrifuge tubes. After the procedure the supernatants were collected in separate tubes and the EV pellets were re-suspended in 80 µL PBS (fine-filtered).

2.17 EVs - analysis using NanoSight

EV concentration and size were analysed using NanoSight NS300 (Malvern Panalytical, UK). Briefly, the EVs were diluted 1000-fold in fine-filtered PBS for a final volume of 1 mL and injected into the NanoSight instrument using a syringe. NanoSight analysis relies on a microscope and camera-driven

detection of scattered light and Brownian motion from nanoparticles passing through a laser beam in a liquid solution. The integrated software is then capable of calculating the particle concentration and hydrodynamic radius using the Stokes-Einstein equation.

2.18 EVs – analysis using flow cytometry

Analysis of PP50-mediated peptide loading into EVs was performed using flow cytometry by Christina Schindler (MedImmune). As free EVs are too small for detection they had to be immobilised on Dynabeads® magnetic beads coated with anti CD9 antibodies, which allows for EV binding on bead surface at a high enough concentration for detection using this method. 40 µL of bead slurry was mixed with 60 µL of the EV sample and topped up with PBS + 0.1% BSA to the total volume of 250 µL. The mixture was left overnight at 8^{o}C, followed by a 3-step wash and analysis using BD LSRFortessa cytometer, detecting the fluorescence of Bim-Cy7. Fresh magnetic beads were used as a negative control.

2.19 PDPH grafting

3-(2-pyridyldithio)propionyl hydrazide (PDPH; 3.2 mg, 0.014 mmol), PP50 (100 mg, 0.28 mmol [COOH]) and DMAP (20 mg, 20 wt% of PP50) were dissolved in anhydrous DMF (400 µL) in a flat bottom, disposable glass tube (5 mL). DCC (3 molar equivalents to PDPH) in anhydrous DMF (40 µL) was added to the previous solution dropwise. The reaction tube was tightly sealed with parafilm and the reaction was left to proceed under magnetic mixing at room temperature for 24 h. Centrifugation was used to spin down dicyclohexylurea (DCU, the by-product of the reaction. The supernatant was collected using a pipette and subsequently rapidly poured into 5 volumes of diethyl ether, where precipitation of crosslinker-grafted polymer (PP50-PDPH) occurred. The precipitate was collected using vacuum filtration and re-dissolved in sodium bicarbonate (0.1 M). Dialysis was performed in order to remove remaining inorganic salts, impurities and solvents using 12-14 kDa MWCO Visking tube membrane (Medicell) against deionised water (48 h). To convert it to the acid form, PP50-PDPH in its sodium salt form was acidified using diluted hydrochloric acid

(0.1 M) after dialysis to cause polymer precipitation (pH 3.0-4.0). The precipitate was spun down using centrifugation, washed with deionised water and freeze-dried to yield dry PP50-PDPH powder. In order to convert to back to the sodium salt form, the PP50-PDPH was dissolved in sodium bicarbonate.

2.20 PDPH characterisation

PP50-PDPH was dissolved in phosphate buffered saline (PBS; pH 7.4) at 1 mg mL^{-1} and its absorbance at 343 nm was measured using a GENESYS 10S UV/Vis Spectrophotometer (Thermo Fisher Scientific, USA). The disulphide bond in PDPH was reduced by addition of excess 0.1 M DTT, and the reaction was allowed to proceed for 90 minutes. The absorbance of 2-mercaptopyridine released from reduced crosslinker was measured at the same wavelength. The difference between the absorbance before and after DTT reduction was used to calculate % grafting with PDPH.

2.21 2-mercaptopyridine release kinetics

The release kinetics of 2-mercapopyridine (small molecule drug model) was studied using the GENESYS 10S UV/Vis Spectrophotometer (Thermo Fisher Scientific, USA). 0.1 mg mL^{-1} PP50-PDPH in PBS (pH 7.4) was incubated with various concentrations of biological reducing agents, glutathione (GSH) and cysteine, at 37^{o}C in order to initiate reduction of disulphide bonds in the PDPH crosslinker. The absorbance of 2-mercaptopyridine released from the crosslinker was recorded using the GENESYS 10S UV/Vis Spectrophotometer at 343 nm over 2 and 24 h periods at chosen time intervals. Reduction with excess DTT was used to establish 100% possible release (positive control), while addition of no reducing agents constituted the negative control.

2.22 Conjugation of PEG-FITC

Thiol-functionalised PEG-FITC was conjugated to PP50-PDPH by dissolving both of the substances in either PBS or DMSO, or a mix of the two to a desired final concentration of PP50-PDPH (1 and 0.66 mg mL^{-1}) and mixing them

together. The amount of PEG-FITC chosen was so that it was in 0.5:1, 1:1 and 2:1 molar ratio with the available PDPH molecules. The reaction was left to proceed at room temperature for up to 24 h. To characterise conjugation effectiveness and kinetics, the GENESYS 10S UV/Vis Spectrophotometer (Thermo Fisher Scientific, USA) was used to measure absorbance of the released 2-mercaptpyridine. Since the absorbance spectra of 2-mercaptpyridne and FITC overlap, a negative control of PEG-FITC at the appropriate concentration was used to establish the actual absorbance reading. The excess of unconjugated PEG-FITC was removed by dialysis against PBS using Spectra-Por® Float-A-Lyzer® G2, 5 mL, MWCO 8-10 kDa dialysis units (Spectrum Labs, USA).

2.23 Conjugation of proteins

Modification with N-succinimidyl S-acetylthioacetate (SATA)

Addition of free sulfhydryl groups on proteins which do not possess free thiols readily available for conjugation was performed using SATA crosslinker, which is reactive to primary amines. For addition of sulfhydryl groups to IgG antibodies, 1 mL of 60 µM protein solution dissolved in PBS (pH 7.4) was prepared. SATA solution (55 mM, 10 µL) dissolved in DMSO, was added to the IgG solution, the samples were placed in a sample rotator and the reaction was allowed to proceed for 30 minutes at room temperature. A 5 mL HiTrap desalting column (VWR, UK) was used to remove unconjugated SATA and the protein fractions were collected and pooled together. Protein concentration was calculated by measuring absorbance at 280 nm using GENESYS 10S UV/Vis Spectrophotometer (Thermo Fisher Scientific, USA). The protective group of SATA was removed by addition of 10 µL of the deacetylation buffer (0.5 M hydroxylamine, 25 mM EDTA in PBS, pH 7.5) to 1 mL SATA-modified protein sample. The reaction was left to proceed for 2 hours at room temperature, and a desalting column was used again to remove hydroxylamine.

The amount of added thiols was quantified in an Ellman's Test. Briefly, 50 µL of 50 mM DTNB was added to 1 M Tris (pH 8.0, 100 µL) and 840 µL dH_2O for each tested sample. 10 µL of protein solution was added to the previously prepared

mixture and left to incubate at room temperature for 5 minutes. Then the absorbance of the solution was measured at 412 nm. The thiol grafting was determined by comparison to a standard curve which was prepared using cysteine.

Conjugation of PP50 and BSA

BSA (or SATA-modified BSA) and PP50 grafted with PDPH were each dissolved in PBS (pH 7.4) and mixed together so that the final concentration of PP50 was 1 mg mL^{-1}. Various amounts of BSA were used, chosen so that they were in e.g. 1:1 and 2:1 molar ratio with the available PDPH molecules. The reaction was allowed to proceed at room temperature for 24 h. The reaction effectiveness was measured by the GENESYS 10S UV/Vis Spectrophotometer (Thermo Fisher Scientific, USA), by measuring the absorbance of 2-mercaptopyridine released from PDPH, separated from the reaction mixture by using Amicon Ultra 0.5 mL 10 kDa MWCO centrifugation units.

Conjugation of PP50 and GFP

GFP and PP50 grafted with PDPH were each dissolved in PBS (pH 7.4) and mixed together so that the final concentration of PP50 was 1 mg mL^{-1}. 1:1 molar ratio of GFP to PDPH was used. The reaction was allowed to proceed at room temperature for 24 h. GFP loading onto PP50 was measured as described above.

Conjugation of PP50 and IgG

PDPH-modified PP50 was mixed with SATA-modified IgG at 1:1 ratio of PDPH and SATA in 1 mL of PBS (pH 7.4) and a final polymer concentration of 1 mg mL^{-1}. The reaction was left to proceed for 24 h at room temperature. The reaction effectiveness was measured as described above.

2.24 Conjugation of Bim and scrBim

Bim and scrBim (as well as Bim-Cy7 and scrBim-Cy7) used herein were designed to contain a free cysteine which enabled conjugation to PP50 via formation of disulphide bonds between the cysteine's sulfhydryl group and

PDPH. 2:1 to 3:1 molar ratios of the peptide to the available PDPH crosslinker on PP50 were used. The peptides were dissolved in a small amount of DMSO and added to the polymer solution dissolver in PBS and mixed vigorously using a benchtop vortex. The Eppendorf tubes containing the materials were mounted on a sample rotator and the reaction was left to proceed for 24 h at full rotation speed. After 24 h, the reaction efficiency was analysed by measuring the amount of 2-mercaptopyridine released from PDPH, separated from the reaction mixture by using Amicon Ultra 0.5 mL 10 kDa MWCO centrifugation units, and compared to a positive control – PDPH-modified PP50 reduced with 20x molar excess of DTT. Unconjugated Bim and scrBim were removed via dialysis against PBS using Spectra-Por® Float-A-Lyzer® G2, 5 mL, MWCO 8-10 kDa dialysis units.

2.25 Bim-Cy7 and scrBim-Cy7 removal by dialysis - analysis

Following conjugation with PP50, the unconjugated Bim-Cy7 and scrBim-Cy7 was attempted to be removed by dialysis using Spectra-Por® Float-A-Lyzer® G2, 5 mL, MWCO 8-10 kDa dialysis units against different buffers for 24 h. The peptide content in the original sample as well as the dialysate were analysed using an Odyssey® infrared fluorescent scanner (LI-COR, Germany). Briefly, 50 µL of the samples were added to 96-well plates (black wall) and read using Odyssey® at λ= 800 nm.

2.26 High Pressure Size Exclusion Chromatography (HPSEC)

High Pressure Size Exclusion Chromatography (HPSEC) was performed Jen Spooner (MedImmune) to analyse the size of PP50, Bim/scrBim and the polymer-peptide conjugates and determine the potential for size-based separation of the peptide. HPSEC was performed using Agilent 1260 HPLC system (Agilent, USA), equipped with a TSKgel G3000SWXL HPSEC column (5 µm, 7.8 mm x 300 mm; Sigma, UK). The flow rate was 1 mL min^{-1} using 0.1 M sodium phosphate dibasic

anhydrous + 0.1 M sodium sulphate, pH 6.8, as the isocratic running buffer. The elutes were analysed using absorbance analysis (λ = 280 nm).

2.27 Endotoxin quantification

Quantification of endotoxin content in conjugate samples prior to immunogenicity and *in vivo* studies was performed by Jen Spooner (MedImmune) using the FDA-approved Limulus Amebocyte Lysate (LAL) Kinetic-QCLTM assay (Lonza Biologics, UK). Briefly, this method relies on detection of Gram-negative bacterial endotoxin by mixing the sample with LAL substrate which contains an endotoxin-sensitive enzyme derived from blood of the horseshoe crab *(Limulus polyphemus*) (Young et al., 1972). Upon catalytic activation by endotoxin, the enzyme reacts with a synthetic substrate to produce p-nitroaniline turning the samples yellow, which can be detected photometrically using a plate reader (λ = 405 nm) and compared to a set of standard endotoxin solutions in order to determine endotoxin concentration. All of the PP50-peptide samples used herein had endotoxin level lower than 50 EU mL^{-1} to prevent toxicity to the animals used in the *in vivo* experiments.

2.28 IL-6 and TNFα ELISAs

Isolation of peripheral blood mononuclear cells (PBMCs) from human blood

Leukocyte cone blood (25 mL) (Addenbrooke's Hospital, Cambridge) diluted in PBS, if necessary, was layered on top of 14 mL Ficoll in 50 mL Falcon tubes and centrifuged for 40 minutes at 400 g. PBMCs were removed from the Ficoll/blood interface using a Pasteur pipette and placed in a new 50 mL Falcon tube, following topping up with PBS to the final volume of 45 mL and second centrifugation step (10 minutes at 200 g) to wash the cells. This step was performed two more times. Following the last wash step, PBMC pellet was collected and resuspended in ACK Red Blood Cell Lysing Buffer and the reaction was left to proceed for 5 minutes at room temperature, following topping up with 45 mL PBS and centrifugation at 200 g for 10 minutes. The pellets were collected and dissolved in 50 mL fresh PBS and the cell number was established

using a haemocytometer and the cells were stored in 90% foetal bovine serum/ 10% DMSO at -80^{o}C.

Incubation with materials

PBMCs were thawed, spun down to remove DMSO and seeded in a 96 well cell culture plate at 5 x 10^5 cells per well in RPMI supplemented with 10% (v/v) FBS, 100 U mL^{-1} penicillin and 100 µg mL^{-1} streptomycin. PP50, PP50-Bim-Cy7, PP50-scrBim-Cy7, Bim-Cy7 and scrBim-Cy7 were added to different cell-containing wells at specified concentrations. Bacterial lipopolysaccharides (LPS) at 10 and 100 ng mL^{-1} were used as a positive control. The cells mixed with different materials were cultured in a humidified incubator at 37 ^{o}C with 5% CO_2 for 24 h, followed by transferring the samples to a U-shaped bottom 96 well plate and centrifugation in order to spin down the cells. The supernatants were transferred to a new plate and frozen at -80^{o}C.

ELISA

Human IL-6 ELISA Duoset and Human TNFα ELSIA Duoset kits were used to analyse the expression levels of IL-6 and TNFα, respectively.

Capture antibody was diluted 1:180 in PBS, and added to Nunc® MaxiSorp™ black 96-well plates (50 µL per well), sealed with a plastic sticker lid and incubated overnight at 4^{o}C. The coated plates were then washed 3 times with PBS and TWEEN® 20 using a plate washer, following addition of 200 µL of 1% Bovine Serum Albumin in PBS (block buffer) and incubation at room temperature for 1 h, followed by a wash step with PBS + TWEEN® 20 (3 times). The supernatants obtained from treatment of PBMCs with the tested materials were thawed and loaded into appropriate wells (50 µL per well). The samples added to the plates containing the TNFα capture antibodies were diluted 1:2 in PBS before addition. After a 2 h incubation at room temperature, the plates were washed 3 times with PBS + TWEEN® 20, followed by addition of biotinylated goat anti-human IgG antibodies diluted 1:180 in 1% BSA solution (50 µL per well) and incubated for 1h at room temperature. The plates were washed 3 times with PBS + TWEEN® 20 and Europium-conjugated streptavidin diluted 1:1000 in DELFIA® Assay Buffer (PerkinElmer, USA) was added to the wells (100 µL) and incubated for another 1 h. The plates were finally washed 7 times with

DELFIA® Assay Buffer, followed by addition of the DELFIA® Enhancement Solution (PerkinElmer, USA) at room temperature (100 µL per well). The plates were shaken for 10 minutes using a rotating plate shaker in the dark. The time-resolved fluorescence of the wells was measured using Envision 2100-series plate reader (PerkinElmer, USA).

2.29 *In vivo* study

CD1-nude mice (Charles River, UK) were used in all the in vivo studies. The experiments were performed on females only older than 8 weeks old and with a body weight equal to or greater than 18 g. Fabien Garcon (MedImmune) supervised the *in vivo* studies. Experimental design was planned by Fabien Garcon and Michal Kopytynski. Michal Kopytynski prepared the conjugate samples. Mice handling was performed by skilled technicians possessing Home Office licenses for animal work.

Cell harvest and preparation

The cell line used to create the xenografts was A549 (ATCC). Briefly, A549 cells were cultured in T175 flasks until reaching 80% confluency and detached using Accutase. The detached cells were diluted with PBS in 50 mL Falcon tubes and spun down at 170 g for 5 minutes using a centrifuge. Cell number was determined using a haemocytometer. 5 x 10^6 cells were diluted in bijoux tubes with PBS and 50% v/v Matrigel Basement Membrane Matrix (Corning, UK) at the final volume of 100 µL which was used for implantation. The samples were sent on ice to the MedImmune animal house (Babraham Research Campus, Cambridgeshire, UK).

Cell Implantation and tumour measurement

Cell implantation was performed by licensed technicians. Briefly, A549 cells, in a volume of 100 µL were implanted subcutaneously in shaved flanks of the CD-1 nude mice. Tumours were measured using graduated callipers taking 2 perpendicular measurements in millimetres (the longest diameter is measured first). Depth of tumour growth is not normally measured. Measurements were performed 3 times a week (usually Monday, Wednesday, Friday). Tumour

volume was calculated to generate a tumour growth curve. Generally, volume = (length x width^2)/ 2. Tumour diameter, which was defined as an average of the length and width, was minimum 15 mm.

Tolerability studies

PP50, PP50-Bim-Cy7 and PP50-scrBim-Cy7 were injected intravenously in tail vein in a volume of 100 µL at a specified concentration. The mice were checked for adverse effect for a period of 60-120 minutes post-injection by observation of the animal behaviour. Usual occurrence is mouse being subdued post-injection, but still being responsive to touch. Full recovery should normally take place within 45 minutes. For the tolerability study, mouse body mass was measured using an electronic scale once a day for 7 days following the last injection.

Non-invasive imaging

The animals were anaesthetised with isoflurane and placed in IVIS Spectrum (PerkinElmer) for imaging of the biodistribution of PP50-Bim-Cy7 and PP50-scrBim-Cy7 administered as an intravenous injection into the tail. The anaesthesia was maintained for the duration of the imaging session. At the endpoint of the study, the animals were culled and different organs were harvested and imaged.

2.30 Statistical analysis

Statistical analysis was performed using GraphPad Prism 7.04. Student's t-tests and ANOVA with Tukey's multiple comparison tests were performed where appropriate. Statistical significance was assigned as follows: P-value ≥ 0.05 – not significant (ns), P-value = 0.01-0.05 – significant (*), P-value = 0.001-0.01 – very significant (**), P-value = 0.0001-0.001 – highly significant (***), P-value < 0.0001 – extremely significant (****).

Chapter 3 - Payload delivery by co-incubation with PP50: mechanism and delivery characterisation

3.1 Introduction

PP50 is a pH-responsive, bio-inspired, amphiphilic polymer which can cause membrane permeabilisation when protonated in a mildly acidic pH environment, enabling payload delivery to the cell interior (Chen et al., 2009c; Lynch et al., 2010). In the cellular milieu, the endosomal pathway, in which endosomes acidify progressively as they mature from early endosomes towards lysosomes, provides an opportunity to trigger pH-responsive delivery agents, such as PP50. This strategy has been previously shown to be capable of delivering siRNA conjugated to another PP-family polymer, PP75, for potential cancer therapy applications (Khormaee et al., 2013).

In contrast, the work in this chapter focuses on another approach in which the pH of the extracellular environment *in vitro* is changed to a mildly acidic one, in order to protonate and activate the polymer before it is internalised by the cell. This approach was used by Lynch et al. (2011), who investigated PP50-mediated delivery of the small molecule trehalose to human erythrocytes for cell preservation applications by simple co-incubation of the polymer with this cargo at mildly acidic pH.

This chapter aims to discuss the mechanism in which PP50 interacts with and permeabilises biological phospholipid bilayers, building on previous work which investigated the interaction of PP50 with artificial DOPC lipid bilayers (Ramadurai et al., 2017), human erythrocytes (Lynch et al., 2011) as well as nucleated mammalian cells (Mercado and Slater, 2016b) and will place these findings in the context of developing PP50 as a universal delivery agent capable of permeabilising the cell membranes in a controlled way, using pH as the trigger. A deeper understanding of the way in which PP50 interacts with biological membranes will help to inform about the capabilities as well as the limitation of this delivery system.

To achieve this, ovine erythrocytes and HeLa cells were used to study the behaviour of fluorescently labelled polymer as well as that of the fluorescent small molecule dye TexasRed and macromolecular dextran, which acted as model payloads. In addition, the effects of the extracellular pH, temperature and the importance of the endosomal acidification on payload delivery into the cytosol were investigated. The analysis was performed by confocal microscopy, flow cytometry and haemolysis assay. This helped to build an explanation of the proposed mechanism underlying payload delivery by simple co-incubation with PP50, which will be discussed.

Furthermore, the delivery process of a fluorescent model payload to HeLa cells was characterised in detail as a function of a number of different parameters. Treatment time, concentration of both the polymer and the cargo as well as the environmental pH are key factors which dictate the delivery efficiency and therefore the amount of payload delivered intracellularly. Here 150 kDa FITC-Dextran was used as the model macromolecular cargo, and the effects of the delivery were analysed using flow cytometry and confocal microscopy.

Understanding the interaction between PP50 and biological membranes, leading to membrane permeabilisation, as well as the characterisation of the delivery efficiency and the crucial parameters ruling the delivery process will help in optimising future experiments whose aim will be to establish PP50-mediated delivery as a platform technology, compatible with different payloads and cell types. This will be further discussed in the following chapter.

3.2 Results and Discussion

3.2.1 pH-responsive interaction with biological membranes

Here, ovine erythrocytes were used as a simplified model of the more complex nucleated mammalian cells. Some of the main differences between these two cell categories include the lack of nucleus and organelles in the erythrocytes as well as low levels of endocytosis, unless chemically induced, compared to nucleated cells (Ginn et al., 1969; Bourgeaux et al., 2016). Erythrocytes are also generally less robust than nucleated cells due to the lack of the intracellular structures, which allows travel though narrow blood vessels and capillaries. It is also interesting to note that red blood cells have been proposed as a potential drug delivery vehicle, and so the ability to load them with the desired payloads possessing biological functions could find clinical uses (Bourgeaux et al., 2016). Building on the results reported by Lynch et al (2011), the interaction between PP50 and the erythrocyte plasma membrane in the context of payload delivery into the cell interior was investigated. A small molecule (fluorescent dye) was used to enable easy detection by microscopy.

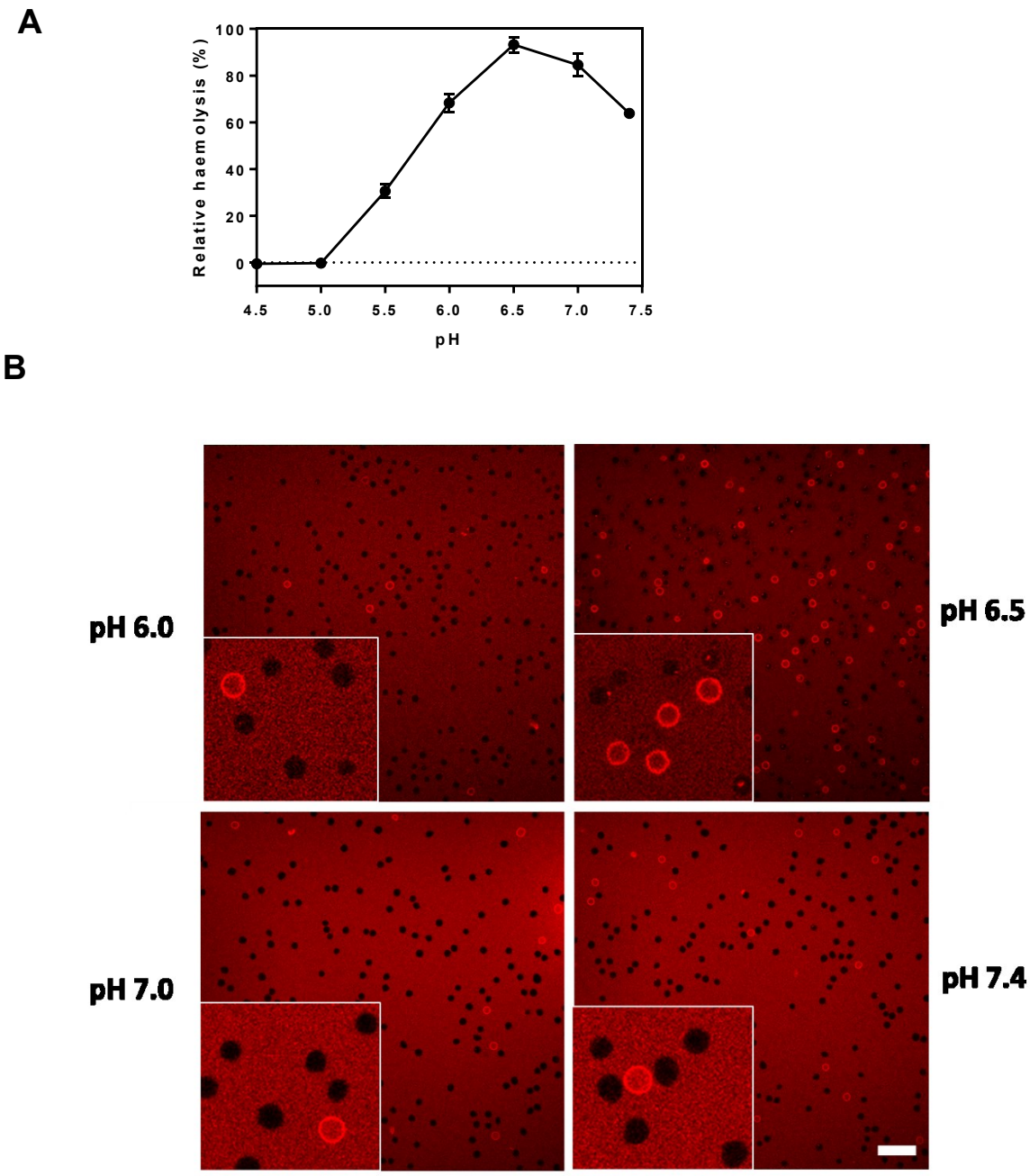


Figure 3-1. (A) Haemolysis of ovine erythrocytes after incubation with PP50 (100 µg mL^{-1}) for 1 h in a shaking water bath at 37°C in 7 different pH environments in the range of pH 4.5-7.4. (B) Delivery of TexasRed dye (0.62 kDa, 1 µM) to ovine erythrocytes by co-incubation with PP50 (50 µg mL^{-1}) at pH 6.0, 6.5, 7.0 and 7.4, as analysed by confocal microscopy. Scale bar = 20 µm.

A haemolysis assay was performed to determine the optimal buffer pH for the treatment of erythrocytes. Incubation of red blood cells with PP50 at pH 6.5 resulted in the highest level of haemoglobin release, compared to pH 4.5, 5.0, 5.5, 6.0, 7.0 and 7.4 (Figure 3-1 A), leading to 90% haemoglobin release, and

thus it was concluded that at this pH value PP50 was the most efficient at permeabilising the erythrocyte plasma membrane and chose it for the following delivery experiments. TexasRed dye (0.62 kDa, Ex 596/ Em 615) was used as a small molecule model for delivery to ovine erythrocytes. TexasRed has been described to bind to the membrane of erythrocytes permeabilised by pH-responsive hyperbranched polymers with high affinity, forming a visible ring, but did not interact with intact erythrocyte membranes (Hughes et al., 2014; Wang and Chen, 2017), thus enabling easy detection of cells modified by membrane permeabilising polymers, such as PP50. The same number of ovine erythrocytes were co-incubated with TexasRed and PP50 at pH 6.0, 6.5, 7.0 and 7.4 for 30 minutes and were subsequently analysed by confocal microscopy (Figure 3-1 B). The treatment with PP50 at pH 6.5 resulted in the highest number of cells bound to by TexasRed as a sub-population of the total cell number, characterised by the clearly visible red ring around the cells. This was in clear contrast to the intact cells which remained impermeable to the dye and appeared as black circles. This is consistent with previously reported results (Chen et al., 2009c; Lynch et al., 2011) showing that pH 6.5 is the optimal pH at which PP50 is in its most membrane-active state due to the protonation and exposure of the hydrophobic pendant groups.

The pH-dependant membrane binding ability was also investigated by Ramadurai et al. (2017), who used microcavity supported lipid bilayers composed of 1,2-Dioleyl-*sn*-glycerophosphocholine (DOPC) as substrate-supported synthetic models of the biological phospholipid bilayer, which offer lipid fluidity similar to that of liposomes. In their study, fluorescently labelled PP50 was incubated with DOPC membranes at pH 7.5, pH 7.05 and pH 6.5, respectively, corresponding to the polymer's deprotonated, partly protonated and fully protonated state, for up to 4 h, and analysed using fluorescence correlation spectroscopy and electrochemical impedance spectroscopy. The results showed that at all the studied pH values PP50 associated with the lipid membrane and diffused along the membrane's aqueous interface, leading to a retardation of lipid diffusion. However, the lipid retardation effect and the increase in film impedance were the strongest and most immediate at pH 6.5, followed by pH 7.05 and pH 7.5, where the effect was weaker and more

temporary, suggesting that more polymer bound to the bilayer in its fully protonated state, the interaction is stronger or that the polymer is more spread out on the membrane surface at pH 6.5.

Furthermore, the study of the electrochemical resistance across the membrane indicated a notable rise after treatment with PP50, suggesting that the polymer did not produce defects or pores in the membrane which would lead to lower resistance. This contrasts with other synthetic delivery agents, such as PEI or poly(L-lysine) (Hong et al., 2006; Wang et al., 2014). These findings also suggest that PP50 does not penetrate deeply into hydrophobic core or span the bilayer, but instead can modify the membrane fluidity by binding on the external leaflet, modifying surface roughness and thickness.

This was also corroborated by Lynch et al. (2011), who visualised the plasma membrane of human erythrocytes after incubation with PP50 at a mildly acidic pH using atomic force microscopy. They observed discrete regions of polymer build-up, increasing the apparent plasma membrane thickness, and presumably, resistivity, as reported by Ramadurai et al. (2017). These regions were surrounded by areas of the membrane whose thickness was depressed by ca. 3 nm, or 35-40% of the total erythrocyte bilayer thickness (Hochmuth et al., 1983; Lynch et al., 2011). The mechanism responsible for this localised membrane thinning was hypothesised to rely on the initial binding of PP50 being mediated by the hydrophilic phase of the polymer binding onto the external, polar regions of the bilayer. This binding leads to a formation of an energetically unstable void in the hydrocarbon chain region, which is quickly eliminated by hydrocarbon tails via trans-gauche isomerisation and chain bends. This promotes the interaction between the hydrophobic core and the hydrophobic phase of PP50, which in turn leads to membrane thinning via disruption of the original bilayer architecture. These areas of localised membrane thinning, or creation of associated membrane perturbations, could be responsible for the reported non-Stokesian diffusion of molecules of interest into the cytosol (i.e. payload delivery). The membrane thinning effect has been also reported upon binding of certain antimicrobial peptides (Ludtke et al., 1995; Mecke et al., 2005).

3.2.2 Formation of ghost cells

There are two possible formats of payload delivery to erythrocytes: (i) delivery to intact cells, with no membrane collapse or (ii) cargo transport to the inside of the erythrocyte ghosts, i.e. membrane shells or cells whose intracellular content has leaked out (Hamidi and Tajerzadeh, 2003; Muzykantov, 2010). Lynch et al., who wanted to deliver trehalose for potential cryopreservation applications, focused on payload transport to red blood cells without causing major haemolysis, which would be highly disadvantageous in the cell preservation context. In experiments presented here, however, the delivery occurred mainly via formation of erythrocyte ghosts.

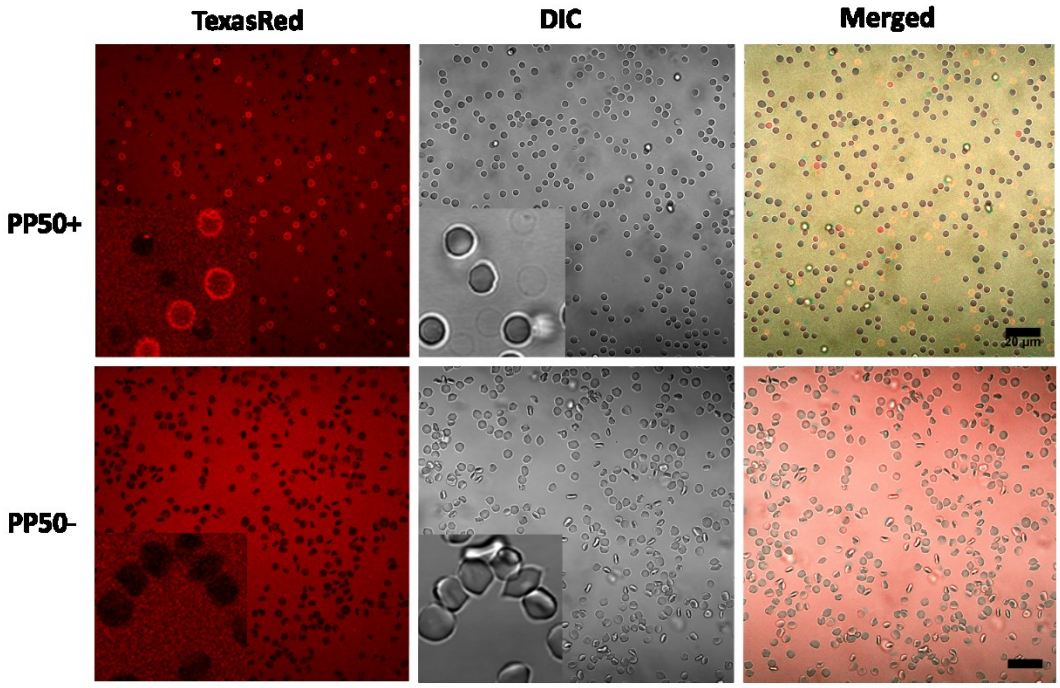


Figure 3-2. Delivery of TexasRed (1 µM) to ovine erythrocytes by co-incubation with PP50 (50 µg mL^{-1}) at pH 6.5 for 30 min in a shaking water bath (37^{o}C), compared to polymer-free control sample, as analysed by confocal microscopy. Red channel represents TexasRed. Differential interference contrast (DIC) is also shown. Scale bar = 20 µm.

To confirm the formation of ghost cells, a more thorough analysis of the cell morphology and a comparison to a suitable negative control was performed After a 30-minute treatment with PP50 mixed with TexasRed at pH 6.5, the samples were visualised using confocal microscopy (Figure 3-2). The formation

of erythrocyte ghosts in the samples treated with the polymer was observed. The ghost cells displayed binding of the small molecule dye on the membrane, resulting in an apparent bright fluorescent ring when observed within a set focal plane, as well as the penetration of the dye into the cell interior. In addition, ghost cells displayed low contrast in the DIC images compared to intact cells, due to the lack of cytosolic haemoglobin. These changes were not observed in the corresponding, polymer-free controls. In addition, TexasRed delivery to intact erythrocytes in the polymer-containing samples was not observed, instead, it appeared that under the studied parameters the full permeabilisation and leakage of cytosolic haemoglobin was a necessary step enabling subsequent molecule delivery in an all-or-nothing manner.

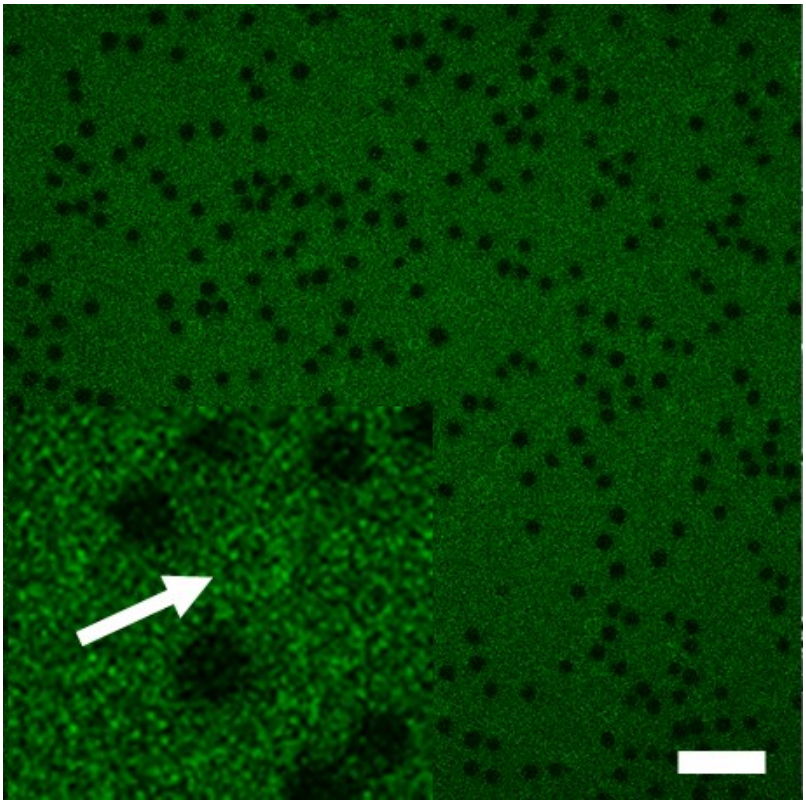


Figure 3-3. Binding of PP50 labelled with fluorescent dye Rhodamine110 (Ex 498/ Em 521 nm) on the membrane of ovine erythrocytes following a 3-minute treatment at 37^{o}C with the polymer at the concertation of 50 µg mL^{-1}. Analysed by confocal microscopy. Scale bar = 20 µm.

Furthermore, PP50 grafted with fluorescent dye Rhodamine110 (Ex 498/ Em 521 nm) was used to observe the behaviour of the polymer and its interaction with red blood cells (Figure 3-3). Following a 30-minute treatment a green ring

forming on a sub-population of the erythrocytes in the sample was observed, which could indicate the polymer binding onto the plasma membrane leading to ghost cell formation and loading of the cells with the molecules present in the extracellular buffer. These findings are also supported by previous results in which fluorescently labelled PP50 was observed to localise on the erythrocyte membrane, creating fluorescent rings, which were significantly brighter at mildly acidic pH, compared to pH 7.4 (Lynch et al., 2011).

3.2.3 Delivery of FITC-Dextran to erythrocyte ghosts

In order to expand the scope of potential applications of PP50, macromolecules were attempted to be delivered into ovine erythrocytes. Here, 10 and 150 kDa FITC-Dextran (Ex 490/ Em 525 nm) were used as surrogate of a small protein/peptide and an IgG antibody, respectively. It was discovered that while 10 kDa FITC-Dextran could penetrate inside the cells, the larger 150 kDa FITC-Dextran did not diffuse in as efficiently under the parameters used in the experiment (Figure 3-4). This might be explained by the potential slower diffusion rate of the larger dextran, or by the existence of a size threshold of the PP50-permeabilised erythrocyte membrane, which would allow for release of haemoglobin (64.5 kDa) from the cytosol and the delivery of the smaller, 10 kDa FITC-Dextran, but would limit the membrane crossing of any larger molecules.

The results above confirm previously published results reporting delivery of a small molecule to red blood cells and provide new evidence that delivery of larger molecules to erythrocyte ghosts is also possible. Further experiments could be carried out to optimise the number of ghost cells formed by varying parameters such as the treatment time as well as the polymer concentration and the polymer/cell ratio. In addition, it could also be possible to deliver macromolecules to erythrocytes without causing the leakage of haemoglobin and membrane collapse, associated with the formation of ghost cells, which would be more advantageous from the therapeutic perspective. Such delivery mode was not observed in the experiments discussed here, however, it was reported by Lynch et al. (2011), who delivered trehalose to intact human erythrocytes by using a higher proportion of red blood cells per available PP50.

Thus, the polymer/cell ratio was a crucial parameter in PP50-mediated payload delivery to erythrocytes, whereby a low polymer/cell ratio led to delivery into intact cells and a high polymer/cell ratio resulted in payload delivery via formation of ghost cells.

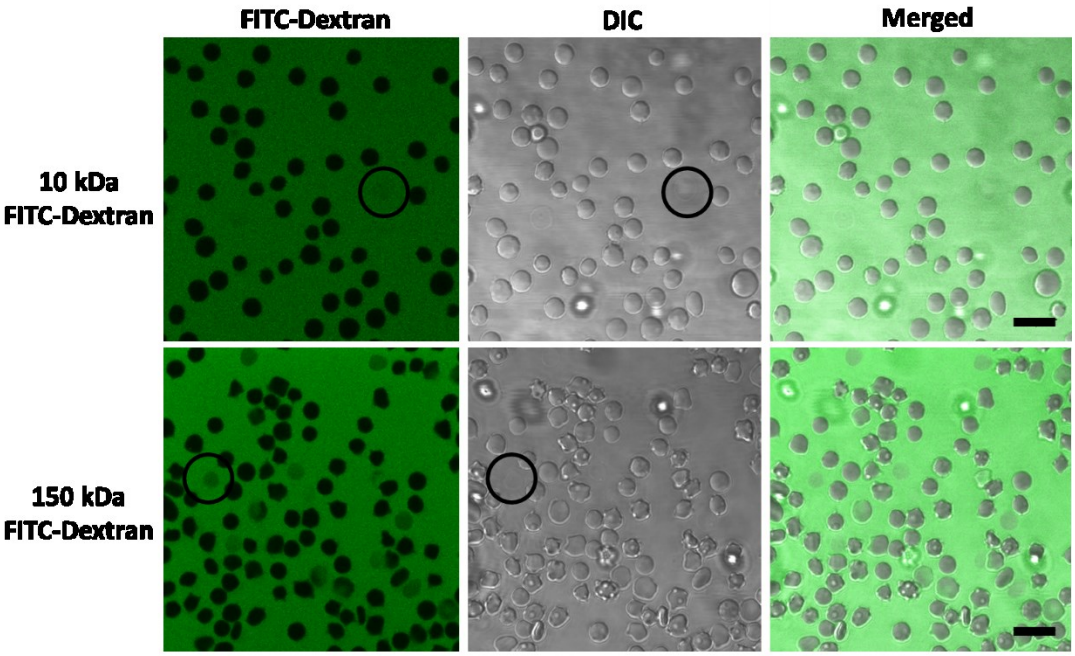


Figure 3-4. Delivery of 10 and 150 kDa FITC-Dextran (10 µM) to ovine erythrocytes following a 30-minute co-incubation with PP50 (100 µg mL^{-1}) at pH 6.5. Analysed by confocal microscopy. Scale bar = 10 µm.

3.2.4 Interaction between PP50 and nucleated mammalian cells

Successful transport of macromolecules to the cytosol of nucleated mammalian cells would be a major advantage of the PP50 delivery platform. In order to investigate how PP50 interacts with such cells, HeLa cells were treated with PP50 labelled with fluorescent dye Cy5 (Ex 633/ Em 647 nm) at pH 6.5. Confocal microscopy pictures obtained at the interval of 10 minutes following the addition of the polymer showed very quick initial PP50-Cy5 binding to the plasma membrane (≤5 minutes after addition) (Figure 3-5 A). The red fluorescent outline of the cells, which was brighter than the surrounding solution, suggesting that PP50-Cy5 binds preferably to the plasma membrane where it reached a concentration sufficient to produce this enhanced signal. It was then

possible to observe progressive migration of the fluorescent signal towards the centre of the cell as well as the gradual appearance of bright spots inside the cells, which could correspond to vesicle-based polymer internalisation or polymer aggregates present in the cytosol.

As reported by Mercado et al. (2016), PP50 is capable of cell entry by escaping the endosomal pathway following incubation at neutral pH in Soas-2 cells. In their study, Mercado et al. blocked specific endocytosis routes, such as clathrin-dependant endocytosis (using hypertonic sucrose), caveloin-mediated endocytosis (using m*β*cd and nystatin) as well as macropinocytosis (using rottlerin) and observed an inhibition of 30%, 50% and 26% in calcein uptake when co-incubated with PP50, respectively. The only partial inhibition of the 3 endocytosis pathways indicates that PP50 is internalised through multiple routes. This combination of cell entry mechanisms is also characteristic of cell penetrating peptides (Fonseca et al., 2009). In addition, Mercado et al. also observed that uptake of 150 kDa dextran, a marker of macropinocytosis, was increased by 35% when co-incubated with PP50 at neutral pH, compared to treatment with dextran alone. They also suggested that PP50 might be affecting the fluidity of the plasma membrane by changing the lipid bilayer viscosity or thickness, which has been reported to increase dextran transport (Ben-Dov and Korenstein, 2015; Mercado et al., 2016). Conducting the treatment at mildly acidic pH could have a synergistic effect of promoting direct membrane permeabilisation due to the earlier triggering of the polymer in the extracellular environment, compared to relying on the endosomal acidification for activating PP50.

As shown in Figure 3-5 B, treatment of HeLa cells with PP50-Cy5 for 1 h at pH 6.5 and pH 7.4 resulted in a similar pattern suggesting membrane binding and high levels of internalisation at both studied pH conditions. This is consistent with the findings of Ramadurai et al. (2017) discussed earlier, which reported that PP50 can bind to artificial membranes at both neutral and mildly acidic pH. More characterisation should be performed, such as the use of atomic force microscopy, to understand the precise polymer-membrane interactions and to explain how the polymer appears to be more membrane permeabilising at mildly acidic pH.

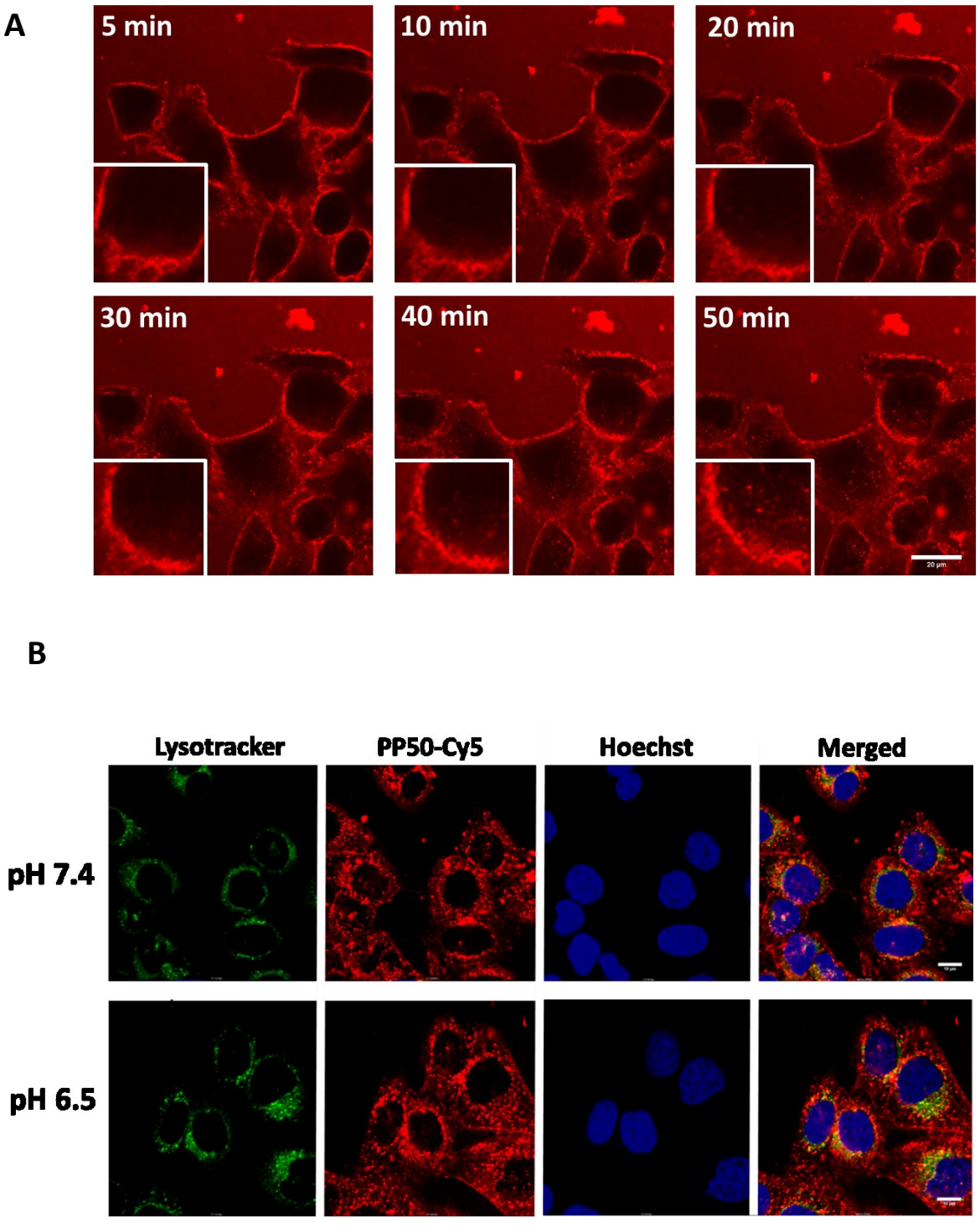


Figure 3-5. Polymer uptake by HeLa cells: (A) Uptake of PP50-Cy5 (0.5 mg mL^{-1}) over a period of 50 minutes after the addition of the polymer at extracellular pH 6.5, visualised by confocal microscopy. Scale bar = 20 μm. (B) Uptake of PP50-Cy5 (1 mg mL^{-1}) following a 1 h treatment at pH 6.5 or pH 7.4 and a further 30 min incubation period in serum-supplemented DMEM following a wash with PBS. Scale bar = 10 μm.

3.2.5 PP50 mediated delivery of FITC-Dextran to HeLa cells

Building on the previously described results indicating a level of delivery of the macromolecular dextran to erythrocytes treated with PP50 at pH 6.5, it was hypothesised that co-incubation of nucleated mammalian cells with a mixture of the polymer and this fluorescent payload should also result in payload delivery to the cytosol. In this instance, HeLa cells were co-incubated with FITC-Dextran and PP50-Cy5 at pH 6.5 for 1 h, after which the cells were analysed by confocal microscopy (Figure 3-6).

FITC-Dextran was used as the model payload as fluorescent dextrans are often used to investigate the permeability of the plasma membrane thanks to their properties such as the weak negative charge, contributing to low non-specific cell surface binding, the ease of detection using methods such as flow cytometry and confocal microscopy, as well as the availability of dextran with different molecular weights at a low cost (Sharei et al., 2013; Li et al., 2015b). To serve as a surrogate for protein delivery, a 150 kDa FITC-Dextran was used in the initial characterisation. This molecular weight corresponds to that of IgG antibodies.

One disadvantage of using FITC as a molecular probe is its pH-sensitive property (Hermanson, 2013). The fluorescence of FITC has been reported to decrease with lowering pH environment, with fluoresence yield obtained at pH 7.4 higher than that at the midly acidic pH equal to 6.0 (Lorenz and Gruenstein, 1999). This can lead to the underestimation of the fluorescent signal of FITC-Dextran present in endosomes and lysosomes, which exhibit lower pH compared to the neutral cytosol and shoul be taken into account when analysing the data presented herein.

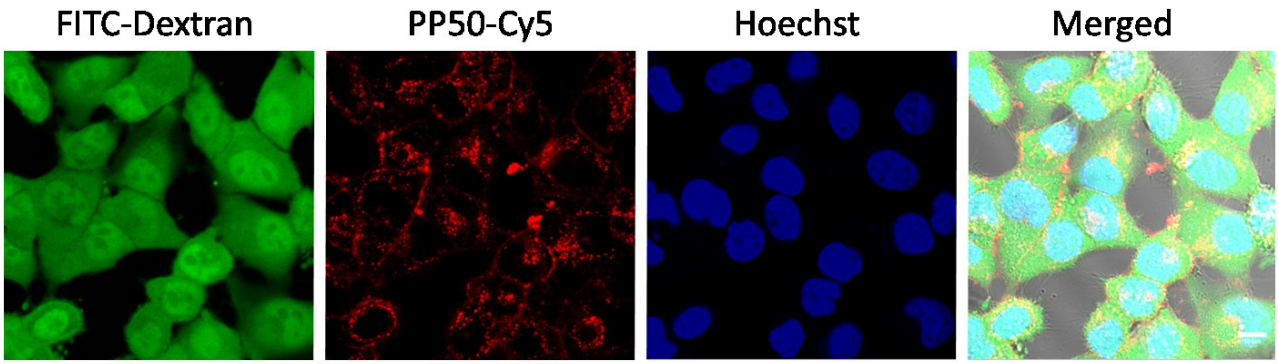


Figure 3-6. Delivery of 150 kDa FITC-Dextran (10 μM) to HeLa cells following co-incubation with Cy5-labelled PP50 (1 mg mL^{-1}) for 1 h at pH 6.5, visualised by confocal microscopy. Scale bar = 20 μm

The green fluorescence signal corresponding to FITC-Dextran was found to be diffused throughout the cytosol, suggesting successful delivery across the plasma membrane. Interestingly, the model payload was consistently found to co-localise with Hoechst. Moreover, the green signal in the nuclear area can be distinguished from the green fluorescence in the cytosol as it appears more dense and brighter. The reason for this was not clear.

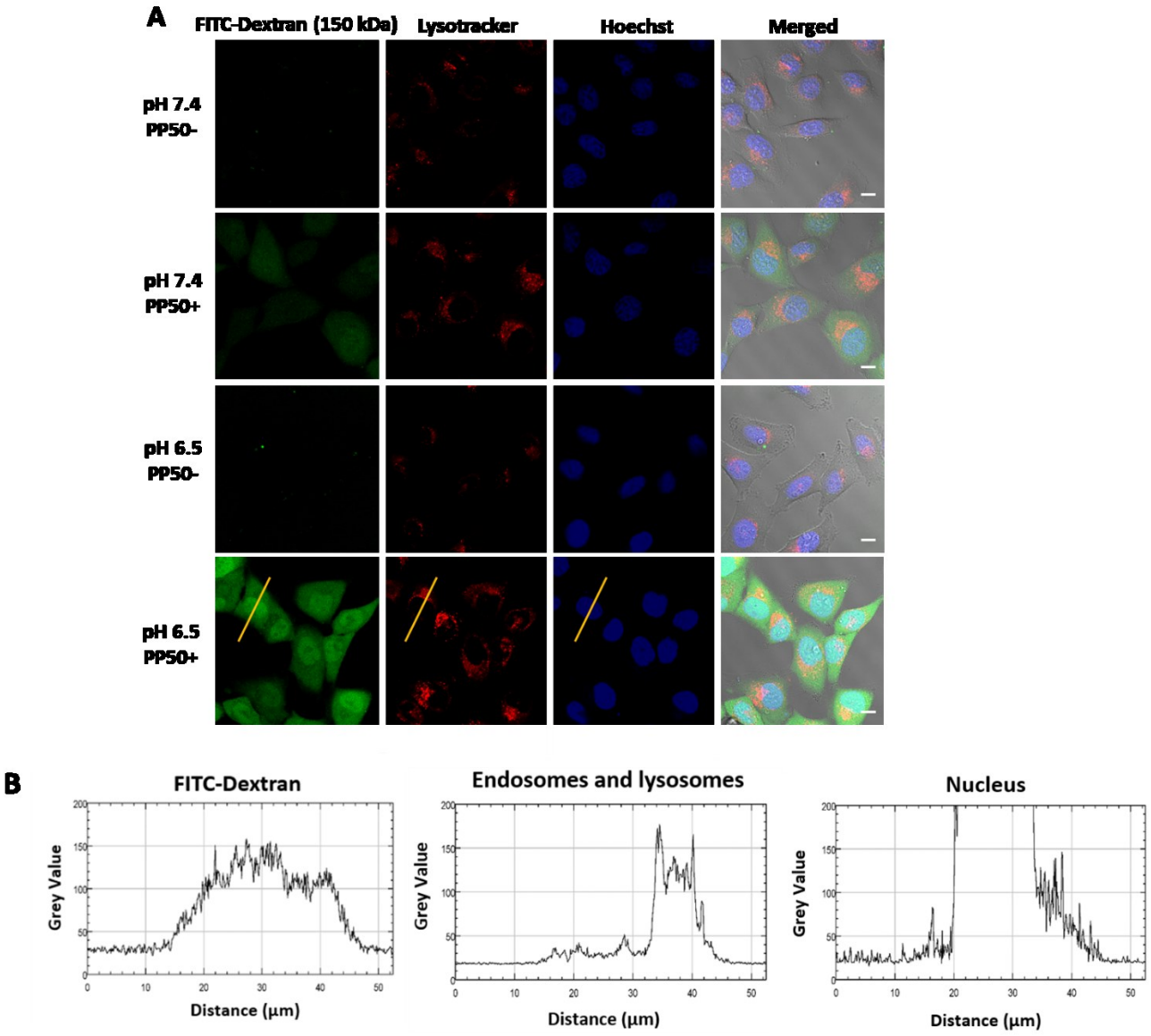


Figure 3-7. (A) Intracellular delivery of 150 kDa FITC-Dextran (10 µM) to HeLa cells by co-incubation with PP50 (0.5 mg mL^{-1}) at pH 7.4 and pH 6.5 for a period of 30 minutes and corresponding polymer-free negative controls (FITC-Dextran only) visualised by confocal microscopy (scale bar = 10 µm) and (B) fluorescence intensity profiles in the cross-sectional area indicated by the yellow lines in the green, red and blue channels, created using ImageJ.

Based on the previously reported findings on the enhanced interaction of PP50 with the membrane at mildly acidic pH, the delivery efficiency was hypothesised to be higher at a lower pH, such as pH 6.5, than at neutral pH. To test this, HeLa cells were co-incubated with 150 kDa FITC-Dextran in either polymer-containing or polymer-free PBS at pH 6.5 and pH 7.4 and analysed using confocal microscopy after a 30-minute treatment (Figure 3-7). The images suggest that

in both tested pH environments the intracellular delivery of FITC-Dextran was successful compared to the polymer-free controls, manifesting in a diffused green fluorescent signal in the cytosol. The uniformity of the cytosolic green fluorescence and the fact that it was not present in the same punctate pattern as the endosomal-lysosomal stain LysotrackerRed (red channel) is indicative of a high level of endosomal escape, or that the problem of endosomal entrapment is overcome in another manner, such as via direct permeabilisation of the plasma membrane (Martens et al., 2014; Erazo-Oliveras et al., 2014).

As expected, treatment at the mildly acidic pH produced a stronger fluorescent signal than that at the neutral pH, which was further confirmed by flow cytometry showing a trend of increased cell brightness when comparing the cells treated at pH 6.5 and pH 7.4 (Figure 3-8). Again, co-localisation of the fluorescent dextran with Hoechst at both pH 7.4 and pH 6.5 was observed, suggesting presence of FITC in the nuclear area. This trend was more pronounced at pH 6.5. This was further confirmed by creation of Z-stack 3D projections showing localisation of the green fluorescent signal inside the nucleus. (Figure 3-9).

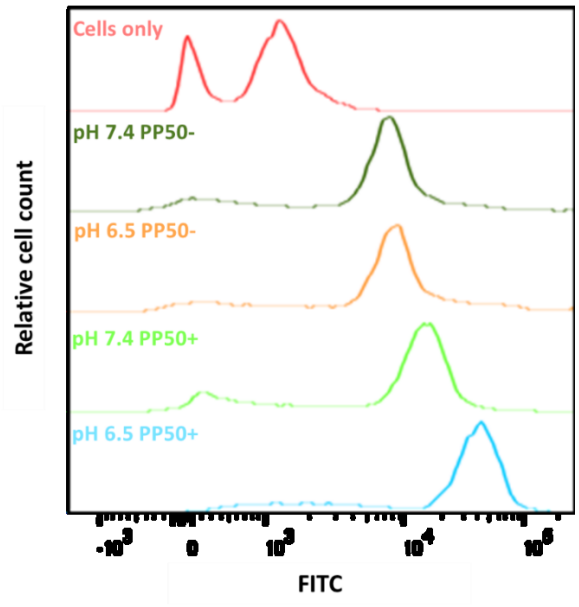


Figure 3-8. Flow cytometry analysis of HeLa cells illustrating fluorescence intensity of intracellular FITC after delivery of FITC-Dextran (5 μM) to HeLa cells by co-incubation with PP50 (0.5 mg mL^{-1}) at pH 6.5 and pH 7.4 for 30 minutes. Results are based on a minimum of 10,000 events analysed.

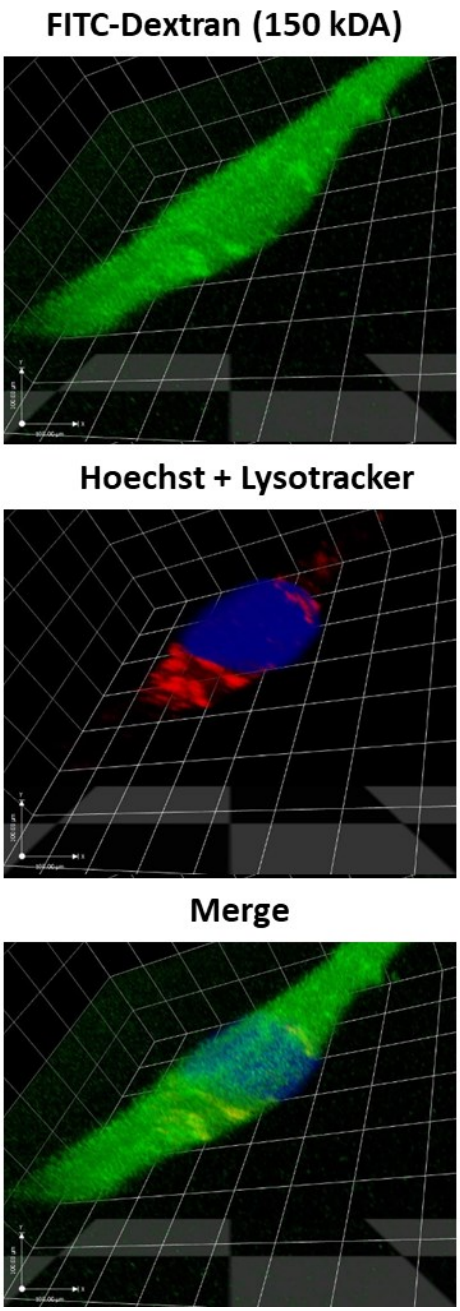


Figure 3-9. 3D projection created using Z-stack obtained via confocal microscopy illustrating the diffused nature of the fluorescent signal throughout the cytosol and the nucleus and the co-localisation of the green signal with blue DNA stain Hoechst following the intracellular delivery of 150 kDa FITC-Dextran (10 μM) to HeLa cells by co-incubation with PP50 (0.5 mg mL^{-1}) at pH 6.5 for 30 minutes.

3.2.6 The effect of temperature on the PP50-mediated delivery

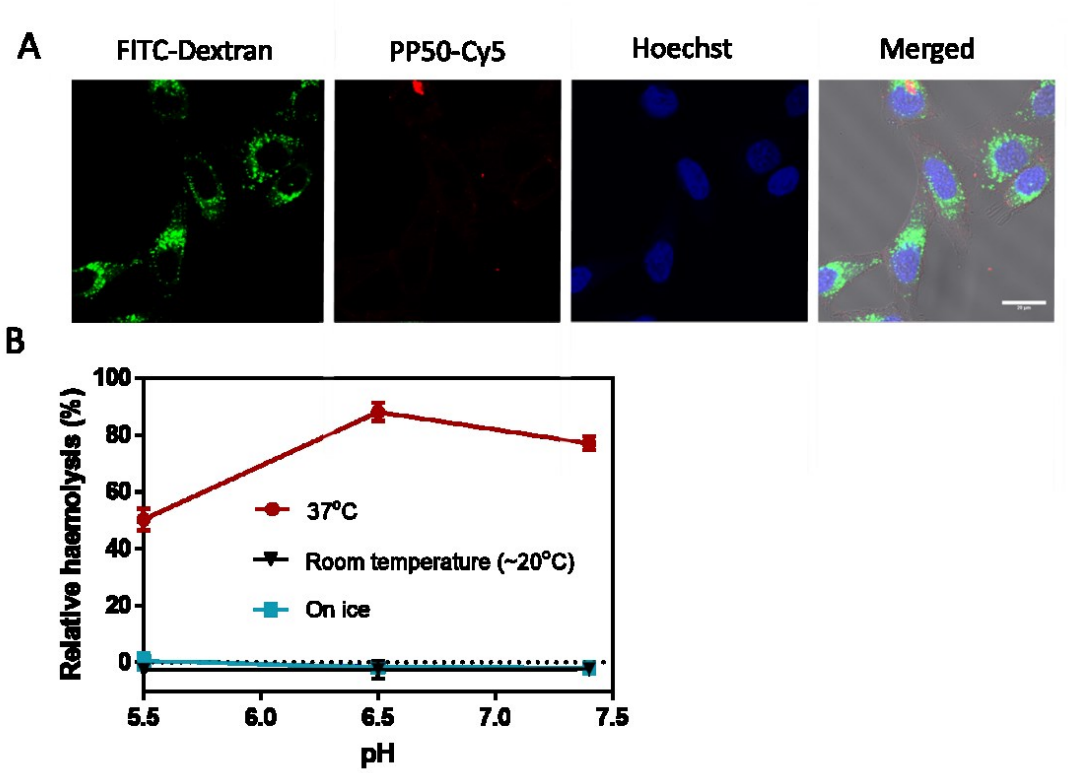


Figure 3-10. (A) Delivery of 150 kDa FITC-Dextran (10 μM) to HeLa cells by co-incubation with PP50-Cy5 (1 mg mL^{-1}) at pH 6.5 for 30 minutes on ice, visualised by confocal microscopy. Scale bar = 10 μm. (B) Haemolysis of ovine erythrocytes following a 1 h incubation with PP50 (100 μg mL^{-1}) at 37°C (water bath), room temperature (20°C, benchtop) as well as on ice. Mean ± standard deviation (SD), n = 3.

It has been reported that a temperature below 37°C can inhibit or block energy-dependent transport processes across the plasma membrane, including the endosomal pathway (Punnonen et al., 1998). When HeLa cells were treated with FITC-Dextran and PP50-Cy5 on ice, no evidence of successful delivery of the payload to the cytosol was observed (Figure 3-10). Punctate areas observed in the green channel were observed, which could correspond to FITC-Dextran taken up by the cells after the treatment on ice had finished due to a potential incomplete wash with PBS. In contrast, no membrane binding or internalisation of the fluorescent PP50 was observed. This could suggest that PP50 internalisation is an energy-dependant process.

To elucidate this, a further experiment was designed in which ovine erythrocytes were treated with PP50 at 37°C, room temperature and on ice. Only the treatment at 37°C, corresponding to the temperature used for delivery to HeLa cells in the previously described figures, caused significant, pH-sensitive haemolysis, reaching up to 90% at pH 6.5. There was no detectable haemolysis in the samples treated with the polymer at room temperature and on ice, compared to appropriate positive controls. It has been reported that endocytotic pathways become inhibited at a temperature below 26°C (Punnonen et al., 1998), which could potentially explain the lack of cytosolic payload delivery in HeLa cells, assuming the process relies heavily on endocytosis, as no FITC-Dextran and PP50-Cy5 were taken up together during the treatment on ice. However, as the levels of endocytosis in mature erythrocytes are normally low, the fact that no haemolysis occurred at room temperature could also suggest that in addition to pH sensitive behaviour, PP50 could also display a thermo-sensitive behaviour in which it does not cause membrane permeabilisation at lower temperatures. This could be reliant on the properties of the phospholipid bilayer since it has been reported that lipid diffusion retardation, which is associated with polymer binding, is directly proportional to temperature in studies of the interactions of a triblock copolymer with synthetic membrane models (Rossi et al., 2011; Ramadurai et al., 2017). In addition, naturally occurring lateral lipid diffusion is also a function of temperature (Bag et al., 2014). It is therefore possible that the decreased membrane fluidity and increased stiffness could be one of the factors preventing membrane permeabilisation, as remodelling of local lipid architecture upon polymer binding is crucial to the proposed permeabilisation by membrane thinning, as described above.

3.2.7 The importance of endosomal acidifaction on PP50-mediated deliviery

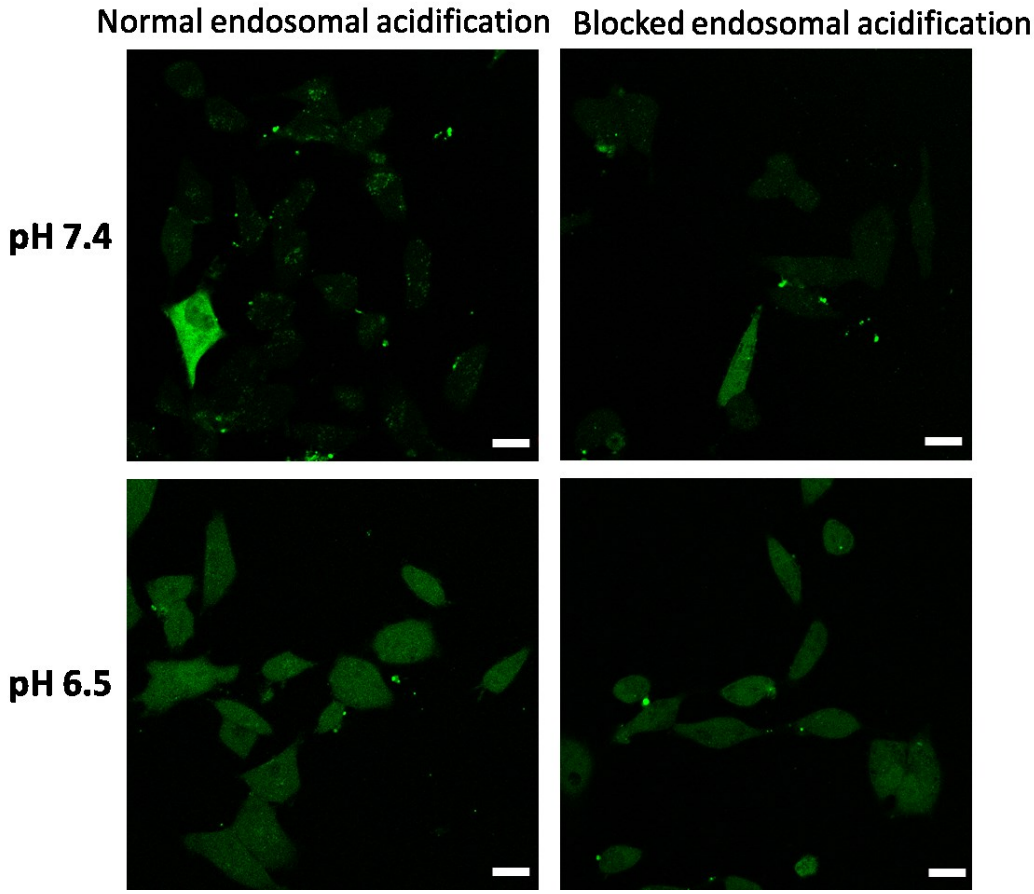


Figure 3-11. Delviery of FITC-Dextran (10 µM) to HeLa cells by co-incubation with PP50 (1 mg mL^{-1}) in 1 h treatment at pH 6.5 and pH 7.4 and with- or without blocking the endosomal acidification by addition of 10 µM NH_4Cl 1 h prior to the treatment, during the treatment, and subsequent to the treatment duirng analysis. The cells were visualised by confocal microscopy. Scale bar = 20 µm.

The delivery pathway was further investigated by blocking the acidification by addition of ammonium chloride prior to, during and following the treatment with FITC-Dextran and PP50 and the results were analysed by confocal microscopy (Figure 3-11). It was observed that the blocking of the endosomal acidification pathway did not contribute substantially to preventing the delivery of FITC-Dextran using PP50 at pH 6.5, as a diffuse green fluorescent signal was observed in the cytosol of both cells incubated with or without ammonium chloride. This could suggest that under the studied conditions dextran delivery

relies to a considerable extent on a pathway which does not require endosomal acidity for activation of the membrane permeabilising activity of PP50.

One can therefore theorise that the efficient intracellular delivery of macromolecular dextran observed at pH 6.5 is most likely attributed to (i) binding to the plasma membrane, causing localised membrane thinning and direct membrane permeabilisation, (ii), efficient endosomal escape, whereby PP50 binds to the plasma membrane and is taken up in its membrane active form, leading to rapid destabilisation of the endosomal vesicles and leakage of their content into the cytosol, or (iii), a combination of these two routes. In the case of route (ii), standard endosomal acidification is not quintessential to allow PP50-mediated membrane permeabilisatiion, as the polymer will have been protonated in the mildly acidic extracellular space and retain this characteristic upon being engulfed into endosomes. When taken up at pH 7.4, the polymer might rely more heavily on the various endocytosis pathways for delivery, and thus requires a longer time until its protonation in the progressively more acidic endosomes. In addition, the strength of the fluorescent signal in the samples with normal endosomal acidification obtained here was weaker than that reported in Figure 3-6, despite using the same delivery parameters. This was thought to be the result of batch-to-bath variation of biological samples.

3.2.8 The effect of payload concentration

The parameters such as treatment time, polymer and payload concentration as well the as buffer pH could have an important effect on the delivery process and thus should be studied in more detail. First, the effect of the extracellular concentrations of the fluorescent payload FITC-Dextran within the range of 0.1-10 μM on the amount of intracellular signal produced after PP50-mediated delivery to HeLa cells was investigated. Unsurprisingly, the strength of the fluorescent signal, determined by flow cytometry, was proportional to the concentration of FITC-Dextran present during the co-incubation with PP50 (Figure 3-12). As described previously, the delivery process was more effective at pH 6.5 than at pH 7.4, which was also observed in this experiment. This enhanced delivery effect in mildly acidic pH scaled down with the payload

concentration, and was still observable at the FITC-Dextram` concentration of 0.1 μM. This experiment illustrates the ability to influence and to some extent, control, the intracellular concentration of the desired payload by varying its extracellular concentration during the delivery process. As the delivery protocol relies on simple co-incubation of the two components, rather than covalent conjugation, this can be done independently of modulating the polymer concentration.

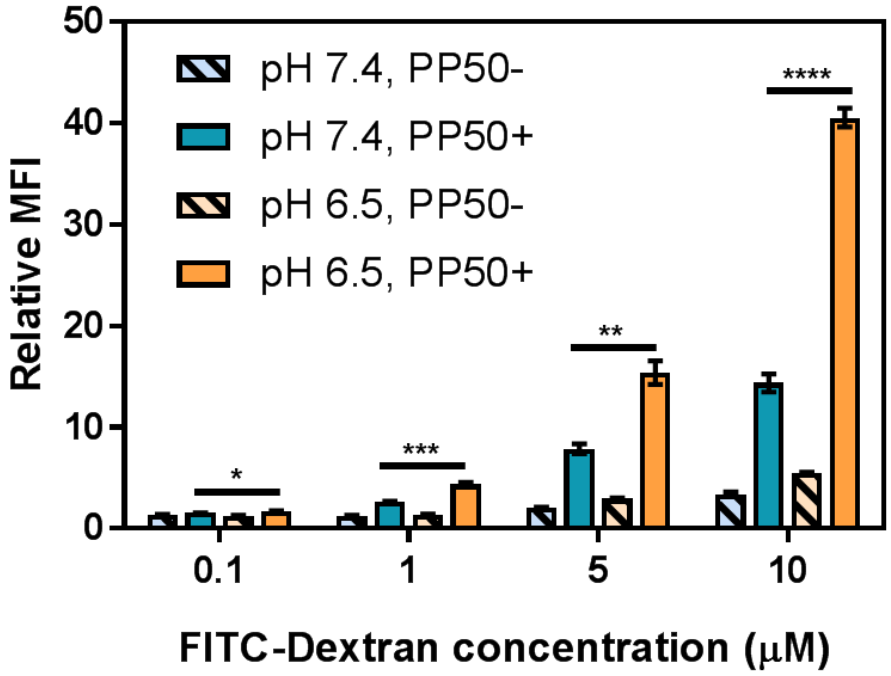


Figure 3-12. Relative median cell fluorescence, analysed by flow cytometry, following a treatment with 150 kDa FITC-Dextran at various concentrations using a fixed concentration of PP50 (0.5 mg mL^{-1}) and a treatment time of 30 minutes. Delivery at pH 6.5 and 7.4, as well as corresponding polymer-free controls, are compared. Mean ± SD, n = 3. Statistical comparison between cells treated with FITC-Dextran and PP50 at pH 7.4 and pH 6.5 at the set payload concentrations was performed using two-tailed unpaired Student's t-test.

3.2.9 The effect of polymer concentration

Another crucial factor determining delivery efficiency is the concentration of the delivery agent. Higher polymer concentration should provide increased membrane binding and permeabilisation (Chen et al., 2009c). Such proportional relationship has been previously reported for other delivery agents, such as poly(acrylic acid)s (Murthy et al., 1999) as well as cell penetrating peptides (Lee

et al., 2010). To test the correlation between PP50 concentration and delivery efficiency, HeLa cells were co-incubated with 150 kDa FITC-Dextran and a polymer concentration range between 50-2000 μg mL^{-1} (Figure 3-13). Interestingly, even the treatment with the lowest concentration of PP50 used here, 50 μg mL^{-1}, resulted in a detectable intracellular fluorescence which was 2-fold brighter at mildly acidic pH than that at neutral pH.

As expected, the median value of cell fluorescence is dependent on polymer concentration and continues increasing up until the polymer concentration of 1 mg mL^{-1}, whereby a plateau is reached. This suggests that under specific conditions there exist a polymer saturation concentration and increasing the amount of polymer in solution will not have a further delivery enhancement effect. This point might be when most of the polymer binds to all of the space available on the plasma membrane initially and would therefore depend on the cell seeding density, cell shape and type, as some cell types might turn over the bound polymer faster than others.

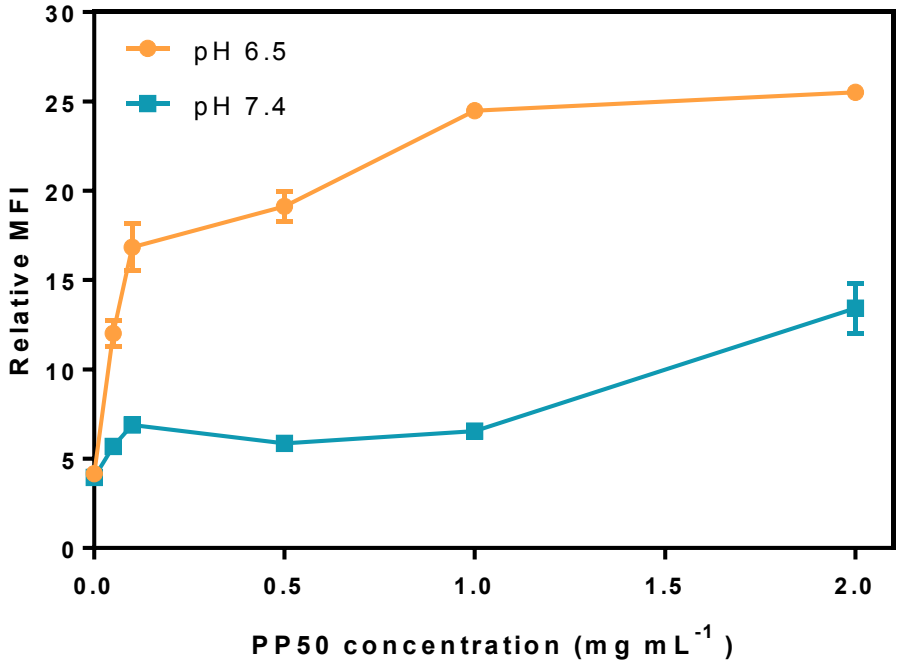


Figure 3-13. Relative median cell fluorescence, analysed by flow cytometry, following a 30-minute treatment with a fixed concentration of FITC-Dextran (10 μM) and PP50 concentration within the range of 50-2000 μg mL^{-1}. Delivery at pH 6.5 and 7.4 is compared. Mean ± SD, n = 3.

3.2.10 The effect of treatment time

The treatment time and its influence on delivery efficiency of FITC-Dextran was also studied (Figure 3-14). The delivery process was observed to be the most efficient within the first 1 h, and it only took between 5-15 minutes for the fluorescent signal to be present at detectable levels in the intracellular space. This fast appearance of such signal suggests that the mechanism responsible for delivery acts very quickly, and could rely on the previously described permeabilisation directly at the plasma membrane or very efficient escape from the endosomal vesicles. The strength of the fluorescent signal was further enhanced by increasing the treatment time up to 3 h and could perhaps be enhanced even further, however, the potential starvation effect of keeping the cells in PBS, which lacks nutrients, for longer periods of time could prevent extending the treatment time considerably.

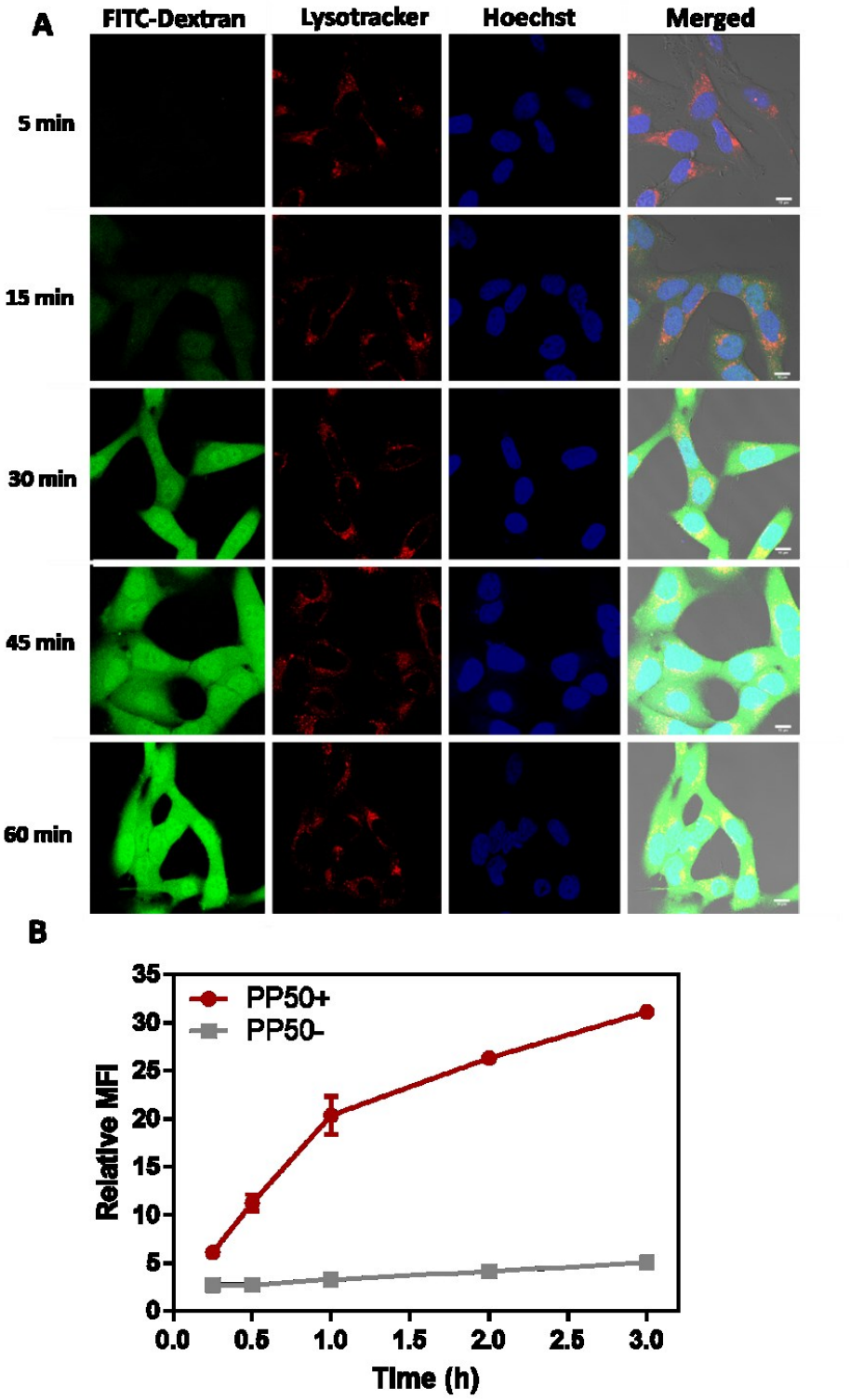


Figure 3-14. Intracellular fluorescence visualised by confocal microscopy, following treatment with a mixture of PP50 (0.5 µg mL^{-}) and 150 kDa FITC-Dextran (2.5 µM) at pH 6.5 for different time periods within the range of 15-180 minutes, compared to polymer-free samples. Scale bar = 10 µm. (B) Relative median cell fluorescence, analysed by flow cytometry, following delivery of 150 kDa FITC-Dextran at pH 6.5 using PP50 (0.5 µg mL^{-1}) and different treatment times. Mean ± SD, n = 3.

3.2.11 The effect of extracellular pH

Lynch et al. (2011) decided to use pH 7.05 to promote mild, yet efficient delivery of small molecule sugar, trehalose, to ovine erythrocytes. In the majority of the presented experiments pH 6.5 was used, which corresponds to the pH of maturing endosomes and some hypoxic tumours, to trigger the membrane-permeabilising ability of the polymer (Kneipp et al., 2010; Anderson et al., 2016). It was demonstrated, however, that lowering the extracellular pH further to pH 5.5-6.0 can further enhance the delivery process to nucleated cells (Figure 3-15). In contrast to the standard cell penetrating peptides, which require additional modifications to become pH-responsive, extracellular pH can be used as a trigger and enhancer of the PP50-mediated payload delivery, with pH lower than pH 6.5 being used in certain circumstances to further increase delivery efficiency. The pH of the PP50- and payload-containing buffer or medium applied to the cells is however limited by its potential cytotoxicity. Mildly acidic pH 6.3 buffer was shown to affect protein synthesis in fibroblast cells, and more acidic buffers with pH equal to pH 5.2 and pH 3.8 were demonstrated to cause 47% and 90% cell death after 3 hours of incubation (Lan et al., 1999). Increasingly acidic buffers can also cause PP50 precipitation (Chen et al., 2009c), limiting the availably of the polymer in solution and potentially causing unwanted, cytotoxic interactions with the cells.

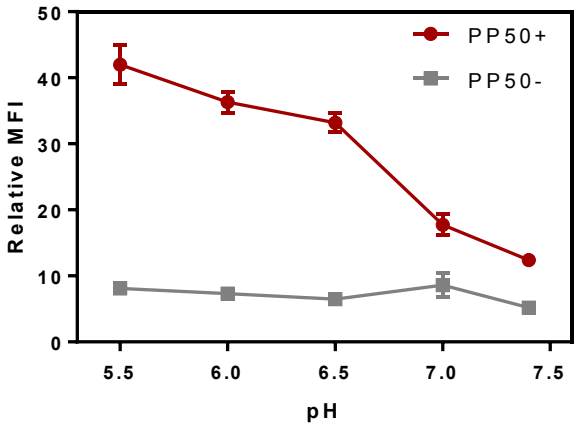


Figure 3-15. Relative median cell fluorescence, analysed by flow cytometry, following delivery of 150 kDa FITC-Dextran (5 μM) using PP50 (0.5 mg mL $^{-1}$) in different pH environments ranging from pH 5.5 to 7.4. Polymer-containing and polymer-free samples are compared. Mean ± SD, n = 3.

3.2.12 Cytotoxicity of PP50-mediated delivery

Finally, safety and lack of cytotoxicity are one of the main requirements for a successful delivery system. As PP50 might deliver the desired cargo by direct membrane permeabilisation or by disrupting endosomes, the cytotoxic effects of this delivery system should be investigated, especially since endosomal leakage has been linked to apoptosis (Erazo-Oliveras et al., 2014).

As reported elsewhere (Chen et al., 2009c; Mercado and Slater, 2016a), PP50 is majorly non-cytotoxic to mammalian cells at neutral pH. In a thorough study on the cellular effects of PP50 on Saos-2 cells, Mercado and Slater (2016a) used various analysis methods, such as trypan blue, MTS, LDS and Annexin V assays as well as microscopy and reported that incubation with the polymer did not bring about any major cytotoxic or morphological effects on the tested osteosarcoma cells at the concentrations used. The reported non-cytotoxicity at neutral pH was also confirmed here by incubating HeLa cells with PP50 at various concentrations for 24 h in DMEM, and by analysing cell survival using AlamarBlue assay (Figure 3-16 A).

In addition, it was necessary to show if the delivery process in which a model payload is introduced and the growth medium is replaced with a harsher, serum-free PBS at a mildly acidic pH 6.5 would have any obvious negative effects on the cells. Using HeLa cells and 10 µM 150 kDa Dextran with a varied PP50 concentration minimal cytotoxicity at both pH 6.5 and pH 7.4 was observed, which were compared here, including at the highest polymer concentration tested of 2000 µg mL^{-1} (Figure 3-16 B). The cell survival dropped to 93% and 87% for pH 7.4 and pH 6.5, respectively, after a prolonged treatment time of 3 h (Figure 3-16 C). These results suggest that PP50-mediated delivery of macromolecules is generally well tolerated by HeLa cells. As opposed to ovine erythrocytes, treatment of nucleated cells with PP50 did not lead to a complete collapse of the plasma membrane which is associated with haemolysis. In contrast, the binding of the polymer on the plasma membrane appeared not to affect the cellular architecture in any major way which could result in cell death.

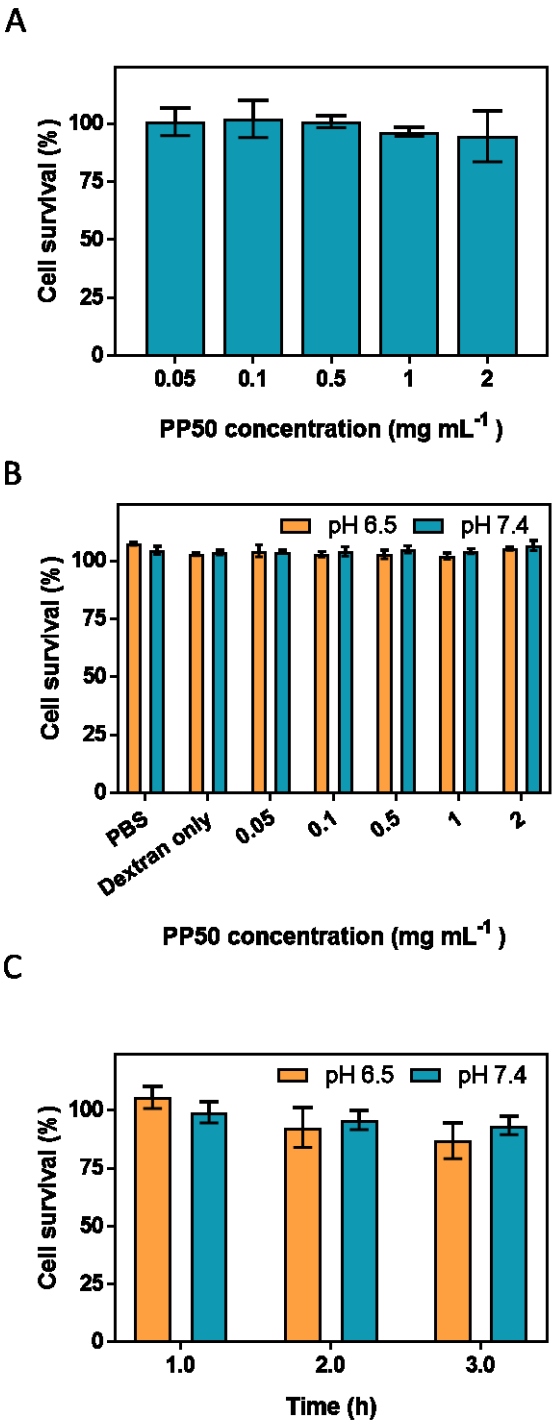


Figure 3-16. (A) Cell survival after a 24 h treatment of HeLa cells with different concentrations of PP50 in DMEM (neutral pH), analysed with AlamarBlue assay (B) Cytotoxicity of the delivery process of 150 kDa Dextran (10 μM) after incubation with PP50 (different concentrations used) for 30 minutes (PBS, pH 6.5 and pH 7.4), determined using AlamarBlue assay and (C) cytotoxicity of the delivery process determined using AlamarBlue assay after incubation with PP50 (1 mg mL^{-1}) and 150 kDa Dextran (10 μM) at pH 6.5 and 7.4, comparing different treatment times (PBS, pH 6.5 and pH 7.4). Mean ± SD, n = 3.

3.2.13 The interaction between PP50 and model payload

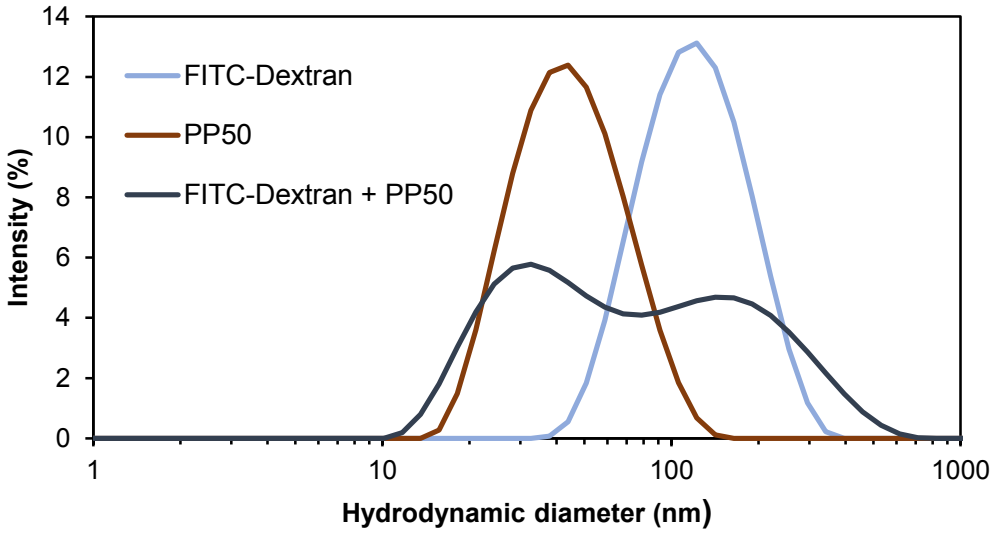


Figure 3-17. Hydrodynamic particle size of FITC-Dextran (150 kDa), PP50 and FITC-Dextran + PP50 mixture at pH 6.5, determined via dynamic light scattering. PP50 concentration was 0.5 mg mL^{-1} and FITC-Dextran concentration was 10 μM.

Table 3-1. Summary of data by analysis of FITC-Dextran (150 kDa) and PP50 using dynamic light scattering and Zeta potential. PP50 concentration was 0.5 mg mL^{-1} and FITC-Dextran concentration was 10 μM.

Sample	Diameter (nm)	Polydispersity (PDI)	Zeta Potential (mV)
FITC-Dextran	94.9	0.268	- 8.8 ± 1.0
PP50	41.9	0.203	- 16.8 ± 2.3
PP50 + FITC-Dextran	55.0 (average of two peaks)	0.456	-13.9 ± 1.9

It was important to characterise the interaction between the delivery agent, PP50, and the macromolecular cargo. The interaction between PP50 and FITC-Dextran was measured using DLS, by comparing the hydrodynamic sizes of PP50 (0.5 mg mL^{-1}) mixed with FIC-Dextran (5 μM) in aqueous solution to those of the two components alone.

The analysis of the size distribution by intensity revealed that the average hydrodynamic size of PP50 and FITC-Dextran was equal to 41.9 (PDI 0.203) and 94.9 (PDI 0.268), respectively (Table 3-1). The average size of the particles in the mixture of those two components was equal to 55.0 (PDI 0.456). The size distribution and the shape of the profile of the PP50 + FITC-Dextran mixture closely resembled the size profiles of the two components alone, with distinct peaks around 30 and 105 nm (Figure 3-17). Along with the increased polydispersity index, this could suggest that there was limited interaction between PP50 and FITC-Dextran subsequent to mixing and the two components were present in the solution without associating or forming complexes which would lead to a more radical change in the particle size and distribution.

This effect could arise due to the electrostatic repulsion between FITC-Dextan and PP50. Zeta potential analysis of both components confirmed their negative charge, which was equal to -8.8 ± 1.0 mV and -16.8 ± 2.3 mV for FITC-Dextran and PP50, respectively (Table 3-1). Interestingly, this did not prevent successful intracellular delivery and overcoming the barrier posed by the plasma membrane, which also harbours a net negative charge.

These results, however, might require confirmation via complimentary methods, such as electron microscopy to elucidate the structure of PP50 and any potential polymer-payload interactions when mixed together. PP50 might interact with different payloads in different ways, based on their size, hydrophobicity/hydrophilicity, charge and a number of other chemical and physical properties. Considering the myriad of possible payloads which the polymer could be used to deliver, it might be beneficial to investigate such interactions by the end user to establish compatibility.

3.3 Conclusions

This chapter aimed to investigate the interaction between PP50 and the plasma membrane in the context of intracellular delivery, as well as to investigate the parameters influencing the delivery process.

Firstly, PP50 was shown to interact with ovine erythrocytes and to bring about the formation of ghost cells at the mildly acidic pH 6.5, where PP50 as shown to have the highest membrane permeabilising activity, as illustrated by the haemolysis assay. Delivery of the small molecule dye TexasRed as well as macromolecular FITC-Dextran to ovine erythrocytes was also demonstrated.

Secondly, PP50 labelled with the fluorescent label Cy5 was shown to be internalised by the cells. Treatment of HeLa cells with a mixture of PP50 and 150 kDa FITC-Dextran resulted in intracellular delivery of the fluorescent macromolecule and the delivery efficiency was higher at mildly acidic pH, perhaps due to a direct permeabilisation of the plasma membrane by PP50 activated by the extracellular pH. The transient mildly acidic extracellular pH during the treatment can enable for a level of delivery control in potential future experimental design. This enhanced delivery in mildly acidic extracellular environment can be further investigated for development of polymer-drug conjugates for targeted *in vivo* delivery to hypoxic tumours, as will be discussed in the following chapters.

Finally, a number of different parameters which dictate the efficiency of the delivery process were studied. PP50-mediated delivery was shown to cause minimal cell perturbation and toxicity while enabling fast and efficient delivery. In addition, intracellular concentration of the desired payload can be controlled by changing the payload concentration present during the treatment, independently of PP50 concentration. PP50 concentration or treatment time can also be varied to achieve a desired level of intracellular delivery

The findings presented in this chapter provided a foundation for the following experiments in which payload delivery to nucleated mammalian cells was made possible by co-incubation with a mixture of PP50 and the cargo while utilising the pH effect to enhance the delivery efficiency.

Chapter 4 - Delivery by co-incubation – technology versatility and investigation of possible uses

4.1 Introduction

Efficient delivery of macromolecules to the intracellular compartments for in vitro and ex vivo applications remains a challenge, mostly due to the difficult task of overcoming the barriers posed by the plasma and endosomal membranes and degradation in lysosomes (Canton and Battaglia, 2012; Stewart et al., 2016b). Many delivery systems have been proposed in the last decades, however, most lack versatility or efficiency to become widely applicable (Khalil et al., 2006; Stewart et al., 2016b). Solving the problem of the rate-limiting entrapment of macromolecular cargo in the endosomal pathway, leading to their ultimate degradation in lysosomes, would unlock a large number of potential uses in the fields of fundamental biology and medicine (Stewart et al., 2016b).

A universal and versatile next generation delivery agent would therefore prove hugely useful. Such delivery agent should possess seven characteristics, as proposed by Stewart et al. (2016b): (i) compatibility with various cell lines, (ii) compatibility with many different payloads i.e. material independence, (iii) the ability to allow for intracellular targeting, (iv) possibility of dosage control, (v) lack of cytotoxicity, (vi) potential and ease of scalability and (vii) low cost. In addition, traits such as trigger-sensitivity and excellent performance for delivery of proteins, which remain a problematic cargo, would be highly desirable (Guillard et al., 2015).

PP-polymers have been successfully used for delivery of siRNA by conjugation (Khormaee et al., 2013), functionalization of liposomal membranes (Chen and Chen, 2016) and delivery of an apoptotic protein by inducing endosomal escape (Liechty et al., 2009). PP50, a member of the PP-family, has been used to deliver trehalose to human erythrocytes and osteosarcoma cells at a mildly

acidic pH for cryo-preservation applications, while causing minimal cytotoxicity (Lynch et al., 2011; Mercado and Slater, 2016b). The previous chapter discussed the mechanisms responsible for the efficient intracellular delivery of model macromolecules by co-incubation with PP50 and the characterisation and optimisation of this process. This chapter will focus on investigating the versatility of the PP50-platform as an *in vitro* and *ex vivo* delivery agent.

Delivery of a model, antibody-sized fluorescent payload to different cell types will be discussed, followed by experiments on delivery to 3D multicellular spheroids and delivery of macromolecular payloads of different type and size. The effect of serum on the delivery process will be also investigated. Furthermore, PP50-mediated intracellular delivery of an apoptotic peptide and its effect will be studied in detail and compared to other commonly used delivery technologies, which will aim to place the PP50 platform in a wider context. Finally, PP-mediated payload loading of extracellular vesicles for potential *in vivo* drug carrier applications will be assessed. The presented results will provide information and aid in development of PP50 as a potential bio-inspired, multi-use, next generation delivery agent, compatible with many model and functional macromolecular payloads and enabling cytosolic delivery to different cell types.

4.2 Results and Discussion

4.2.1 Delivery to different cell lines

In order to prove wide applicability of PP50 as a delivery agent the polymer's ability to deliver a model payload into a number of nucleated mammalian cell types, possessing different characteristics, such as adherent and suspension cell lines, cancerous and non-cancerous cells, stem cells as well as drug resistant cell lines were investigated. In this case, delivery of IgG antibody-sized FITC-Dextran (150 kDa) was tested in 9 cell types by co-incubation with PP50 in mildly acidic condition (pH 6.5) to activate the polymer and analysed using confocal microscopy. The cell types used in this experiment are shown below in Table 4-1.

Table 4-1. Cells types used for PP50-mediated delivery of FITC-Dextran and their details.

Name	Origin	Cell type	Tissue and cell morphology
HeLa	Human	Adherent cancerous	Cervix, epithelial
A549	Human	Adherent cancerous	Lung, epithelial
MES-SA	Human	Adherent cancerous	Uterus, epithelial
MC 3t3	Mouse	Immortalised, suspension	Bone/calvaria, preosteoblast
CHO	Chinese hamster	Adherent, immortalised non-cancerous	Ovary, epithelial
MES-SA/Dx5	Human	Adherent cancerous, Dox resistant	Uterus, epithelial
SU-DHL-8	Human	Immortalised, suspension, non-cancerous	B-lymphocytes, lymphoblast
RAW 264.7	Mouse	Immortalised, mixed adherent and suspension, non-cancerous	macrophage/monocytes
hMSC	Human	Primary, stem cells	Bone marrow, stem cell

The co-incubation with PP50 at pH 6.5 resulted in successful delivery of 150 kDa FITC-Dextran to the cytosol in all 9 of the cell types used in the experiment, manifesting in a uniform, diffused green fluorescent signal in the cytosol (Figure 4-1). Some of the cell types, such as CHO and RAW 264.7 exhibited spots in the cytosolic space in the green channel, which co-localised with the endosomal-lysosomal dye LysotrackerRED, resulting in the appearance of small, punctate yellow or orange areas when the green and red channels were merged. This suggested that some of the fluorescent cargo was trapped in the endosomal pathway, which, however, did not prevent successful and efficient payload delivery to the interior of the cells with as suggested by the strong cytosolic signal in all 9 cell types.

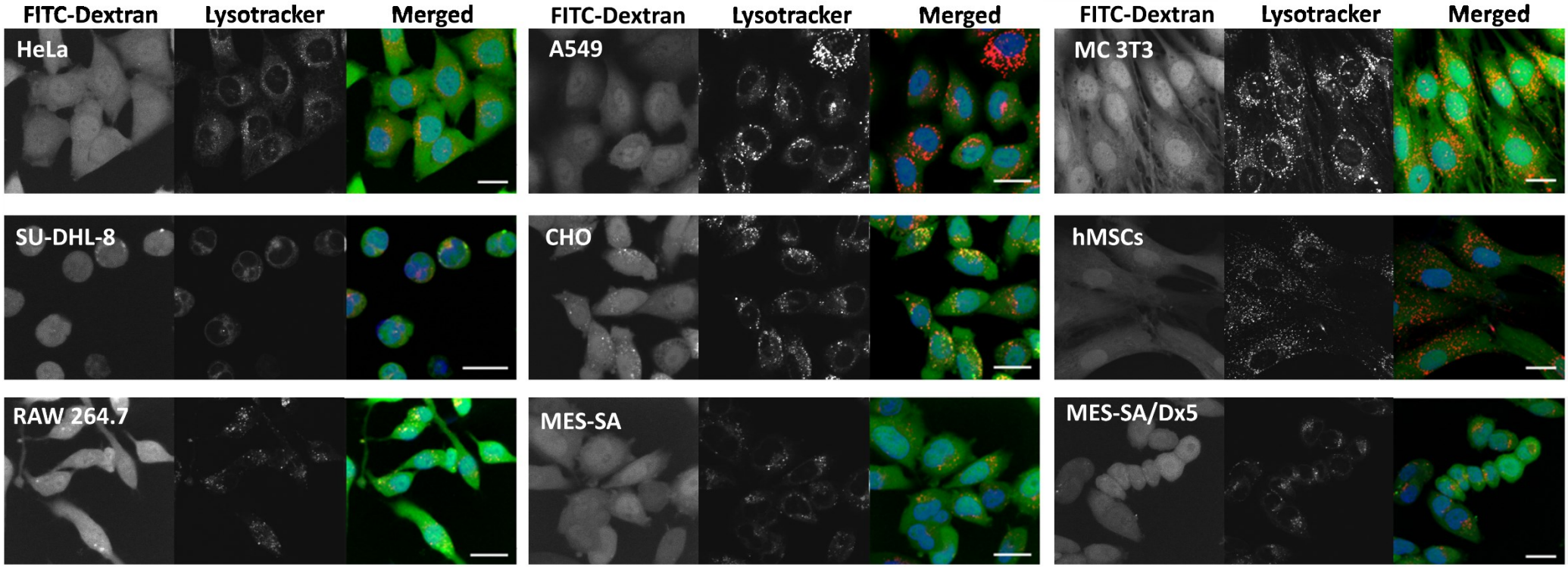


Figure 4-1. Delivery of 150 kDa FITC-Dextran (10 μM) to 9 different cell types using PP50 (1 mg mL^{-1}) using a 1 h treatment (HeLa, A549, MC 3t3, SU-DHL-8, CHO, hMSCs) or the same-sized FITC-Dextran at the concentration equal to 5 μM in 0.5 h treatment using the same polymer concentration (RAW 264.7, MES-SA, MES-SA/Dx5) at pH 6.5. FITC-Dextran and Lysotracker are presented in greyscale. The merged images depict green (FITC-Dextran), red (Lysotracker) and blue (Hoechst) channels. Scale bar = 20 μm.

FITC-Dextran delivery to 9 different cell types was further quantified by flow cytometry, comparing delivery efficiency at pH 7.4 and pH 6.5 (Figure 4-2). The PP50-mediated payload delivery at pH 6.5 was clearly more efficient than that at pH 7.4 and in corresponding polymer-free samples in all but two cell lines: RAW 264.7 and MES-SA. The mean fluorescent intensity of A549 cells incubated with FITC-Dextran and PP50 at 1 mg mL^{-1} was 4 times brighter at pH 6.5 than the cells treated at pH 7.4, which was the largest fold increase between cells incubated at neutral and mildly acidic pH. For A549 cells, payload delivery at neutral pH 7.4 was also similar to polymer-free samples at both pH 6.5 and pH 7.4, illustrating that the extracellular activation of the polymer has a dramatic effect on delivery efficiency in some cell lines. A similar effect was observed for SU-DHL-8 cells and hMSCs. Delivery to HeLa, MC 3t3 and CHO cells was 1.5, 1.75 and 1.45 more efficient at pH 6.5 and pH 7.4, respectively. In these cell lines, however, the delivery at pH 7.4 also occurred to a certain extent, with HeLa, MC 3t3 and CHO cells incubated in the presence of polymer being 5.9, 2.8 and 4.2 brighter than those in the polymer-free samples, which could be illustrating the delivery following endosomal uptake and acidification which activates the polymer and enables endosomal escape following internalisation. Efficient payload uptake via endosomal pathway could play even a more crucial role in RAW 264.7 and MES-SA cells, explaining why extracellular activation of the polymer seems to be having only a small boost effect.

Finally, the cytotoxic effect of the delivery process on the 9 cell types was investigated using AlamarBlue assay following a treatment with 10 μM dextran (150 kDa) and 1 mg mL^{-1} PP50 (Figure 4-3). The delivery of antibody-sized dextran was well tolerated by all the cell types used in the experiment and delivery at pH 6.5 did not have an immediate deleterious effect over delivery at pH 7.4, with cell survival reaching over 90% in majority of the samples. These results confirm the findings discussed in the previous chapter suggesting that PP50-mediated delivery is majorly non-cytotoxic under the parameters required for efficient intracellular delivery.

Based on the confocal microscopy images combined with flow cytometry and cytotoxicity data it was concluded that PP50-mediated delivery has the potential

to be widely applicable across many different cell types, including stem cells and immune cells which remain difficult targets for payload delivery, and that this process is non-cytotoxic and reproducible and can be enhanced in a trigger-sensitive manner by lowering the extracellular pH.

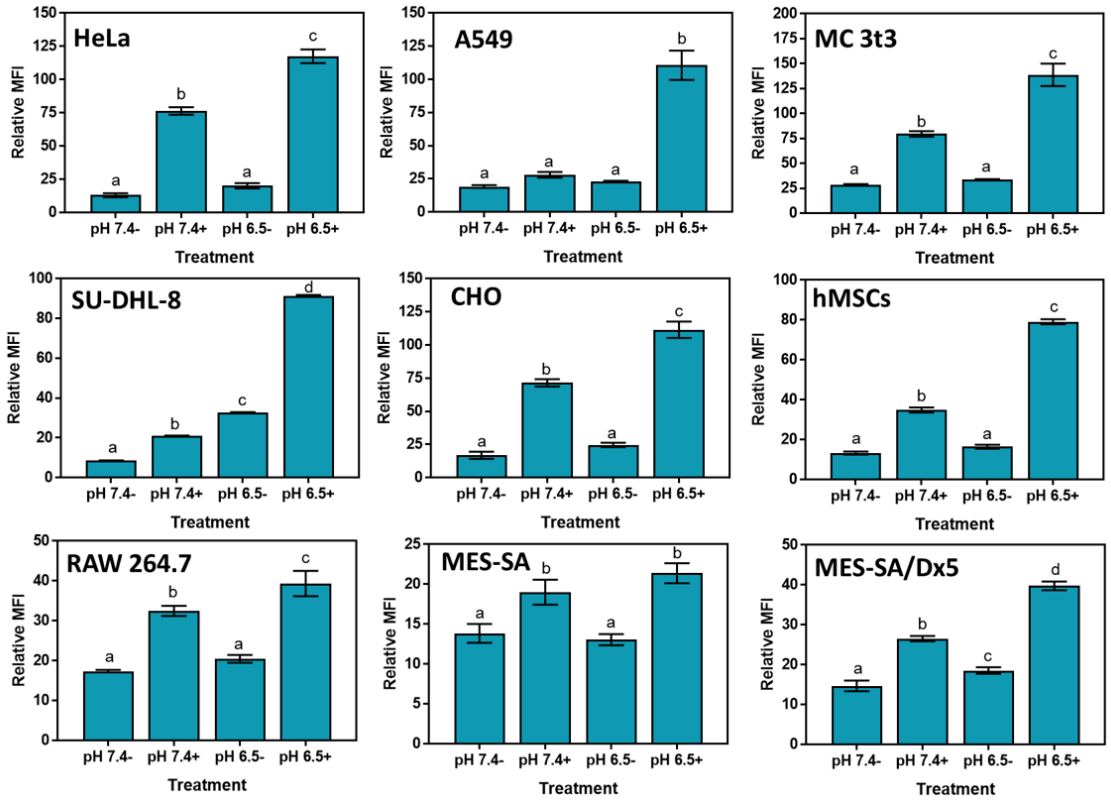


Figure 4-2. Fluorescence intensity of the 9 different cell types after delivery of 10 μM FITC-Dextran using PP50 at the concentration of 1 mg mL^{-1} in 1h treatment. Cells were treated in the absence or presence of polymer at pH 7.4 ("pH 7.4-" and "pH 7.4+", respectively) and at pH 6.5 ("pH 6.5-" and "pH 6.5+", respectively). Mean ± SD, n = 3. One-way ANOVA and Tukey's tests were performed to compare different treatments. Different letters represent statistically significant difference with p-values < 0.5.

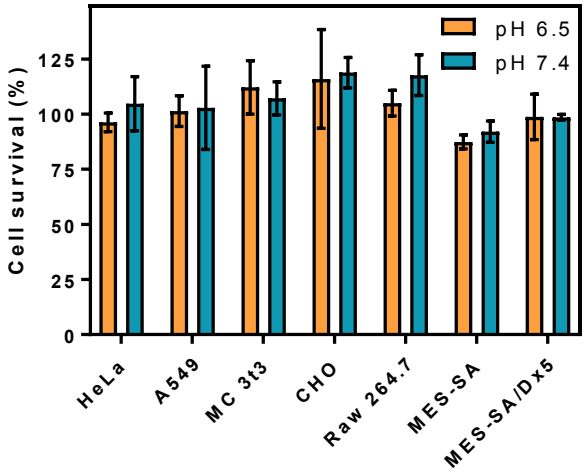


Figure 4-3. Cytotoxicity of the delivery process of 10 μM Dextran using PP50 (1 mg mL^{-1}) to different cell types at pH 7.4 and pH 6.5 following a 1 h treatment as analysed by AlamarBlue assay. Mean ± SD, n = 3.

4.2.2. Delivery to multicellular A549 spheroids

Multicellular spheroids are 3-dimensional, spherical aggregates of cells which can serve as models of tumours and tissues as they accurately mirror their cellular heterogeneity and organisation in layers, gene expression and growth kinetics, the presence of physical barriers, such as the extracellular matrix as well as the oxygen gradient and the distribution of some key metabolites, including glucose, lactate and ATP (Hirschhaeuser et al., 2010; Costa et al., 2016). This complexity makes spheroids a better model of natural *in vivo* environments, compared to 2D cell monolayers, and enables their usage as a relevant tool to study drug development and delivery as well as aspects of cancer and fundamental biology. (Zanoni et al., 2016). The ability to deliver macromolecular cargo, such as proteins and peptides, to spheroids could therefore find many uses in these fields.

Here, 150 kDa FITC-Dextran was attempted to be delivered to A549 spheroids by co-incubation with PP50 at mildly acidic pH 6.5, which was analysed using confocal microscopy (Figure 4-4). 2-day old spheroids were treated with PP50 (0.5 mg mL^{-1}) and 10 μM solution of the fluorescent dextran for a period of 2 h. Successful delivery of FITC-Dextran to the cell interior was observed in the spheroids treated with the polymer and cargo at pH 6.5, where the green

fluorescent signal was uniform and diffused in the cytosol of the spheroid cells, consistent with the previous findings on successful cytosolic delivery of FITC-Dextran reported herein. This was a substantial improvement in comparison to delivery of a fluorescent small molecule mediated by another PP-family polymer at pH 7.4, which was presumed to rely on endosomal disruption for cytosolic entry (Ho et al., 2011).

In addition, this experiment corroborates the enhancement effect of mildly acidic extracellular pH in PP50-mediated delivery. Co-treatment with dextran and the polymer at neutral pH 7.4 resulted in only a very small relative proportion of cells having the bright, diffused fluorescent signal in their cytosol. These were also localised on the external edge of the spheroids only. In contrast, PP50-mediated delivery at pH 6.5 resulted in bright green cells being localised throughout the spheroid, which confirms that this strategy is more efficient and provides better penetration.

In addition, the small number of cells displaying red fluorescent signal as a result of being stained with the dead cell marker propidium iodide in all of the samples, including the spheroids treated with PP50, provides further evidence that the delivery process was majorly non-cytotoxic and is consistent with expected cell viability reported for A549 spheroids (Amann et al., 2014).

This experiment provides some evidence that PP50-mediated delivery could be employed for *in vivo* applications with maximising the therapeutic potential of macromolecular drugs while minimising unwanted side effects. This is because the polymer would not cause delivery to healthy tissues at neutral pH during the circulation in the bloodstream, but could become activated upon reaching the more acidic tumour microenvironment and facilitate drug transport directly into tumour cells.

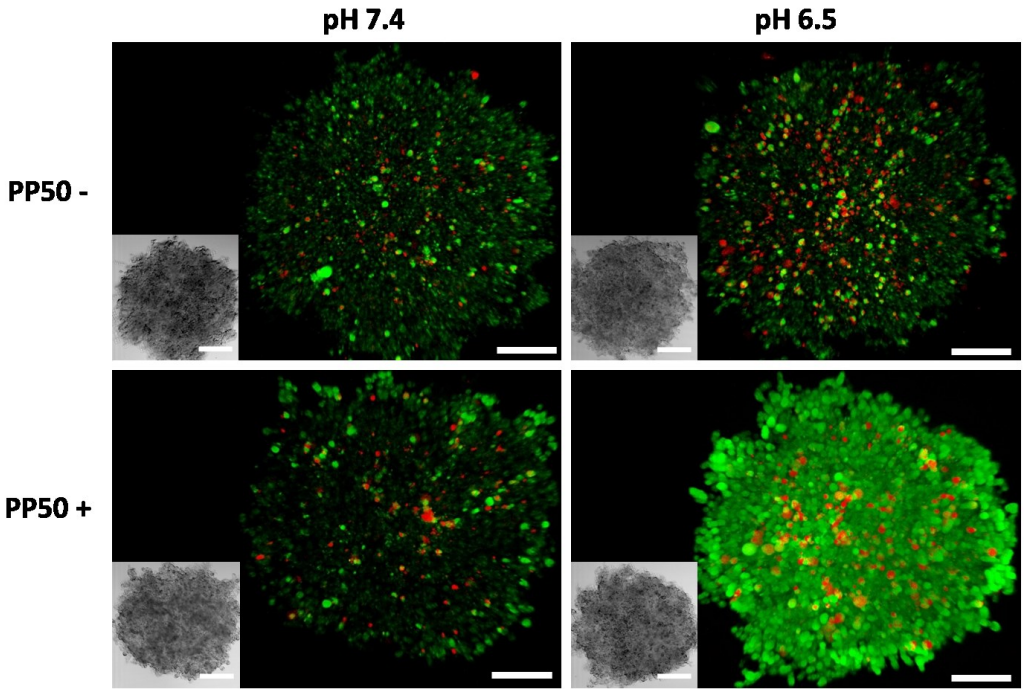


Figure 4-4. Z-stack projections obtained using confocal microscopy illustrating delivery of 150 kDa FITC-Dextran (10 μM) to the A549 spheroids by co-incubation with PP50 (0.5 mg mL^{-1}) for a period of 2 h. Delivery at pH 6.5 and pH 7.4 were compared, in addition to corresponding polymer-free controls. The 3D projections were shown from the top and were a merge of green channel (FITC-Dextran) and red channel (PI stain of dead cells). The insets show bright field images of the corresponding spheroid. Scale bar = 200 μm.

4.2.3 Delivery of different-sized FITC-Dextran

The potential ability of PP50 to facilitate the delivery of payloads of different size would be a hugely advantageous trait of this potential delivery platform. To assess the versatility of PP50 in the aspect, HeLa cells were treated with PP50 and FITC-Dextran with molecular sizes of 10, 70, 150, 500 and 2000 kDa. This size range of the model payload covers a wide range of potential macromolecular cargo, including peptides, protein, siRNAs, antibodies as well as certain nanoparticles and plasmids (Watkins and Chen, 2015). A fixed mass concentration of FITC-Dextran of 0.15 mg mL^{-1} was used to ensure a consistent strength of the fluorescent signal.

Analysis via confocal microscopy revealed that a short, 30-minute treatment at pH 6.5 was enough to obtain a clear cytosolic and nuclear green fluorescent signal, with little evidence of endocytotic entrapment, suggesting successful

delivery (Figure 4-5). Additional confirmation of the delivery was obtained using flow cytometry to quantify the strength of the fluorescent signal. Cells treated with PP50 and different-sized dextran were on average 4.2 ± 0.7 brighter compared to the corresponding polymer-free control samples, suggesting that the payload delivery was due to the contribution of PP50 (Figure 4-6).

The strength of the fluorescent signal of HeLa cells delivered with different-sized FITC-Dextran at a fixed payload and polymer mass concentration varied, with larger dextrans, in general, producing a weaker signal. This could be explained by the fact that larger macromolecules would diffuse through the permeabilised plasma membrane less efficiently than smaller molecules. In addition, since the delivery mechanism could also, to some extent, rely on PP50-mediated endosomal escape, the potential effects of payload size on the internalisation pathway should also be considered. Li *et al*. (2015) showed that different-sized dextrans might use differing endosomal pathways for internalisation, with small dextrans (10 kDa) seeming to internalise via multiple routes, including micro- and macropinocytosis, but larger dextrans switching more towards clathrin- and dynamin-independent macropinocytosis, which might not be as efficient in terms of internalisation throughput (Li et al., 2015b). A surprising exception to this pattern was the largest dextran used herein (2,000 kDa), which produced a very bright intracellular signal, compared to the other dextrans used here. This reproducible effect could be due to a higher degree of grafting with the fluorophore FITC, which was stated to be within 0.003-0.020 mol FITC per mol glucose for all of the dextrans used here and could therefore exhibit batch-to-batch variance, making the largest dextran relatively brighter. These results suggest that PP50 can be used for delivery of dextrans of various size which rely on different endosomal pathways for internalisation, either by polymer-mediated endosomal escape or direct membrane permeabilisation to by-pass the endosomal entrapment altogether.

In agreement with the previous results reported herein, a consistent co-localisation of the green signal with the nuclear marker Hoechst was observed. In some cases the green signal in the nucleus was distinctively stronger than the surrounding cytosolic fluorescence, suggesting accumulation of the cargo fluorescent molecules in the nucleus at a higher concentration than in the

cytosol. It is generally believed that the nuclear pores greatly limit transport of macromolecules which are larger than 50 kDa, with reports that 70 kDa fluorescent dextran, which was transported into the cytosol using a CPP, did not penetrate the nuclear envelope (Gasiorowski and Dean, 2003; Lee et al., 2010; Sui et al., 2011). The data showed here illustrates that even the largest of the tested FITC-Dextran, with the molecular weight of 2,000 kDa, was co-localised inside the nuclei of HeLa cells after co-treatment with PP50 at pH 6.5. Furthermore, since large, 485 kDa, FITC-Dextran has been reported of being stable inside the cell, and not being able of crossing between the cytosol and the nucleus, following injection to either, it was hypothesised that the apparent nuclear delivery is due to the action of PP50 rather than intracellular degradation of the dextran or dye detachment (Ludtke et al., 2002). The precise mechanism by which this occurs is not yet understood and requires further investigation, but could be associated with localisation of PP50 in the perinuclear area of the cell, as reported in the previous chapter, which is also characteristic of certain DNA viruses (Suh et al., 2003; Mercado and Slater, 2016b).

It is also worth noting that whereas all the tested sizes of the FITC-Dextran were successfully delivered to the nucleated cells in the presence of PP50, the delivery of 150 kDa dextran, and presumably any other dextran of similar or larger size, to ovine erythrocytes was much less efficient (See Figure 3-4). This might be a result of different properties of nucleated cells and erythrocytes. One of such differences is the composition of the lipid membrane, which could affect the PP50-membrane interactions, depending on cell type, and leading to the transient membrane permeabilisation whose extent might vary between different cell types, thus affecting cargo delivery rate or even imposing a size limitation (Binder et al., 2003; Lu and Liu, 2007). Other potential explanation is that since mature erytrocytes are believed to lack endocytosis, they would only be able to be delivered with molecules capable of passing through the permeabilised plasma membrane, which might have a size limitation (Marchesi et al., 1976). This contrasts with nucleated cells, whereby macromolecular cargo could be delivered to the cytosol via a combined effect of direct membrane permeabilisation, which might be more efficient for delivery of smaller molecules

(<150 kDa), as well as through PP50-mediated endosomal escape following cargo internalisation in the endosomal vesicles.

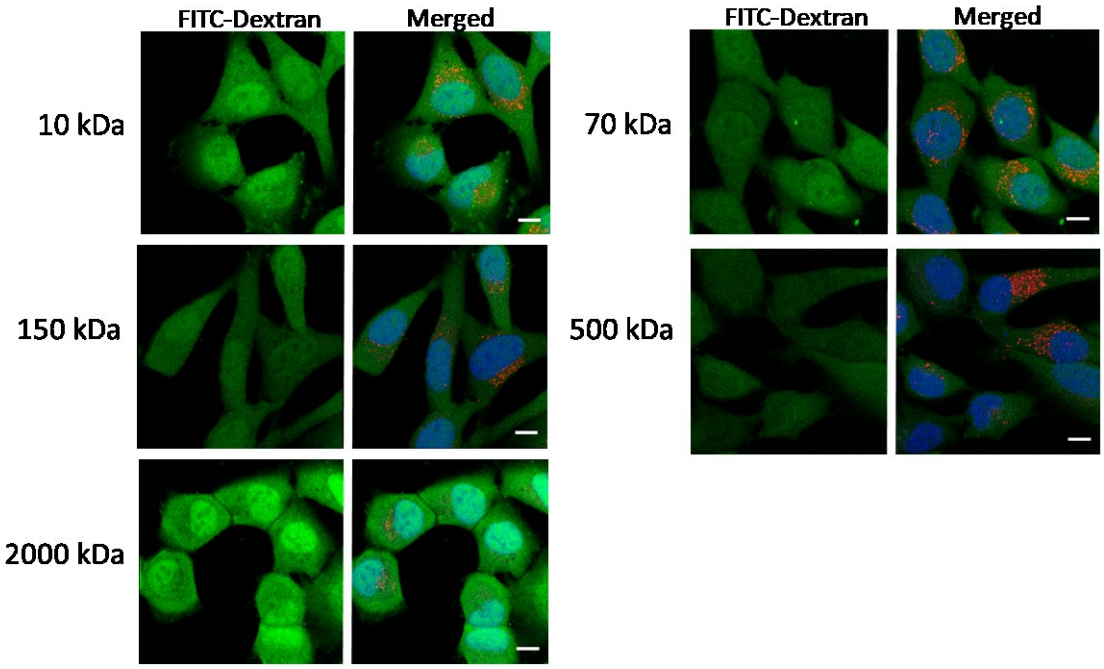


Figure 4-5. Confocal microscopy illustrating delivery of 10, 70, 150 and 2000 kDa FITC-Dextran (0.15 mg mL^{-1}) using PP50 (0.5 mg mL^{-1}) at pH 6.5 in a 30-minute treatment. The merged pictures combine green (FITC-Dextran), red (Lysotracker) and blue (Hoechst) channels. Scale bar = 10 µm.

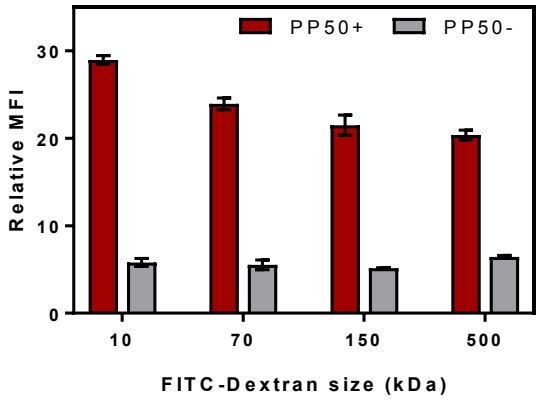


Figure 4-6. Strength of the fluorescent signal of cells as analysed by flow cytometry following a treatment with PP50 (0.5 mg mL^{-1}) and FITC-Dex (0.15 mg mL^{-1}). Treatment time was equal to 1 h. Mean ± SD, n = 3.

4.2.4 Delivery of green fluorescent protein

Green fluorescent protein (GFP) is a 26.9 kDa protein possessing natural fluorescing properties (Ex 488/ Em 510), which has been extensively used in the field of genetics and molecular biology (Prendergast and Mann, 1978; Stepanenko et al., 2008). Here, GFP was used as another model payload to test the versatility of PP50-mediated delivery which is more relevant to potential real lab uses compared to dextran (Figure 4-7). GFP (2 μM) was applied to HeLa cells in the presence or absence of PP50 (0.25 mg mL^{-1}) for 1h and the cells were analysed with confocal microscopy, which resulted in a uniform, diffused signal in the green channel in the cargo- and polymer-positive sample and pH 6.5, suggesting that the protein was successfully delivered to the cells. In contrast, treatment of cells with GFP only at pH 6.5 resulted very limited internalisation, whereas co-treatment with the model protein and PP50 at pH 7.4 produced signal characteristic of endosomal entrapment, which was confirmed using LysotrakcerRed. This experiment provided evidence that on top of being capable of dextran delivery, the PP50 platform was also compatible with payloads with different properties, such as fluorescent proteins.

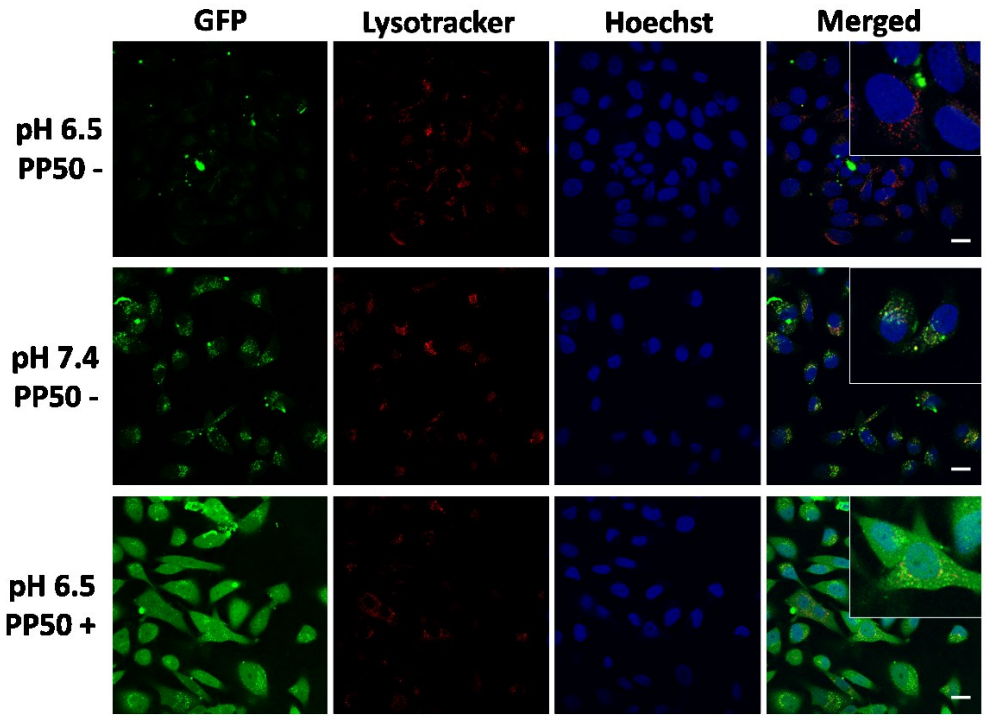


Figure 4-7. Delivery of GFP (2 μM) to HeLa cells using PP50 (0.25 mg mL^{-1}) at pH 6.5 and pH 7.4 following 1 h of treatment. Scale bar = 20 μm.

4.2.5 Delivery in the presence of serum

One of the biggest limitations for many potential delivery platforms is their inhibition by undesired interaction with serum proteins, mainly serum albumin, which could lead to total loss of the membrane permeabilisation activity (Yang et al., 2014; Xu et al., 2018). This can occur when the desired buffer or medium used for the delivery contains foetal bovine serum, or similar, and can prevent successful transition of this technology from *ex vivo* to *in vivo* applications. It is therefore necessary to investigate the effect of serum on PP50-mediated delivery.

To test this, HeLa cells were treated with 10 μM FITC-Dextran and PP50 (0.5 mg mL^{-1}) at pH 6.5 and pH 7.4 in the presence or absence of 10% FBS, and payload delivery was analysed using confocal microscopy (Figure 4-8). The relatively long treatment time of 3 h resulted in efficient delivery of the fluorescent dextran at both pH 6.5 and pH 7.4 in the serum-free samples, with the cells treated at pH 6.5 being noticeably brighter, which is consistent with the results described above. When the cells were treated in PBS containing 10% FBS, however, there was no payload delivery observed at neutral pH, while delivery at pH 6.5 was still possible and resulted in a diffused fluorescent signal throughout the cells, albeit the signal was weaker in comparison to serum-free samples at the same pH. This was most likely due to inhibition of the polymer by serum proteins, which decreases delivery efficiency. As delivery at pH 6.5 has been shown to be more efficient than at neutral pH, the inhibition effect is not sufficient to fully prevent intracellular delivery. Another potential reason contributing to the observed difference between the serum-free and serum-containing samples could be increased endocytosis in serum-starved cells as a means of scavenging for nutrients by the cells (Muranen et al., 2017).

It is possible that the delivery efficiency can be further enhance by prolonging the treatment time or by increasing the polymer/serum ratio. The latter was tested by treating HeLa cells with dextran and polymer concentration at 0.5, 1 and 2 mg mL^{-1} in the presence of 10% FBS, and compared to delivery in serum-free PBS using 0.5 mg mL^{-1} PP50 (Figure 4-9). While addition of serum to the system seems to half the delivery efficiency at a set polymer concentration, it

was possible to restore it up to 85% of the original value by increasing the polymer concentration from 0.5 to 2 mg mL^{-1}, as analysed by flow cytometry. This experiment demonstrates that PP50-mediated delivery can be applicable to serum-containing environments at mildly acidic conditions, although with a decreased efficiency. Thus, PP50 could be applicable for *in vivo* applications.

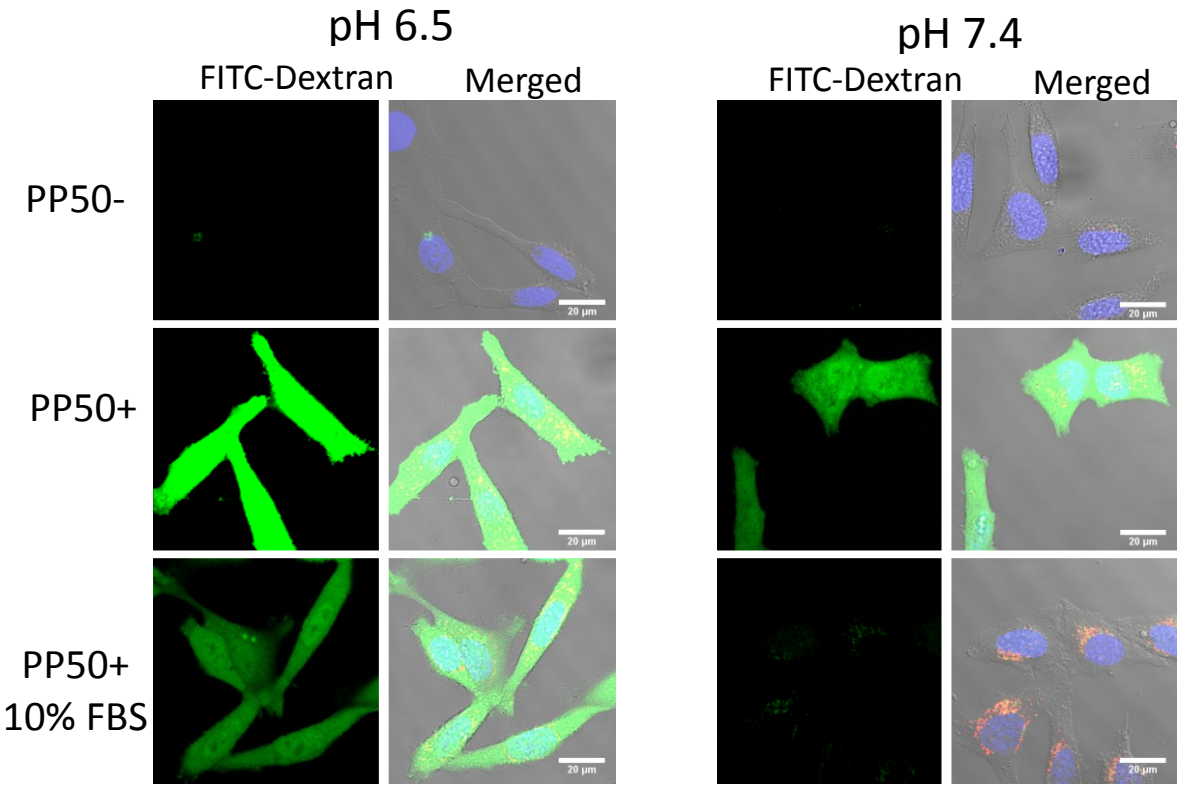


Figure 4-8. Delivery of 150 kDa FITC-Dextran (10 µM) to HeLa cells by co-incubation with PP50 (0.5 mg mL^{-1}) in a 3 h treatment, analysed by confocal microscopy. The merged pictures combine green (FITC-Dextran), red (Lysotracker) and blue (Hoechst) channels. Scale bar = 20 µm.

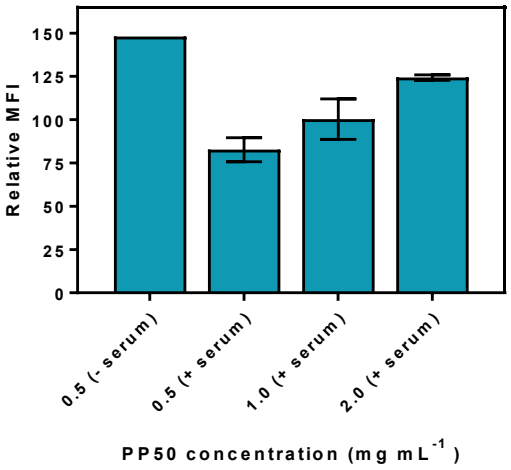


Figure 4-9. Flow cytometry of HeLa cells following a 4 h treatment with PP50 and 150 kDa FITC-Dextran (5 μM) at pH 6.5 with or without FBS at 10% v/v. Mean ± SD, n = 3.

4.2.6 Strength of intracellular fluorescence over time and topping-up

The stability of the fluorescent signal inside the cells post-delivery using PP50 was also investigated. While this could be very payload- and cell type-dependent, the current study focused on using HeLa cells and FITC-Dextran (150 kDa). Following a delivery of this model payload in a short, 30-minute treatment with PP50 in PBS at pH 6.5 and pH 7.4, cell fluorescence was analysed using confocal microscopy (Figure 4-10 A) and flow cytometry (Figure 4-10 B and C) at 0.5, 6 and 24 h after a wash and return to regular growing medium, in this case DMEM supplemented with 10% FBS.

Both analysis methods revealed that HeLa cells treated at pH 6.5 started with higher initial strength of the fluorescent signal, consistent with previous findings. Subsequent to that, both of the cell groups started to lose their fluorescence signal, approximately by half between 0.5 and 6 h and again, between 6 h and 24 h. By the last analysis at 24 h post-treatment, the cells treated originally at pH 7.4 lost almost all of the cytosolic FITC signal detectable by fluorescent microscopy, while the cells treated at pH 6.5 still possessed a clear, diffused green fluorescent signal.

This was confirmed by the analysis of the percentage of fluorescent cells as a subpopulation of all the cells present in the sample (Figure 4-10 C). This analysis revealed that in both treatment groups 100% of the cells were classed as possessing a detectable level of intracellular fluorescence, as compared to a FITC-Dextran and PP50-negative control group, and nearly 100% of the cells treated at pH 6.5 retained detectable fluorescence by 24 h post-treatment while the percentage of fluorescent cells in the pH 7.4 group dropped by 40%. It is further possible that this fluorescent signal in the pH 7.4 group was contributed by the punctuate green areas observed in the microscopy images, rather than the uniform, diffused fluorescent signal which would suggest presence of the model payload in the cytosol. This difference arises most likely due to the higher degree of loading with FITC-Dextran during the treatment at mildly acidic pH, which enabled delivery of more of the payload to the cytosol and therefore the decrease of the fluorescent signal, most likely due to removal of FITC-Dextran by the cell, occurs more slowly.

This effect is theorised to arise due to the exocytosis of the delivered FITC-Dextran. Post-delivery exocytosis of nanoparticles has been widely reported for various molecules and nanoparticle types, and its efficiency is thought to depend on a number of parameters, such as the cell type and particle size, shape and surface properties, and can range from ~ 30 minutes for poly lactic-co-glycolic acid (PLGA), 4 – 12 h for gold and mesoporous silica of various size and a minimum of 6 days for nanodiamonds (Fang et al., 2011; Slowing et al., 2011; Sakhtianchi et al., 2013; Yanes et al., 2013; Oh and Park, 2014). In addition, it has been reported that nanoparticles which leave the exosome/lysosome system and translocate to the cytosol can take a longer time to be exocytosed (Stayton et al., 2009)

The potential ability to increase the strength of cytosolic fluorescent signal post-treatment by subjecting the cells to another co-treatment with PP50 and FITC-Dextran, or “topping-up”, were also investigated (Figure 4-11). The fluorescence profile obtained using flow cytometry demonstrated that the cytosolic levels of FITC-Dextran, which was lost in the period of 24 h following PP50-mediated delivery at pH 6.5, was restored to the levels directly following the original treatment by subsequent topping-up treatment. Furthermore, this process was

proven to be repeatable, with at least 3 treatments possible, each delivering a very similar amount of the model payload to the cells without causing critical cell damage. This property of the PP50-platform could be useful in application whereby a target cell population needs to be repeatedly delivered with a desired protein or other macromolecular cargo to ensure high cytosolic levels.

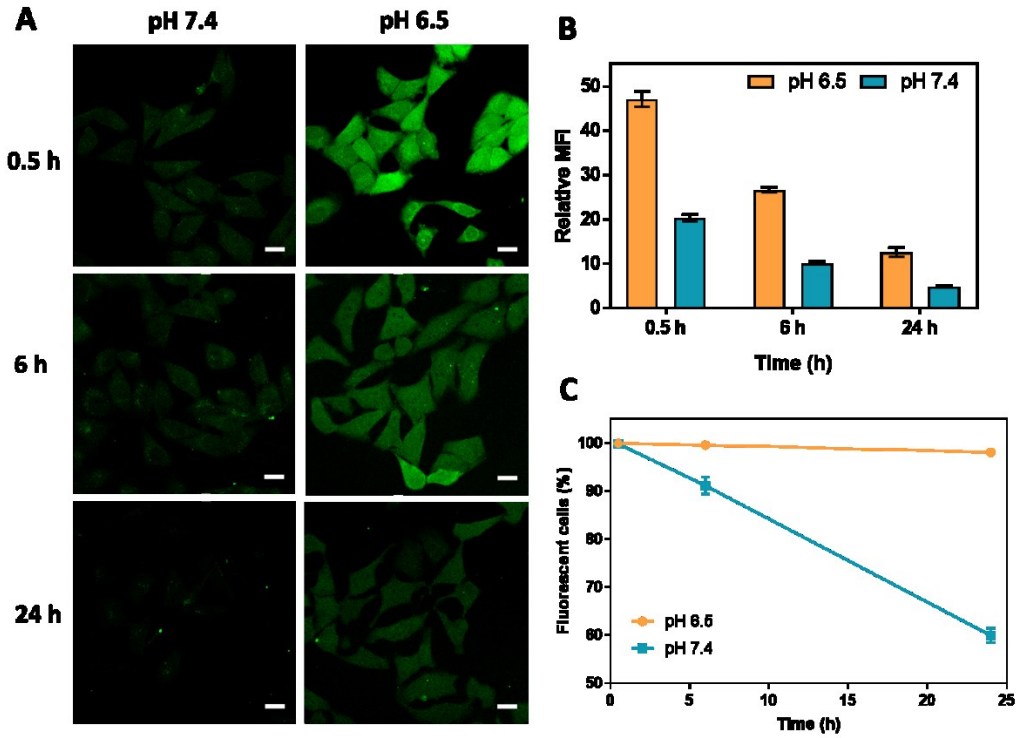


Figure 4-10. Cytosolic fluorescence of HeLa cells delivered with 150 kDa FITC-Dextran (10 µM) in a 30-minutes treatment with PP50 (0.5 mg mL^{-1}) in PBS at pH 6.5 and pH 7.4. (A) Analysed by confocal microscopy at 0.5, 6 and 24 h post-treatment, scale bar = 10 µm, and analysed by flow cytometry at the same time points and expressed as (B) Median fluorescence intensity of the cells and (C), percentage of fluorescent cells compared to a negative control. Mean ± SD, n = 3.

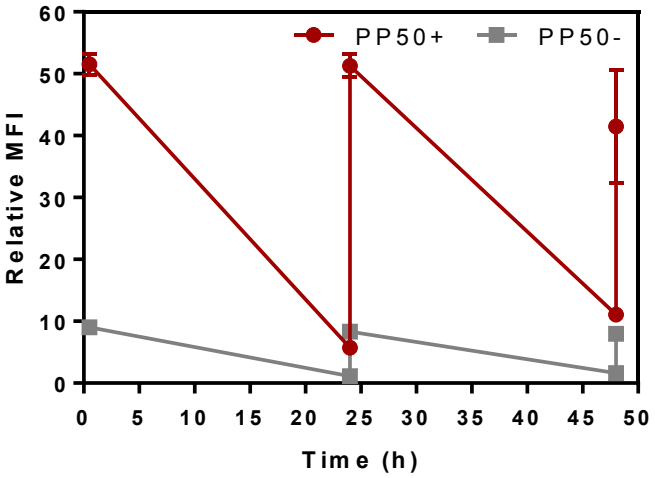


Figure 4-11. Multiple dosing of 150 kDa FITC-Dextran (10 μM) in HeLa cells by repeated delivery with PP50 (0.5 mg $mL^{-1)}$ in a 30-minute treatment at pH 6.5, compared to a polymer-free control, analysed by flow cytometry. Mean ± SD, n = 3.

4.2.7 Antibody delivery

The ability to deliver antibodies would be another big advantage of the PP50 platform. Here, the delivery of Anti-non-muscle myosin IIA antibody labelled with AF647 (Ex 650/ Em 665) using PP50 at pH 6.5 was tested and compared to delivery of the same amount of the antibody to fixed and permeabilised cells and analysed using confocal microscopy (Figure 4-12). The difference between the two treatment groups was obvious, with the fixed and permeabilised cells displaying clear and bright staining of the myosin network whereas the fluorescence inside the live cells treated with the polymer and this payload displayed a much more punctate fluorescent pattern with partial binding to the myosin network in some of the cells (indicated by white arrows). This suggests that PP50 has a potential to deliver functional antibodies to the cell interior but the precise protocol might require further optimisation to establish the most optimal parameters to improve the efficiency of this process.

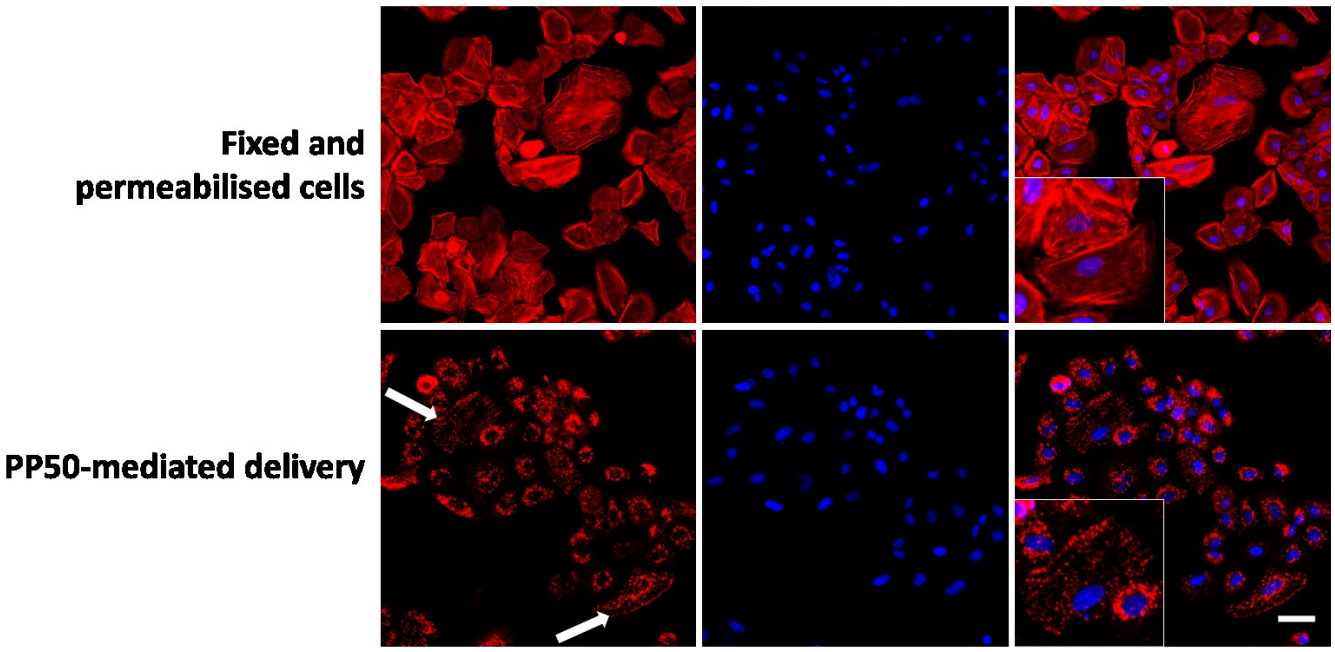


Figure 4-12. Delivery of Anti-non-muscle Myosin IIA antibody (Alexa Fluor® 647) to A549 cells: comparison of PP50-mediated delivery (0.5 mg mL^{-1}) of the antibody (50 µg mL^{-1}or 333 nM) in a 1 h treatment at pH 6.5 against passive delivery to fixed and permeabilised cells of the same antibody concentration in 1 h treatment. Scale bar = 10 µm.

4.2.8 Plasmid delivery

Delivery of nucleic acids, including plasmid DNA, for genetic engineering of cells and gene therapy remains a challenging task. Here, dsRed plasmid was attempted to be delivered to HeLa cells by co-incubation with PP50 at pH 6.5 for 2 h and the expression of the encoded reporter protein, red fluorescent protein (RFP; Ex 558/ Em 583nm) was quantified using laser scanning confocal microscopy. As illustrated in Figure 4-13, the expression of RFP following the treatment with the plasmid and PP50 did not reach detectable levels and was similar to the background signal obtained from analysing HeLa cells which had not been treated. This suggests that the intracellular delivery of dsRed was not successful. Different treatment regimens (such as pre-treatment with PP50 alone, followed by a wash and addition of either dsRed or dsRed mixed with PP50) and increasing the further incubation period up to 24 h following the treatment were attempted but plasmid delivery did not appear to have been achieved by varying those parameters (data not shown). The difficulty with

PP50-mediated delivery of nucleic acids using the co-incubation approach can arise from the fact that both the payload and the cargo have negative charge, which can result in electrostatic repulsion and inhibition of membrane binding and internalisation of these two components.

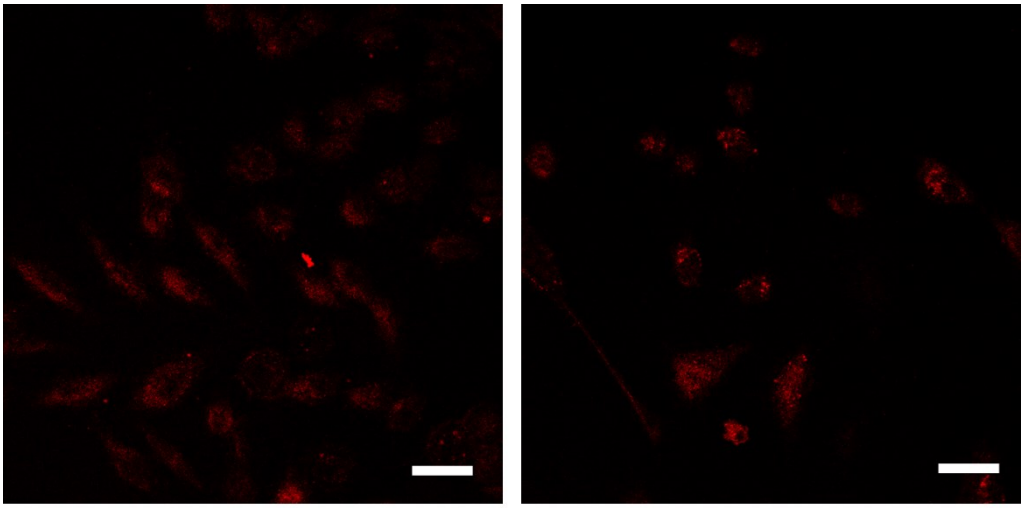


Figure 4-13. Delivery of dsRED (1 μg mL^{-1}) to HeLa cells by co-incubation with PP50 (0.5 mg mL^{-1}) at pH 6.5. Treatment time was equal to 2 h. Scale bar = 10 μm.

4.2.9 Delivery of Bim

The ability to deliver functional payloads to the cell interior with preserving its function is a pre-requisite for any versatile delivery platform candidate, such as PP50. To investigate this aspect of the PP50-platform and to expand the work on model payloads pro-apoptotic peptide, Bim, was used as the functional cargo in the following experiments. Bim is a 3 kDa peptide which can interact with Bcl-2 proteins – a protein family localised on the nuclear envelope, endoplasmic reticulum as well as the external mitochondrial membrane and playing an important role in regulating the progression of cell death via apoptosis (O'Connor et al., 1998; Strasser et al., 2000). A specific region of the Bim peptide, called BH3, is capable of interacting with the proteins in the Bcl-2 family leading to their inactivation and initiation of apoptosis utilising the Caspase 9 pathway (Strasser et al., 2000).

4.2.9.1 Caspase activation and cell survival

First, delivery of Bim was tested by co-treatment of A549 cells with the peptide and PP50 at pH 6.5 and pH 7.4, for comparison, and the functional activity of the payload, i.e. apoptosis, was analysed by detection of Caspase 9 and Caspase 3/7, which are known as apoptosis executioners. Furthermore, the cell survival post-delivery was also assessed using an AlamarBlue assay.

Bim (20 μM) co-incubated with PP50 (1 mg mL^{-1}) at the mildly acidic pH, but not at neutral pH, was capable of inducing a strong Caspase 3/7 and 9 activation response (Figure 4-14). This is consistent with the results discussed above noting that the extracellular activation of PP50 greatly enhanced its delivery potential. The PP50-mediated delivery of Bim was compared to a number of controls to ensure validity of this result. Treatment of A549 cells with Bim alone, PP50 alone or a mixture of PP50 and inactive version of Bim peptide (scrBim) did not induce caspase activation. In addition, small molecule, membrane permeable Bcl-2 inhibitor and BH3 mimic, ABT-737, were used as a positive control (van Delft et al., 2006). In both cases of Caspase 9 and Caspase 3/7, the PP50-mediated response fell within the same order of magnitude as that induced by the small molecule, with the differences between the two arising potentially due to their action working in different time frames because of different dynamics.

In addition, the cell survival following a 24 h period of further incubation after the treatment, a PBS wash and media exchange was analysed by AlamarBlue assay (Figure 4-15). The cell survival profile corresponded to the caspase activation results, with only 37% of the cells treated with PP50 and Bim at pH 6.5 surviving, but no major decrease in cell survival the experimental sample at pH 7.4 nor in any of the negative controls, as compared to untreated cells. Surprisingly, delivery of ABT-737 did not seem to decrease cell survival in such a dramatic way as PP50-mediated delivery of Bim, causing 77% cell survival, even though their caspase activation was similar. This might arise due to the ABT-737 response being more short-lived and requiring constant presence of the small molecule in the growth medium for a prolonged period of time, as

opposed to PP50-mediated delivery, which relies on short and efficient permeabilisation leading to the internalisation of the cargo.

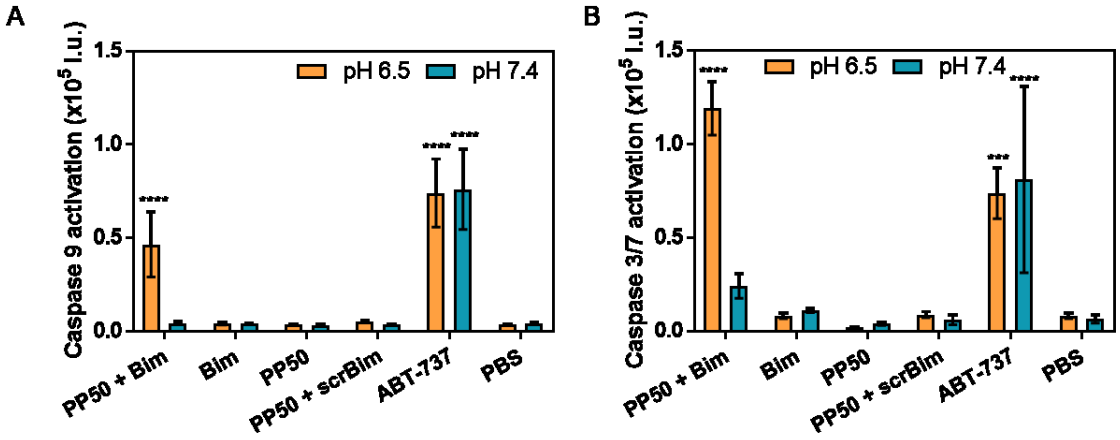


Figure 4-14. Caspase activation after delivery of Bim (20 μM) by co-incubation with PP50 (1 mg mL^{-1}) for a period of 3 h at pH 6.5 and pH 7.4, as compared to controls: PP50 mediated delivery of scrambled Bim, and cells incubated with Bim, PP50 or PBS alone, analysed using (A) Caspase 9 Glo and (B) Caspase 3/7 Glo assays. Membrane permeable small molecule Bim mimetic, ABT-737 (20 μM), was used as a positive control. Mean ± SD, n = 3. Two-way ANOVA and Tukey's tests were performed to compare the cells treated with the different materials to PBS-treated cells.

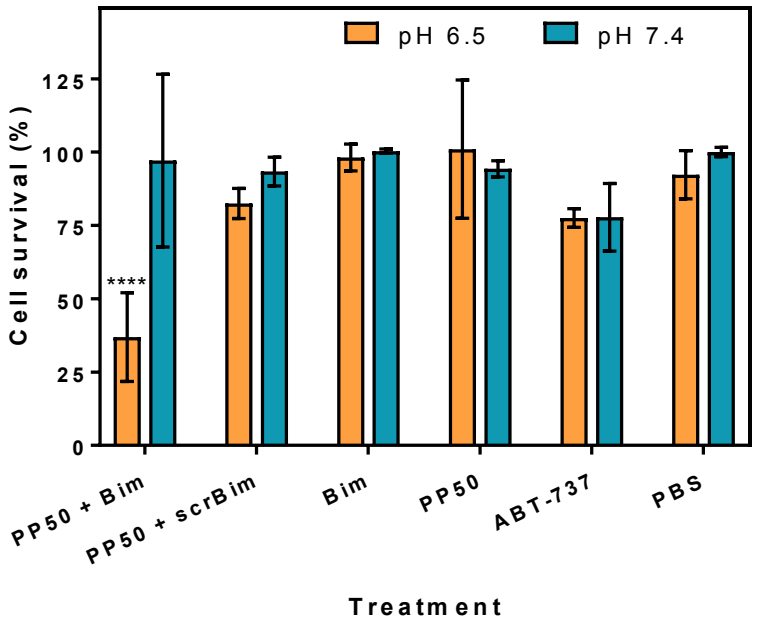


Figure 4-15. Survival of cells after delivery of Bim (20 μM) by co-incubation with PP50 (1 mg mL^{-1}) for a period of 3 h at pH 6.5 and pH 7.4 following a further incubation period of 24 h, analysed using AlamarBlue assay. Mean ± SD, n = 3. Two-way ANOVA and Tukey's test was performed to compare the cells treated with the different materials to PBS-treated cells.

4.2.9.2 Delivery of Bim – time

In order to investigate the dynamics of PP50-mediated delivery of Bim, as well as to elucidate the difference in the apoptosis induction speed by Bim and by ABT-737, a time-course study was performed using IncuCyte®. A549 cells were either delivered with 20 uM Bim in a 4 h treatment with PP50 at pH 6.5, followed by a wash and media replacement, or treated with the same concentration of ABT-737 throughout the duration of the IncuCyte® experiment. The samples were then supplemented with IncuCyte® Caspase-3/7 Green Apoptosis Assay reagent and analysed every 2 hours (Figure 4-16). Cells treated with the peptide were observed to change their morphology from spread out to rounded very quickly and this was obvious at the time of the first scan post-treatment (t = 0 h). The cells then followed the apoptotic pathway and became stained with the assay reagent detecting high levels of Caspase 3/7, which results in green fluorescence. This was most efficient within the first 8 hours, as quantified by the IncuCyte® (Figure 4-17), and resulted in a visibly decreased cell survival leading to lower confluency by t = 18 h, as compared to cells treated with PBS only. Treatment with ABT-737 also led to rapid rounding of A549 cells, but failed to push them onto the apoptotic route, as indicated by the assay, up until t = 18-20 h, where an increase in green fluorescence was observed. Along with the previous results this indicates that the mode of action of ABT-737 is slower than PP50-mediated Bim delivery.

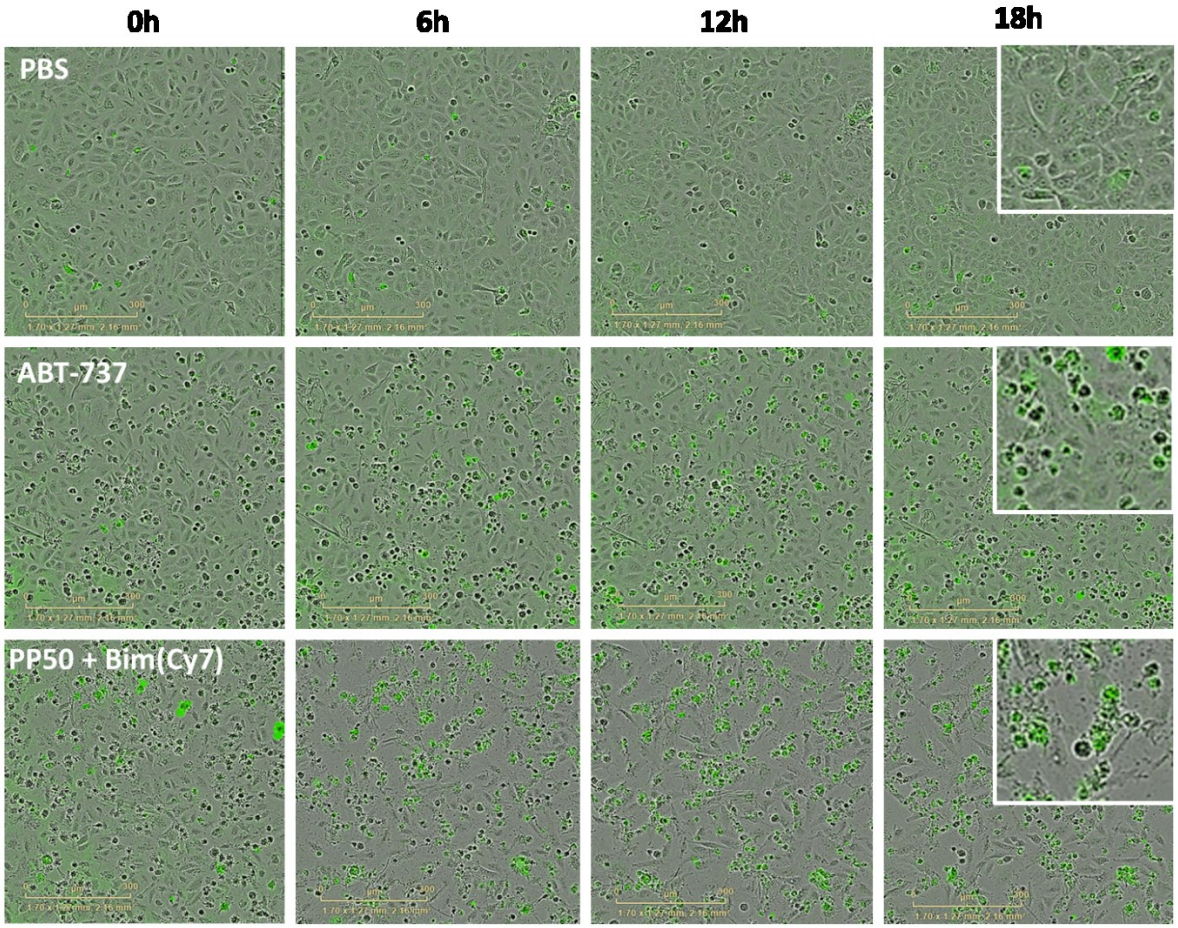


Figure 4-16. Cell morphology and death followed by delivery of Bim (20 μM) by co-incubation with PP50 (1 mg mL^{-1}) at pH 6.5 in a 4 h treatment compared to cell death caused by continuous treatment with ABT-737 (20 μM), analysed in IncuCyte® using Caspase-3/7 Green Apoptosis Assay.

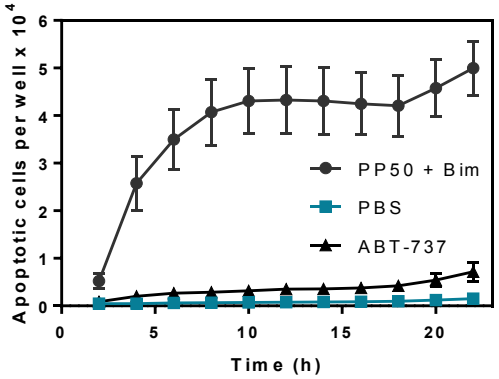


Figure 4-17. Number of apoptotic cells following delivery of Bim (20 μM) by co-incubation with PP50 (1 mg mL^{-1}) at pH 6.5 in a 4 h treatment compared to cell death caused by continuous treatment with ABT-737 (20 μM), analysed in IncuCyte® using Caspase-3/7 Green Apoptosis Assay over a 20 h period. Mean ± SD, n = 3.

4.2.9.3 Delivery of Bim – dose titration

To further characterise the PP50-mediated delivery of Bim, a dose titration study of the peptide was performed at a fixed polymer concentration of 0.5 mg mL^{-1} (Figure 4-18). The extracellular concentrations of Bim and scrBim, used for comparison, were equal to 0.1, 0.5, 1, 5, 10 and 20 μM. The initial Caspase 3/7 response was detected at 5 μM, and further increased 3-fold for 10 μM extracellular Bim. No obvious Caspase 3/7 activation was observed for the scrBim delivered via PP50. These findings are in line with reports about delivery of Tat-Bim conjugates, whereby the apoptosis activation was recorded after treatment with 2-5 μM of the constructs, depending on cell type (Kashiwagi et al., 2007). Like previously, the Caspase activation assay was performed in parallel to an AlamarBlue cell survival assay after a further 24 h period post-treatment (Figure 4-19). As expected, the cell survival was highly dependent on the peptide concentration used during the treatment, with half maximal effective concentration (EC50) of Bim delivered using PP50, as defined by the percentage of dead cells, equal to 11.2 μM. This also illustrates that for PP50-mediated delivery of this peptide, caspase activation is a good predictor of cell survival. In comparison, Caspase activation induced by the treatment with ABT-737 was not a reliable indicator of cell survival, as was shown in Figure 4-14 and Figure 4-15.

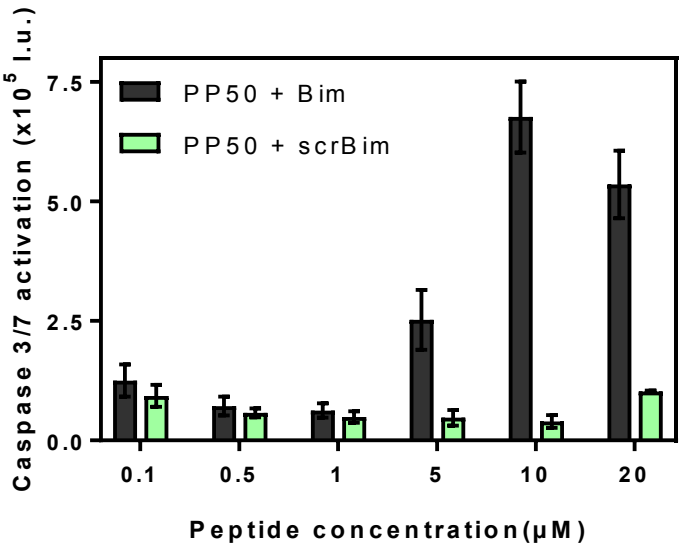


Figure 4-18. Caspase 3/7 activation following a treatment with PP50 (0.5 mg mL^{-1}) and either Bim or scrBim in the concentration range of 0.1-20 μM at pH 6.5. Treatment time was equal to 3 h, followed by a wash and 4 h of further incubation and analysis using the Caspase 3/7 Glo Assay. Mean ± SD, n = 3.

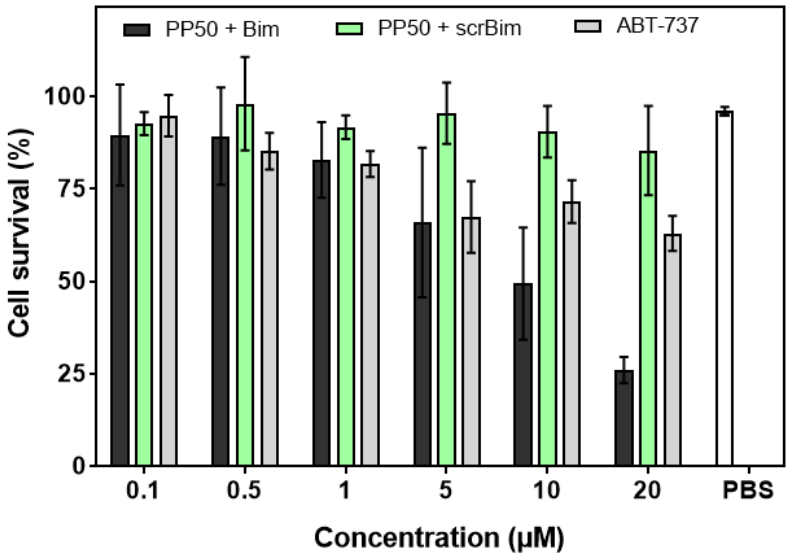


Figure 4-19. Survival of cells following a treatment with PP50 (0.5 mg mL^{-1}) and either Bim or scrBim in the concentration range of 0.1-20 μM at pH 6.5 or treatment with ABT-737 in the same concentration range. Treatment time was equal to 3 h, followed by a wash and analysis using AlamarBlue assay 24 h post-treatment. Mean ± SD, n = 3.

4.2.9.4 Delivery of Bim-Cy7

To provide further evidence for intracellular delivery of Bim, a Cy7 (Ex 750/ Em 773) labelled version of this peptide was used, along with the inactive control, scrBim-Cy7, to quantify the PP50-mediated delivery to A549 cells (Figure 4-20). Following a 1 h treatment with the polymer and the peptides at pH 6.5, or peptides alone, the cells were characterised using flow cytometry. In both cases of Bim-Cy7 and scrBim-Cy7 there was a clear effect of co-treatment with polymer, which resulted in brighter cells, compared to the polymer-free samples. This suggests that both of the peptides were being delivered to the cell interior but, as shown in previous figures, only Bim was capable of inducing apoptosis, which further validated scrBim as a valid, inactive control in the experiments presented herein.

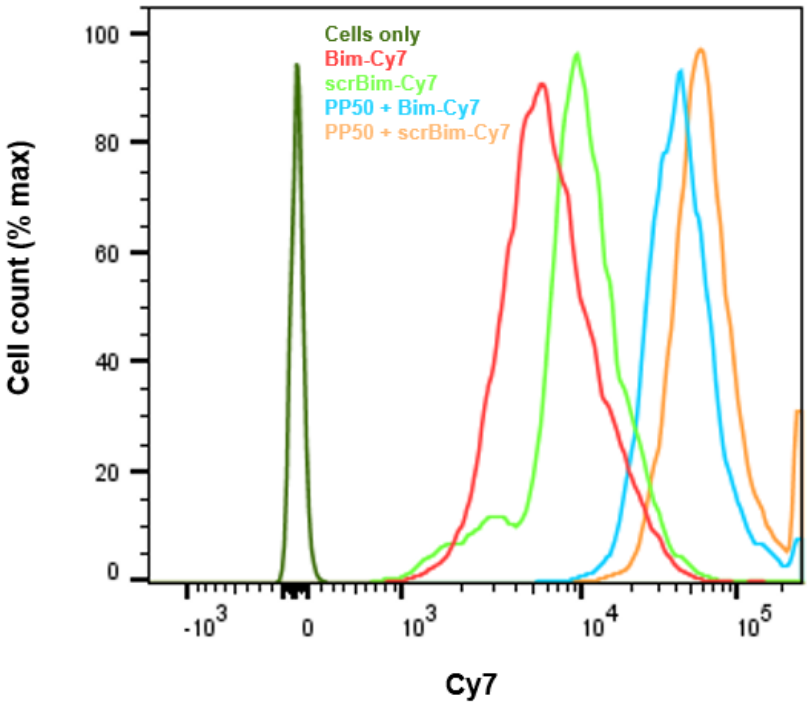


Figure 4-20. Flow cytometry of A549 cells following a 1 h treatment with PP50 (1 mg mL^{-1}) and either Bim-Cy7 or scrBim-Cy7 (10 μM) at pH 6.5. Corresponding polymer-free controls were used for comparison.

4.2.9.5 Delivery of Bim - comparison against other delivery methods

In order to place the PP50-mediated payload delivery in a wider context, the delivery of Bim and scrBim using this platform was compared against 8 other delivery technologies and the results were analysed in terms of cell survival following the treatment. Bim and scrBim (15 μM) were attempted to be delivered via the techniques listed in Table 4-2. In each case, optimal concentration and treatment time were established via literature research and optimisation experiments (data not shown).

Table 4-2. Delivery techniques used in the comparison study.

Delivery technique	Carrier Type	Molar concentration	Mass concentration	Reference
PP50	Polymer	22 μM	1 mg mL^{-1}	(Chen et al., 2009c; Mercado and Slater, 2016b)
PLP	Polymer	29 μM	1 mg mL^{-1}	(Eccleston et al., 2000; Eccleston et al., 2005)
PEI 0.6 kDa	Polymer	1.7 mM	1 mg mL^{-1}	(Godbey et al., 1999a; Wiseman et al., 2003)
PEI 25 kDa	Polymer	10 μM	0.25 mg mL^{-1}	(Godbey et al., 1999a; Wiseman et al., 2003)
Melittin	CPP	1 μM	2.85 μg mL^{-1}	(Kyung et al., 2018)
Tat	CPP	20 μM	31 μg mL^{-1}	(Erazo-Oliveras et al., 2014)
Penetratin	CPP	20 μM	47 μg mL^{-1}	(Derossi et al., 1994; Weill et al., 2008)
PULSin®	Commercial kit	Unknown	Unknown	
BioPORTER®	Commercial kit	Unknown	Unknown	(Bottger et al., 2010)
Electroporation	Physical method	N/A	N/A	(Ma et al., 2014)

In all cases, cell survival was analysed 24h post-treatment using the CellTiter Glo 2.0 assay, which quantifies ATP and therefore the presence of metabolically active cells in the samples. The results showed that PP50-mediated delivery performed best out of all the techniques used as comparison, resulting in 21.4 ± 1.5% cell survival in the cell samples treated with Bim, compared to 89.7 ± 3.3% survival in the cells delivered with the scrBim control (Figure 4-21). This method significantly outperformed the runner-up technique which was the delivery using 25 kDa PEI which resulted in a cell survival equal to 65.2 ± 5.9% and 52.7 ± 7.5% for Bim and scrBim, respectively. The high level of cell death observed when delivering scrBim using PEI (25 kDa) suggests a level of cytotoxicity of this delivery agent which was the most likely cause of cell death, rather than the action of delivered Bim. This comparison provides evidence that the PP50 platform is clearly a more potent delivery agent than some commonly used CPPs, PEI, electroporation and even two commercially available protein delivery kits, PULSin® and BioPORTER®, at peptide delivery by using the simple co-incubation strategy.

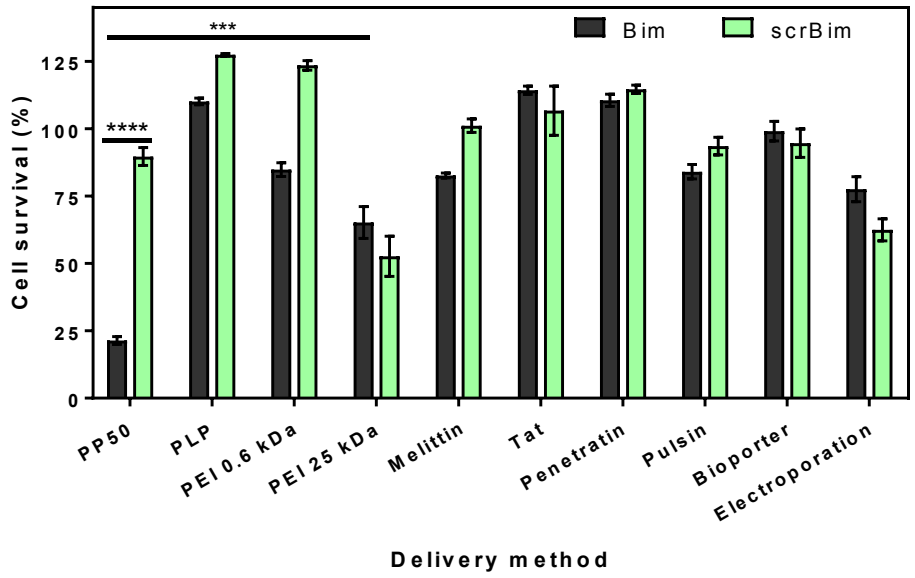


Figure 4-21. Comparison of cell death caused by the delivery of 15 μM Bim(Cy7) using different delivery methods. For the chemical delivery agents, the treatment time was equal to 4h. Cell survival was quantified using CellTiter-Glo 2.0 assay 24 h after the end of the treatment. Mean ± SD, n = 3. Statistical comparison between PP50-mediated delivery of Bim-Cy7 and scrBim-Cy7, as well as between PP50 and PEI 25 kDa (delivery of Bim-Cy7) was performed using two-tailed unpaired Student's t-test.

4.2.10 Delivery to extracellular vesicles

Extracellular vesicles are nanovesicles which can be produced by many different cell types including blood cells, stem cells and tumour cells, and occur naturally (Gangadaran et al., 2018). EVs play an important role in mediating long-distance intercellular communication as they can transfer different macromolecules, including nucleic acids (DNA, mRNA, non-coding RNA), lipids, receptors and proteins (Ha et al., 2016; Guo et al., 2017).

EVs are currenly being intensively studied as a potential drug carrier for *in vivo* applications and have already been shown of being capable of delivering small molecule anti-cancer drugs, proteins and nucleic acids (Ha et al., 2016). In contrast to liposomes and polymeric nanoparticles, EVs have a lower chance of inducing an immunogenic response due the similarity of membrane composition to that of the rest of the cells in the body when used autologously (Ha et al., 2016). In addition, EVs have been suggested to offer good tissue penetration and long systemic circulation due to negative charge and evasion of degradation (Gangadaran et al., 2018).

Currently used techniques for drug loading of EVs can be used either prior to extracellular isolation, most commonly via transfection of the desired cargo, or after isolation of the vesciles, via physical methods such as extrusion, sonication and electroporation (Vader et al., 2016). Here, the PP50-platform was investigated as a means of using a polymeric delivery agent for EV loading subseuent to their isolation from cells. EVs were kindly donated by Dr Christina Schindler (MedImmune) who also performed the analysis by flow cytometry.

Initial steps included charaterisation of the effects which PP50-mediated delivery has on EVs and confirmation of the delivery outcome. EVs obtained from HEK293 cells were incubated with 20 µM Bim-Cy7 for 1 h at pH 6.5 in the presence and absence of PP50 (1 mg mL^{-1}), followed by EV isolation using ultracentrifugation, which produced a good yield of 75% as analysed via NanoSight (Figure 4-22). This analysis also revealed that the treatment with the polymer and peptide did not affect the EV size, which stayed at ca. 130 nm

(Figure 4-23). These results indicate that PP50 does not have a disruptive effect on the vesicles.

The outcome of PP50-mediated delviery of Bim-Cy7 was analysed using flow cytometry. EVs incubated with the polymer and peptide using the same paramteres and isolation as above were immobilised on magnetic beads coated with anti-CD9 antibody, which concentrated the vesicles and allowed their visualisation using flow cytometry (Figure 4-24). The EVs incubated in the presence of both the peptide and the polymer were over 2-fold brighter than those in the polymer-negative samples, which suggests succseful loading of the fluorescent peptide into the vesciles. Interestingly, PP50-negative samples displayed a noticeable increase in fluorescence over the samples containing beads only, suggesting a level of membrane binding of the peptide on EV surface, passive loading or, most likely, incomplete peptide removal in the process of EV isolation which should therefore be further optimised.

Finally, the apoptotic effect of EVs loaded with Bim-Cy7 was assessed by treatment of A549 cells for 24 h, followed by cells survival analysis using CellTiter Glo2.0 assay. The EV samples containing 1.5 x 10^{12} vesicles per mL were dilluted 10-fold in DMEM and applied to A549 cells grown in 96-well plates. Iterestingly, the cell survival in the cells treated with EVs loaded with Bim-Cy7 in the presence of PP50 dropped by 20%, compared to the cell treated with EVs which had been incubated in the presence of the peptide alone. This promising result indicates that PP50 could have the ability to load EVs with an apoptotic macromomolecue, following by use of the vesicles as a a drug carrier. However, both the laoding and the cell treatment parts of the experiment need furhter optimisation to produce lower cell survival.

In addition, further studies need to be performed to evaluate and compare PP50-mediated delviery of Bim to EVs with other methods of EV loading, including sonication and extrusion (Vader et al., 2016). In addition, it might be possible to load the desired cargo to EV-producing cells prior to isoloation to ensure their incorporation into the vesicles, assuming the payload does not have an immediate deleterious effect on the producer cell, such as the apoptoic Bim

peptide. The payload concentration in the cytosol can be then kept at high level by periodic topping-up, as demonstrated earlier.

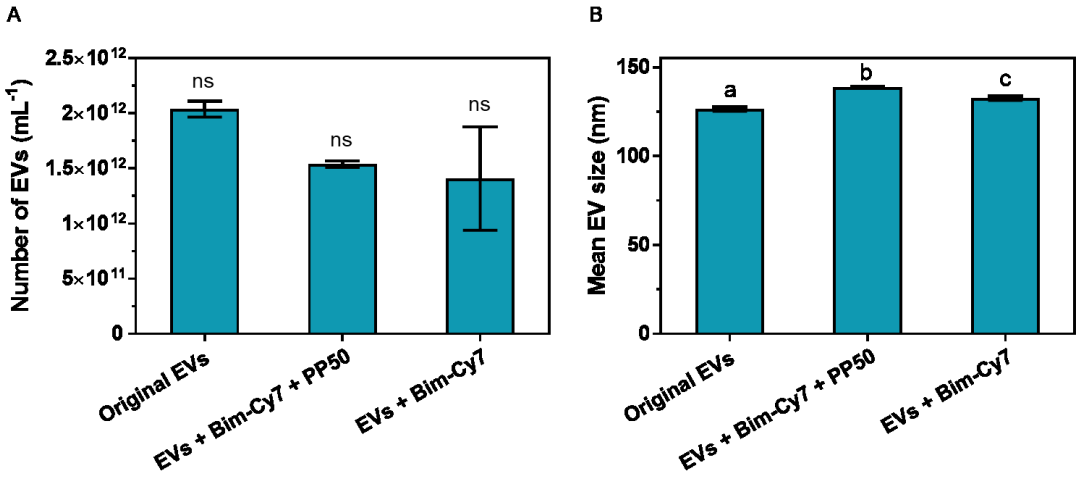


Figure 4-22. (A) concentration and (B) means size of EVs following loading of Bim-Cy7 (20 μM) by co-incubation with PP50 (1 mg mL^{-1}) at pH 6.5 for 1.5 h and EV isolation by ultracentrifugation, compared to the original EV concentration and size, analysed by NanoSight. Mean ± SD, n = 3. One-way ANOVA and Tukey's tests were performed for comparison. Different letters represent statistically significant difference with p-values < 0.5.

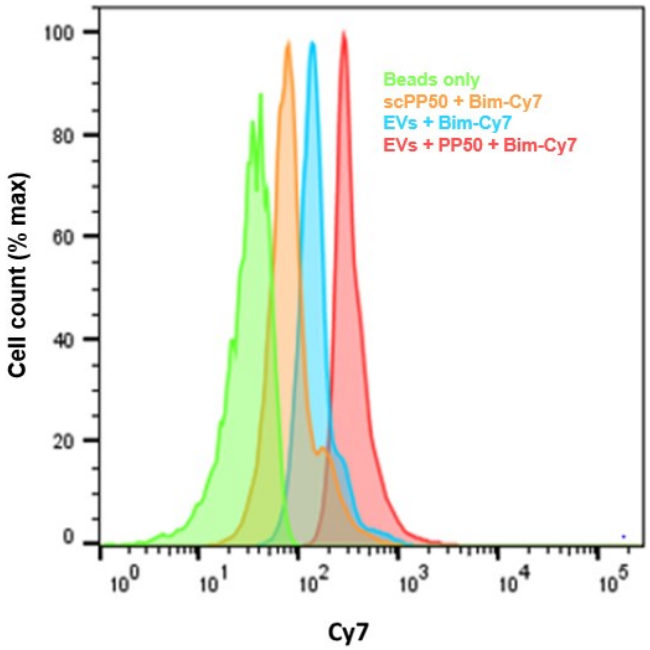


Figure 4-23. Fluorescence of EVs concentrated on magnetic beads following loading of Bim-Cy7 (20 μM) by co-incubation with PP50 (1 mg mL^{-1}) at pH 6.5 for 1.5 h and EV isolation by ultracentrifugation, analysed by flow cytometry. Flow cytometry of EVs was performed by Christina Schindler (MedImmune).

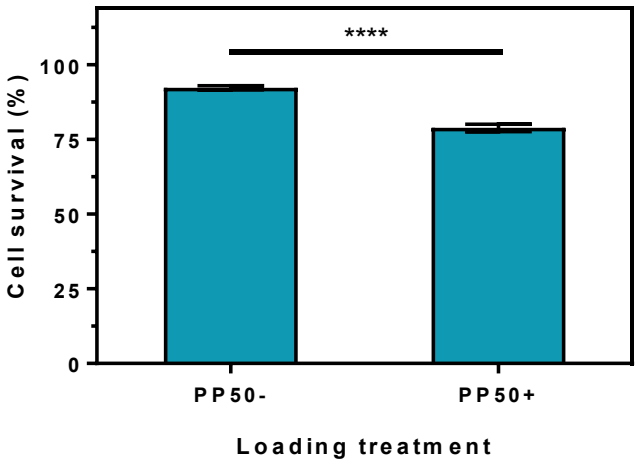


Figure 4-24. Survival of A549 cells treated with EVs loaded with Bim-Cy7 using PP50 at pH 6.5, following a continous treatment over 24 h, analysed using CellTiterGlo 2.0 Assay. Mean ± SD, n = 3. P-values were calculated using unpaired Student's t-test.

4.3 Conclusions

This chapter investigated the use of PP50 – a trigger responsive, membrane permeabilising polymer – as a versatile delivery agent for intracellular delivery of macromolecules. Based on the presented results, PP50 appears to be a good candidate to become a potential verstaile, next generation delivery agent with many potential uses *in vitro* and *ex vivo* (Stewart et al., 2016b).

It was demonstrated that treatment of nucleated mammalian cells with the polymer and a model antibody-sized payload in a simple, 2-step protocol, resulted in delivery to all 9 of the cell lines tested, including delivery to hard-to-transfect human mesenchymal stem cells. Based on this, PP50-mediated delivery is assumed to be compatible with many more cell lines. Furthermore, the PP50 platform performed well in delivery of a fluorescent model payload to 3D spheroids. This could allow to study cells and tumour models in a more unperturbed state, in contrast to payload delivery achieved by cell squeezing and other mechanical methods, which are often compatible only with single cell suspensions. Payload delivery to extracellular vesicles also appeared to be possible, but requires further optimisation. EVs loaded with the help of PP50 could be potentially used as drug carriers in *in vivo* applications.

PP50 sucesfully delivered various payload types, including a wide size range of fluorescent dextrans, proteins and a peptide. Additional studies are needed to fully asses the potential of PP50 to deliver nucleic acids by co-incubation, however, a PP-family polymer has already been reported to sucesfully deliver siRNA by conjugation for cancer therapy applications (Khormaee et al., 2013). Importantly, PP50 enabled the delivery of an apoptotic peptide, resulting in considerable cell death in a process which proved to be more efficient than some major competing technologies, such as CPPs and electroporation.

Since PP50 was shown to be capable of cytosolic delivery of macromolecules, it is therefore compatible with intracellular targeting strategies. The concentration of the desired payload in the cytosol can be controlled to certain extent by multiple delivery when necessary, as was demonstrated. The co-incubation protocol, in contrast to covalent conjugation, ensures that macromolecules delivered with the use of PP50 retain their functional properties upon cell entry. In addition, the consistent co-localisation of FITC-Dextran with the nuclear dye Hoechst suggest that PP50 might be capable of nuclear delivery. If this is confirmed, PP50 could allow for cell modification using the CRISPR/Cas9 system for genome editing (Li et al., 2015a).

Finally, the PP50 platform could be easily scaled up and could perform just as well with a small and large number of cells, with the restricting factors being the materials supply and the size of the cell culture vessel, in contrast to microfluidic-based delivery devices, which can be prone to clogging, limiting their throughput. In addition, PP50 is obtained using well established organic chemistry and has a low cost of production compared to cell penetrating peptides which require more complex synthesis.

In conclusion, PP50 has been shown to be a versatile platform technology which is compatible with different macromolecular cargo of different size and with different chemical and physical properties as well as suitable for delivery to different cell lines and to cells grown in different formats, and one which is potentially a more efficient delivery agent than a number of commonly used chemical and physical delivery techniques.

Chapter 5 - Payload delivery by conjugation with PP50

5.1 Introduction

The second mode of PP50-mediated intracellular delivery investigated is by payload conjugation to the polymer. In general, linkage of a cargo molecule to the delivery agent has a number of advantages over delivery by simple mixing, especially in *in vivo* settings. Firstly, payload conjugation prevents passive diffusion of drugs in the blood stream and their separation from the delivery agent, which can be pertinent for their intracellular delivery (Lee et al., 2017b). This is especially important for molecules which have inherent off-target effects and cytotoxicity, and therefore whose spread throughout the body should be avoided. Secondly, payload conjugation to a delivery agent can decrease the amount of the required drug by increasing its local concentration. This might allow the use of drugs which otherwise have low bioavailability, resulting in a low therapeutic utility (Bareford and Swaan, 2007). Thirdly, conjugation can increase the circulation time and drug stability in the blood stream (Suk et al., 2016).

PP-polymers have been used for payload delivery by conjugation before. Khormaee et al. (2013) conjugated thiol-modified siRNA onto PP75, a PP-family polymer with a 67% stoichiometric ratio of L-phenylalanine grafting. In their study, succinimidyl 3-(2-pyridyldithio)propionate (SPDP) was used as the crosslinker. The current work replaced this approach with conjugation using a disulphide containing crosslinker 3-(2-pyridyldithio)propionyl hydrazide (PDPH). This was built on expertise existing in the group. The cleavable nature of the crosslinker should enable payload release following reduction of the disulphide bond between the polymer and the macromolecular cargo in the intracellular environment.

This chapter describes the development of novel conjugate constructs containing the PP50 polymer linked to different-sized model payloads via

disulphide bond formation. First, 3.4 kDa PEG-FTIC was used as a model of a peptide-sized payload. Aspects of the conjugation reaction, such as the efficiencyynamics and payload release, using a small molecule model, were investigated. This was followed by the development and optimisation of PP50-protein conjugation procedure which used the inexpensive and readily available, medium-sized BSA as a model. Based on this newly developed conjugation protocol, green fluorescent protein (GFP) and immunoglobulin G (IgG) antibody, which were used as surrogates of small and large therapeutic proteins, respectively, were linked to PP50 via PDPH. Intracellular payload delivery was analysed using confocal fluorescent microscopy, which was made possible by using PEG and IgG antibody labelled with the fluorescent dye FITC and by using the intrinsic fluorescence of GFP.

The data presented herein illustrate the potential as well as the limitations of cargo delivery following conjugation to PP50, especially due to the payload size. The shown work also informs the development of polymer conjugates with functional payloads, which will be discussed in the following chapter.

5.2 Results and Discussion

5.2.1 PDPH grafting

PP50 was grafted with the thiol reactive crosslinker PDPH via amide bonds to enable subsequent polymer-macromolecular cargo conjugation. PDPH has been previously used to conjugate IgG antibodies with poly-L-lysine (Suh et al., 2001), maleimide-containing liposomes (Ansell et al., 1996) and a small molecule drug (Lee et al., 2017a) and for creation of poly(D,L-lactic-co-glycolic acid)-siRNA and Doxorubicin-gold conjugates, among others (Lee et al., 2011; Lee et al., 2015).

The crosslinker grafting degree can be defined and controlled by using a specific molar ratio of PDPH and the polymer. PDPH contains a protective 2-pyridyldithio group, which can be easily reduced by a thiol-contacting payload or a reducing agent to allow formation of a new disulphide bond. This results in the

displacement of 2-mercaptopyridine from the crosslinker, whose absorbance can be measured, enabling quantitative characterisation of the PDPH amount in solution, and thus the crosslinker grafting efficiency.

The level of grafting was determined using the following equation based on the Lambert-Beer Law:

$$\text{moles of PDPH addition per moles polymer unit} = \frac{\Delta A}{\varepsilon} \times \frac{\text{Mw polymer unit}}{\text{conc.}}$$

where:

- ΔA is the change of absorbance at 343 nm before and after DTT addition, as determined by UV-Vis spectrophotmotery (ΔA= (Average A_{343} after DTT) – (Average A_{343} before DTT)
- ε is the molar extinction coefficient of 2-mercaptopyridine in PBS and at 343 nm is equal to 8.08 x 10^3 $M^{-1}cm^{-1}$ (as per manufacturer's manual).
- Mw of PP50 unit is equal to 354 g mol^{-1}.
- Conc. is the concentration of PP50-PDPH used in the UV-Vis study and here is equal to 1 mg mL^{-1}.

In the first instance, the stoichiometric ratio of PDPH and the polymer of 5%, was used during the grafting reaction. This was assumed of being able to provide a sufficient number of 2-pyridyldithio groups on the polymer to enable payload conjugation. The actual degree of PDPH grafting on PP50 was established to be 2.86% ± 0.46% (n = 5). This means that ca. 2.86% of the available carboxyl groups located in the PP50 monomer units formed an amide bond with the crosslinker. With the desired grafting level of 5%, the efficiency of the grafting reaction was ca. 60 %. Knowledge of the PDPH grafting reaction efficiency was helpful in designing batches of polymer with a specific number of crosslinkers per polymer chain, as dictated by the needs of the payload being used.

5.2.2 Membrane disruptive ability of PP50-PDPH vs PP50

Since grafting of extra molecules onto PP50 might alter its properties, the membrane disruptive ability of the crosslinker-modified polymer was investigated. The membrane lytic capacities of PDPH-modified PP50 was compared to that of the original PP50 polymer. This analysis was performed using a haemolysis assay employing ovine erythrocytes, as described above. The haemolytic capacities were investigated at the polymer concentration of 0.1 mg mL^{-1} (Figure 5-1).

The pH-dependent membrane disruptive profile of PP50 was similar to previously published results, describing the membrane lytic ability of PP75 (Chen et al., 2009c). PP50-induced relative haemolysis peaked at pH 6.5, reaching a value of 90%.

The membrane disruptive profile of PP50-PDPH as a function of environmental pH showed high similarity to that of PP50 alone, with the highest level of relative haemolysis (ca. 85%) recorded at pH 6.5 for both PP50 with 0.9% and 1.7% grafting with PDPH. As pH 6.5 is typical of early endosomes, this can ensure release of engulfed materials in the early stages of endosomal trafficking to prevent degradation in lysosomes (Gao et al., 2010). The apparent drop of membrane lytic ability, noticeable especially at pH 6.0 and pH 7.4, might result from reduction in the number of free carboxyl groups, replaced with PDPH via amide bonding and is not surprising as changes in the carboxyl/hydrophobic group ratio of membrane-active polymers have been linked with substantial changes in their haemolytic properties (El-Sayed et al., 2005). However, due to the overall similarity and the high level of haemolysis achieved, it is possible to conclude that grafting with the PDPH crosslinker at ca. 2% substitution rate should not have a negative effect on overall polymer functionality and that the PP50-PDPH construct could be used in further payload delivery studies.

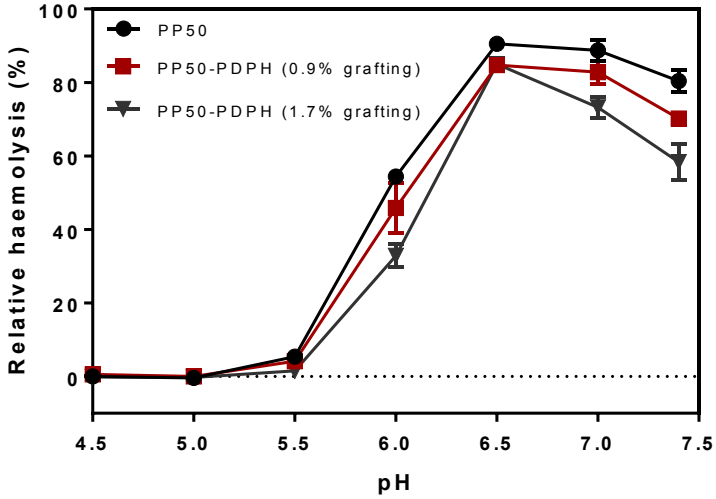


Figure 5-1. Relative haemolysis of red blood cells using PP50 and PP50-PDPH at 100 µg mL^{-1}. Incubation time = 1 h, temperature = 37°C. Mean ± SD, n = 3.

5.2.3 Release of 2-mercaptpyridine – a small molecule drug model

Polymer-payload conjugates should be stable during circulation in the bloodstream, while remaining sensitive to the intracellular environment and being capable of releasing the active substance inside the targeted cells. Glutathione (GSH) is a thiol-containing, biological antioxidant, abundantly present in the cytosol (Kurtoglu et al., 2009). The cytosolic concentration of glutathione is 0.5 – 10 mM, while plasma concentration is much lower, at around 2 µM (Maher, 2005; Lushchak, 2012). In addition, GSH concentration is also elevated in certain tumour types, including breast, ovarian and lung cancer (Gamcsik et al., 2012). Similarly, cysteine (Cys), which is another important biological reducing agent, shows a clear difference between the cytosol and plasma concentrations which are equal to 20 µM and 100 µM, respectively (Dröge et al., 1991; Lu, 1999). This gradient of redox conditions enables usage of crosslinkers with reducible disulphide bonds, such as PDPH.

2-mercaptopyridine (Mw = 111.16 g mol^{-1}) is a structural part of PDPH (Figure 5-2) where it acts as a protective component, preventing the thiol group from unwanted side reactions. In this set of experiments, 2-mercaptopyridine was

treated as a small molecule drug model conjugated to the crosslinker via a cleavable disulphide bond.

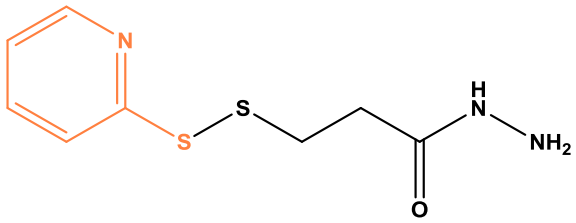


Figure 5-2. Structure of PDPH with 2-mercaptopyridine highlighted.

The release profiles of 2-mercaptopryridine from PDPH-modified PP50 in redox conditions at physiological pH 7.4 were studied using GSH and Cys as the reducing agents. The results are presented in Figure 5-3 and Figure 5-4. At the average blood concentration of GSH (2 μM), PP50-PDPH was stable with barely any detectable release of 2-mercaptopyridine. 25% and 58% of the total pool of the small molecule was however readily released at the concentrations corresponding to the lowest and highest limits of the intracellular concentration of GSH, respectively, following 2 h of incubation. Similarly, the release of 2-mercaptopyridine following incubation with Cys was higher at the intracellular concentration of this amino acid (25%), compared to that at the plasma-like concentration (10%). These results indicate that at intracellular concentrations, GSH was more efficient at reducing the disulphide bond of PDPH and releasing 2-mercaptopyridine than Cys.

In order to study a prolonged time-dependant profile of 2-mercaptopyridine release, the observation time was extended to 24 h. As before, the trends suggesting lower release levels in the environments mimicking the extracellular concentrations of GSH and cysteine and higher release levels in the environment mimicking the cytosol concentrations of these reducing agents were apparent. Furthermore, it was noticed that the initial release of the small molecule drug model was very rapid, with the majority of 2-mercaptopyridine released within the first 15 minutes, and was followed by a period of slower release until a plateau is reached between 2-6 hours of incubation, with 78% and 35% total release at the end of the 24 h observation period in the samples treated with GSH and Cys, respectively. The rapid release of the model payload is in line with the values reported for GSH-induced peptide-small molecule drug

conjugate disulphide cleavage (Lee et al., 2012). The reason why 100% release was not obtained here was not clear. A complementary technique, such as the measurement of payload fluorescence, could be performed to validate the model cargo release data.

The results presented in this section illustrate that the PP50-payload conjugates linked by disulphide bonds should remain stable in the bloodstream, but allow rapid payload release from the polymer once localised in the cytosol due to the high local concentration of the reducing agents such as glutathione and, to a lesser extent, cysteine.

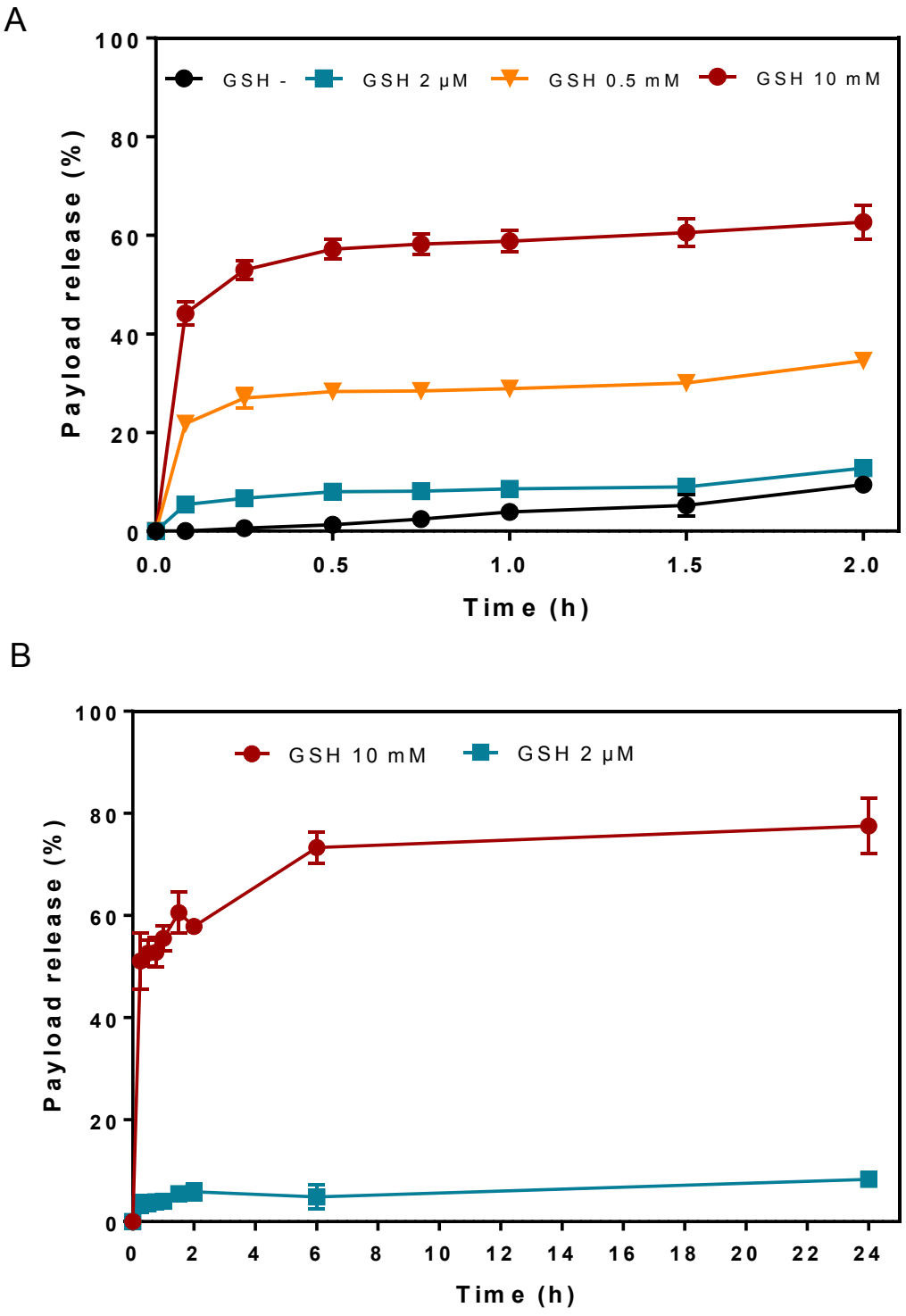
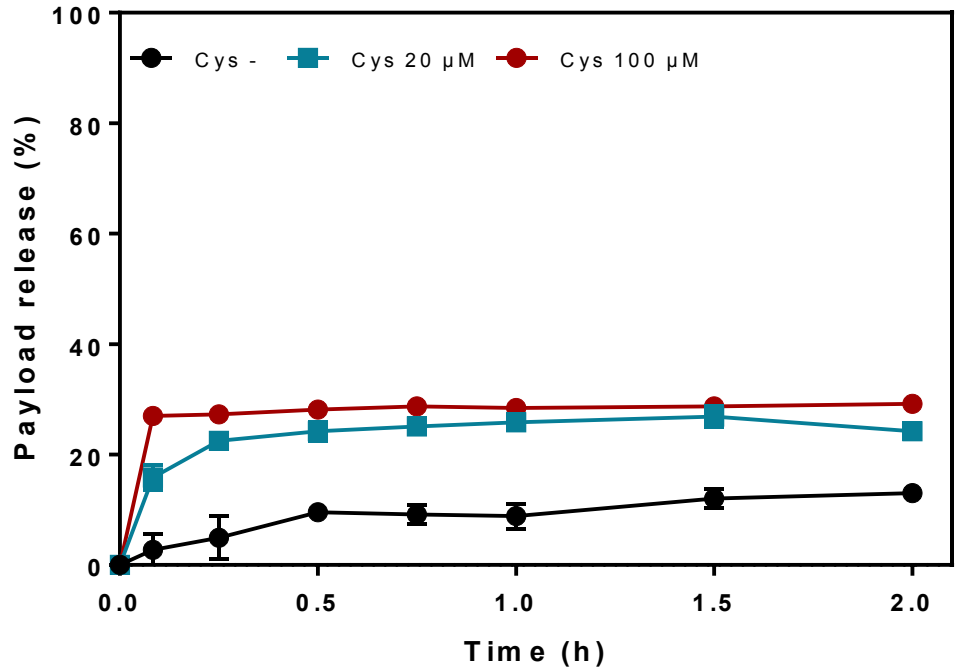


Figure 5-3. Release of 2-mercaptopyrine from PP50-PDPH using the cytosol (0.5 and/or 10 mM) and plasma (2 µM) concentrations of GSH (A) over a period of 2 h and (B) 24 h from the start of the reaction. Mean ± SD, n = 3.

A



B

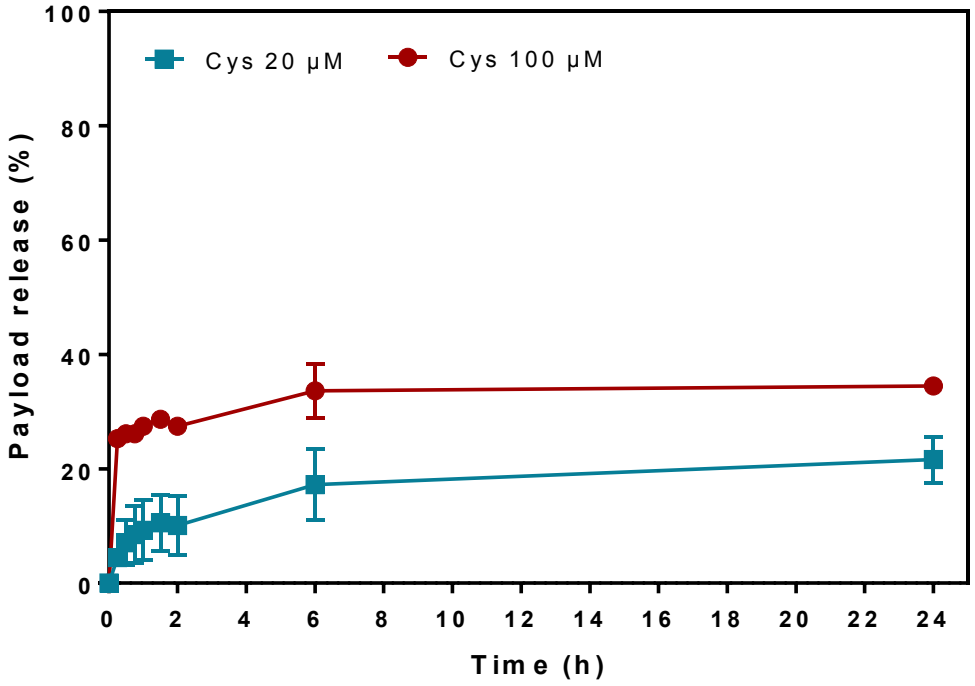


Figure 5-4. Release of 2-mercaptopyrine from PP50-PDPH using the cytosol (100 µM) and plasma (20 µM) concentrations of cysteine (A) over a period of 2 h and (B) 24 h from the start of the reaction. Mean ± SD, n = 3.

5.2.4 Conjugation and delivery of PEG-FITC

PEG-FITC is a poly(ethylene glycol) (PEG) polymer conjugated with a fluorescein (FITC) molecule, which enables tracking in cellular studies, as well as functionalised with a thiol group, allowing conjugation to other molecules via a cleavable disulphide bond (Figure 5-5*).* The molecular weight of the PEG-FITC used in this study was equal to 3.4 kDa, with the aim of using this fluorescent cargo as a peptide-sized model payload. In addition, non-fluorescent, thiol-functionalised PEGs with the molecular weight of 2 and 6 kDa were used in the haemolysis and cell toxicity study, in order to avoid potential interference with these measurements.

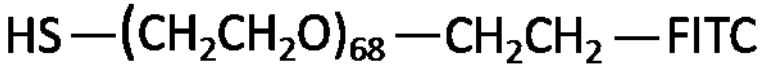


Figure 5-5. Structure of PEG-FITC

5.2.4.1 Conjugation efficiency and kinetics

Conjugation efficiency, defined as the ratio of payload molecules loaded onto a delivery agent to the total number of crosslinker sites available for binding, is of great interest in the process of preparation of polymer-payload conjugates. High conjugation efficiency simplifies the subsequent purification process, or removes a need for one altogether in scenarios when the reaction is nearly 100% efficient. Furthermore, since therapeutic payloads are often expensive, high conjugation efficiency lies in economic interest. Here, two parameters which dictate the efficiency of payload loading were studied: (i) the molar ratio of payload to crosslinker as well as (ii) the composition of the solution in which the reaction took place.

Firstly, the conjugation kinetics and efficiency of PEG-FITC onto PDPH-modified PP50 using 3 different molar ratios of the payload to the crosslinker were investigated. The molar ratios of PEG-FITC to PDPH used were equal to 0.5:1, 1:1 and 2:1. The results are presented in Figure 5-6 and Figure 5-7. As

suggested by the sharp slope of the three curves in the initial 5 minutes, the conjugation process occurred very rapidly, with the majority of the possible conjugation taking place before the first measurement was taken. This was followed by a period with a slower increase in payload loading observed at the 0.5:1 and 1:1 molar ratios, after which the conjugation reaction reached a plateau. Unsurprisingly, it was observed that the speed and the final level of conjugation were directly proportional to the molar ratio of the payload to the available PDPH crosslinkers used in the reaction, with the highest conjugation effectiveness following a 24 h reaction equal to 73%, followed by 62% and 39% for 2:1, 1:1 and 0.5:1 molar ratios, respectively. The thiol exchange kinetics shown here were similar to those reported by the group of Ansell et al. (1996) who used PDPH for protein-liposome conjugation, observing the majority of the reaction occurring within the first 1 h.

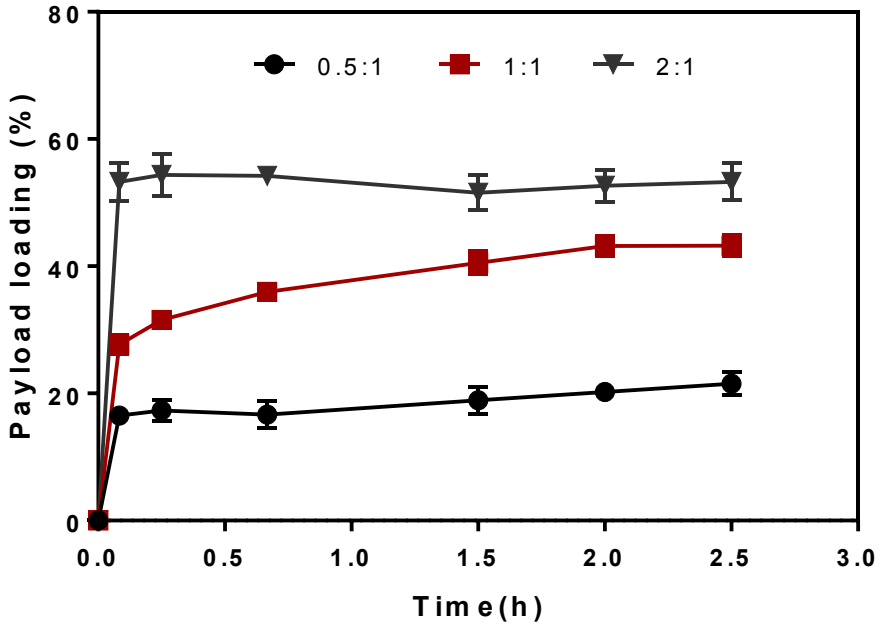


Figure 5-6. Kinetics of the conjugation of FITC-PEG-Thiol onto PP50-PDPH in PBS (pH 7.4) at 0.5:1, 1:1 and 2:1 molar ratios of payload to PDPH over 2.5 hours at room temperature. Mean ± SD, n = 3.

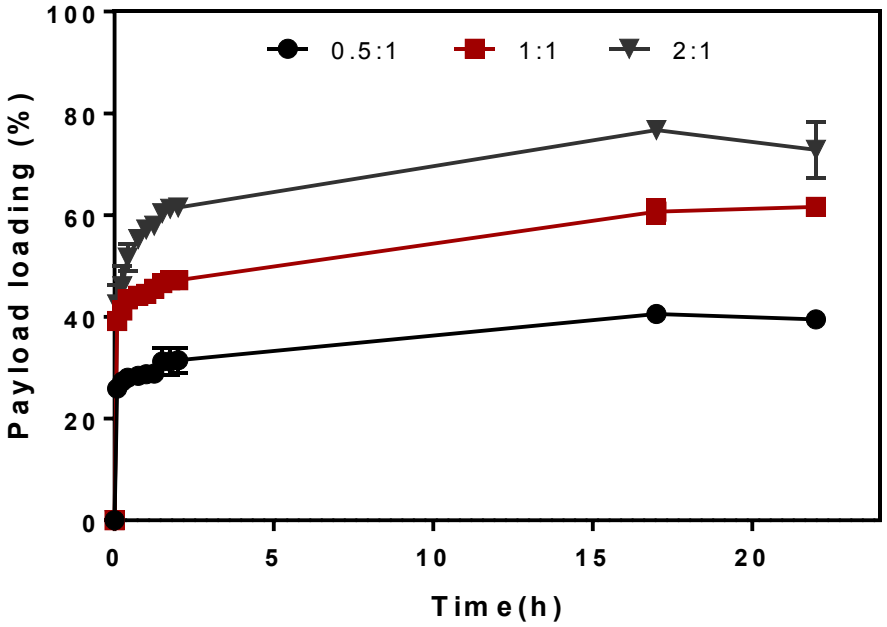


Figure 5-7. Kinetics of the conjugation of FITC-PEG-Thiol on PP50-PDPH in PBS (pH 7.4) at 0.5:1, 1:1 and 2:1 molar ratios of the payload to PDPH over 22 hours at room temperature. Mean ± SD, n = 3.

In addition, the effect of the reaction environment on reaction efficiency was also studied (Figure 5-8). The presented results suggest that the use of a PBS/DMSO mixture could further enhance the conjugation efficiency. Higher proportions of DMSO exceeding 50% were seemingly worse for conjugation effectiveness than buffers containing 50% DMSO. It is possible that a mixed solvent system, containing 50% DMSO/50% PBS could be most potent for a desirable reaction efficiency for some payloads. This effect was perhaps due to a more open structure of both the PP50 and the PEG-FITC payload in these conditions, which promotes the interaction between the thiol on the payload and the crosslinker, encouraging efficient formation of disulphide bonds.

These experiments suggest that it is possible to increase the efficiency of the conjugation reaction between PDPH-modified PP50 and a peptide-sized, thiol containing payloads by modulating their molar ratio as well as changing the reaction environment. They also provided base knowledge about the conjugation kinetics between the two components which can prove useful in future conjugation experiments, especially when designing their timing. In the

following experiments, the 2:1 ratio of payload to crosslinker was used to ensure high conjugation efficiency and the excess PEG was removed by dialysis.

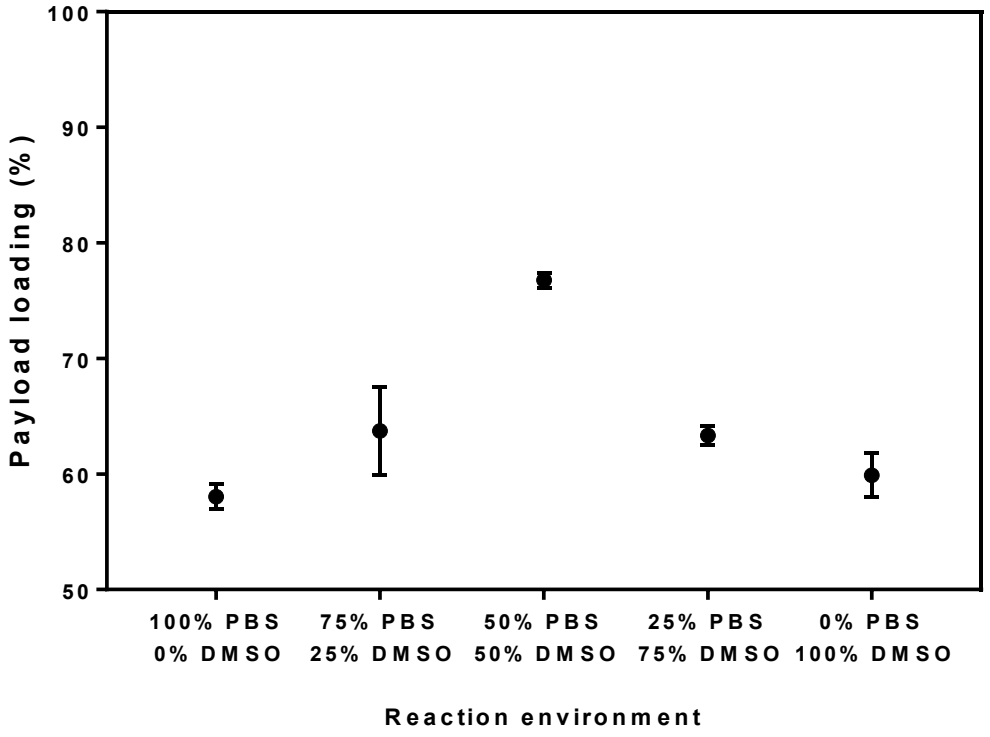


Figure 5-8. The efficiency of the conjugation reaction between PEG-FITC and PP50-PDPH in different reaction environments at a 1:1 molar ratio of the payload to the crosslinker, measured by quantifying the release of 2-mercaptopyridine by UV-Vis spectroscopy. The conjugation was performed at room temperature, t = 5 h. PP50-PDPH concentration = 1 mg mL^{-1}. Mean ± SD, n = 3.

5.2.4.2 Membrane permeabilisation by PP50-PEG conjugates – haemolysis assay

The membrane permeabilising ability of PP50 conjugated to PEG was characterised in a haemolysis assay (Figure 5-9). PP50 conjugated to either 2 kDa or 6 kDa PEG at one payload per polymer chain were used. Molarity was used to describe conjugate concentration, based on the average Mw of PP50 = 46 kDa (Chen et al., 2009c; Lynch et al., 2010). The profile of haemoglobin release from ovine erythrocytes following 1 h treatment in 7 different pH environments was similar to that of PP50 alone, with an average decrease of 14% in terms of haemolysis efficiency for the conjugates. This difference was most evident at pH 6.0, where the relative haemolysis for PP50 was equal 62%

but only 24% for PP50-PEG. Nevertheless, the conjugates achieved a very high level of haemoglobin release at pH 6.5 of 74% and 80% for the conjugates with 6 kDa and 2 kDa PEG, respectively. This high level of membrane activity leading to haemolysis at mildly acidic pH values, typical of early endosomes, would enable payload release before potential degradation in lysosomes.

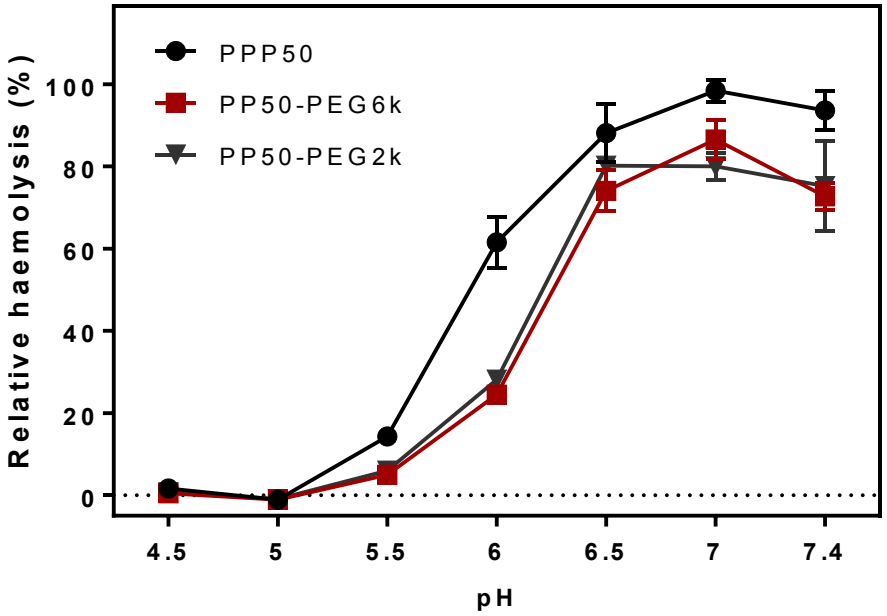


Figure 5-9. Relative haemolysis of PP50 and PP50-PEG (PEG size equal to 2 or 6 kDa, one PEG payload conjugated per 1 polymer chain). Polymer concentration was equal to 100 μg mL^{-1} (2.2 μM) and conjugate concentration was 2.2 μM. The incubation time was 1 h. The treatment was performed at 37°C in a shaking water bath. Mean ± SD, n = 3.

5.2.4.3 Cytotoxicity of PP50-PEG conjugates

Before imaging of the delivery to nucleated mammalian cells, the cytotoxic effect of the PP50 conjugates with the peptide-sized 2kDa PEG payload on HeLa cells was quantified. HeLa cells used in this study were treated with PP50 alone, PDPH-modified PP50, or PP50-PEG2k at concentrations in the range of 0.05 to 1 mg mL^{-1} for 24 h, and the cell survival was determined using the AlamarBlue assay (Figure 5-10). The results showed very high cell survival for all of the samples, as compared to untreated cells, indicating that neither the PP50 nor the PP50-PEG2k conjugate should pose a major risk in terms of cytotoxicity to the cells during the delivery process.

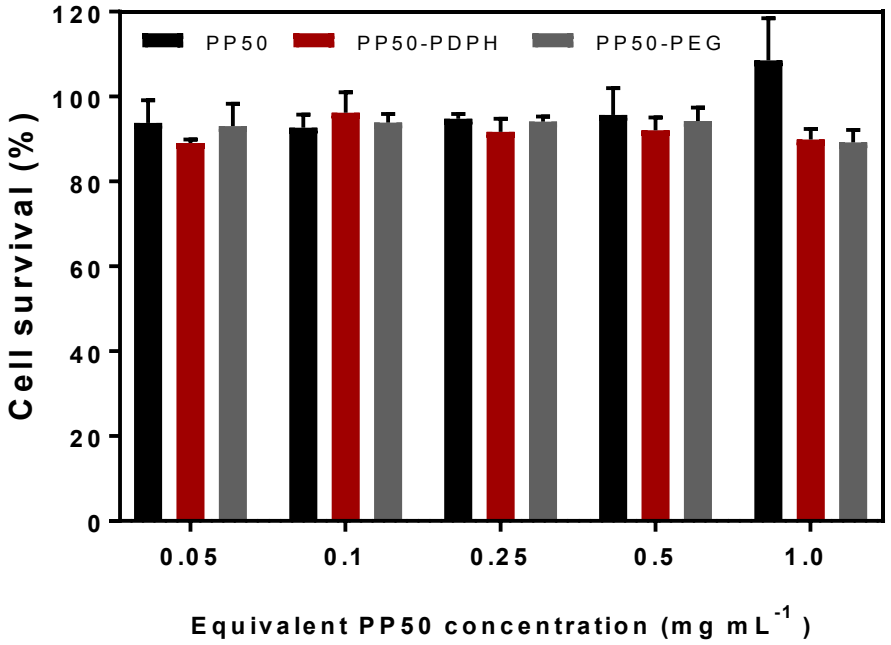


Figure 5-10. Survival of HeLa cells, determined by AlamarBlue assay, following a 24 h treatment with various concentrations of PP50, PP50-PDPH and PP50-PEG2k (1.3 PEG molecules per 1 polymer chain) at equivalent PP50 concentrations. Mean ± SD, n = 3.

5.2.4.4 Intracellular delivery of PP50-PEG conjugates

The ability to deliver a fluorescent, peptide-sized PEG by PP50 was investigated. PP50-PEG-FITC was applied to HeLa cells at pH 7.4 and pH 6.5 and analysed with confocal microscopy (Figure 5-11). The delivery efficiency was also compared to cells treated with PEG-FITC alone at both pH 7.4 and pH 6.5.

As illustrated in the green channel, the delivery of the peptide-sized payload was successful following conjugation to PP50, resulting in a presence of a diffused green fluorescence signal in the intracellular space, indicative of intracellular delivery of the payload. This was in obvious contrast to the cells treated with PEG-FITC alone, which did not result in a detectable fluorescent signal following washing and did not stimulate endocytosis to the same extent as the treatment with PP50-PEG-FITC, as illustrated by LysotrackerRED (red channel).

Successful delivery of PEG-FITC by conjugation with PP50 was observed at both pH 6.5 and pH 7.4. In addition, presence of bright green spots in the green channel, which colocalised with LysotrackerRED, suggests partial entrapment in the endosomes, which did not however prevent intracellular delivery. This fluorescence pattern contrasts with delivery achieved by mixing PP50 with fluorescent payloads in two ways: (i) following delivery of fluorescent dextrans by co-incubation, there was no obvious endosomal entrapment as indicated by bright spots and (ii) payload delivery at pH 6.5 appeared to be much more efficient than at pH 7.4. These changes could be explained by the fact that payload conjugation to PP50 might affects its ability to permeabilise the plasma membrane. Such effect was reported for cationic CPPs which were conjugated to a cargo oligonucleotide, resulting in switching of the uptake route from fast direct penetration to a slower, endosome-mediated internalisation (Räägel et al., 2010).

It is therefore possible that covalently linking a payload, such as PEG-FITC, to the PP50 polymer would also have a similar effect, with the consequence being internalisation via the less efficient endosomal route. This effect could greatly depend on the size and properties of the conjugated cargo, and not all payloads might dampen the delivery efficiency in such manner. This will be illustrated in the following chapter.

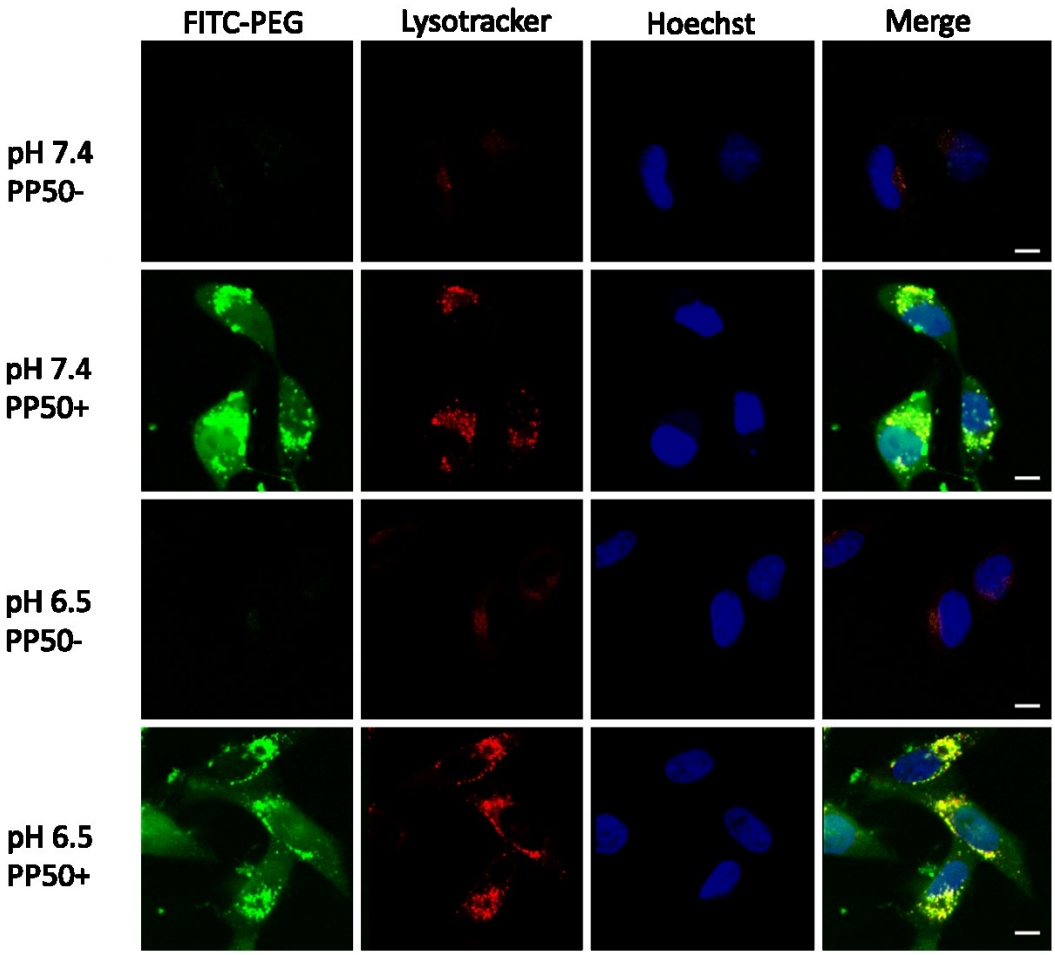


Figure 5-11. Delivery of PP50-PEG-FITC (11 μM) to HeLa, as analysed by confocal microscopy. 2 PEG-FTIC molecules were conjugation via the PDPH crosslinker per each one PP50 chain. Cells were treated in the absence or presence of polymer at pH 7.4 ("pH 7.4 PP50-" and "pH 7.4 PP50+", respectively) and at pH 6.5 ("pH 6.5 PP50-" and "pH 6.5 PP50+", respectively) for 1 h, which was followed by cell washing and 3 h of further incubation in serum-supplemented DMEM. Channels: Red = LysoTracker, Blue = Hoechst33342, Green = FITC-PEG. Scale bar = 10 μm.

5.2.5 Conjugation and delivery of proteins

Proteins are large macromolecules composed of amino acids and exist in many different sizes and with various properties and functions, including their potential to be used as therapeutics. A number of FDA-approved protein therapeutics are covalently linked to PEG to improve their half-life in the bloodstream (Pelegri-O'Day et al., 2014). Polymeric substitutes of poly(ethylene glycol) for protein conjugation have also been developed to counteract possible problems of PEG, such as tissue accumulation and immune response promotion (Pelegri-O'Day

et al., 2014), while improving or introducing new properties to the protein, such as increased stability or functional activity (Keefe and Jiang, 2011; Lee et al., 2013). In this chapter, proteins were attempted to be conjugated to PP50 via the PDPH crosslinker and be delivered to the interior of HeLa cells via the polymer-induced membrane permeabilisation.

5.2.5.1 Conjugation of Bovine Serum Albumin

BSA is an inexpensive protein with M_w of 66.5 kDa, which was used as a model of a medium-sized functional protein. It has one free thiol group on Cysteine 34 (Figure 5-12), which can react with PDPH-grafted PP50 to form a cleavable disulphide link. Here, the reaction efficiency between BSA and PP50-PDPH was investigated using different molar ratios of the protein and the crosslinker-grafted polymer, different polymer concentrations, inclusion of DMSO in the reaction solution, as well as by increasing the number of free thiols on BSA by grafting with N-succinimidyl S-acetylthioacetate (SATA). BSA conjugation to PP50 was used as a model to inform about the crucial parameters dictating the efficiency of PP50-protein conjugation and to help with design of protocols for conjugation of other proteins which are more relevant in the context of payload delivery, such as IgG and GFP, whose intracellular delivery was investigated in the following experiments.

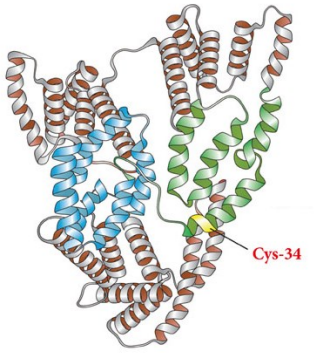


Figure 5-12. The structure of Albumin with free cysteine highlighted. Modified from Kim and Lee (2012).

Firstly, different molar ratios of PP50-PDPH and BSA were used (Figure 5-13 A). The effectiveness of the conjugation reaction was equal to 19 % at 0.5:1 molar ratio of BSA to the available PDPH molecules, 37 % at 1:1 and 41 % at 2:1. Interestingly, the reaction effectiveness recorded at 1:1 and 2:1 were very similar, suggesting that increasing the molar excess of BSA over PDPH might not result in a better efficiency of the reaction.

In an attempt to increase the efficiency of the conjugation reaction, the concentration of PP50-PDPH was increased from 1 to 2 and 5 mg mL^{-1} (the concentration of BSA was increased accordingly to match the 1:1 molar ratio of BSA to available PDPH). As shown in Figure 5-13 B, the increase in concentration did not cause a corresponding increase in conjugation effectiveness, with maximum detected conjugation levels just below 40% for all the studied concentrations. The limited protein loading might be a result of the large size of BSA which could lead to steric hindrance, preventing sufficient levels of interaction with other large sized molecules, such as the polymer used (Veronese et al., 2009).

The following step included addition of extra sulfhydryl groups using the SATA crosslinker. Introduction of sulfhydryl groups has been suggested in the literature for enabling or improving the development of protein-polymer conjugates (Gauthier and Klok, 2008). SATA, which binds to primary amines of proteins, introduced 1.5 moles of sulfhydryl per 1 mole of BSA, for the total of 2.5 sulfhydryl groups per BSA molecule, as detected by Ellman's reaction. The following conjugation reaction with PP50-PDPH at a 1:1 ratio of BSA to PDPH resulted in 84% protein loading, compared to 40% for unmodified BSA (Figure 5-13). These results suggest that addition of extra sulfhydryl groups on protein might increase the efficiency of the conjugation reaction.

Finally, the conjugation efficiency of PP50 to the SATA-modified BSA was compared to the conjugation efficiency of unmodified BSA in a solution containing 50% DMSO, which was shown to increase the PEG conjugation efficiency. As illustrated in Figure 5-13 D, both SATA-modified BSA and BSA conjugated in a solution containing 50% DMSO achieved high levels of loading onto PP50 which was equal to 76% and 85%, respectively. This might be a

result of partial or complete unfolding of the protein structure subjected to the organic solvent, leading to a high level of exposure of BSA's free thiol (Ashok et al., 2013). Since protein unfolding can lead to loss of function, this approach is however not recommended for this type of macromolecular payloads unless refolding is a viable option after removal of DMSO.

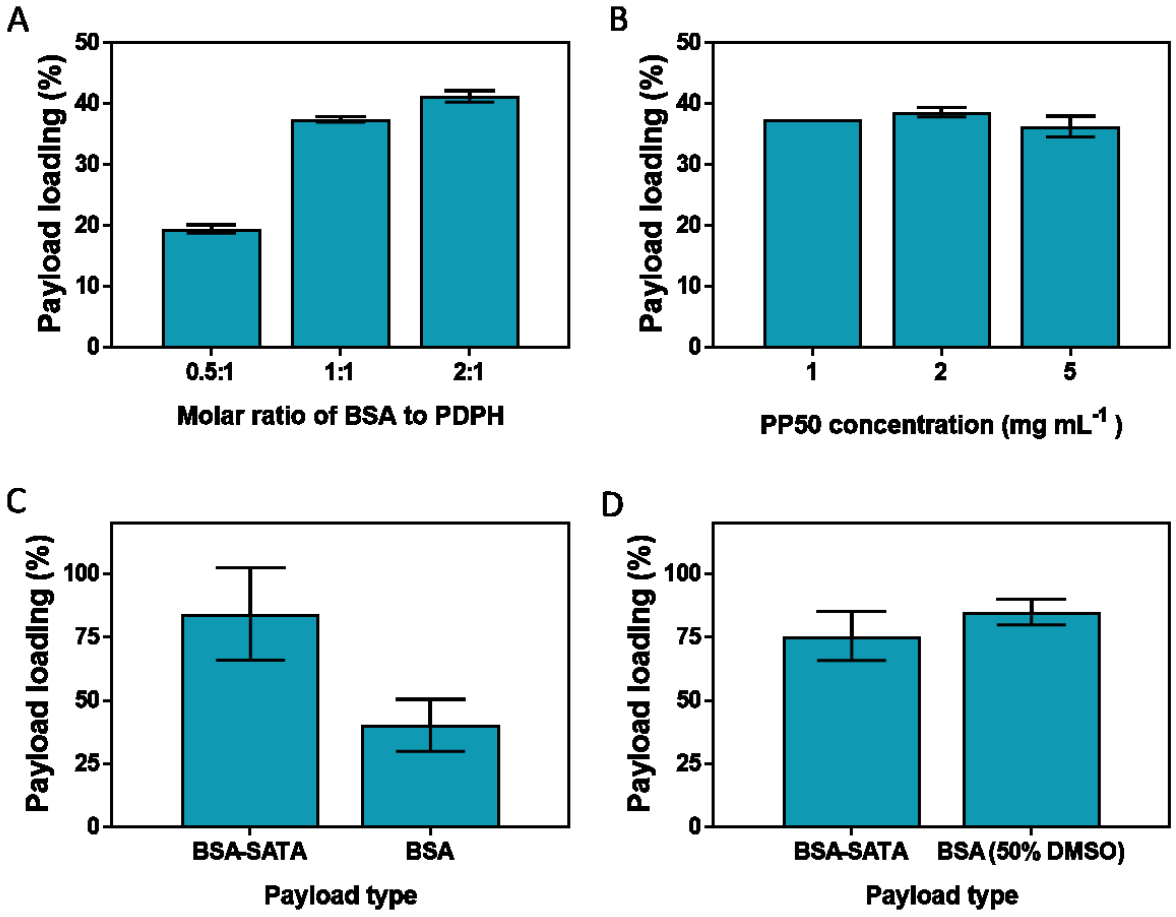


Figure 5-13. The efficiency of BSA conjugation to PDPH-modified PP50, analysed by the 2-mercaptopyridine release assay: (A) Conjugation of BSA to PP50-PDPH at 0.5, 1:1 and 2:1 molar ratios of BSA to PDPH. Concentration of PP50-PDPH = 1 mg mL^{-1}. (B) Conjugation of BSA to PP50-PDPH at 1:1 protein to PDPH molar ratio. Concentration of PP50-PDPH = 1, 2 and 5 mg mL^{-1}. (C) Conjugation efficiency of PP50-PDPH to SATA-modified BSA compared to conjugation of unmodified BSA in PBS. Concentration of PP50-PDPH = 1 mg mL^{-1} (D) Conjugation efficiency of PP50-PDPH to SATA-modified BSA in PBS compared to conjugation of unmodified SATA in 50%DMSO/50% PBS. Concentration of PP50-PDPH = 1 mg mL^{-1}. All reactions were performed at room temperature. Reaction time was equal to 24 hours. Mean ± SD, n = 3.

5.2.5.2 Conjugation and delivery of green fluorescent protein

GFP (Mw = 26.9 kDa) was used as a model of small-sized proteins and its intracellular delivery was investigated by conjugation to PP50. GFP is a chromophore-containing protein, with excitation and emission peaks at 395 nm and 509 nm, respectively. GFP also possess a free cysteine at the position 48 which is exposed to the solvent. (Inouye and Tsuji, 1994; Ormo et al., 1996). The thiol group of the free cysteine was used here as a point of attachment via the PDPH crosslinker to the polymer, as described above. The conjugation reaction resulted in approximately 1.1 GFP molecule per polymer chain, as analysed using the 2-mercapotpyridine release assay.

Preliminary experiments were then carried out to test the general deliverability of PP50-GFP at pH 7.4 to HeLa cells and characterised by confocal microscopy. Cells treated with PP50-GFP for 1 h in serum-free DMEM (pH 7.4), followed by a wash and a period of 6 h of further incubation were compared to cells treated with GFP alone under the same conditions. The confocal microscopy images presented in Figure 5-14 illustrate successful delivery of GFP following conjugation with PP50, which resulted in a clear diffused green fluorescent signal throughout the cell. However, a high level of colocalization with the endosome-lysosome marker LysotrackerRED evident by the yellow fluorescence observed in the merged channel, suggests a level of endosomal entrapment which could have, to a certain extent, inhibited the delivery efficiency. This pattern, however, suggested a higher level of cytosolic delivery than GFP delivered by conjugation to CPPs, such as Tat and Hepta-arginine (Fu et al., 2014; Nischan et al., 2015). In contrast to PP50-GFP, GFP alone appeared only to internalise in endosomes and was not capable of cytosolic entry.

These results suggest that PP50 is able of delivering small-sized proteins, such as GFP, by conjugation. Further experiments could be carried out to test the potential synergistic effect of GFP delivery by conjugation to PP50 and of the mildly acidic extracellular pH which could further enhance delivery efficiency.

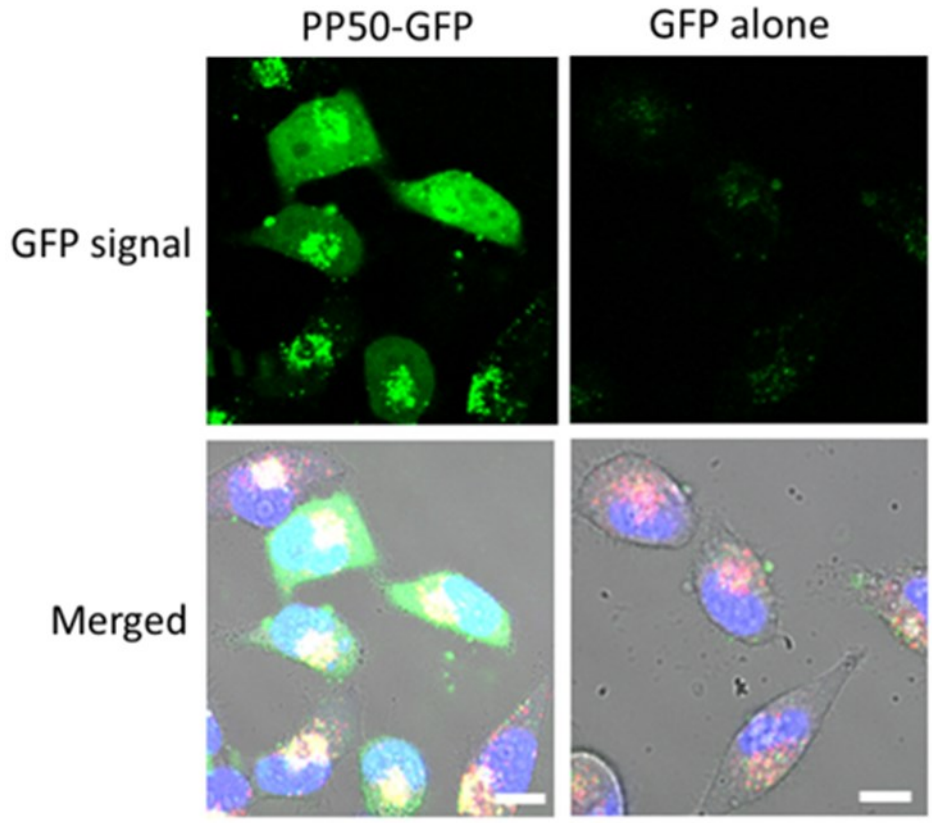


Figure 5-14. Delivery of GFP to HeLa cells following conjugation to PDPH-modified PP50, analysed by confocal microscopy. GFP was conjugated to PP50-PDPH at 1.1 protein per 1 polymer chain (PP50-GFP concentration = 24 μM) and compared to delivery of GFP alone (4.6 μM). The materials were applied in serum-free DMEM for 1 h, followed by cell washing and 6 h of further incubation in serum-complemented DMEM. Channels: Green = GFP; Merge = Green channel + Red (LysoTrackerRED) and Blue (Hoechst33342). Scale bar = 10 μm.

5.2.5.3 Conjugation and delivery of IgG

PP50 was conjugated to IgG labelled with FITC. As IgG antibodies do not possess free thiols which are readily available for conjugation, additional thiols were added to the antibodies using SATA. SATA-modified IgG antibodies were subsequently conjugated to PP50 grafted with the thiol-containing crosslinker, PDPH, resulting in addition of ca. 4 polymer chains per 1 IgG molecule.

The membrane activity of the PP50-IgG conjugate was investigated via a haemolysis assay (Figure 5-15). Following incubation with ovine red blood cells at 6 different pH values, the absorbance of the released haemoglobin was

analysed. The PP50-IgG conjugate achieved >95% haemolysis at mildly acidic pH values between pH 6.5-7.0. The haemolysis profile was similar to that of a mixture of PP50 and IgG, which was used for comparison. This suggested that the polymer-antibody conjugates had high membrane permeabilisation potential.

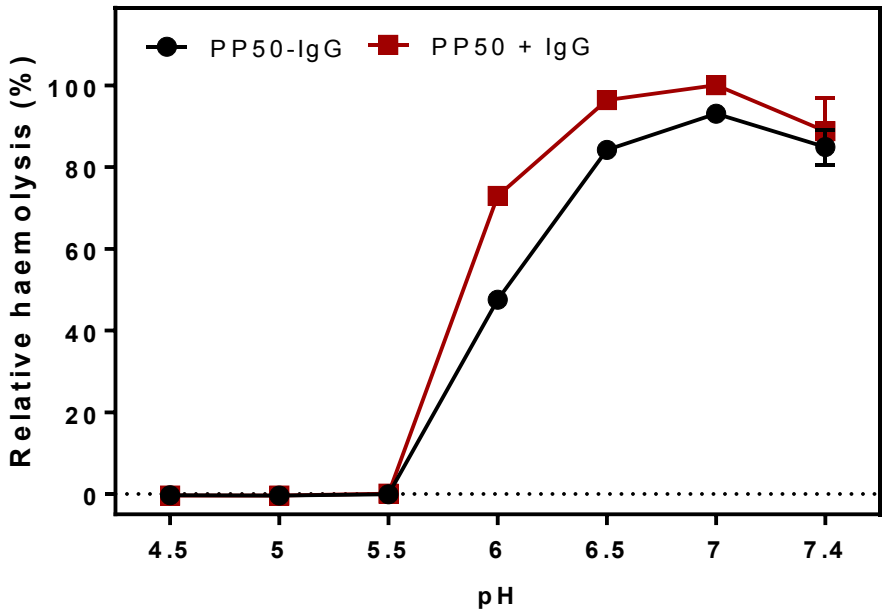


Figure 5-15. Relative haemolysis of PP50-IgG (0.27 μM, 4 polymer chains per IgG) and IgG mixed with PP50 (IgG concentration was equal to 0.27 μM, PP50 concentration was 50 μg mL^{-1} or 1.1 μM). Mean ± SD, n = 3.

The preliminary deliverability of the PP50-IgG-FITC conjugate to HeLa cells at neutral pH was analysed using confocal microscopy. The delivery of the conjugate was compared to an unconjugated mixture of PP50 and IgG-FITC. As illustrated in Figure 5-16, the treatment with the conjugate produced a pattern of fluorescent green spots, which co-localised with the endosomal-lysosomal dye (red channel). In contrast, the mixture of PP50 and the fluorescent antibody resulted in a diffused green signal in the cytosol of the treated cells. These results suggest that the polymer-antibody conjugate was unable to escape the endosomal entrapment under the conditions tested. The feat of endosomal escape by a construct consisting of poly(propylacrylic acid) conjugated to a monoclonal antibody was reported by Berguig et al. (2012), who used a ratiometirc fluorescence approach to note that 45% of their antibody-polymer

conjugate was localised in the cytosol after a 6 h treatment. The unsatisfactory cytosolic localisation of PP50-IgG-FITC might be a result of a diminished membrane permeabilising potential of PP50 following conjugation. Further optimisation, such as the use of a mildly acidic pH or increasing the treatment time, could be performed to try to counteract this.

Interestingly, the confocal microscopy data contrasts with the haemolysis results shown, which suggested that the conjugate was efficient at permeabilising the membranes of ovine erythrocytes leading to haemoglobin release. This highlights the important difference between the erythrocyte and the nucleated cell models, suggesting caution when trying to apply result from one of those systems to the other, as they might not be directly transferable.

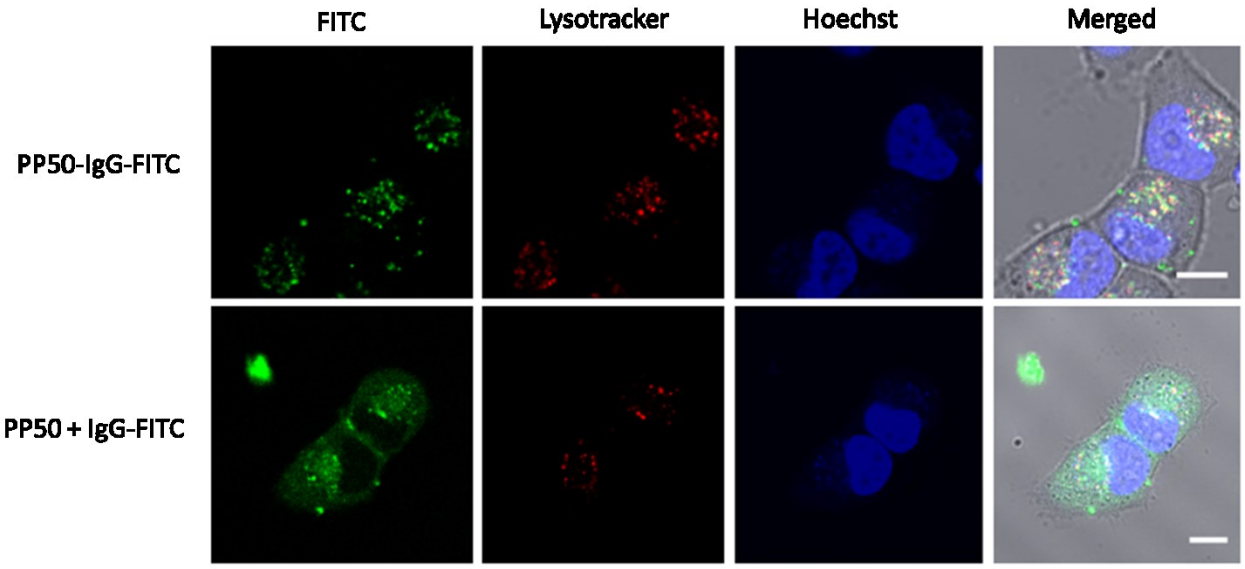


Figure 5-16. Delivery of IgG-FITC to HeLa cells following conjugation to PP50-PDPH, analysed by confocal microscopy. IgG-FITC was conjugated to PP50-PDPH at 4 polymer chains per 1 IgG molecule (PP50-IgG-FITC concentration was equal to 5.4 μM) and compared to delivery of IgG-FITC mixed with PP50 (polymer conc. = 1 mg mL^{-1} or 22 μM, IgG-FITC conc. = 4.8 μM). The materials were applied in serum-free DMEM for 1 h, followed by cell washing and 6 h of further incubation in serum-supplemented DMEM. Channels: Green = GFP, Red = LysoTrackerRED, Blue = Hoechst33342. Scale bar = 10 μm.

5.3 Conclusions

Grafting of PDPH crosslinker onto pendant carboxylic groups of the PP50 polymer via amide bonds has been achieved. The efficiency of the reaction was estimated to be 60%, which is helpful in designing polymer constructs with a specific number of attachment points available for the cargo. Using a haemolysis assay, it was shown that grafting with PDPH had negligible effects on the desired, membrane disruptive properties of PP50 as a function of pH.

Release profiles of 2-mercaptopyrdine which was treated as a small-molecule model drug from PP50-PDPH under reducing conditions was investigated, showing a negligible release of the model payload in samples mimicking plasma concentration of GSH and Cys, and a high release in samples mimicking intracellular concentrations of those reducing agents; up to 78% after 24h incubation with GSH. This suggested that payloads loaded on PP50 would be efficiently realised following internalisation.

The PDPH crosslinker allowed conjugation of various model macromolecular payloads of differing size to PP50 such as PEG-FITC, GFP and IgG, enabling synthesis of novel polymer-payload constructs. The conjugation reaction was shown to be rapid, with majority of the conjugates being formed in the first 15 minutes. The reaction efficiency can be increased by increasing the molar excess of payload over crosslinker, addition of extra sulfhydryls on the payload or by including an organic solvent, such as DMSO, in the reaction environment, as was demonstrated by using BSA as a model in the conjugation reaction. The first two methods are better suited for creation of conjugates with proteins due to the potential effects of DMSO.

The preliminary confocal microscopy analysis of the deliverability of GFP and IgG-FITC conjugated to PP50 suggests that that delivery of proteins might be possible but requires further optimisation, especially in the case of the larger IgG which exhibited endosomal entrapment. The encountered problems might be a result of steric hindrance, whereby the large macromolecules limit or inhibit the conformational change of PP50 following conjugation, which in turns lowers the efficiency with which PP50 can permeabilise the cell or endosomal

membrane. Thus, payload size might be a critical parameter dictating the efficiency and the outcome of delivery by conjugation to PP50.

This work provides a new understanding of the capacity of PP50 to form conjugates with various, different-sized model molecules as well as its membrane disruption and payload release abilities. The delivery of a peptide-sized model payload was discovered to be the most consistently successful. This could suggest that in the current state of the technology PP50 is best suited for delivery of smaller macromolecules, such as peptides, which carry a lower risk of causing steric hindrance and limiting the membrane permeabilisation.

Chapter 6 - Development and *in vivo* delivery of PP50-Bim conjugates

6.1 Introduction

Building on the results describing the development of novel conjugates of PP50 with model payloads, and their delivery, this chapter focuses on the delivery of functional payloads by the same method. Specifically, the apoptotic peptide Bim was attempted to be delivered to A549 human lung carcinoma cells *in vitro* and *in vivo*, in a mouse model.

Bim modified for increased affinity to Bcl-X_L, a member of the Bcl-2 family proteins, obtained by rational substitution of four residues on the wild type Bim with natural and non-natural amino acids, has been used in *in vivo* experiments (Ponassi et al., 2008). The modification also included addition of the *Antennapedia* homeodomain polypeptide– a cationic polypeptide shown to translocate through the plasma membrane via macropinocytosis and whose third α-helix has been widely used as “Penetratin” (Wu and Gehring, 2014). Ponassi et al. (2008) demonstrated that intravenous administration of their modified Bim to NOD/SCID mice bearing xenografts of human acute myeloid leukaemia cells resulted in no off-target tissue toxicity and a selectivity effect of the peptide for cancer cells, leading to a significant delay of leukemic cell growth upon treatment. The reason for the selectivity of the peptide for cancer cells, which has also been reported for other BH3 mimetics, was not understood, but was hypothesised to rely on the higher sensitivity of tumours to BH3-proteins and BH3-mimetics due to an abnormal balance of Bcl-2 family proteins in such cells, compared to cells in healthy tissues, which makes them “primed for death” when exogenous BH3-containing molecules are introduced (Certo et al., 2006). In the current study Bim with an unmodified main sequence was attempted to be delivered to CD-1 nude mice bearing xenografts of A549 cells (human lung carcinoma) – a cell line which was demonstrated herein to be sensitive to Bim-induced apoptosis.

In contrast to payload delivery by co-incubation with PP50, an approach in which the mildly acidic buffer was used to trigger the conformational change of the polymer, making it membrane permeabilising, a different approach was required for *in vivo* delivery. This is because a small volume of the buffer would become diluted in the blood stream post injection, due to the near-neutral pH value of blood (Kellum, 2000). One of the solutions to overcome this issue would be to rely on the tumour environment to trigger the polymer conformational change. The microenvironment of solid tumours is known to be more acidic than that of the surrounding healthy tissues (Wike-Hooley et al., 1984; Anderson et al., 2016). This is due to abnormal metabolism, in which anaerobic glycolysis leads to a build-up of lactic acid – so called "Warburg effect" (Warburg et al., 1927; Harris, 2002). The mildly acidic environment of tumours could therefore lead to triggering of the polymer directly and specifically at the tumour site. This would lead to membrane permeabilisation of the cancer cells and internalisation of the PP50-Bim conjugates and release of the apoptosis-promoting cargo following reduction of the disulphide crosslinker.

However, a delivery approach relying on such passive targeting of the tumour carries a risk of not being sufficient to result in a high enough local concentration of the conjugates at the site of the diseased tissue to cause a significant apoptotic effect. Another risk is the polymer becoming triggered in other areas of the body with lower pH. In such case, the addition of a targeting ligand might be considered to enable a more active and specific targeting of the cancer cells.

This chapter discusses firstly the development of PP50-Bim conjugates and the assessment of their apoptotic potential *in vitro*. The immunogenicity of the conjugates is investigated by treatment of human leukocytes. In addition, the tolerability of the conjugates is tested in CD-1 nude mice, followed by visualisation of the biodistribution of the conjugates in the animals.

The *in vivo* work presented in this chapter was supervised by Dr Fabien Garcon (MedImmune). Fabien Garcon and Michal Kopytynski designed the experiments. Mice handling was performed by skilled technicians possessing Home Office licenses for animal work at MedImmune.

6.2 Results and Discussion

6.2.1 Conjugation of Bim and scrBim to PP50

The results described in Chapter 5 suggest that conjugation of large payloads, such as IgG, might decrease the membrane permeabilising potential of PP50, perhaps by blocking the conformational change by the mechanism of steric hindrance. To minimise this, PP50 with 0.8 mol% crosslinker grafting was synthesised and used in all the experiments described in this chapter. This corresponds to approximately 1 crosslinker available per polymer chain of average 130 monomer units (Chen et al., 2009c; Lynch et al., 2010).

PP50 conjugation to Bim and scrBim via PDPH was quantified by measuring the absorption of 2-mercaptopyridine released from the crosslinker following conjugation, as described above. Both Bim and scrBim demonstrated efficient disulphide exchange leading to 84.0 ± 7.1% and 74.7 ± 15.2% (n = 3) of the available crosslinker molecules being conjugated to scrBim and Bim, respectively, at molar excess of the peptides to PDPH ranging from 1.5:1 to 3:1. The excess, unconjugated peptide was removed by dialysis.

6.2.2 Apoptotic effect of PP50-Bim and PP50-scrBim – Caspase 3/7 assay

The potency of the novel PP50-peptide conjugates was assessed by analysis of Caspase 3/7 activation in A549 cells. Cells were treated with PP50 alone, PP50-Bim and PP50-scrBim at 22, 12 and 17 μM, respectively for 3 hours (pH 6.5 and pH 7.4), followed by addition of the Caspase-Glo® 3/7 reagent, and the luminescence of the samples was quantified.

The results presented in Figure 6-1 indicate that neither PP50 on its own nor PP50-scrBim were capable of eliciting a detectable Caspase 3/7 response in A549 cells at both pH 6.5 and pH 7.4. In contrast, the conjugate constructs containing the active peptide were efficient at activating Caspase 3/7. This suggests that PP50 is capable of delivering Bim to the cell interior, and that the peptide retains its functional pro-apoptotic activity following conjugation to the

polymer, delivery and intracellular release. Successful delivery of Bim by conjugation with PP50 suggest that scrBim was also delivered in a similar manner, but as expected, failed to activate the Caspase 3/7 pathway, which further validates scrBim as a pertinent negative control.

Interestingly, PP50-Bim mediated Caspase 3/7 response at pH 6.5 was 2-fold higher than that at pH 7.4. This is in contrast to the delivery of FITC-PEG reported in Chapter 5, whereby the delivery of the fluorescently labelled PEG was comparable at both of these pH environments – an effect which was thought to be caused by potential steric hindrance and partial inhibition of the polymer's membrane permeabilising ability, forcing the constructs to rely more on the endosomal pathway for internalisation. The fact that PP50-Bim seems to be more potent at pH 6.5 might suggest that this effect does not play such a significant role in this scenario and supports the hypothesis that the extent of the PP50 inhibition by steric hindrance is payload-dependent. The observed enhanced delivery at the mildly acidic pH might be exploited for delivery to hypoxic, solid tumours with acidic microenvironments (Liu et al., 2014; Tannock and Rotin, 1989).

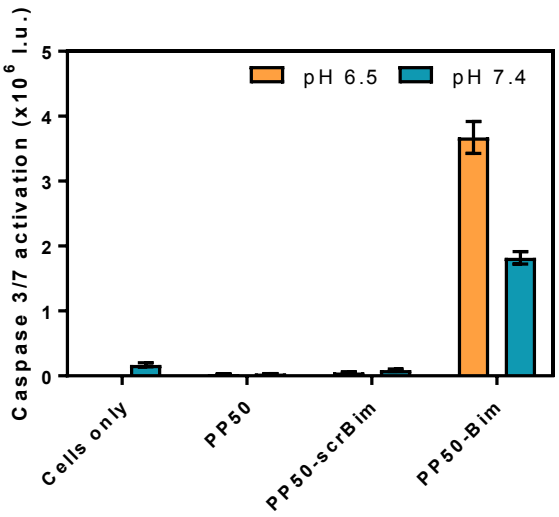


Figure 6-1. Caspase 3/7 activation in A549 cells following delivery of Bim and scrBim conjugated to PP50 polymer (one PDPH crosslinker per polymer chain). Concentrations of PP50, PP50-Bim and PP50-scrBim used in the experiment were equal to 22, 12 and 17 μM, respectively. The treatment time was equal to 1.5 h, followed by wash with PBS, replacement of DMEM and a 3 h period of further incubation. Mean ± SD, n = 3.

6.2.3 Conjugation of Bim-Cy7 and scrBim-Cy7 to PP50 and peptide purification

In preparation for studying the effects of PP50-mediated delivery *in vivo*, Bim and scrBim peptides labelled with a fluorescent dye Cy7 were obtained. Cy7 fluoresces in the near infra-red part of the spectrum, which enables visualisation of biodistribution in mice after injection.

The conjugation efficiency of Bim-Cy7 and scrBim-Cy7 to PP50 was analysed using the 2-mercaptopyridine release assay, following the reaction where 2:1 or 2.5:1 molar ratio of peptide to PDPH available on PP50 was performed. The conjugation efficiency for both peptides exhibited high-batch to batch variation, with average peptide loading of 77.3 ± 23.2% and 78.0 ± 28.0% for Bim-Cy7 and scrBim-Cy7, respectively (n = 6), when being conjugated to PP50 containing one crosslinker per polymer chain.

Given that a portion of the unconjugated peptide was present in the solution post-reaction, a purification step was attempted. However, in contrast to the unlabelled peptides used previously, Bim-Cy7 and scrBim-Cy7 exhibited a decreased solubility in a number of tested buffers containing organic solvents, manifesting in precipitation of the fluorescent peptide or visibly high turbidity, which posed a problem for the purification efficiency. A number of purification methods were tested to remove the free peptide, including dialysis, size exclusion and anion exchange chromatography, centrifugation using Amicon centrifugal filter units as well as desalting columns. During dialysis against a number of different buffers, no fluorescent peptide was detected in the dialysate as measured by Odyssey, which suggested that the peptide could not cross the 14 kDa MWCO membrane of the dialysis tube, despite it being nearly 4 times larger than the peptide itself (Figure 6-2). Similarly, no membrane crossing was observed using centrifugal filter units.

Following the failure to purify out the unconjugated peptides using membrane and filter-based methods, column-based methods were tested. High Performance Size Exclusion Chromatography (HPSEC) was first used to characterise the size of Bim, PP50 and PP50-Bim conjugates (Figure 6-3). The analysis revealed a considerable peak overlap between Bim, PP50 and the conjugate resulting in too

poor a resolution to attempt column separation based on size. This could be perhaps due to the linear nature of the polymer, which migrates through the column faster than globular proteins of similar size, or due to the interaction between the polymer or the peptide and the beads, resulting in the materials eluting in similar fractions.

Finally, anion exchange chromatography was tested for peptide purification. In this method, the negatively charged PP50 was hoped to bind to the resin, allowing to remove the unconjugated peptide. However, all the fluorescent material seemed to bind strongly to the resin and proved too difficult to elute to make anion exchange chromatography technically feasible for this application (data not shown).

Based on this and in the interest of time, it was decided to proceed without the separation of the unconjugated peptide. One problem with this approach is that the presence of the unconjugated peptide could result in an overestimation of the pro-apoptotic activity. This could arise as a result of the unconjugated peptide "piggy backing" on the membrane permeabilisation caused by the polymer and being transported to the cell interior. This potential effect, however, was not judged to constitute a problem during the planned *in vivo* studies as the unconjugated peptide would get separated from the conjugates in the bloodstream.

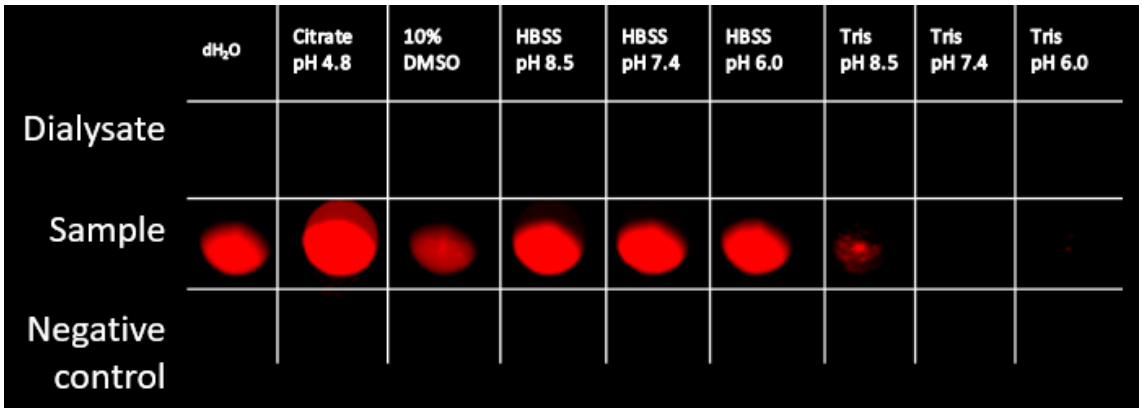


Figure 6-2. Qualitative analysis of the dialysis efficiency performed by exciting aliquots from the dialysate, sample undergoing dialysis and negative control (buffer only) at 800 nm using Odyssey.

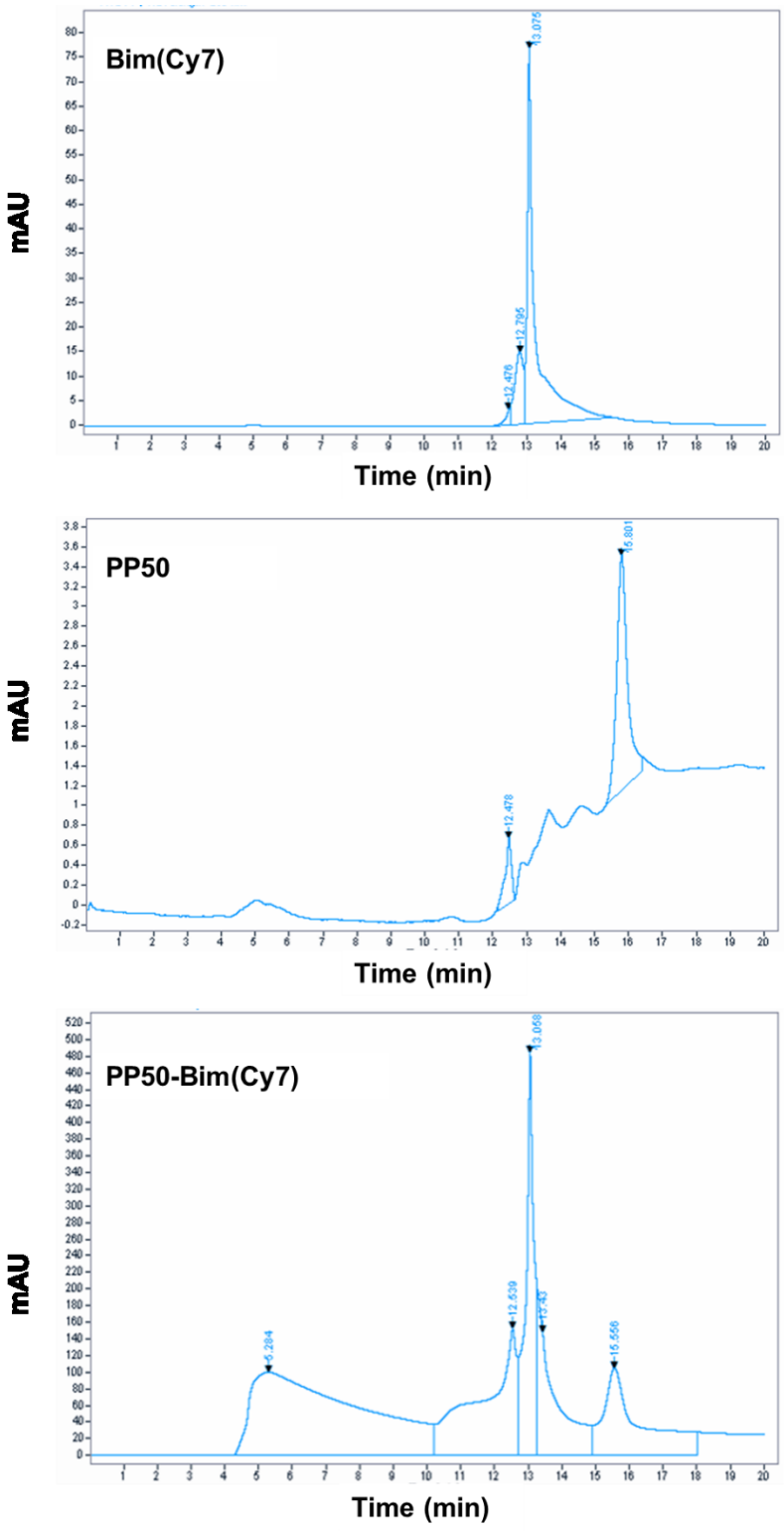


Figure 6-3. Size spectra of Bim-Cy7, PP50 and PP50-Bim-Cy7 obtained by High Performance Size Exclusion Chromatography. HPSEC was performed by Jen Spooner (MedImmune).

6.2.4 Apoptotic effect of PP50-Bim-Cy7 and PP50-scrBim-Cy7 – Caspase 3/7 activation

The effect of the novel PP50-Bim-Cy7 and PP50-scrBim-Cy7 conjugates on A549 cells was assessed by analysis of Caspase 3/7 activation. Cells were treated with PP50-Bim-Cy7 and PP50-scrBim-Cy7 at three different concentrations equal to 3, 6 and 12.5 μM for 3 h at pH 6.5. Due to the incomplete removal of the unconjugated peptide, the solutions also contained ca. 7, 14 and 27.5 μM of free Bim-Cy7 and scrBim-Cy7 for the three increasing conjugate concentrations mentioned above, respectively (based on 80% reaction efficiency at 2.5:1 molar excess of peptide to crosslinker). Therefore, the ratio of peptide in the conjugate form to the free peptide in solution was equal to ca. 0.4:1.

The treatment was followed by a wash and 3 h of further incubation and addition of the Caspase-Glo® 3/7 reagent, and the luminescence of the samples was quantified. The results shown in Figure 6-4 suggest that PP50-Bim-Cy7 induced Caspase 3/7 response in A549 cells, compared to PP50-scrBim-Cy7, which did not stimulate Caspase 3/7 expression. The PP50-Bim-Cy7-induced Caspase 3/7 response was most prominent in the cell samples treated the highest concentration of the conjugates (12.5 μM). In addition, the delivery of PP50-Bim-Cy7 and PP50-scrBim-Cy7 at 3 μM was compared to the delivery of the same amount of the conjugates supplemented with 0.5 mg mL^{-1} (or 11 μM) of extra, free PP50, which produced a high Caspase 3/7 response in the samples containing Bim-Cy7, suggesting that addition of free PP50 can enhance the functional delivery of this peptide.

The magnitude of Caspase 3/7 activation by PP50-Bim-Cy7 shown here was lower than that described in Figure 6-1, which was induced by PP50-Bim at a similar concentration of 12 μM. This difference could arise from the fact that the treatment time used here was 1.5 h longer than before, and thus a different time point of the dynamic Caspase 3/7 reaction could have been captured by the Caspase-Glo® 3/7 analysis. Another potential explanation is that the addition of the dye and the described low solubility of the peptide resulted in a lower

effective dose of Bim-Cy7 being delivered to the cells, compares to unlabelled Bim.

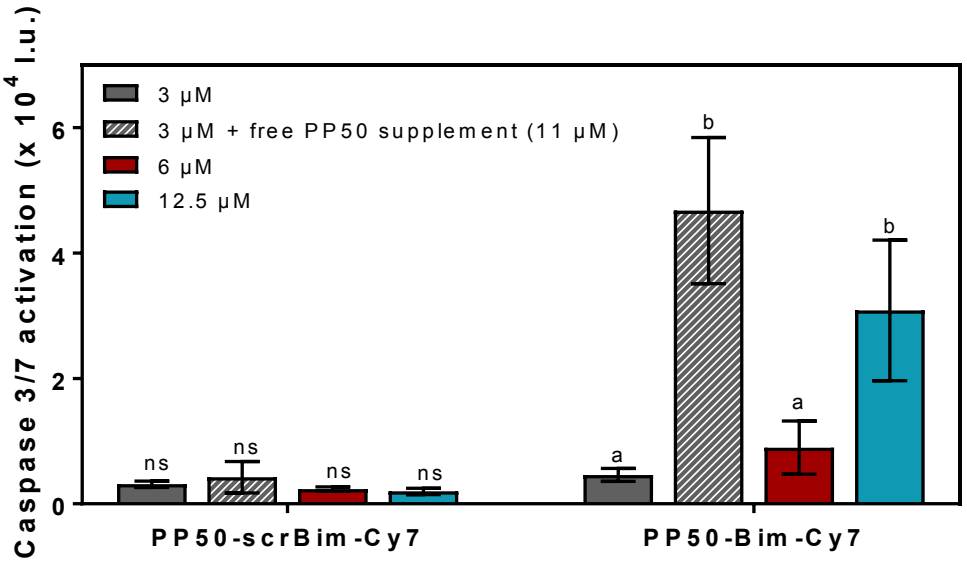


Figure 6-4. Caspase 3/7 activation in A549 cells following delivery of Bim-Cy7 and scrBim-Cy7 conjugated to PP50 via PDPH (one crosslinker per polymer chain) and a mixture of the conjugates and free PP50. PP50-Bim-Cy7 and PP50-scrBim-Cy7 concentrations of 3, 6 and 12.5 µM were used. Delivery of conjugates at 3 µM was compared to the delivery of the same amount of conjugates supplement with free PP50 at 0.5 mg mL^{-1} (or 11 µM). The treatment was performed at pH 6.5 for 3 h, followed by a wash with PBS, replacement of DMEM and a 3 h period of further incubation. Mean ± SD, n = 3. One-way ANOVA and Tukey's tests were performed for comparison of samples within the PP50-scrBim-Cy7 and PP50-Bim-Cy7 groups. Different letters represent statistically significant difference with P-values < 0.5.

6.2.5 Apoptotic effect of PP50-Bim-Cy7 and PP50-scrBim-Cy7 – Incucyte analysis

Further analysis of cell survival following treatment with PP50-Bim-Cy7 and PP50-scrBim-Cy7 was evaluated using the IncuCyte©, a time dependent imaging system for *in vitro* cell culture. A549 cells cultured in 96-well plates were treated with the conjugates at 9, 17 and 35 µM at pH 6.5 and pH 7.4. Again, due to the difficulty of removal, there was free Bim-Cy7 and scrBim-Cy7 present in the solution at the same ratio as described in Section 6.2.4.

After 1 h of treatment, the conjugate solutions were replaced with DMEM containing the IncuCyte©Caspase-3/7 Green Apoptosis reagent, placed inside the IncuCyte© chamber and imaged every hour for the first 4 hours, then every 2 hours up until 24 hours post-treatment. IncuCyte© images illustrating the cells treated at pH 6.5 are shown in Figure 6-5. At time t = 0 h, the morphology of the cells treated with both conjugates – PP50-Bim-Cy7 and PP50-scrBim-Cy7, appeared similar. However, at t = 1 h, while there was no change in the morphology of the cells treated with PP50-scrBim-Cy7, those cells treated with PP50-Bim-Cy7 became less confluent and visibly shrivelled and rounded up, indicative of apoptosis (Häcker, 2000). The altered morphological state of the cells persisted at t = 10 h and t = 20 h, with many cells starting to appear green due to the reaction with the Caspase 3/7 stain. Again, this was not observed in the cells treated with PP50-scrBim-Cy7, which displayed normal, spread out morphology throughout the experiment and did not stain with the assay reagent.

Quantitative analysis of the cells was performed using the integrated IncuCyte© software (Figure 6-6). The treatment with PP50-scrBim-Cy7 did not produce a notable number of apoptotic cells neither at pH 6.5 nor pH 7.4, as expected. The treatment with PP50-Bim-Cy7 at pH 6.5 produced up to approximately 1.8×10^4, 1.2×10^4 and 6.0×10^3 apoptotic cells per well at the conjugate concentrations of 35, 17 and 9 μM, respectively. The appearance of apoptotic cells was the fastest within the first 8 h post-treatment, after which a plateau was reached. In contrast, the delivery of the active peptide by conjugation to PP50 was less potent at pH 7.4, where highest number of apoptotic cells per well was 3×10^3 for PP50-Bim-Cy7 at 35 μM - a 6-fold decrease compared to the delivery in the mildly acidic environment.

The IncuCyte© experiments confirmed the ability of the PP50-Bim-Cy7 conjugates to promote apoptosis, leading to eventual cell death, and provided further evidence that the delivery of this payload was more efficient at pH 6.5 than at pH 7.4, which can be exploited in cancer therapy, as explained in Section 6.1. One potential issue with this study is that due to the inability to remove the unconjugated peptide the potency of the conjugates might have been overestimated. This is because some of the Bim-Cy7 which promoted cell death in this case could have originated from the pool of the unconjugated peptide

present in the solution, rather than from the peptide loaded on the polymer. In *in vivo* scenarios the unconjugated peptide is expected to become separated from the conjugates in the blood stream and the pool of the locally available Bim might therefore be lower, possibly resulting in lower evident promotion of apoptosis at corresponding polymer concentrations.

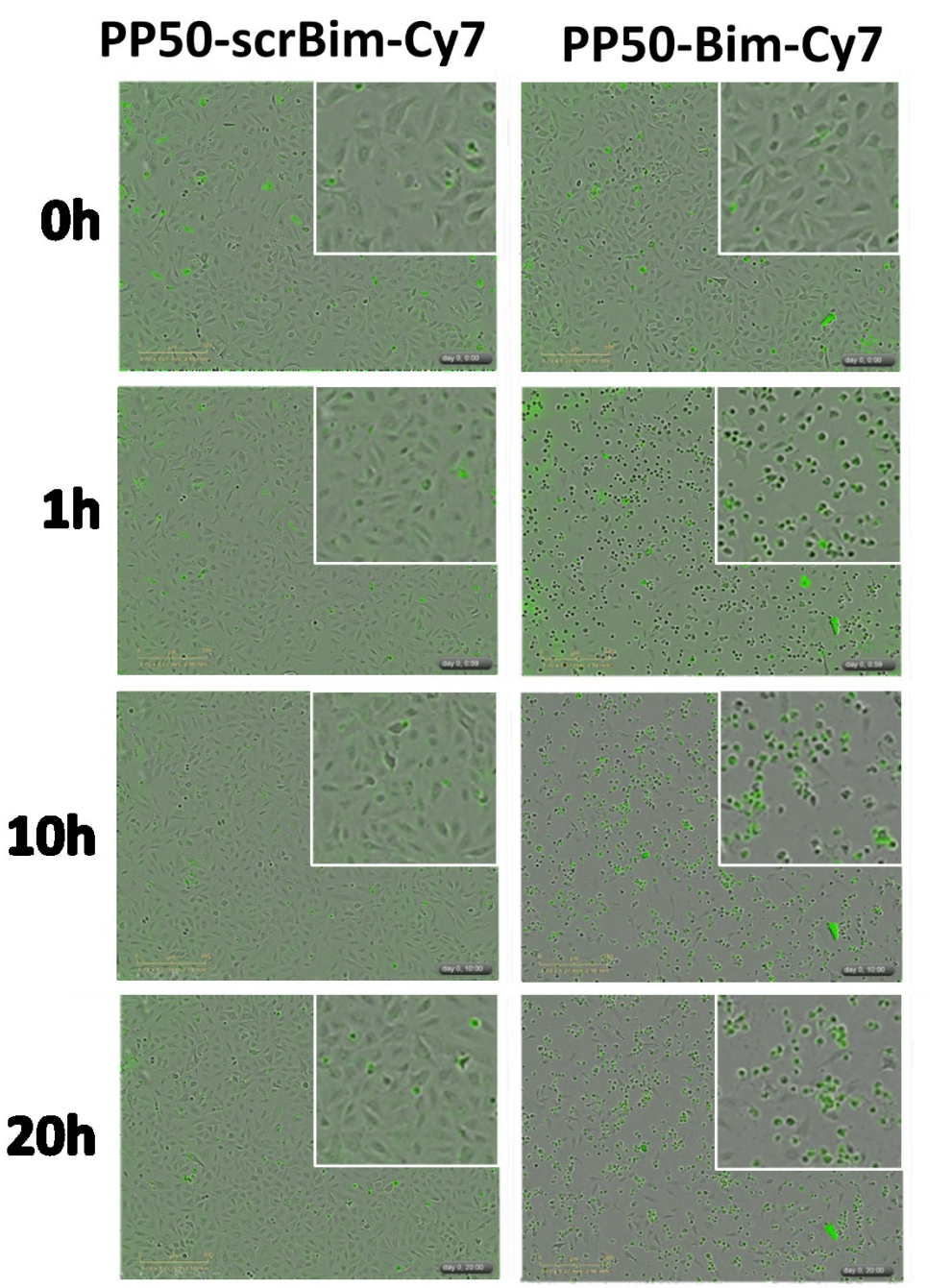


Figure 6-5. Images of A549 cells following treatment with 35 µM PP50-Bim-Cy7- or PP50-scrBim-Cy7. The IncuCyte® Caspase-3/7 Green Apoptosis reagent present in the growth medium was excited at 488 nm to indicate apoptotic cells.

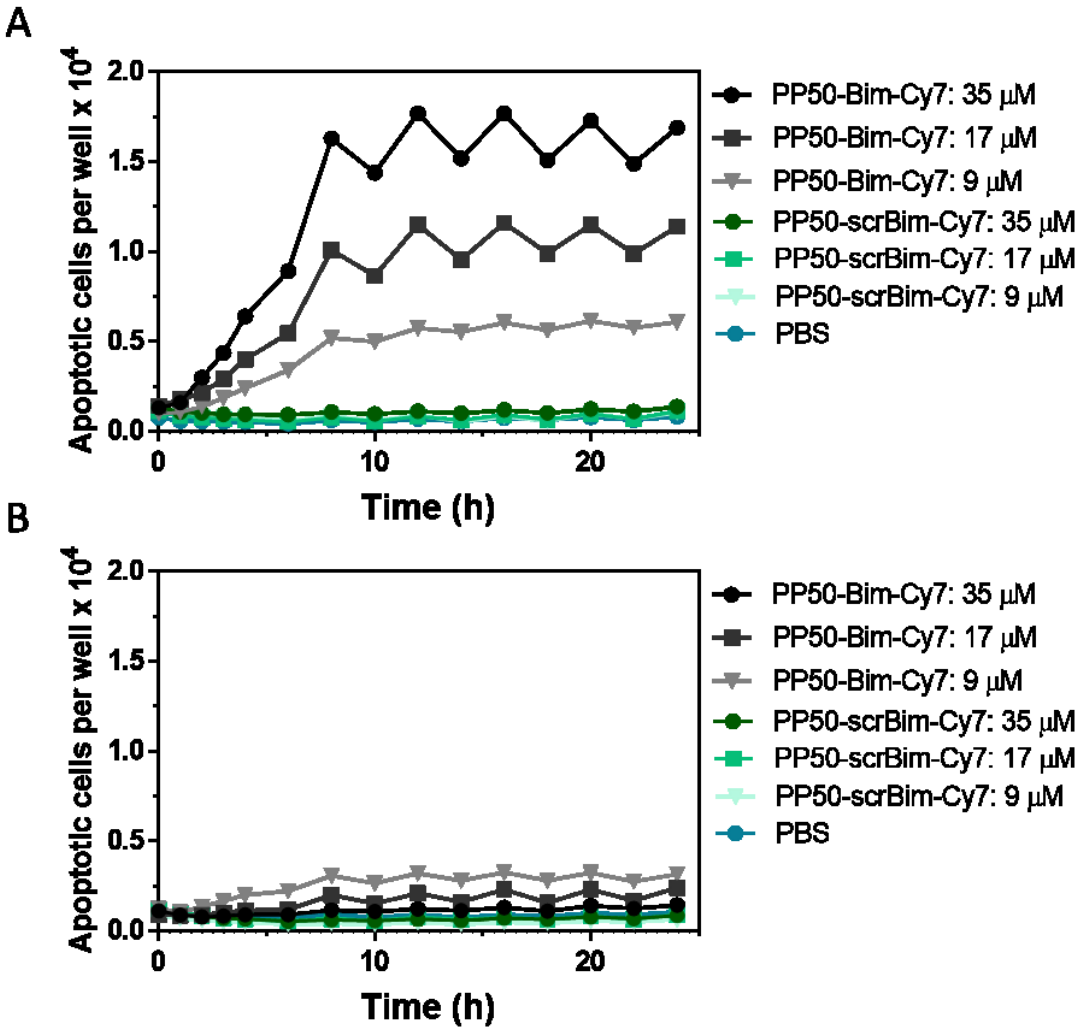


Figure 6-6. Number of apoptotic A549 cells following treatment with different concentrations of PP50 conjugated with Bim-Cy7 or scrBim-Cy7 at pH 6.5 (A) or pH 7.4 (B) over a 24 h period post-treatment. n = 1.

6.2.6 Immunogenicity of PP50-Bim

In vitro assays can be used to predict the potential immunogenicity of novel therapeutics prior to the *in vivo* testing phase. This is crucial to minimise the chance of any significant immune reactions which could lead to an immune shock and the death post-injection. Peripheral blood mononucleated cells (PBMC)-based assays in particular have been used to characterise the immunogenicity of therapeutic proteins and for detection of unwanted product quality attributes (Joubert et al., 2016).

Quantification of the immunogenic effect can be performed by measurement of expression levels of proteins involved in the immune response, such as the Tumour Necrosis Factor Alpha (TNFα), which is known as the “master regulator” of the cytokine cascade, as well as Interleukin-6 (IL-6) – a cytokine responsible for stimulation of the acute immune reaction following injury or infection (Parameswaran and Patial, 2010; Tanaka et al., 2014). TNFα is produced chiefly by macrophages, whereas IL-6 is secreted by both T-cells and macrophages.

To quantify the immune response to the conjugates, PBMCs isolated from human blood (3 different donors) were incubated with PP50 alone, PP50-Bim-Cy7, PP50-scrBim-Cy7, Bim-Cy7 and scrBim-Cy7 for 24 h. Following the incubation, ELISAs were performed to investigate the expression levels of TNFα and IL-6. The results illustrated in Figure 6-7 indicate that the expression of the two immunity markers following the treatment with the peptides and the novel conjugates was similar to the baseline of the negative control (cells only). This was in obvious contrast with the expression levels of TNFα and IL-6 stimulated by bacterial lipopolysaccharides, which were used as a positive control. These results suggest that the chance for an acute and potentially dangerous immune response following injection of the materials *in vivo* is quite low and provided a level of confidence regarding the safety profile of the conjugates, allowing for progression to studies involving mice.

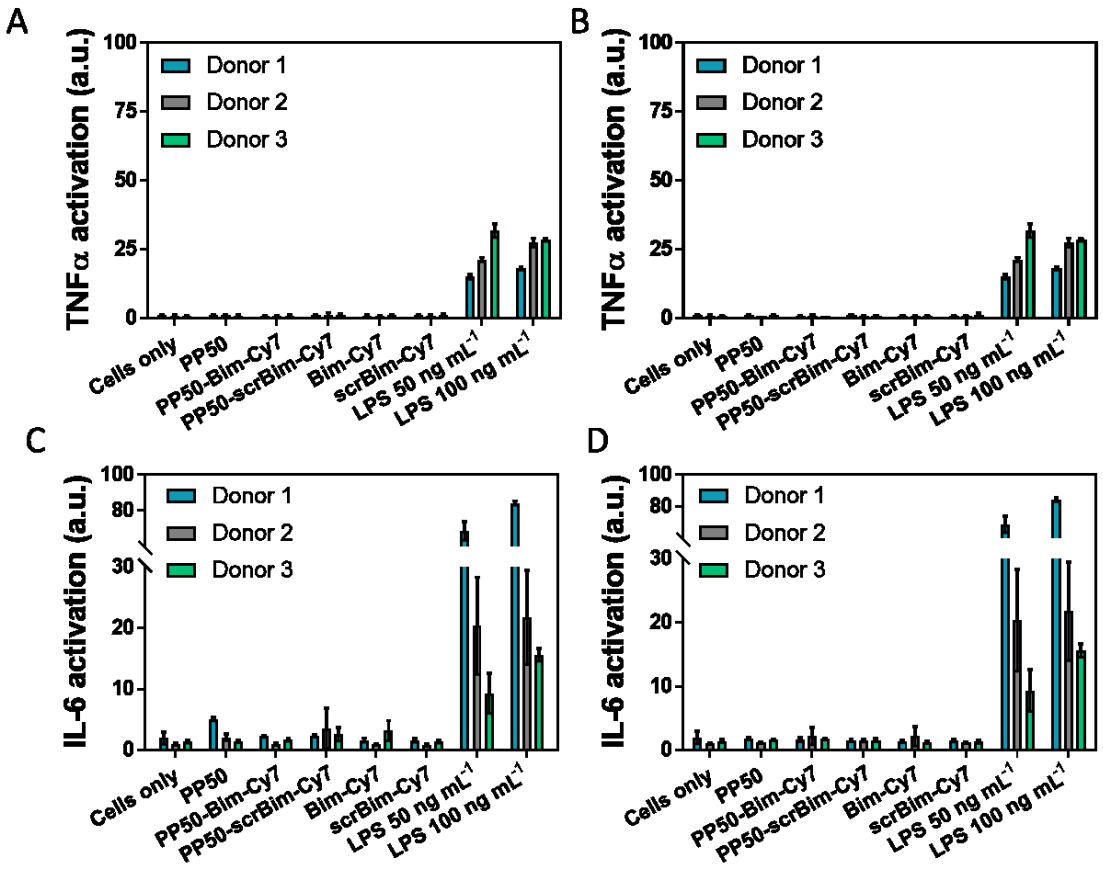


Figure 6-7. In vitro stimulation of the immune response by PP50-Bim-Cy7 and PP50-scrBim-Cy7 following incubation of human PBMCs, determined by ELISA. Expression of two immunity markers was analysed: TNFα (A) and (B) as well as IL-6 (C) and (D). Cells were treated following concentrations of materials: PP50 = 11 μM (or 0.5 mg mL^{-1}), Bim-Cy7 and scrBim-Cy7 = 27 μM, PP50-Bim-Cy7 and PP50-scrBim-Cy7 = 8 μM in (A) and (C) as well as PP50 = 2.2 μM (or 0.1 mg mL^{-1}), Bim-Cy7 and scrBim-Cy7 = 5.4 μM, PP50-Bim-Cy7 and PP50-scrBim-Cy7 = 1.6 μM in (B) and (D). Mean ± SD, n = 3.

6.2.7 Tolerability studies

6.2.7.1 Tolerability of PP50

The aim of the first *in vivo* study was to test PP50 tolerability in non-tumour bearing CD-1 nude mice. This was to ensure that the polymer on its own would not have any deleterious effect on the animals. Polymer tolerability was tested by injection of 80 mg kg^{-1} of the polymer intra-venously to 3 mice. For a 25 g mouse, 80 mg kg^{-1} corresponds to PP50 blood concentration of 1.4 mg mL^{-1} (or 30 μM), assuming fast and even distribution in the blood stream. The behaviour

and body mass of the animals were subsequently observed in the 7 days following the injection (Figure 6-8). The results showed that the body mass of the 3 mice did not change in the 7 days following injection with PP50, staying at approximately 22 g. In addition, the observations of the animal behaviour did not record any abnormal behaviour, such as hunching or convulsing, which could be indicative of pain. These results suggest that PP50 was well tolerated by the animals.

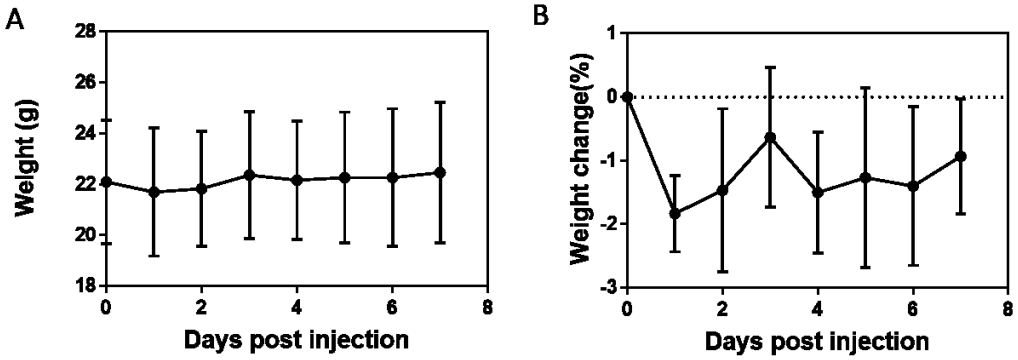


Figure 6-8. Body weight of mice measured 7 days post-injection with PP50. Mean ± SD, n = 3.

6.2.7.2 Optimisation of buffer formulation for peptide solubilisation

The low solubility of the peptides has a risk of causing unwanted effects *in vivo* due to potential aggregations which could lead to blockage of blood vessels resulting in the death of the mice. To avoid this issue, 6 different buffer formulations were tested and analysed in respect to their peptide solubilisation ability (Table 6-1). Following dissolution in the specific buffer, centrifugation and filtration with 0.22 µm syringe-driven filters were performed to remove any potential precipitates and aggregates. Figure 6-9 illustrates the peptide recovery, suggesting that Formulation 5 was most effective for solubilising Bim-Cy7 resulting in an only 10% loss of the peptide, followed by Formulation 2, with a 35% loss. ScrBim-Cy7 proved to have a worse solubility profile than the active peptide, with Formulations 2, 5 and 6 all enabling 45-55% peptide recoveries. The critical factor for the improved solubility appeared to be the DMSO content – buffers containing 10% DMSO offered better solubility for both Bim-Cy7 and

scrBim-Cy7 than those with 2% DMSO. The DMSO content could not be increased further due to safety concerns.

Based on these results, Formulation 5 was chosen and used in the *in vivo* experiments for injection of the novel PP50-peptide conjugates. However, the viability of this data is limited due to only one replicate being used here (n = 1) and should therefore be used as a guide only. More studies need to be performed to optimise the buffer formulation.

Table 6-1. Compositions of the buffer formulations tested for the *in vivo* study

Formulation 1	PBS, 2% DMSO
Formulation 2	PBS, 10% DMSO
Formulation 3	PBS, 10% DMSO + DTT
Formulation 4	Phosphate buffer pH 9.0, 2% DMSO, 5% mannitol
Formulation 5	Phosphate buffer pH 9.0, 10% DMSO. 5% mannitol
Formulation 6	Phosphate buffer pH 10.0, 10% DMSO, 5% mannitol

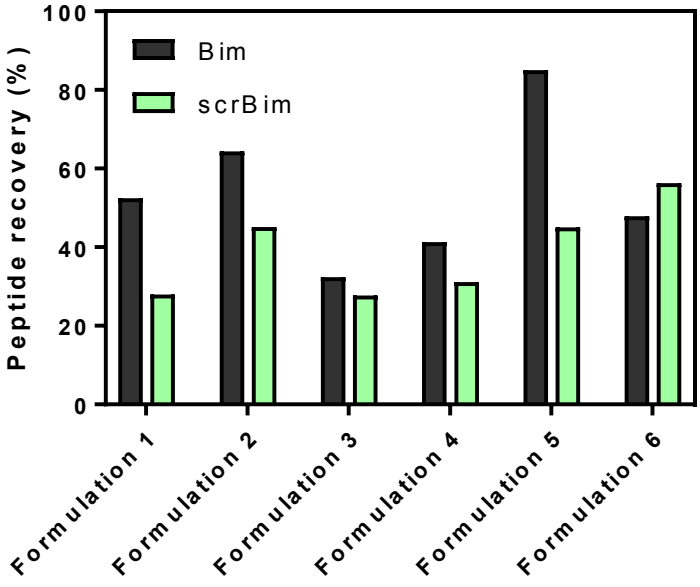


Figure 6-9. Recovery of Bim-Cy7 and scrBim-Cy7 dissolved in 6 buffers with different compositions. Measurement of peptide absorbance at 220 nm followed centrifugation and filtration to ensure removal of any precipitates and was compared to the initial absorbance to calculate the percentage of peptide recovery. n = 1.

6.2.7.3 Tolerability of conjugates - single dose

The tolerability of PP50-Bim-Cy7 and PP50-scrBim-Cy7 was tested by intravenous injection of the materials at a conjugate concentration of 17.5 μM (equivalent PP50 concentration equal to 60 mg kg^{-1}, or 1 mg mL^{-1} of blood) into non-tumour bearing CD1-nude mice divided into two groups of 6 animals, each receiving either the polymer conjugated with the active or the inactive peptide. Observation of the animals' behaviour was performed as described above, noting that some of the animals dosed with PP50-scrBim-Cy7 exhibited a degree of hunching, while remaining reactive to touch. This issue resolved within minutes and was thought to be caused by a level of precipitation of the scrambled peptide within the bloodstream. This was not surprising as scrBim-Cy7 was shown to have a relatively low stability in solution. The mice treated with PP50-Bim-Cy7, which was demonstrated to have better solubility, did not exhibit any abnormal behaviour. Despite the initial, temporary adverse reaction in some of the animals dosed with PP50-scrBim-Cy7, the animals in both groups appeared to be healthy and retained their initial body weight in the 7 days following the injections (Figure 6-10). Thus, it was concluded that conjugates were well tolerated by the CD1-nude mice following a single injection.

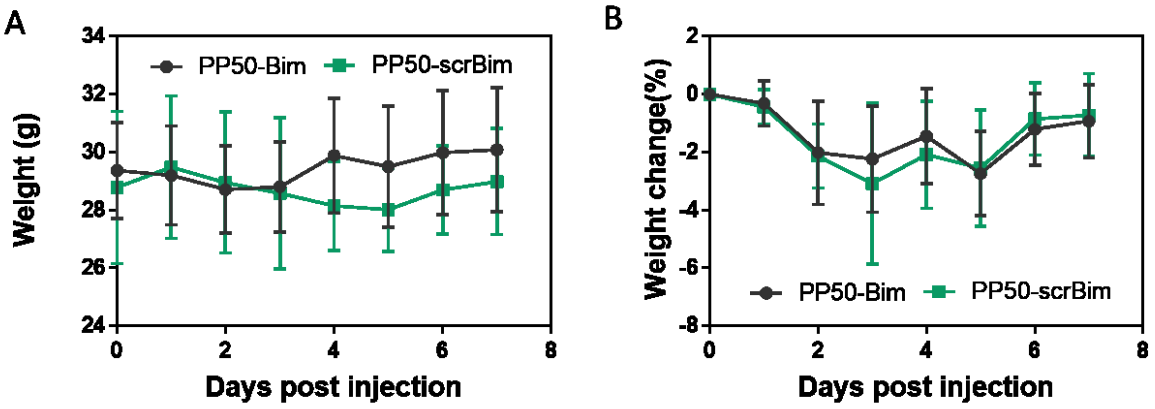


Figure 6-10. Body weight of mice measured for 7 days following a single injection with PP50-Bim-Cy7 and PP50-scrBim-Cy7 at 17.5 μM. Mean ± SD, n = 6.

6.2.7.4 Tolerability of conjugates - multiple dose

A similar study was performed to evaluate the tolerability of PP50-Bim-Cy7 and PP50-scrBim-Cy7 dosed twice within 48 h (Figure 6-11). Multiple injections might be required if the pharmacokinetics of the conjugates would indicate very fast systemic clearance, in order to ensure a high enough concentration to reach the effective dose. Non-tumour bearing CD1-nude mice divided into two groups (6 animals each) were dosed with PP50-Bim-Cy7 and PP50-scrBim-Cy7 on day 0 and day 2. As above, the animals injected with PP50-scrBim-Cy7 exhibited mild adverse effect immediately post injection, which resolved within minutes. The animal body weight remained consistent in 2 days following the first injection and in 7 days after the second injection. These results indicated that the conjugates were safe and well tolerated in case a multiple injection strategy was needed.

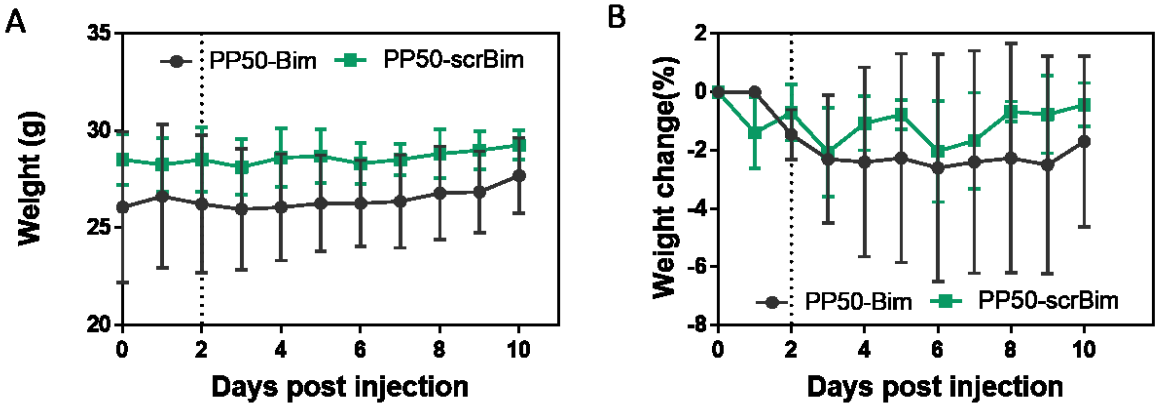


Figure 6-11. Body weight of mice following two injections with PP50-Bim-Cy7 and PP50-scrBim-Cy7 at 17.5 µM. The first injection was performed on day 0, followed by the second injection on day 2. Mean ± SD, n= 6.

6.2.8 Biodistribution

The biodistribution of PP50-Bim-Cy7 and PP50-scrBim-Cy7 was analysed using the IVIS Spectrum *In Vivo* Imaging System. CD-1 nude mice bearing A549 tumour xenografts on their lower right flank were injected once with either PP50-

Bim-Cy7 or PP50-scrBim-Cy7 at 17.5 μM (n = 2 for each group). The conjugates were administered intravenously into the tails of the animals.

Shortly after injection with PP50-scrBim-Cy7, the animals started exhibiting signs of pain, hunching and laboured breathing which did not subside with time and had to be culled for ethical reasons and the treatment with PP50-scrBim-Cy7 was discontinued. This was somewhat contrasting with the previously described tolerability studies which demonstrated that despite some initial abnormal behaviour following treatment with the scrBim conjugate the mice did not suffer from any longer-lasting negative effects. Mice treated with PP50-Bim-Cy7 exhibited similar but milder effects, which shortly subsided. This again was in contrast to the previous tolerability study, where PP50-Bim-Cy7-treated mice did not show any adverse effects.

This result could be potentially explained by the fact that tumour-bearing mice whose biological systems could have been under more stress due to the presence of the tumour were used here, compared to non-tumour bearing mice used in the tolerability studies. The adverse effects of the Cy7-labelled Bim and scrBim arose most likely due to their poor solubility and tendency to precipitate out of aqueous solution, which was observed throughout their use in the experiments presented herein. Further investigations, therefore, are needed to improve the solubility of these peptides, perhaps by adjusting the buffer formulation. In addition, scrBim-Cy7 should be replaced with another peptide possessing a similar, scrambled sequence but with a better solubility profile. Finally, lower dose during the treatment could be used to limit or prevent the appearance of the symptoms described above.

Following their recovery, the two animals dosed with PP50-Bim-Cy7 were imaged using the IVIS Spectrum System 1 h post injection (Figure 6-12). The analysis revealed a strong fluorescent Cy7 signal originating from the tumour in both mice, which did not appear prior to the treatment, as illustrated in the images showing the original tissue autofluorescence. The non-invasive whole-body imaging of the animals was followed by culling of the two mice and harvesting of their internal organs, followed by imaging with the IVIS Spectrum (Figure 6-13). Corroborating the results from the whole-body imaging, the

harvested tumours exhibited a much stronger fluorescent signal than the kidneys, spleen, liver, lungs, heart or brain in both animals.

These results suggest that the treatment with PP50-Bim-Cy7 resulted in the presence of a clear fluorescent signal which appeared to localise in the A549 tumour xenografts in the studied CD-1 nude mice, suggesting a high local concentration of the systemically-administered conjugate only 1 h post-injection. This discovery suggests that the conjugates are not rapidly cleared out from the blood stream, which would have resulted in an accumulation in the liver, spleen or kidneys. This advantageous trait can therefore allow PP50 to be used as a potential drug carrier in future studied, however, more experiments are needed to determine the precise pharmacokinetics profile.

The observed advantageous tumour accumulation is a result of passive tumour targeting only as no targeting ligand was used in this study. It is possible that the tumour localisation is a result of (i) passive targeting provided by the pH-responsive properties of PP50, leading to efficient plasma membrane binding at the mildly acidic pH characteristic to the tumour microenvironment and intracellular trafficking, (ii) the inherent specificity of Bim for cancer cells, as described in Section 6.1 (Ponassi et al., 2008), or (iii) a combination of those effects. The precise mechanism can be further elucidated by injection of Bim-Cy7 alone and observing if the peptide alone also tends to accumulate in the tumour. The negative charge of PP50-Bim-Cy7 is thought to play an important role in enabling safe and stable passage to the tumour site while avoiding interaction with negatively charge serum proteins, in contrast to cationic polymers which can interact with anionic proteins and plasma membranes during circulation, which can limit their stability, circulation time and biodistribution (Zhang et al., 2007).

The currently observed preferential accumulation of PP50-Bim-Cy7 in the tumour should be followed by tumour growth inhibition experiments in which the tumour size in conjugate-dosed mice is measured for a prolonged period of time, to determine the therapeutic effect of this novel conjugate and delivery method.

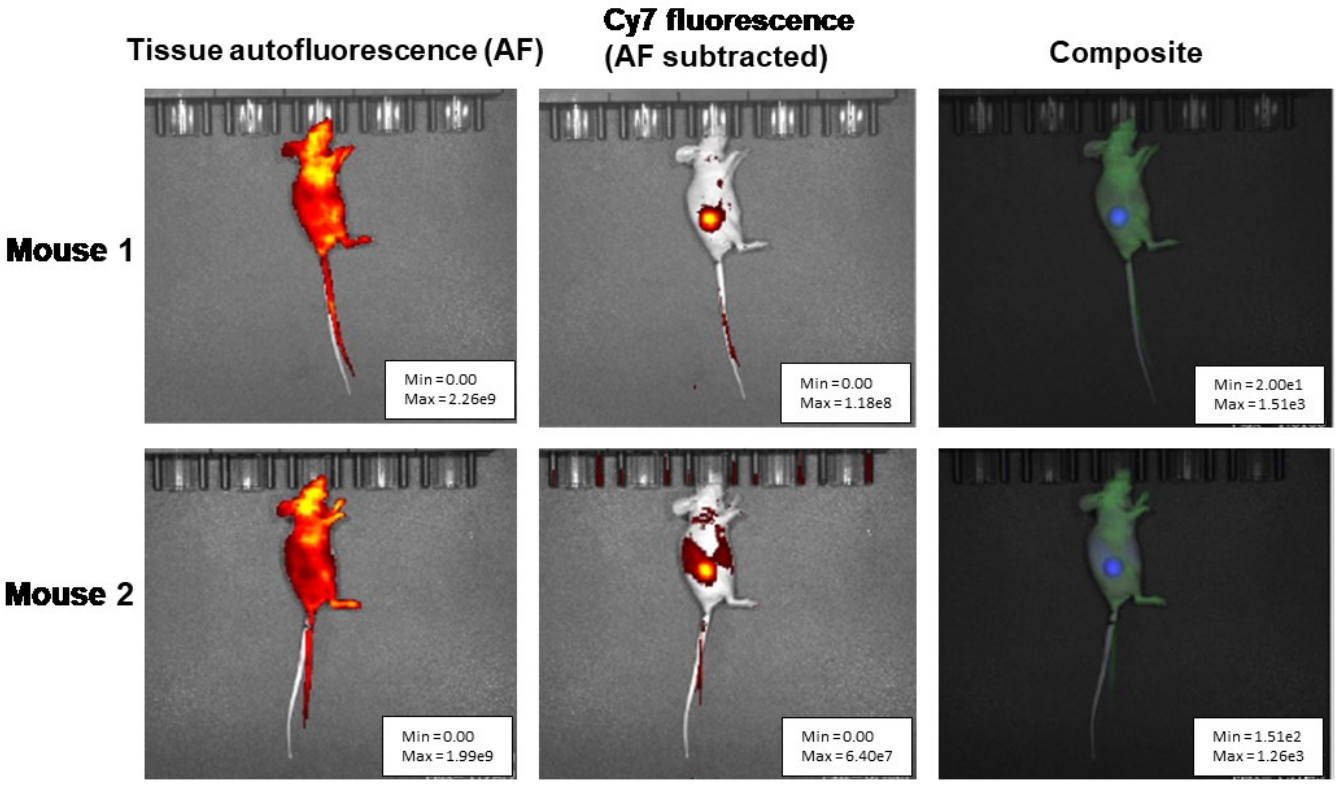


Figure 6-12. Distribution of the Cy7 fluorescent signal in tumour-bearing CD-1 nude mice (lateral view) 1 h after intravenous injection of PP50-Bim-Cy7 at 17.5 μM. The bright yellow and orange areas correspond to a stronger fluorescent signal. The composite image shows the tissue autofluorescence in green and the Cy7 specific signal in blue, indicating preferential accumulation of the conjugate in the tumours. The minimum and maximum recorded fluorescence values are presented in the insets for each image.

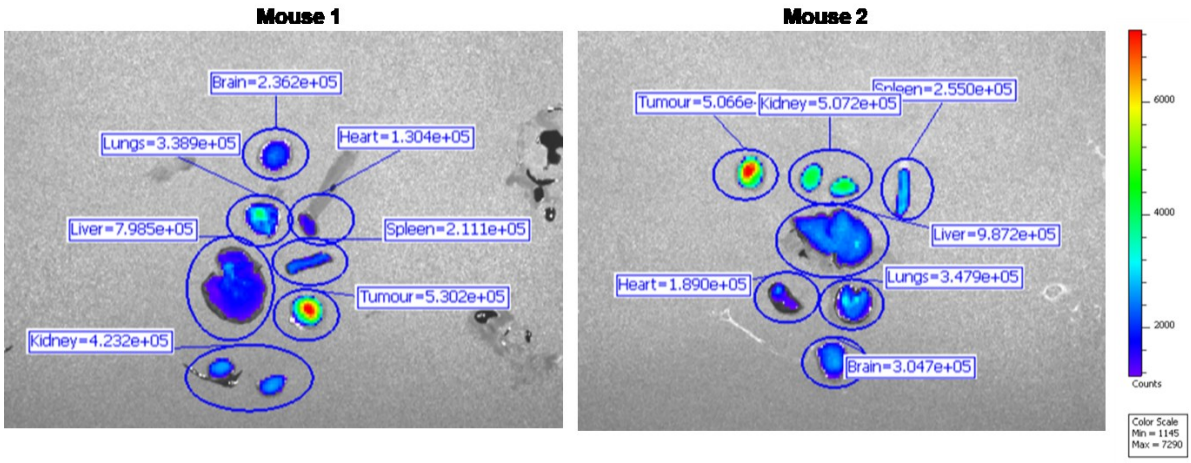


Figure 6-13. Distribution of the Cy7 signal in internal organs of two CD-1 mice dosed with PP50-Bim-Cy7 at 17.5 μM. The organs were harvested and screened following the imaging of whole animals at t = 1 h post-injection.

6.3 Conclusions

In this work, novel conjugates of the PP50 polymer and the apoptotic peptide Bim were synthesised. The conjugates were shown to activate Caspase 3/7 in A549 cells *in vitro* and promote cell death via apoptosis. Conjugates with an inactive version of the Bim peptide (scrBim) did not exhibit similar properties and were generally well tolerated by the cells.

These results encouraged the development of PP50 conjugates with Bim and scrBim labelled with the near-infrared dye Cy7, which can be used to visualise the peptide biodistribution in mice. PP50-Bim-Cy7 and PP50-scrBim-Cy7 were demonstrated to promote cell death in a pH dependant manner, with treatments in the mildly acidic buffer (pH 6.5) resulting in a 6-fold increase in the number of apoptotic cells compared to treatments at neutral pH, as analysed by the IncuCyte©, suggesting that the conjugates would be potent in the tumour microenvironment. However, the inability to efficiently remove the excess, unconjugated peptide from the solution following the conjugation reaction could have resulted in an overestimation of the exact apoptotic potency of the conjugates. More studies are needed to investigate if it is possible to remove the free peptide from the solution. One of potential purification methods would be reversed-phase chromatography.

The conjugates were shown to not promote the expression of TNFα and IL-6 following incubation with PBMCs in an *in vitro* assay as well as to be generally well tolerated by non-tumour bearing CD-1 nude mice under single and multiple injections dosing regimens at 17.5 μM. These studies provided evidence that PP50-Bim-Cy7 and PP50-scrBim-Cy7 are non-immunogenic and generally well tolerated by healthy mice. Finally, the distribution of PP50-Bim-Cy7 in tumour-bearing mice was explored, revealing preferential conjugate accumulation in the tumour. The observed level of toxicity to tumour-bearing mice was thought to be the result of poor peptide solubility and can be potentially counteracted by improving the buffer formulation or using a lower conjugate concentration in future studies.

The results presented in this chapter verify that mildly-acidic, tumour-like extracellular pH can be used to enhance the delivery efficiency of functional macromolecules, such as Bim/Bim-Cy7, by conjugation to PP50. In addition, the efficient passive targeting of A549 tumour xenografts by PP50-Bim-Cy7 with no targeting ligand was shown, which, together with the potent cell-killing activity at tumour-like pH, promise a good therapeutic potential of the conjugate.

Chapter 7 – Conclusions and Future Work

7.1 Research summary and project novelties

Delivery of macromolecules, such as proteins and peptides, across the plasma membrane poses a significant challenge. PP50 is a pH responsive polymer which is capable of undergoing a coil-to-globule conformation change triggered by acidifying environment, and gaining the ability to permeabilise the plasma membrane.

Previously published work introduced PP50 as a promising delivery agent of the small molecule cryopreservant trehalose, which was delivered to human erythrocytes and an osteosarcoma cancer cell line.

The goal of the research presented in this thesis was to greatly extend the capabilities of PP50 and to establish it as a versatile delivery platform by exploring intracellular delivery potential of the polymer in *in vitro* and *in vivo* scenarios. The research summary and novelties of this project are discussed below:

1. **PP50 is capable of erythrocyte ghost cell formation**

PP50 synthesised in-house was analysed for its membrane permeabilising activity using ovine erythrocytes. The polymer was shown to efficiently release haemoglobin from the cells and to promote formation of erythrocyte ghosts – an effect which was the most pronounced at the mildly acidic extracellular pH 6.5. The formation of ghost cells was also associated with the delivery of the small molecule dye TexasRed as well as macromolecular dextran to the cell interior, as was demonstrated by confocal microscopy.

2. **PP50 enables efficient delivery of a model macromolecule to nucleated cells by co-incubation**

The interaction between PP50 and cultured nucleated mammalian cells (HeLa) was studied *in vitro*. Fluorescently labelled PP50 was shown to very rapidly bind

to the plasma membrane followed by internalisation. The polymer mixed with fluorescent dextran (150 kDa) enabled the delivery of this cargo to the cell interior, with fluorescent patterns suggesting very little to none endosomal entrapment. Again, this effect was much more evident at the mildly acidic extracellular pH as compared to neutral pH. The work presented herein is the first to report the PP50-mediated delivery of large model macromolecules using mildly acidic extracellular pH to overcome the drawbacks of other delivery methods, often resulting in low delivery efficiency due to endosomal entrapment.

In addition, PP50-mediated payload delivery using the co-incubation approach was demonstrated to depend on a number of parameters, such as the cargo and polymer concentration, treatment time, the presence or absence of serum as well as the extracellular pH. Manipulation of these parameters, in particular the treatment time, allows to increase the delivery efficiency.

3. PP50 is a versatile delivery agent compatible with various payloads and cell types for intracellular payload delivery by co-incubation

Novel *in vitro* applications of PP50 were explored as well as the versatility and potential limitations of this delivery approach. PP50-mediated delivery of 150 kDa FITC-Dextran was successful in 9 different cell lines, including cells grown as adherent culture, a suspension as well as 3D spheroids, which mimic solid tumours. The delivery process was also shown to be non-toxic and well tolerated by different cell lines. Delivery of other payloads, such as GFP and the apoptotic peptide Bim, was also achieved by co-incubation with the polymer. The delivery of the peptide to A549 cells using PP50 at pH 6.5 resulted in activation of Caspases 9 and 3/7 leading to apoptosis and death of 80% of the treated cells. PP50-mediated delivery of Bim was also shown to be more potent than 9 other delivery methods used for comparison, which either did not produce a notable apoptotic effect via delivery of the peptide or exhibited a high level of toxicity to the cells.

4. PP50 can enable intracellular delivery of macromolecules by conjugation

This project developed novel conjugates of the polymer with different-sized model and functional payloads linked by a cleavable crosslinker for *in vivo*, whereby it is desirable to avoid the separation of the delivery agent and the cargo in the blood stream. Conjugation of model payloads to PP50 via disulphide bonds was achieved using the reducible crosslinker PDPH, which had been grafted onto the polymer. The payload loading kinetics and efficiency were analysed using different-sized PEG and BSA as model payloads, showing that the conjugation occurs rapidly. In addition, payload release kinetics using reducing agents indicated that cargo-polymer constructs should remain stable during circulation but readily release the payload following internalisation.

Based on this, novel conjugates between PP50 and either fluorescently labelled PEG (3.4 kDa) and IgG (150 kDa) or GFP (26.9 kDa) were synthesised. These molecules were chosen as surrogates of various therapeutic macromolecules of different size. The delivery of the conjugates was tested in HeLa cells and analysed using laser scanning confocal microscopy, which revealed successful delivery of PP50-PEG and PP50-GFP resulting in diffused fluorescent signal in the cytosol. The delivery efficiency, however, appeared to be lower compared to the co-incubation approach, as evident by a high level of colocalisation with the endosomal stain LysoTracker. In addition, the delivery of the fluorescent IgG following conjugation to PP50 was not successful. This was theorised to be a result of steric hindrance.

5. PP50 conjugated to an apoptotic peptide is potent at tumour-like pH and shows preferential accumulation in tumour xenografts *in vivo*

Finally, novel conjugates of PP50 and the apoptotic peptide Bim and scrBim, as well as the Cy7-labelled versions of these peptides, were synthesised and tested *in vitro*, demonstrating a potent cell killing activity at tumour-like pH. PP50-Bim-Cy7 and PP50-scrBim-Cy7 conjugates were also demonstrated to not upregulate the expression of TNFα and IL-6 in PBMCs, suggesting that the novel constructs are not immunogenic.

This project is also the first to investigate the systemic tolerability of PP50 *in vivo* following intravenous injection and the biodistribution of PP50-peptide conjugates. PP50 as well as the polymer-Bim conjugate exhibited good tolerability in non-tumour bearing CD1 nude mice. The biodistribution of PP50-Bim-Cy7 showed excellent accumulation in A549 tumour xenograft. Together with the *in vitro* studies, this result suggests a good therapeutic potential of PP50-Bim-Cy7 but buffer formulation needs to be further improved.

7.2 Future work

7.2.1 Delivery to EVs

Potential for PP50-mediated delivery to extracellular vesicles was demonstrated in the current work. A549 cells treated with Bim-loaded EVs exhibited a decreased survival, compared to corresponding controls. This effect, however, was only marginal. Further work is required to optimise the PP50-mediated loading process of EVs in order to find an appropriate apoptotic dose. This could be performed by changing the loading parameters such as the concentrations of the polymer, Bim or the loading time and pH. Following removal of the unloaded peptide, cell treatment and cell survival assays can be used to determine the effectiveness of the drug-containing EVs. In addition, other payloads, including fluorescent model macromolecules, could be used to analyse the delivery effectiveness, kinetics as well as the intracellular fate of the cargo.

7.2.2 Delivery of nucleic acids

Delivery of nucleic acids using PP50 should be further investigated. In the current work, the intracellular delivery of plasmids by co-incubation with PP50 was not achieved. This could arise from the fact that both nucleic acids and the polymer have negative charge, which would result in electrostatic repulsion between the two components, greatly inhibiting or fully preventing payload delivery by the mixing strategy. To overcome this issue, calcium phosphate could be used to promote the initial binding of plasmid DNA to the negatively charged plasma membrane, followed by treatment with PP50, which is hypothesised to enable delivery of such complexes into the cell interior (Wu and Yuan, 2011; Khan et al.,

2016). Alternatively, nucleic acid delivery could be achieved by conjugation to PP50, as has been demonstrated for another PP-family polymer (Khormaee et al., 2013). In addition, intracellular delivery of the CRISPR-Cas9 system by co-incubation with PP50 for in vitro applications should be investigated (Liu et al., 2017a). Demonstration of successful delivery of nucleic acids for transfection and gene editing applications would greatly expand the potential scope of PP50 uses.

7.2.3 Delivery of large proteins by conjugation

It was demonstrated that the delivery of larger proteins, such as the 150 kDa IgG antibody remains a challenge. This could be because of steric hindrance interactions between the macromolecular payload and the polymer, which can prevent successful coil-to-globule transition and/or binding onto the membrane, leading to its permeabilisation. One potential solution to this problem could be increasing the amount of conjugated polymer chains per protein molecule from 4 used in the current study in order to counteract the potential detrimental effects of the large cargo. In addition, a longer crosslinker between PP50 and the cargo could be employed, as it could have a chance to minimise the unwanted interactions between the two components. Finally, a larger repertoire of proteins should be studied, including proteins of differing size, surface charge and shape, including different antibodies transcription factors and enzymes, in order to confirm which of these parameters is the most crucial in preventing the successful delivery as well as to further explore and expand the potential uses of the PP50 platform for protein delivery, including its limitations.

7.2.4 Tumour growth inhibition effect *in vivo*

The passive targeting of PP50-Bim-Cy7, leading to conjugate localisation in the tumour, together with *in vitro* experiments showing a high cell-killing potency at tumour-like pH make this novel construct a promising therapeutic agent. Further *in vivo* studies should be carried out to analyse the effect of PP50-Bim-Cy7 on the growth kinetics and possible size reduction of A549 tumours in CD-1 nude mice.

7.3 Closing remarks

The research presented in this PhD thesis expands the current understanding of polymer-mediated intracellular delivery of macromolecules. Insight into the versatility of PP50-mediated intracellular delivery of different payloads has been gained, in addition to the exploration and full optimisation of the main parameters influencing this process. Novel conjugates of PP50 with both model and functional payloads have been synthesised and characterised in terms of their intracellular delivery potential. Finally, *in vivo* delivery of an apoptotic peptide by conjugation to PP50 was tested. The reported research provides solid foundation for further work investigating the delivery of macromolecular payloads using PP50 to different cell lines for various applications, both *in vitro/ex vivo* as well as *in vivo*.

Bibliography

ADAMS, M. L., LAVASANIFAR, A. & KWON, G. S. 2003. Amphiphilic block copolymers for drug delivery. *Journal of Pharmaceutical Sciences,* 92**,** 1343-1355.

AGYEI, D., AHMED, I., AKRAM, Z., IQBAL, H. M. & DANQUAH, M. K. 2017. Protein and Peptide Biopharmaceuticals: An Overview. *Protein Pept Lett,* 24**,** 94-101.

AL-MUALLEM, H. A., WAZEER, M. I. M. & ALI, S. A. 2002. Synthesis and solution properties of a new pH-responsive polymer containing amino acid residues. *Polymer,* 43**,** 4285-4295.

ALAVI, M., KARIMI, N. & SAFAEI, M. 2017. Application of Various Types of Liposomes in Drug Delivery Systems. *Advanced pharmaceutical bulletin,* 7**,** 3-9.

ALEXANDER, C. 2006. Temperature- and pH-responsive smart polymers for gene delivery. *Expert Opinion on Drug Delivery,* 3**,** 573-581.

ALLEN, T. M. & CULLIS, P. R. 2013. Liposomal drug delivery systems: from concept to clinical applications. *Adv Drug Deliv Rev,* 65**,** 36-48.

AMANN, A., ZWIERZINA, M., GAMERITH, G., BITSCHE, M., HUBER, J. M., VOGEL, G. F., BLUMER, M., KOECK, S., PECHRIGGL, E. J., KELM, J. M., HILBE, W. & ZWIERZINA, H. 2014. Development of an innovative 3D cell culture system to study tumour--stroma interactions in non-small cell lung cancer cells. *PLoS One,* 9**,** e92511.

ANDERSON, M., MOSHNIKOVA, A., ENGELMAN, D. M., RESHETNYAK, Y. K. & ANDREEV, O. A. 2016. Probe for the measurement of cell surface pH in vivo and ex vivo. *Proc Natl Acad Sci U S A,* 113**,** 8177-81.

ANGELINI, A., DI ILIO, C., CASTELLANI, M. L., CONTI, P. & CUCCURULLO, F. 2010. Modulation of multidrug resistance p-glycoprotein activity by flavonoids and honokiol in human doxorubicin- resistant sarcoma cells (MES-SA/DX-5): implications for natural sedatives as chemosensitizing agents in cancer therapy. *J Biol Regul Homeost Agents,* 24**,** 197-205.

ANSELL, S. M., TARDI, P. G. & BUCHKOWSKY, S. S. 1996. 3-(2-pyridyldithio)propionic acid hydrazide as a cross-linker in the formation of liposome-antibody conjugates. *Bioconjug Chem,* 7**,** 490-6.

ASHOK, P., SATYAJIT, P. & ANUNAY, S. 2013. Structural Transformation of Bovine Serum Albumin Induced by Dimethyl Sulfoxide and Probed by Fluorescence Correlation Spectroscopy and Additional Methods. *ChemPhysChem,* 14**,** 2441-2449.

AUTHIER, F., POSNER, B. I. & BERGERON, J. J. M. 1996. Endosomal proteolysis of internalized proteins. *FEBS Letters,* 389**,** 55-60.

AYUNI, E. L., GAZDHAR, A., GIRAUD, M. N., KADNER, A., GUGGER, M., CECCHINI, M., CAUS, T., CARREL, T. P., SCHMID, R. A. & TEVAEARAI, H. T. 2010. In vivo electroporation mediated gene delivery to the beating heart. *PLoS One,* 5**,** e14467.

BAG, N., YAP, D. H. X. & WOHLAND, T. 2014. Temperature dependence of diffusion in model and live cell membranes characterized by imaging fluorescence correlation spectroscopy. *Biochimica et Biophysica Acta (BBA) - Biomembranes,* 1838**,** 802-813.

BAREFORD, L. M. & SWAAN, P. W. 2007. ENDOCYTIC MECHANISMS FOR TARGETED DRUG DELIVERY. *Advanced drug delivery reviews,* 59**,** 748-758.

BAUDIS, S., BEHL, M. & LENDLEIN, A. 2014. Smart Polymers for Biomedical Applications. *Macromolecular Chemistry and Physics,* 215**,** 2399-2402.

BEHR, J.-P. 1997. The Proton Sponge: a Trick to Enter Cells the Viruses Did Not Exploit. *CHIMIA International Journal for Chemistry,* 51**,** 34-36.

BEN-DOV, N. & KORENSTEIN, R. 2015. The uptake of HIV Tat peptide proceeds via two pathways which differ from macropinocytosis. *Biochimica et Biophysica Acta (BBA) - Biomembranes,* 1848**,** 869-877.

BENVEGNU, T., LEMIEGRE, L. & CAMMAS-MARION, S. 2009. New generation of liposomes called archaeosomes based on natural or synthetic archaeal lipids as innovative formulations for drug delivery. *Recent Pat Drug Deliv Formul,* 3**,** 206-20.

BERGUIG, G. Y., CONVERTINE, A. J., SHI, J., PALANCA-WESSELS, M. C., DUVALL, C. L., PUN, S. H., PRESS, O. W. & STAYTON, P. S. 2012. Intracellular delivery and trafficking dynamics of a lymphoma-targeting antibody-polymer conjugate. *Mol Pharm,* 9**,** 3506-14.

BINDER, W. H., BARRAGAN, V. & MENGER, F. M. 2003. Domains and rafts in lipid membranes. *Angew Chem Int Ed Engl,* 42**,** 5802-27.

BISCHOFBERGER, M., IACOVACHE, I. & VAN DER GOOT, F. G. 2012. Pathogenic pore-forming proteins: function and host response. *Cell Host Microbe,* 12**,** 266-75.

BLANCO, E., SHEN, H. & FERRARI, M. 2015. Principles of nanoparticle design for overcoming biological barriers to drug delivery. *Nature Biotechnology,* 33**,** 941.

BOLHASSANI, A. 2011. Potential efficacy of cell-penetrating peptides for nucleic acid and drug delivery in cancer. *Biochim Biophys Acta,* 1816**,** 232-46.

BORLE, A. B. & SNOWDOWNE, K. W. 1982. Measurement of intracellular free calcium in monkey kidney cells with aequorin. *Science,* 217**,** 252-4.

BOTTGER, D., ULLRICH, C. & HUMPEL, C. 2010. Monocytes deliver bioactive nerve growth factor through a brain capillary endothelial cell-monolayer in vitro and counteract degeneration of cholinergic neurons. *Brain Res,* 1312**,** 108-19.

BOURGEAUX, V., LANAO, J. M., BAX, B. E. & GODFRIN, Y. 2016. Drug-loaded erythrocytes: on the road toward marketing approval. *Drug Design, Development and Therapy,* 10**,** 665-676.

BOUSSIF, O., LEZOUALC'H, F., ZANTA, M. A., MERGNY, M. D., SCHERMAN, D., DEMENEIX, B. & BEHR, J. P. 1995. A versatile vector for gene and oligonucleotide transfer into cells in culture and in vivo: polyethylenimine. *Proc Natl Acad Sci U S A,* 92**,** 7297-301.

BRANNON-PEPPAS, L. & BLANCHETTE, J. O. 2004. Nanoparticle and targeted systems for cancer therapy. *Advanced Drug Delivery Reviews,* 56**,** 1649-1659.

BROCK, R. 2014. The Uptake of Arginine-Rich Cell-Penetrating Peptides: Putting the Puzzle Together. *Bioconjugate Chemistry,* 25**,** 863-868.

BROOKS, H., LEBLEU, B. & VIVES, E. 2005. Tat peptide-mediated cellular delivery: back to basics. *Adv Drug Deliv Rev,* 57**,** 559-77.

CAIRNS, R., PAPANDREOU, I. & DENKO, N. 2006. Overcoming physiologic barriers to cancer treatment by molecularly targeting the tumor microenvironment. *Mol Cancer Res,* 4**,** 61-70.

CANTON, I. & BATTAGLIA, G. 2012. Endocytosis at the nanoscale. *Chem Soc Rev,* 41**,** 2718-39.

CAPECCHI, M. R. 1980. High efficiency transformation by direct microinjection of DNA into cultured mammalian cells. *Cell,* 22**,** 479-88.

CERTO, M., DEL GAIZO MOORE, V., NISHINO, M., WEI, G., KORSMEYER, S., ARMSTRONG, S. A. & LETAI, A. 2006. Mitochondria primed by death signals determine cellular addiction to antiapoptotic BCL-2 family members. *Cancer Cell,* 9**,** 351-65.

CHALOUNI, C. & DOLL, S. 2018. Fate of Antibody-Drug Conjugates in Cancer Cells. *Journal of experimental & clinical cancer research : CR,* 37**,** 20-20.

CHANG, H.-I. & YEH, M.-K. 2012. Clinical development of liposome-based drugs: formulation, characterization, and therapeutic efficacy. *International Journal of Nanomedicine,* 7**,** 49-60.

CHATIN, B., MEVEL, M., DEVALLIERE, J., DALLET, L., HAUDEBOURG, T., PEUZIAT, P., COLOMBANI, T., BERCHEL, M., LAMBERT, O., EDELMAN, A. & PITARD, B. 2015. Liposome-based Formulation for Intracellular Delivery of Functional Proteins. *Mol Ther Nucleic Acids,* 4**,** e244.

CHAUDHARY, N., GOMEZ, G. A., HOWES, M. T., LO, H. P., MCMAHON, K. A., RAE, J. A., SCHIEBER, N. L., HILL, M. M., GAUS, K., YAP, A. S. & PARTON, R. G. 2014. Endocytic

crosstalk: cavins, caveolins, and caveolae regulate clathrin-independent endocytosis. *PLoS Biol,* 12**,** e1001832.
CHEN, B., DAI, W., HE, B., ZHANG, H., WANG, X., WANG, Y. & ZHANG, Q. 2017. Current Multistage Drug Delivery Systems Based on the Tumor Microenvironment. *Theranostics,* 7**,** 538-558.
CHEN, C., SMYE, S. W., ROBINSON, M. P. & EVANS, J. A. 2006. Membrane electroporation theories: a review. *Med Biol Eng Comput,* 44**,** 5-14.
CHEN, R., ECCLESTON, M. E., YUE, Z. & SLATER, N. K. H. 2009a. Synthesis and pH-responsive properties of pseudo-peptides containing hydrophobic amino acid grafts. *Journal of Materials Chemistry,* 19**,** 4217-4224.
CHEN, R., KHORMAEE, S., ECCLESTON, M. E. & SLATER, N. K. H. 2009b. Effect of l-Leucine Graft Content on Aqueous Solution Behavior and Membrane-Lytic Activity of a pH-Responsive Pseudopeptide. *Biomacromolecules,* 10**,** 2601-2608.
CHEN, R., KHORMAEE, S., ECCLESTON, M. E. & SLATER, N. K. H. 2009c. The role of hydrophobic amino acid grafts in the enhancement of membrane-disruptive activity of pH-responsive pseudo-peptides. *Biomaterials,* 30**,** 1954-1961.
CHEN, R., YUE, Z., ECCLESTON, M. E. & SLATER, N. K. H. 2008. Aqueous solution behaviour and membrane disruptive activity of pH-responsive PEGylated pseudo-peptides and their intracellular distribution. *Biomaterials,* 29**,** 4333-4340.
CHEN, R., YUE, Z., ECCLESTON, M. E., WILLIAMS, S. & SLATER, N. K. H. 2005. Modulation of cell membrane disruption by pH-responsive pseudo-peptides through grafting with hydrophilic side chains. *Journal of Controlled Release,* 108**,** 63-72.
CHEN, S. & CHEN, R. 2016. A Virus-Mimicking, Endosomolytic Liposomal System for Efficient, pH-Triggered Intracellular Drug Delivery. *ACS Applied Materials & Interfaces,* 8**,** 22457-22467.
CHENG, W., GU, L., REN, W. & LIU, Y. 2014. Stimuli-responsive polymers for anti-cancer drug delivery. *Materials Science and Engineering: C,* 45**,** 600-608.
CHENG, Y., YUMUL, R. C. & PUN, S. H. 2016. Virus-Inspired Polymer for Efficient In Vitro and In Vivo Gene Delivery. *Angew Chem Int Ed Engl,* 55**,** 12013-7.
CHETTY, C., LAKKA, S. S., BHOOPATHI, P., KUNIGAL, S., GEISS, R. & RAO, J. S. 2008. Tissue Inhibitor of Metalloproteinase 3 Suppresses Tumor Angiogenesis in Matrix Metalloproteinase 2–Down-regulated Lung Cancer. *Cancer Research,* 68**,** 4736-4745.
CHEUNG, A., BAX, H. J., JOSEPHS, D. H., ILIEVA, K. M., PELLIZZARI, G., OPZOOMER, J., BLOOMFIELD, J., FITTALL, M., GRIGORIADIS, A., FIGINI, M., CANEVARI, S., SPICER, J. F., TUTT, A. N. & KARAGIANNIS, S. N. 2016. Targeting folate receptor alpha for cancer treatment. *Oncotarget,* 7**,** 52553-52574.
CHRISTIE, R. J. & GRAINGER, D. W. 2003. Design strategies to improve soluble macromolecular delivery constructs. *Advanced Drug Delivery Reviews,* 55**,** 421-437.
COPOLOVICI, D. M., LANGEL, K., ERISTE, E. & LANGEL, Ü. 2014. Cell-Penetrating Peptides: Design, Synthesis, and Applications. *ACS Nano,* 8**,** 1972-1994.
COSTA, E. C., MOREIRA, A. F., DE MELO-DIOGO, D., GASPAR, V. M., CARVALHO, M. P. & CORREIA, I. J. 2016. 3D tumor spheroids: an overview on the tools and techniques used for their analysis. *Biotechnology Advances,* 34**,** 1427-1441.
CRAIK, D. J., FAIRLIE, D. P., LIRAS, S. & PRICE, D. 2013. The future of peptide-based drugs. *Chem Biol Drug Des,* 81**,** 136-47.
DAVID, R. M. & DOHERTY, A. T. 2017. Viral Vectors: The Road to Reducing Genotoxicity. *Toxicological Sciences,* 155**,** 315-325.
DAVIDSON, B. L. & BREAKEFIELD, X. O. 2003. Viral vectors for gene delivery to the nervous system. *Nature Reviews Neuroscience,* 4**,** 353.
DE COCK, I., ZAGATO, E., BRAECKMANS, K., LUAN, Y., DE JONG, N., DE SMEDT, S. C. & LENTACKER, I. 2015. Ultrasound and microbubble mediated drug delivery: acoustic

pressure as determinant for uptake via membrane pores or endocytosis. *J Control Release,* 197**,** 20-8.
DE DUVE, C., DE BARSY, T., POOLE, B., TROUET, A., TULKENS, P. & VAN HOOF, F. 1974. Commentary. Lysosomotropic agents. *Biochem Pharmacol,* 23**,** 2495-531.
DE LA TORRE, B. G. & ALBERICIO, F. 2018. The Pharmaceutical Industry in 2017. An Analysis of FDA Drug Approvals from the Perspective of Molecules. *Molecules,* 23.
DEORA, A. A., DIAZ, F., SCHREINER, R. & RODRIGUEZ-BOULAN, E. 2007. Efficient Electroporation of DNA and Protein into Confluent and Differentiated Epithelial Cells in Culture. *Traffic (Copenhagen, Denmark),* 8**,** 1304-1312.
DERFUS, A. M., CHAN, W. C. W. & BHATIA, S. N. 2004. Intracellular Delivery of Quantum Dots for Live Cell Labeling and Organelle Tracking. *Advanced Materials,* 16**,** 961-966.
DEROSSI, D., JOLIOT, A. H., CHASSAING, G. & PROCHIANTZ, A. 1994. The third helix of the Antennapedia homeodomain translocates through biological membranes. *J Biol Chem,* 269**,** 10444-50.
DINCER, S., TURK, M. & PISKIN, E. 2005. Intelligent polymers as nonviral vectors. *Gene Ther,* 12**,** S139-S145.
DING, X., STEWART, M. P., SHAREI, A., WEAVER, J. C., LANGER, R. S. & JENSEN, K. F. 2017. High-throughput nuclear delivery and rapid expression of DNA via mechanical and electrical cell-membrane disruption. *Nature Biomedical Engineering,* 1**,** 0039.
DRÖGE, W., ECK, H. P., GMÜNDER, H. & MIHM, S. 1991. Modulation of lymphocyte functions and immune responses by cysteine and cysteine derivatives. *The American Journal of Medicine,* 91**,** S140-S144.
DUNCAN, R. 2006. Polymer conjugates as anticancer nanomedicines. *Nat Rev Cancer,* 6**,** 688-701.
DUNCAN, R. & RICHARDSON, S. C. 2012. Endocytosis and intracellular trafficking as gateways for nanomedicine delivery: opportunities and challenges. *Mol Pharm,* 9**,** 2380-402.
DUTTA, D. & DONALDSON, J. G. 2012. Search for inhibitors of endocytosis: Intended specificity and unintended consequences. *Cellular logistics,* 2**,** 203-208.
ECCLESTON, M. E., KUIPER, M., GILCHRIST, F. M. & SLATER, N. K. H. 2000. pH-responsive pseudo-peptides for cell membrane disruption. *Journal of Controlled Release,* 69**,** 297-307.
ECCLESTON, M. E., SLATER, N. K. H. & TIGHE, B. J. 1999. Synthetic routes to responsive polymers; co-polycondensation of tri-functional amino acids with diacylchlorides. *Reactive and Functional Polymers,* 42**,** 147-161.
ECCLESTON, M. E., WILLIAMS, S. L., YUE, Z., CHEN, R., LEE, C. K., ANIKINA, E., PAWLYN, C., BARRAND, M. A. & SLATER, N. K. H. 2005. Design and In-vitro Testing of Effective Poly(l-Lysine Iso-Phthalamide) Based Drug Targeting Systems for Solid Tumours. *Food and Bioproducts Processing,* 83**,** 141-146.
EGEBLAD, M. & WERB, Z. 2002. New functions for the matrix metalloproteinases in cancer progression. *Nat Rev Cancer,* 2**,** 161-74.
EL-SAYED, M. E., HOFFMAN, A. S. & STAYTON, P. S. 2005. Smart polymeric carriers for enhanced intracellular delivery of therapeutic macromolecules. *Expert Opinion on Biological Therapy,* 5**,** 23-32.
ELKIN, S. R., LAKODUK, A. M. & SCHMID, S. L. 2016. Endocytic pathways and endosomal trafficking: a primer. *Wiener Medizinische Wochenschrift,* 166**,** 196-204.
ELVIN, J. G., COUSTON, R. G. & VAN DER WALLE, C. F. 2013. Therapeutic antibodies: Market considerations, disease targets and bioprocessing. *International Journal of Pharmaceutics,* 440**,** 83-98.
ERAZO-OLIVERAS, A., NAJJAR, K., DAYANI, L., WANG, T.-Y., JOHNSON, G. A. & PELLOIS, J.-P. 2014. Protein delivery into live cells by incubation with an endosomolytic agent. *Nature Methods,* 11**,** 861.

ERBACHER, P., BETTINGER, T., BRION, E., COLL, J. L., PLANK, C., BEHR, J. P. & REMY, J. S. 2004. Genuine DNA/polyethylenimine (PEI) complexes improve transfection properties and cell survival. *J Drug Target,* 12**,** 223-36.

FACCIABENE, A., PENG, X., HAGEMANN, I. S., BALINT, K., BARCHETTI, A., WANG, L. P., GIMOTTY, P. A., GILKS, C. B., LAL, P., ZHANG, L. & COUKOS, G. 2011. Tumour hypoxia promotes tolerance and angiogenesis via CCL28 and T(reg) cells. *Nature,* 475**,** 226-30.

FANG, C. Y., VAIJAYANTHIMALA, V., CHENG, C. A., YEH, S. H., CHANG, C. F., LI, C. L. & CHANG, H. C. 2011. The exocytosis of fluorescent nanodiamond and its use as a long-term cell tracker. *Small,* 7**,** 3363-70.

FIEDLER, U., REICHEN, C., TAYLOR, J., SCHILDKNECHT, P., BARSIN, S., METZ, C., SCHLEGEL, A., FONTAINE, S., VILLEMAGNE, D., AHLSKOG, J., KAUFMANN, Y., LINK, A., RIGAMONTI, N., HEPP, J. & STUMPP, M. T. 2018. Abstract 4552: Tumor-restricted immune modulation by multispecific molecules from the DARPin toolbox. *Cancer Research,* 78**,** 4552-4552.

FISCHER, D., BIEBER, T., LI, Y., ELSÄSSER, H.-P. & KISSEL, T. 1999. A Novel Non-Viral Vector for DNA Delivery Based on Low Molecular Weight, Branched Polyethylenimine: Effect of Molecular Weight on Transfection Efficiency and Cytotoxicity. *Pharmaceutical Research,* 16**,** 1273-1279.

FLEIGE, E., QUADIR, M. A. & HAAG, R. 2012. Stimuli-responsive polymeric nanocarriers for the controlled transport of active compounds: concepts and applications. *Adv Drug Deliv Rev,* 64**,** 866-84.

FONSECA, S. B., PEREIRA, M. P. & KELLEY, S. O. 2009. Recent advances in the use of cell-penetrating peptides for medical and biological applications. *Adv Drug Deliv Rev,* 61**,** 953-64.

FRIDEN, P. M., WALUS, L. R., WATSON, P., DOCTROW, S. R., KOZARICH, J. W., BACKMAN, C., BERGMAN, H., HOFFER, B., BLOOM, F. & GRANHOLM, A. C. 1993. Blood-brain barrier penetration and in vivo activity of an NGF conjugate. *Science,* 259**,** 373-7.

FU, A., TANG, R., HARDIE, J., FARKAS, M. E. & ROTELLO, V. M. 2014. Promises and Pitfalls of Intracellular Delivery of Proteins. *Bioconjugate Chemistry,* 25**,** 1602-1608.

GAMCSIK, M. P., KASIBHATLA, M. S., TEETER, S. D. & COLVIN, O. M. 2012. Glutathione Levels in Human Tumors. *Biomarkers : biochemical indicators of exposure, response, and susceptibility to chemicals,* 17**,** 671-691.

GANGADARAN, P., HONG, C. M. & AHN, B.-C. 2018. An Update on in Vivo Imaging of Extracellular Vesicles as Drug Delivery Vehicles. *Frontiers in Pharmacology,* 9.

GAO, W., CHAN, J. M. & FAROKHZAD, O. C. 2010. pH-Responsive nanoparticles for drug delivery. *Molecular pharmaceutics,* 7**,** 1913-1920.

GARCÍA, K. P., ZARSCHLER, K., BARBARO, L., BARRETO, J. A., O'MALLEY, W., SPICCIA, L., STEPHAN, H. & GRAHAM, B. 2014. Zwitterionic-Coated "Stealth" Nanoparticles for Biomedical Applications: Recent Advances in Countering Biomolecular Corona Formation and Uptake by the Mononuclear Phagocyte System. *Small,* 10**,** 2516-2529.

GARNOCK-JONES, K. P., KEATING, G. M. & SCOTT, L. J. 2010. Trastuzumab: A review of its use as adjuvant treatment in human epidermal growth factor receptor 2 (HER2)-positive early breast cancer. *Drugs,* 70**,** 215-39.

GASIOROWSKI, J. Z. & DEAN, D. A. 2003. Mechanisms of nuclear transport and interventions. *Advanced Drug Delivery Reviews,* 55**,** 703-716.

GAUTHIER, M. A. & KLOK, H. A. 2008. Peptide/protein-polymer conjugates: synthetic strategies and design concepts. *Chem Commun (Camb)***,** 2591-611.

GERWECK, L. E., KOZIN, S. V. & STOCKS, S. J. 1999. The pH partition theory predicts the accumulation and toxicity of doxorubicin in normal and low-pH-adapted cells. *Br J Cancer,* 79**,** 838-42.

GILLERON, J., QUERBES, W., ZEIGERER, A., BORODOVSKY, A., MARSICO, G., SCHUBERT, U., MANYGOATS, K., SEIFERT, S., ANDREE, C., STÖTER, M., EPSTEIN-BARASH, H., ZHANG, L., KOTELIANSKY, V., FITZGERALD, K., FAVA, E., BICKLE, M., KALAIDZIDIS, Y., AKINC, A.,

MAIER, M. & ZERIAL, M. 2013. Image-based analysis of lipid nanoparticle–mediated siRNA delivery, intracellular trafficking and endosomal escape. *Nature Biotechnology,* 31**,** 638.

GINN, F. L., HOCHSTEIN, P. & TRUMP, B. F. 1969. Membrane alterations in hemolysis: Internalization of plasmalemma induced by primaquine. *Science,* 164**,** 843-5.

GODA, T., GOTO, Y. & ISHIHARA, K. 2010. Cell-penetrating macromolecules: Direct penetration of amphipathic phospholipid polymers across plasma membrane of living cells. *Biomaterials,* 31**,** 2380-2387.

GODBEY, W. T., WU, K. K. & MIKOS, A. G. 1999a. Size matters: Molecular weight affects the efficiency of poly(ethylenimine) as a gene delivery vehicle. *Journal of Biomedical Materials Research,* 45**,** 268-275.

GODBEY, W. T., WU, K. K. & MIKOS, A. G. 1999b. Tracking the intracellular path of poly(ethylenimine)/DNA complexes for gene delivery. *Proceedings of the National Academy of Sciences,* 96**,** 5177-5181.

GREENFIELD, R. S., KANEKO, T., DAUES, A., EDSON, M. A., FITZGERALD, K. A., OLECH, L. J., GRATTAN, J. A., SPITALNY, G. L. & BRASLAWSKY, G. R. 1990. Evaluation in vitro of adriamycin immunoconjugates synthesized using an acid-sensitive hydrazone linker. *Cancer Res,* 50**,** 6600-7.

GREISH, K. 2010. Enhanced Permeability and Retention (EPR) Effect for Anticancer Nanomedicine Drug Targeting. *In:* GROBMYER, S. R. & MOUDGIL, B. M. (eds.) *Cancer Nanotechnology.* Humana Press.

GUIDOTTI, G., BRAMBILLA, L. & ROSSI, D. 2017. Cell-Penetrating Peptides: From Basic Research to Clinics. *Trends in Pharmacological Sciences,* 38**,** 406-424.

GUILLARD, S., MINTER, R. R. & JACKSON, R. H. 2015. Engineering therapeutic proteins for cell entry: the natural approach. *Trends in Biotechnology,* 33**,** 163-171.

GUO, W., GAO, Y., LI, N., SHAO, F., WANG, C., WANG, P., YANG, Z., LI, R. & HE, J. 2017. Exosomes: New players in cancer (Review). *Oncol Rep,* 38**,** 665-675.

GURTOVENKO, A. A., ANWAR, J. & VATTULAINEN, I. 2010. Defect-mediated trafficking across cell membranes: insights from in silico modeling. *Chem Rev,* 110**,** 6077-103.

HA, D., YANG, N. & NADITHE, V. 2016. Exosomes as therapeutic drug carriers and delivery vehicles across biological membranes: current perspectives and future challenges. *Acta Pharmaceutica Sinica B,* 6**,** 287-296.

HAAG, R. & KRATZ, F. 2006. Polymer therapeutics: concepts and applications. *Angew Chem Int Ed Engl,* 45**,** 1198-215.

HÄCKER, G. 2000. The morphology of apoptosis. *Cell and Tissue Research,* 301**,** 5-17.

HALLOW, D. M., SEEGER, R. A., KAMAEV, P. P., PRADO, G. R., LAPLACA, M. C. & PRAUSNITZ, M. R. 2008. Shear-induced intracellular loading of cells with molecules by controlled microfluidics. *Biotechnology and bioengineering,* 99**,** 846-854.

HAMIDI, M. & TAJERZADEH, H. 2003. Carrier Erythrocytes: An Overview. *Drug Delivery,* 10**,** 9-20.

HARADA, H., KIZAKA-KONDOH, S. & HIRAOKA, M. 2005. Optical imaging of tumor hypoxia and evaluation of efficacy of a hypoxia-targeting drug in living animals. *Mol Imaging,* 4**,** 182-93.

HARRIS, A. L. 2002. Hypoxia — a key regulatory factor in tumour growth. *Nature Reviews Cancer,* 2**,** 38.

HARRIS, J. M. & CHESS, R. B. 2003. Effect of pegylation on pharmaceuticals. *Nat Rev Drug Discov,* 2**,** 214-221.

HATAKEYAMA, H., AKITA, H., KOGURE, K., OISHI, M., NAGASAKI, Y., KIHIRA, Y., UENO, M., KOBAYASHI, H., KIKUCHI, H. & HARASHIMA, H. 2006. Development of a novel systemic gene delivery system for cancer therapy with a tumor-specific cleavable PEG-lipid. *Gene Therapy,* 14**,** 68.

HE, X., AMIN, A. A., FOWLER, A. & TONER, M. 2006. Thermally Induced Introduction of Trehalose into Primary Rat Hepatocytes. *Cell Preservation Technology,* 4**,** 178-187.
HE, X., LI, J., AN, S. & JIANG, C. 2013. *PH-Sensitive drug-Delivery systems for tumor targeting*.
HEINEMANN, M. L. & VYKOUKAL, J. 2017. Sequential Filtration: A Gentle Method for the Isolation of Functional Extracellular Vesicles. *Methods Mol Biol,* 1660**,** 33-41.
HEITZ, F., MORRIS, M. C. & DIVITA, G. 2009. Twenty years of cell-penetrating peptides: from molecular mechanisms to therapeutics. *Br J Pharmacol,* 157**,** 195-206.
HELLER, D. A., BAIK, S., EURELL, T. E. & STRANO, M. S. 2005. Single-Walled Carbon Nanotube Spectroscopy in Live Cells: Towards Long-Term Labels and Optical Sensors. *Advanced Materials,* 17**,** 2793-2799.
HERCE, H. D. & GARCIA, A. E. 2007. Molecular dynamics simulations suggest a mechanism for translocation of the HIV-1 TAT peptide across lipid membranes. *Proceedings of the National Academy of Sciences,* 104**,** 20805-20810.
HERMANSON, G. T. 2013. Chapter 10 - Fluorescent Probes. *In:* HERMANSON, G. T. (ed.) *Bioconjugate Techniques (Third Edition).* Boston: Academic Press.
HIROSE, H., TAKEUCHI, T., OSAKADA, H., PUJALS, S., KATAYAMA, S., NAKASE, I., KOBAYASHI, S., HARAGUCHI, T. & FUTAKI, S. 2012. Transient Focal Membrane Deformation Induced by Arginine-rich Peptides Leads to Their Direct Penetration into Cells. *Molecular Therapy,* 20**,** 984-993.
HIRSCHHAEUSER, F., MENNE, H., DITTFELD, C., WEST, J., MUELLER-KLIESER, W. & KUNZ-SCHUGHART, L. A. 2010. Multicellular tumor spheroids: An underestimated tool is catching up again. *Journal of Biotechnology,* 148**,** 3-15.
HO, V. H. B., SLATER, N. K. H. & CHEN, R. 2011. pH-responsive endosomolytic pseudo-peptides for drug delivery to multicellular spheroids tumour models. *Biomaterials,* 32**,** 2953-2958.
HOCHMUTH, R. M., EVANS, C. A., WILES, H. C. & MCCOWN, J. T. 1983. Mechanical measurement of red cell membrane thickness. *Science,* 220**,** 101-2.
HOFFMAN, A. S. 2013. Stimuli-responsive polymers: Biomedical applications and challenges for clinical translation. *Advanced Drug Delivery Reviews,* 65**,** 10-16.
HONG, S., LEROUEIL, P. R., JANUS, E. K., PETERS, J. L., KOBER, M. M., ISLAM, M. T., ORR, B. G., BAKER, J. R., JR. & BANASZAK HOLL, M. M. 2006. Interaction of polycationic polymers with supported lipid bilayers and cells: nanoscale hole formation and enhanced membrane permeability. *Bioconjug Chem,* 17**,** 728-34.
HOU, S., ZIEBACZ, N., WIECZOREK, S. A., KALWARCZYK, E., SASHUK, V., KALWARCZYK, T., KAMINSKI, T. S. & HOLYST, R. 2011. Formation and structure of PEI/DNA complexes: quantitative analysis. *Soft Matter,* 7**,** 6967-6972.
HRUBÝ, M., FILIPPOV, S. K. & ŠTĚPÁNEK, P. 2015. Smart polymers in drug delivery systems on crossroads: Which way deserves following? *European Polymer Journal,* 65**,** 82-97.
HU, Y.-B., DAMMER, E. B., REN, R.-J. & WANG, G. 2015. The endosomal-lysosomal system: from acidification and cargo sorting to neurodegeneration. *Translational neurodegeneration,* 4**,** 18-18.
HUGHES, L. D., RAWLE, R. J. & BOXER, S. G. 2014. Choose Your Label Wisely: Water-Soluble Fluorophores Often Interact with Lipid Bilayers. *PLOS ONE,* 9**,** e87649.
IMAI, K. & TAKAOKA, A. 2006. Comparing antibody and small-molecule therapies for cancer. *Nat Rev Cancer,* 6**,** 714-727.
INOUYE, S. & TSUJI, F. I. 1994. Evidence for redox forms of the Aequorea green fluorescent protein. *FEBS Letters,* 351**,** 211-214.
IVERSEN, T.-G., SKOTLAND, T. & SANDVIG, K. 2011. Endocytosis and intracellular transport of nanoparticles: Present knowledge and need for future studies. *Nano Today,* 6**,** 176-185.

JAIMES-AGUIRRE, L., GIBBENS-BANDALA, B. V., MORALES-AVILA, E., OCAMPO-GARCIA, B. E., SEYEDEH-FATEMEH, M. & AMIRHOSEIN, A. 2016. Polymer-Based Drug Delivery Systems, Development and Pre-Clinical Status. *Curr Pharm Des,* 22**,** 2886-903.

JAIN, N. K., TARE, M. S., MISHRA, V. & TRIPATHI, P. K. 2015. The development, characterization and in vivo anti-ovarian cancer activity of poly(propylene imine) (PPI)-antibody conjugates containing encapsulated paclitaxel. *Nanomedicine: Nanotechnology, Biology, and Medicine,* 11**,** 207-218.

JAIN, R. K. 2001. Normalizing tumor vasculature with anti-angiogenic therapy: a new paradigm for combination therapy. *Nat Med,* 7**,** 987-9.

JIAO, C. Y., DELAROCHE, D., BURLINA, F., ALVES, I. D., CHASSAING, G. & SAGAN, S. 2009. Translocation and endocytosis for cell-penetrating peptide internalization. *J Biol Chem,* 284**,** 33957-65.

JOUBERT, M. K., DESHPANDE, M., YANG, J., REYNOLDS, H., BRYSON, C., FOGG, M., BAKER, M. P., HERSKOVITZ, J., GOLETZ, T. J., ZHOU, L., MOXNESS, M., FLYNN, G. C., NARHI, L. O. & JAWA, V. 2016. Use of In Vitro Assays to Assess Immunogenicity Risk of Antibody-Based Biotherapeutics. *PLoS ONE,* 11**,** e0159328.

JOZALA, A. F., GERALDES, D. C., TUNDISI, L. L., FEITOSA, V. D. A., BREYER, C. A., CARDOSO, S. L., MAZZOLA, P. G., OLIVEIRA-NASCIMENTO, L. D., RANGEL-YAGUI, C. D. O., MAGALHÃES, P. D. O., OLIVEIRA, M. A. D. & PESSOA, A., JR. 2016. Biopharmaceuticals from microorganisms: from production to purification. *Brazilian journal of microbiology : [publication of the Brazilian Society for Microbiology],* 47 Suppl 1**,** 51-63.

JUNTTILA, M. R. & DE SAUVAGE, F. J. 2013. Influence of tumour micro-environment heterogeneity on therapeutic response. *Nature,* 501**,** 346-54.

KAKSONEN, M. & ROUX, A. 2018. Mechanisms of clathrin-mediated endocytosis. *Nat Rev Mol Cell Biol,* 19**,** 313-326.

KANAMALA, M., WILSON, W. R., YANG, M., PALMER, B. D. & WU, Z. 2016. Mechanisms and biomaterials in pH-responsive tumour targeted drug delivery: A review. *Biomaterials,* 85**,** 152-167.

KASHIWAGI, H., MCDUNN, J. E., GOEDEGEBUURE, P. S., GAFFNEY, M. C., CHANG, K., TRINKAUS, K., PIWNICA-WORMS, D., HOTCHKISS, R. S. & HAWKINS, W. G. 2007. TAT-Bim Induces Extensive Apoptosis in Cancer Cells. *Annals of Surgical Oncology,* 14**,** 1763-1771.

KAUFMANN, B. A. & LINDNER, J. R. 2007. Molecular imaging with targeted contrast ultrasound. *Curr Opin Biotechnol,* 18**,** 11-6.

KEEFE, A. J. & JIANG, S. 2011. Poly(zwitterionic)protein conjugates offer increased stability without sacrificing binding affinity or bioactivity. *Nature Chemistry,* 4**,** 59.

KELLUM, J. A. 2000. Determinants of blood pH in health and disease. *Critical Care,* 4**,** 6.

KHALIL, I. A., KOGURE, K., AKITA, H. & HARASHIMA, H. 2006. Uptake pathways and subsequent intracellular trafficking in nonviral gene delivery. *Pharmacol Rev,* 58**,** 32-45.

KHAN, M. A., WU, V. M., GHOSH, S. & USKOKOVIĆ, V. 2016. Gene delivery using calcium phosphate nanoparticles: Optimization of the transfection process and the effects of citrate and poly(l-lysine) as additives. *Journal of colloid and interface science,* 471**,** 48-58.

KHORMAEE, S., CHOI, Y., SHEN, M. J., XU, B., WU, H., GRIFFITHS, G. L., CHEN, R., SLATER, N. K. H. & PARK, J. K. 2013. Endosomolytic Anionic Polymer for the Cytoplasmic Delivery of siRNAs in Localized In Vivo Applications. *Advanced Functional Materials,* 23**,** 565-574.

KIKUCHI, T., SHIMIZU, H., AKIYAMA, Y. & TANIGUCHI, S. 2017. In situ delivery and production system of trastuzumab scFv with Bifidobacterium. *Biochem Biophys Res Commun,* 493**,** 306-312.

KIM, D., KIM, C. H., MOON, J. I., CHUNG, Y. G., CHANG, M. Y., HAN, B. S., KO, S., YANG, E., CHA, K. Y., LANZA, R. & KIM, K. S. 2009a. Generation of human induced pluripotent stem cells by direct delivery of reprogramming proteins. *Cell Stem Cell,* 4**,** 472-6.

KIM, H., KIM, S., PARK, C., LEE, H., PARK, H. J. & KIM, C. 2010. Glutathione-Induced Intracellular Release of Guests from Mesoporous Silica Nanocontainers with Cyclodextrin Gatekeepers. *Advanced Materials,* 22**,** 4280-4283.
KIM, K. J. & LEE, B.-W. 2012. The Roles of Glycated Albumin as Intermediate Glycation Index and Pathogenic Protein. *Diabetes & Metabolism Journal,* 36**,** 98-107.
KIM, S., KIM, J. H., JEON, O., KWON, I. C. & PARK, K. 2009b. Engineered polymers for advanced drug delivery. *Eur J Pharm Biopharm,* 71**,** 420-30.
KIRCHEIS, R., WIGHTMAN, L. & WAGNER, E. 2001. Design and gene delivery activity of modified polyethylenimines. *Advanced Drug Delivery Reviews,* 53**,** 341-358.
KLEIN, T. M., WOLF, E. D., WU, R. & SANFORD, J. C. 1987. High-velocity microprojectiles for delivering nucleic acids into living cells. *Nature,* 327**,** 70.
KNEIPP, J., KNEIPP, H., WITTIG, B. & KNEIPP, K. 2010. Following the Dynamics of pH in Endosomes of Live Cells with SERS Nanosensors. *The Journal of Physical Chemistry C,* 114**,** 7421-7426.
KNIGHT, S., COLLINS, M. & TAKEUCHI, Y. 2013. Insertional mutagenesis by retroviral vectors: current concepts and methods of analysis. *Curr Gene Ther,* 13**,** 211-27.
KOLLMANNSPERGER, A., SHAREI, A., RAULF, A., HEILEMANN, M., LANGER, R., JENSEN, K. F., WIENEKE, R. & TAMPÉ, R. 2016. Live-cell protein labelling with nanometre precision by cell squeezing. *Nature Communications,* 7**,** 10372.
KOPEČEK, J., KOPEČKOVÁ, P., MINKO, T. & LU, Z.-R. 2000. HPMA copolymer–anticancer drug conjugates: design, activity, and mechanism of action. *European Journal of Pharmaceutics and Biopharmaceutics,* 50**,** 61-81.
KOREN, E., APTE, A., JANI, A. & TORCHILIN, V. P. 2012. Multifunctional PEGylated 2C5-immunoliposomes containing pH-sensitive bonds and TAT peptide for enhanced tumor cell internalization and cytotoxicity. *J Control Release,* 160**,** 264-73.
KOSTRITSKII, A. Y., KONDINSKAIA, D. A., NESTERENKO, A. M. & GURTOVENKO, A. A. 2016. Adsorption of Synthetic Cationic Polymers on Model Phospholipid Membranes: Insight from Atomic-Scale Molecular Dynamics Simulations. *Langmuir,* 32**,** 10402-10414.
KOTNIK, T., FREY, W., SACK, M., HABERL MEGLIČ, S., PETERKA, M. & MIKLAVČIČ, D. 2015. Electroporation-based applications in biotechnology. *Trends in Biotechnology,* 33**,** 480-488.
KUHN, S. J., FINCH, S. K., HALLAHAN, D. E. & GIORGIO, T. D. 2006. Proteolytic surface functionalization enhances in vitro magnetic nanoparticle mobility through extracellular matrix. *Nano Lett,* 6**,** 306-12.
KUPPEN, P. J. K., VAN DER EB, M. M., JONGES, L. E., HAGENAARS, M., HOKLAND, M. E., NANNMARK, U., GOLDFARB, R. H., BASSE, P. H., FLEUREN, G. J., HOEBEN, R. C. & VAN DE VELDE, C. J. H. 2001. Tumor structure and extracellular matrix as a possible barrier for therapeutic approaches using immune cells or adenoviruses in colorectal cancer. *Histochemistry and Cell Biology,* 115**,** 67-72.
KUPPUSAMY, P., LI, H., ILANGOVAN, G., CARDOUNEL, A. J., ZWEIER, J. L., YAMADA, K., KRISHNA, M. C. & MITCHELL, J. B. 2002. Noninvasive imaging of tumor redox status and its modification by tissue glutathione levels. *Cancer Res,* 62**,** 307-12.
KUROSAKI, T., KITAHARA, T., FUMOTO, S., NISHIDA, K., NAKAMURA, J., NIIDOME, T., KODAMA, Y., NAKAGAWA, H., TO, H. & SASAKI, H. 2009. Ternary complexes of pDNA, polyethylenimine, and gamma-polyglutamic acid for gene delivery systems. *Biomaterials,* 30**,** 2846-53.
KUROSAKI, T., KITAHARA, T., NAKAMURA, T., NISHIDA, K., FUMOTO, S., KODAMA, Y., NAKAGAWA, H., HIGUCHI, N. & SASAKI, H. 2012. Development of effective cancer vaccine using targeting system of antigen protein to APCs. *Pharm Res,* 29**,** 483-9.
KURTOGLU, Y. E., NAVATH, R. S., WANG, B., KANNAN, S., ROMERO, R. & KANNAN, R. M. 2009. Poly(amidoamine) dendrimer-drug conjugates with disulfide linkages for intracellular drug delivery. *Biomaterials,* 30**,** 2112-21.

KYUNG, H., KIM, H., LEE, H. & LEE, S. J. 2018. Enhanced intracellular delivery of macromolecules by melittin derivatives mediated cellular uptake. *Journal of Industrial and Engineering Chemistry,* 58**,** 290-295.

LACKEY, C. A., PRESS, O. W., HOFFMAN, A. S. & STAYTON, P. S. 2002. A biomimetic pH-responsive polymer directs endosomal release and intracellular delivery of an endocytosed antibody complex. *Bioconjug Chem,* 13**,** 996-1001.

LALE, S. V., KUMAR, A., NAZ, F., BHARTI, A. C. & KOUL, V. 2015. Multifunctional ATRP based pH responsive polymeric nanoparticles for improved doxorubicin chemotherapy in breast cancer by proton sponge effect/endo-lysosomal escape. *Polymer Chemistry,* 6**,** 2115-2132.

LAMICHHANE, N., UDAYAKUMAR, T. S., D'SOUZA, W. D., SIMONE, C. B., 2ND, RAGHAVAN, S. R., POLF, J. & MAHMOOD, J. 2018. Liposomes: Clinical Applications and Potential for Image-Guided Drug Delivery. *Molecules,* 23.

LAN, W. C., LAN, W. H., CHAN, C. P., HSIEH, C. C., CHANG, M. C. & JENG, J. H. 1999. The effects of extracellular citric acid acidosis on the viability, cellular adhesion capacity and protein synthesis of cultured human gingival fibroblasts. *Aust Dent J,* 44**,** 123-30.

LEE, H., BHANG, S. H., LEE, J. H., KIM, H. & HAHN, S. K. 2017a. Tocilizumab–Alendronate Conjugate for Treatment of Rheumatoid Arthritis. *Bioconjugate Chemistry,* 28**,** 1084-1092.

LEE, J., LIN, E.-W., LAU, U. Y., HEDRICK, J. L., BAT, E. & MAYNARD, H. D. 2013. Trehalose Glycopolymers as Excipients for Protein Stabilization. *Biomacromolecules,* 14**,** 2561-2569.

LEE, K. Y. J., WANG, Y. & NIE, S. 2015. In vitro study of a pH-sensitive multifunctional doxorubicin–gold nanoparticle system: therapeutic effect and surface enhanced Raman scattering. *RSC Advances,* 5**,** 65651-65659.

LEE, M. H., KIM, J. Y., HAN, J. H., BHUNIYA, S., SESSLER, J. L., KANG, C. & KIM, J. S. 2012. Direct Fluorescence Monitoring of the Delivery and Cellular Uptake of a Cancer-Targeted RGD Peptide-Appended Naphthalimide Theragnostic Prodrug. *Journal of the American Chemical Society,* 134**,** 12668-12674.

LEE, M. S., DEES, E. C. & WANG, A. Z. 2017b. Nanoparticle-Delivered Chemotherapy: Old Drugs in New Packages. *Oncology (Williston Park),* 31**,** 198-208.

LEE, S. H., MOK, H., LEE, Y. & PARK, T. G. 2011. Self-assembled siRNA–PLGA conjugate micelles for gene silencing. *Journal of Controlled Release,* 152**,** 152-158.

LEE, Y. J., ERAZO-OLIVERAS, A. & PELLOIS, J. P. 2010. Delivery of macromolecules into live cells by simple co-incubation with a peptide. *Chembiochem,* 11**,** 325-30.

LERICHE, G., CHISHOLM, L. & WAGNER, A. 2012. Cleavable linkers in chemical biology. *Bioorg Med Chem,* 20**,** 571-82.

LI, J., WANG, B., JUBA, B. M., VAZQUEZ, M., KORTUM, S. W., PIERCE, B. S., PACHECO, M., ROBERTS, L., STROHBACH, J. W., JONES, L. H., HETT, E., THORARENSEN, A., TELLIEZ, J.-B., SHAREI, A., BUNNAGE, M. & GILBERT, J. B. 2017. Microfluidic-Enabled Intracellular Delivery of Membrane Impermeable Inhibitors to Study Target Engagement in Human Primary Cells. *ACS Chemical Biology,* 12**,** 2970-2974.

LI, L., HE, Z. Y., WEI, X. W., GAO, G. P. & WEI, Y. Q. 2015a. Challenges in CRISPR/CAS9 Delivery: Potential Roles of Nonviral Vectors. *Hum Gene Ther,* 26**,** 452-62.

LI, L., WAN, T., WAN, M., LIU, B., CHENG, R. & ZHANG, R. 2015b. The effect of the size of fluorescent dextran on its endocytic pathway. *Cell Biology International,* 39**,** 531-539.

LIECHTY, W. B., CHEN, R., FARZANEH, F., TAVASSOLI, M. & SLATER, N. K. H. 2009. Synthetic pH-Responsive Polymers for Protein Transduction. *Advanced materials (Deerfield Beach, Fla.),* 21**,** 3910-3914.

LIU, C., ZHANG, L., LIU, H. & CHENG, K. 2017a. Delivery strategies of the CRISPR-Cas9 gene-editing system for therapeutic applications. *J Control Release,* 266**,** 17-26.

LIU, J., HUANG, Y., KUMAR, A., TAN, A., JIN, S., MOZHI, A. & LIANG, X.-J. 2014. pH-Sensitive nano-systems for drug delivery in cancer therapy. *Biotechnology Advances,* 32**,** 693-710.

LIU, Y., WANG, Z., LIU, Y., ZHU, G., JACOBSON, O., FU, X., BAI, R., LIN, X., LU, N., YANG, X., FAN, W., SONG, J., WANG, Z., YU, G., ZHANG, F., KALISH, H., NIU, G., NIE, Z. & CHEN, X. 2017b. Suppressing Nanoparticle-Mononuclear Phagocyte System Interactions of Two-Dimensional Gold Nanorings for Improved Tumor Accumulation and Photothermal Ablation of Tumors. *ACS Nano,* 11**,** 10539-10548.

LORENZ, J. N. & GRUENSTEIN, E. 1999. A simple, nonradioactive method for evaluating single-nephron filtration rate using FITC-inulin. *Am J Physiol,* 276**,** F172-7.

LU, Q. L., LIANG, H. D., PARTRIDGE, T. & BLOMLEY, M. J. 2003. Microbubble ultrasound improves the efficiency of gene transduction in skeletal muscle in vivo with reduced tissue damage. *Gene Ther,* 10**,** 396-405.

LU, S. C. 1999. Regulation of hepatic glutathione synthesis: current concepts and controversies. *The FASEB Journal,* 13**,** 1169-1183.

LU, Y. & LIU, J. 2007. Erythrocyte membrane proteins and membrane skeleton. *Frontiers of Biology in China,* 2**,** 247-255.

LUDTKE, J. J., SEBESTYÉN, M. G. & WOLFF, J. A. 2002. The Effect of Cell Division on the Cellular Dynamics of Microinjected DNA and Dextran. *Molecular Therapy,* 5**,** 579-588.

LUDTKE, S., HE, K. & HUANG, H. 1995. Membrane thinning caused by magainin 2. *Biochemistry,* 34**,** 16764-16769.

LUSHCHAK, V. I. 2012. Glutathione Homeostasis and Functions: Potential Targets for Medical Interventions. *Journal of Amino Acids,* 2012**,** 26.

LYNCH, A. L., CHEN, R., DOMINOWSKI, P. J., SHALAEV, E. Y., YANCEY, R. J., JR. & SLATER, N. K. 2010. Biopolymer mediated trehalose uptake for enhanced erythrocyte cryosurvival. *Biomaterials,* 31**,** 6096-103.

LYNCH, A. L., CHEN, R. & SLATER, N. K. 2011. pH-responsive polymers for trehalose loading and desiccation protection of human red blood cells. *Biomaterials,* 32**,** 4443-9.

MA, S., SCHROEDER, B., SUN, C., LOUFAKIS, D. N., CAO, Z., SRIRANGANATHAN, N. & LU, C. 2014. Electroporation-based delivery of cell-penetrating peptide conjugates of peptide nucleic acids for antisense inhibition of intracellular bacteria. *Integr Biol (Camb),* 6**,** 973-8.

MAEDA, H., BHARATE, G. Y. & DARUWALLA, J. 2009. Polymeric drugs for efficient tumor-targeted drug delivery based on EPR-effect. *Eur J Pharm Biopharm,* 71**,** 409-19.

MAHER, P. 2005. The effects of stress and aging on glutathione metabolism. *Ageing Res Rev,* 4**,** 288-314.

MAHONEY, B. P., RAGHUNAND, N., BAGGETT, B. & GILLIES, R. J. 2003. Tumor acidity, ion trapping and chemotherapeutics. I. Acid pH affects the distribution of chemotherapeutic agents in vitro. *Biochem Pharmacol,* 66**,** 1207-18.

MALLAKPOUR, S. & DINARI, M. 2011. *Progress in Synthetic Polymers Based on Natural Amino Acids*.

MARCHESI, V. T., FURTHMAYR, H. & TOMITA, M. 1976. The red cell membrane. *Annu Rev Biochem,* 45**,** 667-98.

MARSCHALL, A. L., ZHANG, C., FRENZEL, A., SCHIRRMANN, T., HUST, M., PEREZ, F. & DUBEL, S. 2014. Delivery of antibodies to the cytosol: debunking the myths. *MAbs,* 6**,** 943-56.

MARTENS, T. F., REMAUT, K., DEMEESTER, J., DE SMEDT, S. C. & BRAECKMANS, K. 2014. Intracellular delivery of nanomaterials: How to catch endosomal escape in the act. *Nano Today,* 9**,** 344-364.

MAYOR, S. & PAGANO, R. E. 2007. Pathways of clathrin-independent endocytosis. *Nat Rev Mol Cell Biol,* 8**,** 603-12.

MAYOR, S., PARTON, R. G. & DONALDSON, J. G. 2014. Clathrin-independent pathways of endocytosis. *Cold Spring Harb Perspect Biol,* 6.

MCNEIL, P. L. 1988. Chapter 10 Incorporation of Macromolecules into Living Cells. *In:* WANG, Y.-L., TAYLOR, D. L. & JEON, K. W. (eds.) *Methods in Cell Biology.* Academic Press.
MECKE, A., LEE, D. K., RAMAMOORTHY, A., ORR, B. G. & BANASZAK HOLL, M. M. 2005. Membrane thinning due to antimicrobial peptide binding: an atomic force microscopy study of MSI-78 in lipid bilayers. *Biophys J,* 89**,** 4043-50.
MELLMAN, I. 1996. Endocytosis and molecular sorting. *Annu Rev Cell Dev Biol,* 12**,** 575-625.
MERCADO, S. A., ORELLANA-TAVRA, C., CHEN, A. & SLATER, N. K. H. 2016. The intracellular fate of an amphipathic pH-responsive polymer: Key characteristics towards drug delivery. *Materials Science and Engineering: C,* 69**,** 1051-1057.
MERCADO, S. A. & SLATER, N. K. H. 2016a. The functional and structural effects of an amphipathic pH responsive biopolymer: A comprehensive study in osteosarcoma cells. *European Polymer Journal,* 74**,** 158-167.
MERCADO, S. A. & SLATER, N. K. H. 2016b. Increased cryosurvival of osteosarcoma cells using an amphipathic pH-responsive polymer for trehalose uptake. *Cryobiology,* 73**,** 175-180.
MERDAN, T., KOPECEK, J. & KISSEL, T. 2002. Prospects for cationic polymers in gene and oligonucleotide therapy against cancer. *Adv Drug Deliv Rev,* 54**,** 715-58.
METTLEN, M., CHEN, P.-H., SRINIVASAN, S., DANUSER, G. & SCHMID, S. L. 2018. Regulation of Clathrin-Mediated Endocytosis. *Annual Review of Biochemistry,* 87**,** 871-896.
MIELE, E., SPINELLI, G. P., MIELE, E., DI FABRIZIO, E., FERRETTI, E., TOMAO, S. & GULINO, A. 2012. Nanoparticle-based delivery of small interfering RNA: challenges for cancer therapy. *Int J Nanomedicine,* 7**,** 3637-57.
MIKLAVCIC, D., SEMROV, D., MEKID, H. & MIR, L. M. 2000. A validated model of in vivo electric field distribution in tissues for electrochemotherapy and for DNA electrotransfer for gene therapy. *Biochim Biophys Acta,* 1523**,** 73-83.
MILLA, P., DOSIO, F. & CATTEL, L. 2012. PEGylation of proteins and liposomes: a powerful and flexible strategy to improve the drug delivery. *Curr Drug Metab,* 13**,** 105-19.
MOITRA, K., LOU, H. & DEAN, M. 2011. Multidrug Efflux Pumps and Cancer Stem Cells: Insights Into Multidrug Resistance and Therapeutic Development. *Clinical Pharmacology & Therapeutics,* 89**,** 491-502.
MOORKENS, E., MEUWISSEN, N., HUYS, I., DECLERCK, P., VULTO, A. G. & SIMOENS, S. 2017. The Market of Biopharmaceutical Medicines: A Snapshot of a Diverse Industrial Landscape. *Frontiers in pharmacology,* 8**,** 314-314.
MORILLE, M., PASSIRANI, C., VONARBOURG, A., CLAVREUL, A. & BENOIT, J. P. 2008. Progress in developing cationic vectors for non-viral systemic gene therapy against cancer. *Biomaterials,* 29**,** 3477-96.
MOUSAVI, S. A., MALEROD, L., BERG, T. & KJEKEN, R. 2004. Clathrin-dependent endocytosis. *Biochem J,* 377**,** 1-16.
MUKHERJEE, S., GHOSH, R. N. & MAXFIELD, F. R. 1997. *Endocytosis*.
MURANEN, T., IWANICKI, M. P., CURRY, N. L., HWANG, J., DUBOIS, C. D., COLOFF, J. L., HITCHCOCK, D. S., CLISH, C. B., BRUGGE, J. S. & KALAANY, N. Y. 2017. Starved epithelial cells uptake extracellular matrix for survival. *Nature Communications,* 8**,** 13989.
MURTHY, N., CAMPBELL, J., FAUSTO, N., HOFFMAN, A. S. & STAYTON, P. S. 2003. Design and synthesis of pH-responsive polymeric carriers that target uptake and enhance the intracellular delivery of oligonucleotides. *Journal of Controlled Release,* 89**,** 365-374.
MURTHY, N., CHANG, I., STAYTON, P. & HOFFMAN, A. 2001. pH-sensitive hemolysis by random copolymers of alkyl acrylates and acrylic acid. *Macromolecular Symposia,* 172**,** 49-56.
MURTHY, N., ROBICHAUD, J. R., TIRRELL, D. A., STAYTON, P. S. & HOFFMAN, A. S. 1999. The design and synthesis of polymers for eukaryotic membrane disruption. *J Control Release,* 61**,** 137-43.
MUZYKANTOV, V. R. 2010. Drug delivery by red blood cells: vascular carriers designed by Mother Nature. *Expert opinion on drug delivery,* 7**,** 403-427.

NAKAMURA, Y., MOCHIDA, A., CHOYKE, P. L. & KOBAYASHI, H. 2016. Nanodrug Delivery: Is the Enhanced Permeability and Retention Effect Sufficient for Curing Cancer? *Bioconjugate Chemistry,* 27**,** 2225-2238.

NEEVES, K. B., SAWYER, A. J., FOLEY, C. P., SALTZMAN, W. M. & OLBRICHT, W. L. 2007. Dilation and degradation of the brain extracellular matrix enhances penetration of infused polymer nanoparticles. *Brain Res,* 1180**,** 121-32.

NEL, A., RUOSLAHTI, E. & MENG, H. 2017. New Insights into "Permeability" as in the Enhanced Permeability and Retention Effect of Cancer Nanotherapeutics. *ACS Nano,* 11**,** 9567-9569.

NELSON, A. L. 2010. Antibody fragments: hope and hype. *MAbs,* 2**,** 77-83.

NISCHAN, N., HERCE, H. D., NATALE, F., BOHLKE, N., BUDISA, N., CARDOSO, M. C. & HACKENBERGER, C. P. R. 2015. Covalent Attachment of Cyclic TAT Peptides to GFP Results in Protein Delivery into Live Cells with Immediate Bioavailability. *Angewandte Chemie International Edition,* 54**,** 1950-1953.

O'CONNOR, L., STRASSER, A., O'REILLY, L. A., HAUSMANN, G., ADAMS, J. M., CORY, S. & HUANG, D. C. 1998. Bim: a novel member of the Bcl-2 family that promotes apoptosis. *Embo j,* 17**,** 384-95.

OGRIS, M., BRUNNER, S., SCHULLER, S., KIRCHEIS, R. & WAGNER, E. 1999. PEGylated DNA/transferrin-PEI complexes: reduced interaction with blood components, extended circulation in blood and potential for systemic gene delivery. *Gene Ther,* 6**,** 595-605.

OH, N. & PARK, J.-H. 2014. Endocytosis and exocytosis of nanoparticles in mammalian cells. *International Journal of Nanomedicine,* 9**,** 51-63.

ORMO, M., CUBITT, A. B., KALLIO, K., GROSS, L. A., TSIEN, R. Y. & REMINGTON, S. J. 1996. Crystal structure of the Aequorea victoria green fluorescent protein. *Science,* 273**,** 1392-5.

OWENS, D. E. & PEPPAS, N. A. 2006. Opsonization, biodistribution, and pharmacokinetics of polymeric nanoparticles. *International Journal of Pharmaceutics,* 307**,** 93-102.

PACK, D. W., HOFFMAN, A. S., PUN, S. & STAYTON, P. S. 2005. Design and development of polymers for gene delivery. *Nat Rev Drug Discov,* 4**,** 581-93.

PAIN, D. & SUROLIA, A. 1981. Preparation of protein A-peroxidase monoconjugate using a heterobifunctional reagent, and its use in enzyme immunoassays. *J Immunol Methods,* 40**,** 219-30.

PARAMESWARAN, N. & PATIAL, S. 2010. Tumor necrosis factor-alpha signaling in macrophages. *Crit Rev Eukaryot Gene Expr,* 20**,** 87-103.

PARTON, R. G. & SIMONS, K. 2007. The multiple faces of caveolae. *Nat Rev Mol Cell Biol,* 8**,** 185-194.

PELEGRI-O'DAY, E. M., LIN, E.-W. & MAYNARD, H. D. 2014. Therapeutic Protein–Polymer Conjugates: Advancing Beyond PEGylation. *Journal of the American Chemical Society,* 136**,** 14323-14332.

PÉREZ-HERRERO, E. & FERNÁNDEZ-MEDARDE, A. 2015. Advanced targeted therapies in cancer: Drug nanocarriers, the future of chemotherapy. *European Journal of Pharmaceutics and Biopharmaceutics,* 93**,** 52-79.

PLANK, C., OBERHAUSER, B., MECHTLER, K., KOCH, C. & WAGNER, E. 1994. The influence of endosome-disruptive peptides on gene transfer using synthetic virus-like gene transfer systems. *J Biol Chem,* 269**,** 12918-24.

PLANK, C., ZAUNER, W. & WAGNER, E. 1998. Application of membrane-active peptides for drug and gene delivery across cellular membranes. *Advanced Drug Delivery Reviews,* 34**,** 21-35.

PONASSI, R., BIASOTTI, B., TOMATI, V., BRUNO, S., POGGI, A., MALACARNE, D., CIMOLI, G., SALIS, A., POZZI, S., MIGLINO, M., DAMONTE, G., COZZINI, P., SPYRAKIS, F., CAMPANINI, B., BAGNASCO, L., CASTAGNINO, N., TORTOLINA, L., MUMOT, A.,

FRASSONI, F., DAGA, A., CILLI, M., PICCARDI, F., MONFARDINI, I., PERUGINI, M., ZOPPOLI, G., D'ARRIGO, C., PESENTI, R. & PARODI, S. 2008. A novel Bim-BH3-derived Bcl-XL inhibitor: biochemical characterization, in vitro, in vivo and ex-vivo anti-leukemic activity. *Cell Cycle,* 7**,** 3211-24.

PRENDERGAST, F. G. & MANN, K. G. 1978. Chemical and physical properties of aequorin and the green fluorescent protein isolated from Aequorea forskalea. *Biochemistry,* 17**,** 3448-3453.

PRENTICE, P., CUSCHIERI, A., DHOLAKIA, K., PRAUSNITZ, M. & CAMPBELL, P. 2005. Membrane disruption by optically controlled microbubble cavitation. *Nature Physics,* 1**,** 107.

PUNNONEN, E. L., RYHANEN, K. & MARJOMAKI, V. S. 1998. At reduced temperature, endocytic membrane traffic is blocked in multivesicular carrier endosomes in rat cardiac myocytes. *Eur J Cell Biol,* 75**,** 344-52.

RÄÄGEL, H., SÄÄLIK, P. & POOGA, M. 2010. Peptide-mediated protein delivery—Which pathways are penetrable? *Biochimica et Biophysica Acta (BBA) - Biomembranes,* 1798**,** 2240-2248.

RAJENDRAN, L., KNOLKER, H.-J. & SIMONS, K. 2010. Subcellular targeting strategies for drug design and delivery. *Nat Rev Drug Discov,* 9**,** 29-42.

RAMACHANDRAN, D. & URBAN, M. W. 2011. Sensing macromolecular rearrangements in polymer networks by stimuli-responsive crosslinkers. *Journal of Materials Chemistry,* 21**,** 8300-8308.

RAMADURAI, S., WERNER, M., SLATER, N. K. H., MARTIN, A., BAULIN, V. A. & KEYES, T. E. 2017. Dynamic studies of the interaction of a pH responsive, amphiphilic polymer with a DOPC lipid membrane. *Soft Matter,* 13**,** 3690-3700.

RINGSDORF, H. 1975. Structure and properties of pharmacologically active polymers. *Journal of Polymer Science: Polymer Symposia,* 51**,** 135-153.

RIZZUTI, M., NIZZARDO, M., ZANETTA, C., RAMIREZ, A. & CORTI, S. 2015. Therapeutic applications of the cell-penetrating HIV-1 Tat peptide. *Drug Discovery Today,* 20**,** 76-85.

ROSSI, G., MONTICELLI, L., PUISTO, S. R., VATTULAINEN, I. & ALA-NISSILA, T. 2011. Coarse-graining polymers with the MARTINI force-field: polystyrene as a benchmark case. *Soft Matter,* 7**,** 698-708.

RUOSLAHTI, E. 2017. Tumor penetrating peptides for improved drug delivery. *Advanced Drug Delivery Reviews,* 110-111**,** 3-12.

SAGA, T., NEUMANN, R. D., HEYA, T., SATO, J., KINUYA, S., LE, N., PAIK, C. H. & WEINSTEIN, J. N. 1995. Targeting cancer micrometastases with monoclonal antibodies: a binding-site barrier. *Proc Natl Acad Sci U S A,* 92**,** 8999-9003.

SAITO, G., SWANSON, J. A. & LEE, K.-D. 2003. Drug delivery strategy utilizing conjugation via reversible disulfide linkages: role and site of cellular reducing activities. *Advanced Drug Delivery Reviews,* 55**,** 199-215.

SAKHTIANCHI, R., MINCHIN, R. F., LEE, K.-B., ALKILANY, A. M., SERPOOSHAN, V. & MAHMOUDI, M. 2013. Exocytosis of nanoparticles from cells: Role in cellular retention and toxicity. *Advances in Colloid and Interface Science,* 201-202**,** 18-29.

SARANTIS, H. & GRINSTEIN, S. 2012. Subversion of Phagocytosis for Pathogen Survival. *Cell Host & Microbe,* 12**,** 419-431.

SASIENI, P. D., SHELTON, J., ORMISTON-SMITH, N., THOMSON, C. S. & SILCOCKS, P. B. 2011. What is the lifetime risk of developing cancer?: the effect of adjusting for multiple primaries. *British Journal of Cancer,* 105**,** 460-465.

SAUNG, M. T., SHAREI, A., ADALSTEINSSON, V. A., CHO, N., KAMATH, T., RUIZ, C., KIRKPATRICK, J., PATEL, N., MINO-KENUDSON, M., THAYER, S. P., LANGER, R., JENSEN, K. F., LISS, A. S. & LOVE, J. C. 2016. A Size-Selective Intracellular Delivery Platform. *Small*.

SAWANT, R. R., SRIRAMAN, S. K., NAVARRO, G., BISWAS, S., DALVI, R. A. & TORCHILIN, V. P. 2012. Polyethyleneimine-lipid conjugate-based pH-sensitive micellar carrier for gene delivery. *Biomaterials,* 33**,** 3942-51.

SCHMALJOHANN, D. 2006. Thermo- and pH-responsive polymers in drug delivery. *Advanced Drug Delivery Reviews,* 58**,** 1655-1670.

SCHOEN, B. & MACHLUF, M. 2016. *Cell Ghosts: Cellular Membranes for Drug Delivery*.

SCOTT, G. K., ROBLES, R., PARK, J. W., MONTGOMERY, P. A., DANIEL, J., HOLMES, W. E., LEE, J., KELLER, G. A., LI, W. L., FENDLY, B. M. & ET AL. 1993. A truncated intracellular HER2/neu receptor produced by alternative RNA processing affects growth of human carcinoma cells. *Mol Cell Biol,* 13**,** 2247-57.

SEKI, K. & TIRRELL, D. A. 1984. pH-Dependent complexation of poly(acrylic acid) derivatives with phospholipid vesicle membranes. *Macromolecules,* 17**,** 1692-1698.

SHAPIRO, G., WONG, A. W., BEZ, M., YANG, F., TAM, S., EVEN, L., SHEYN, D., BEN-DAVID, S., TAWACKOLI, W., PELLED, G., FERRARA, K. W. & GAZIT, D. 2016. Multiparameter evaluation of in vivo gene delivery using ultrasound-guided, microbubble-enhanced sonoporation. *J Control Release,* 223**,** 157-164.

SHAREI, A., POCEVICIUTE, R., JACKSON, E. L., CHO, N., MAO, S., HARTOULAROS, G. C., JANG, D. Y., JHUNJHUNWALA, S., EYERMAN, A., SCHOETTLE, T., LANGER, R. & JENSEN, K. F. 2014. Plasma membrane recovery kinetics of a microfluidic intracellular delivery platform. *Integr Biol (Camb),* 6**,** 470-5.

SHAREI, A., ZOLDAN, J., ADAMO, A., SIM, W. Y., CHO, N., JACKSON, E., MAO, S., SCHNEIDER, S., HAN, M.-J., LYTTON-JEAN, A., BASTO, P. A., JHUNJHUNWALA, S., LEE, J., HELLER, D. A., KANG, J. W., HARTOULAROS, G. C., KIM, K.-S., ANDERSON, D. G., LANGER, R. & JENSEN, K. F. 2013. A vector-free microfluidic platform for intracellular delivery. *Proceedings of the National Academy of Sciences,* 110**,** 2082-2087.

SIEGEL, R. L., MILLER, K. D. & JEMAL, A. 2017. Cancer statistics, 2017. *CA: A Cancer Journal for Clinicians,* 67**,** 7-30.

SIEGLER, E., LI, S., KIM, Y. J. & WANG, P. 2017. Designed Ankyrin Repeat Proteins as Her2 Targeting Domains in Chimeric Antigen Receptor-Engineered T Cells. *Human gene therapy,* 28**,** 726-736.

SLAMON, D. J., GODOLPHIN, W., JONES, L. A., HOLT, J. A., WONG, S. G., KEITH, D. E., LEVIN, W. J., STUART, S. G., UDOVE, J., ULLRICH, A. & ET AL. 1989. Studies of the HER-2/neu proto-oncogene in human breast and ovarian cancer. *Science,* 244**,** 707-12.

SLOWING, I. I., VIVERO-ESCOTO, J. L., ZHAO, Y., KANDEL, K., PEERAPHATDIT, C., TREWYN, B. G. & LIN, V. S.-Y. 2011. Exocytosis of Mesoporous Silica Nanoparticles from Mammalian Cells: From Asymmetric Cell-to-Cell Transfer to Protein Harvesting. *Small,* 7**,** 1526-1532.

SOLIMAN, M., NASANIT, R., ABULATEEFEH, S. R., ALLEN, S., DAVIES, M. C., BRIGGS, S. S., SEYMOUR, L. W., PREECE, J. A., GRABOWSKA, A. M., WATSON, S. A. & ALEXANDER, C. 2012. Multicomponent Synthetic Polymers with Viral-Mimetic Chemistry for Nucleic Acid Delivery. *Molecular Pharmaceutics,* 9**,** 1-13.

SONAWANE, N. D., SZOKA, F. C., JR. & VERKMAN, A. S. 2003. Chloride accumulation and swelling in endosomes enhances DNA transfer by polyamine-DNA polyplexes. *J Biol Chem,* 278**,** 44826-31.

SPETH, P. A. J., VAN HOESEL, Q. G. C. M. & HAANEN, C. 1988. Clinical Pharmacokinetics of Doxorubicin. *Clinical Pharmacokinetics,* 15**,** 15-31.

STAYTON, I., WINIARZ, J., SHANNON, K. & MA, Y. 2009. Study of uptake and loss of silica nanoparticles in living human lung epithelial cells at single cell level. *Analytical and Bioanalytical Chemistry,* 394**,** 1595-1608.

STEPANENKO, O. V., VERKHUSHA, V. V., KUZNETSOVA, I. M., UVERSKY, V. N. & TUROVEROV, K. K. 2008. Fluorescent Proteins as Biomarkers and Biosensors: Throwing Color Lights on Molecular and Cellular Processes. *Current protein & peptide science,* 9**,** 338-369.

STEWART, M. P., LORENZ, A., DAHLMAN, J. & SAHAY, G. 2016a. Challenges in carrier-mediated intracellular delivery: moving beyond endosomal barriers. *Wiley Interdisciplinary Reviews: Nanomedicine and Nanobiotechnology,* 8**,** 465-478.

STEWART, M. P., SHAREI, A., DING, X., SAHAY, G., LANGER, R. & JENSEN, K. F. 2016b. In vitro and ex vivo strategies for intracellular delivery. *Nature,* 538**,** 183-192.

STRASSER, A., PUTHALAKATH, H., BOUILLET, P., HUANG, D. C., O'CONNOR, L., O'REILLY, L. A., CULLEN, L., CORY, S. & ADAMS, J. M. 2000. The role of bim, a proapoptotic BH3-only member of the Bcl-2 family in cell-death control. *Ann N Y Acad Sci,* 917**,** 541-8.

STUMPP, M. T., BINZ, H. K. & AMSTUTZ, P. 2008. DARPins: A new generation of protein therapeutics. *Drug Discovery Today,* 13**,** 695-701.

SUH, J., PAIK, H. J. & HWANG, B. K. 1994. Ionization of Poly(ethylenimine) and Poly(allylamine) at Various pH's. *Bioorganic Chemistry,* 22**,** 318-327.

SUH, J., WIRTZ, D. & HANES, J. 2003. Efficient active transport of gene nanocarriers to the cell nucleus. *Proceedings of the National Academy of Sciences,* 100**,** 3878-3882.

SUH, W., CHUNG, J.-K., PARK, S.-H. & KIM, S. W. 2001. Anti-JL1 antibody-conjugated poly (l-lysine) for targeted gene delivery to leukemia T cells. *Journal of Controlled Release,* 72**,** 171-178.

SUI, M., LIU, W. & SHEN, Y. 2011. Nuclear drug delivery for cancer chemotherapy. *Journal of Controlled Release,* 155**,** 227-236.

SUK, J. S., XU, Q., KIM, N., HANES, J. & ENSIGN, L. M. 2016. PEGylation as a strategy for improving nanoparticle-based drug and gene delivery. *Advanced drug delivery reviews,* 99**,** 28-51.

SWANSON, J. A. 2008. Shaping cups into phagosomes and macropinosomes. *Nat Rev Mol Cell Biol,* 9**,** 639-649.

SZETO, G. L., VAN EGEREN, D., WORKU, H., SHAREI, A., ALEJANDRO, B., PARK, C., FREW, K., BREFO, M., MAO, S., HEIMANN, M., LANGER, R., JENSEN, K. & IRVINE, D. J. 2015. Microfluidic squeezing for intracellular antigen loading in polyclonal B-cells as cellular vaccines. *Scientific Reports,* 5**,** 10276.

TANAKA, T., NARAZAKI, M. & KISHIMOTO, T. 2014. IL-6 in Inflammation, Immunity, and Disease. *Cold Spring Harbor Perspectives in Biology,* 6**,** a016295.

TANNOCK, I. F. & ROTIN, D. 1989. Acid pH in Tumors and Its Potential for Therapeutic Exploitation. *Cancer Research,* 49**,** 4373-4384.

TARANEJOO, S., LIU, J., VERMA, P. & HOURIGAN, K. 2015. A review of the developments of characteristics of PEI derivatives for gene delivery applications. *Journal of Applied Polymer Science,* 132.

TEIXEIRA, M., PY, B. F., BOSC, C., LAUBRETON, D., MOUTIN, M.-J., MARVEL, J., FLAMANT, F. & MARKOSSIAN, S. 2018. Electroporation of mice zygotes with dual guide RNA/Cas9 complexes for simple and efficient cloning-free genome editing. *Scientific Reports,* 8**,** 474.

THAMBI, T., DEEPAGAN, V. G., YOON, H. Y., HAN, H. S., KIM, S. H., SON, S., JO, D. G., AHN, C. H., SUH, Y. D., KIM, K., KWON, I. C., LEE, D. S. & PARK, J. H. 2014. Hypoxia-responsive polymeric nanoparticles for tumor-targeted drug delivery. *Biomaterials,* 35**,** 1735-43.

THAMBI, T., SON, S., LEE, D. S. & PARK, J. H. 2016. Poly(ethylene glycol)-b-poly(lysine) copolymer bearing nitroaromatics for hypoxia-sensitive drug delivery. *Acta Biomaterialia,* 29**,** 261-270.

THOMAS, C. E., EHRHARDT, A. & KAY, M. A. 2003. Progress and problems with the use of viral vectors for gene therapy. *Nat Rev Genet,* 4**,** 346-58.

THOMAS, J. L., DEVLIN, B. P. & TIRRELL, D. A. 1996. Kinetics of membrane micellization by the hydrophobic polyelectrolyte poly(2-ethylacrylic acid). *Biochimica et Biophysica Acta (BBA) - Biomembranes,* 1278**,** 73-78.

TIMOTHY, E. M., ANATOLI, V. M., GUY, D. G., MICHAEL, A. G., VLADIMIR, I. M., FRANCISCO, S., DALE, K. H., MITCHEL, J. D., DOUGLAS, H. L. & MICHAEL, L. S. 2003. Intracellular

integration of synthetic nanostructures with viable cells for controlled biochemical manipulation. *Nanotechnology,* 14**,** 551.
TOMIZAWA, M., SHINOZAKI, F., MOTOYOSHI, Y., SUGIYAMA, T., YAMAMOTO, S. & SUEISHI, M. 2013. Sonoporation: Gene transfer using ultrasound. *World Journal of Methodology,* 3**,** 39-44.
TONG, R. T., BOUCHER, Y., KOZIN, S. V., WINKLER, F., HICKLIN, D. J. & JAIN, R. K. 2004. Vascular normalization by vascular endothelial growth factor receptor 2 blockade induces a pressure gradient across the vasculature and improves drug penetration in tumors. *Cancer Res,* 64**,** 3731-6.
TORCHILIN, V. P. 2005. Recent advances with liposomes as pharmaceutical carriers. *Nat Rev Drug Discov,* 4**,** 145-160.
TORCHILIN, V. P. 2008. Cell penetrating peptide-modified pharmaceutical nanocarriers for intracellular drug and gene delivery. *Biopolymers,* 90**,** 604-10.
TORCHILIN, V. P. 2014. Multifunctional, stimuli-sensitive nanoparticulate systems for drug delivery. *Nat Rev Drug Discov,* 13**,** 813-827.
TSUKAKOSHI, M., KURATA, S., NOMIYA, Y., IKAWA, Y. & KASUYA, T. 1984. A novel method of DNA transfection by laser microbeam cell surgery. *Applied Physics B,* 35**,** 135-140.
VADER, P., MOL, E. A., PASTERKAMP, G. & SCHIFFELERS, R. M. 2016. Extracellular vesicles for drug delivery. *Advanced Drug Delivery Reviews,* 106**,** 148-156.
VAIDYANATHAN, S., ANDERSON, K. B., MERZEL, R. L., JACOBOVITZ, B., KAUSHIK, M. P., KELLY, C. N., VAN DONGEN, M. A., DOUGHERTY, C. A., ORR, B. G. & HOLL, M. M. B. 2015. Quantitative Measurement of Cationic Polymer Vector and Polymer/pDNA Polyplex Intercalation into the Cell Plasma Membrane. *ACS nano,* 9**,** 6097-6109.
VAN DELFT, M. F., WEI, A. H., MASON, K. D., VANDENBERG, C. J., CHEN, L., CZABOTAR, P. E., WILLIS, S. N., SCOTT, C. L., DAY, C. L., CORY, S., ADAMS, J. M., ROBERTS, A. W. & HUANG, D. C. 2006. The BH3 mimetic ABT-737 targets selective Bcl-2 proteins and efficiently induces apoptosis via Bak/Bax if Mcl-1 is neutralized. *Cancer Cell,* 10**,** 389-99.
VANDER HEIDEN, M. G., CANTLEY, L. C. & THOMPSON, C. B. 2009. Understanding the Warburg effect: the metabolic requirements of cell proliferation. *Science,* 324**,** 1029-33.
VARKOUHI, A. K., SCHOLTE, M., STORM, G. & HAISMA, H. J. 2011. Endosomal escape pathways for delivery of biologicals. *J Control Release,* 151**,** 220-8.
VAUPEL, P., KALLINOWSKI, F. & OKUNIEFF, P. 1989. Blood flow, oxygen and nutrient supply, and metabolic microenvironment of human tumors: a review. *Cancer Res,* 49**,** 6449-65.
VENSLAUSKAS, M. S. & SATKAUSKAS, S. 2015. Mechanisms of transfer of bioactive molecules through the cell membrane by electroporation. *Eur Biophys J,* 44**,** 277-89.
VERCAUTEREN, D., VANDENBROUCKE, R. E., JONES, A. T., REJMAN, J., DEMEESTER, J., DE SMEDT, S. C., SANDERS, N. N. & BRAECKMANS, K. 2010. The use of inhibitors to study endocytic pathways of gene carriers: optimization and pitfalls. *Molecular therapy : the journal of the American Society of Gene Therapy,* 18**,** 561-569.
VERONESE, F., MERO, A. & PASUT, G. 2009. Protein PEGylation, basic science and biological applications. *In:* VERONESE, F. (ed.) *PEGylated Protein Drugs: Basic Science and Clinical Applications.* Birkhäuser Basel.
WANG, J., LI, S., LUO, T., WANG, C. & ZHAO, J. 2012a. Disulfide linkage: a potent strategy in tumor-targeting drug discovery. *Curr Med Chem,* 19**,** 2976-83.
WANG, J., SEGATORI, L. & BISWAL, S. L. 2014. Probing the association of triblock copolymers with supported lipid membranes using microcantilevers. *Soft Matter,* 10**,** 6417-24.
WANG, S. & CHEN, R. 2017. pH-Responsive, Lysine-Based, Hyperbranched Polymers Mimicking Endosomolytic Cell-Penetrating Peptides for Efficient Intracellular Delivery. *Chemistry of Materials,* 29**,** 5806-5815.

WANG, T., UPPONI, J. R. & TORCHILIN, V. P. 2012b. Design of multifunctional non-viral gene vectors to overcome physiological barriers: dilemmas and strategies. *Int J Pharm,* 427**,** 3-20.
WANG, Y., LI, P., CHEN, F., JIA, L., XU, Q., GAI, X., YU, Y., DI, Y., ZHU, Z., LIANG, Y., LIU, M., PAN, W. & YANG, X. 2017. A novel pH-sensitive carrier for the delivery of antitumor drugs: histidine-modified auricularia auricular polysaccharide nano-micelles. *Scientific Reports,* 7**,** 4751.
WANLING, L. & JENNY, K. W. L. 2012. Endosomal Escape Pathways for Non-Viral Nucleic Acid Delivery Systems.
WARBURG, O., WIND, F. & NEGELEIN, E. 1927. THE METABOLISM OF TUMORS IN THE BODY. *The Journal of General Physiology,* 8**,** 519-530.
WATANABE, Y., HORIE, S., FUNAKI, Y., KIKUCHI, Y., YAMAZAKI, H., ISHII, K., MORI, S., VASSAUX, G. & KODAMA, T. 2010. Delivery of Na/I symporter gene into skeletal muscle using nanobubbles and ultrasound: visualization of gene expression by PET. *J Nucl Med,* 51**,** 951-8.
WATKINS, K. A. & CHEN, R. 2015. pH-responsive, lysine-based hydrogels for the oral delivery of a wide size range of molecules. *Int J Pharm,* 478**,** 496-503.
WATSON, D. S., ENDSLEY, A. N. & HUANG, L. 2012. Design considerations for liposomal vaccines: influence of formulation parameters on antibody and cell-mediated immune responses to liposome associated antigens. *Vaccine,* 30**,** 2256-72.
WEI, M., GAO, Y., LI, X. & SERPE, M. J. 2017. Stimuli-responsive polymers and their applications. *Polymer Chemistry,* 8**,** 127-143.
WEI, X., LUO, Q., SUN, L., LI, X., ZHU, H., GUAN, P., WU, M., LUO, K. & GONG, Q. 2016. Enzyme- and pH-Sensitive Branched Polymer–Doxorubicin Conjugate-Based Nanoscale Drug Delivery System for Cancer Therapy. *ACS Applied Materials & Interfaces,* 8**,** 11765-11778.
WEILL, C. O., BIRI, S., ADIB, A. & ERBACHER, P. 2008. A practical approach for intracellular protein delivery. *Cytotechnology,* 56**,** 41-48.
WENDLAND, B. 2002. Epsins: adaptors in endocytosis? *Nat Rev Mol Cell Biol,* 3**,** 971-977.
WHITEHEAD, K. A., LANGER, R. & ANDERSON, D. G. 2009. Knocking down barriers: advances in siRNA delivery. *Nat Rev Drug Discov,* 8**,** 129-138.
WIKE-HOOLEY, J. L., HAVEMAN, J. & REINHOLD, H. S. 1984. The relevance of tumour pH to the treatment of malignant disease. *Radiotherapy and Oncology,* 2**,** 343-366.
WILSON, W. R. & HAY, M. P. 2011. Targeting hypoxia in cancer therapy. *Nat Rev Cancer,* 11**,** 393-410.
WISEMAN, J. W., GODDARD, C. A., MCLELLAND, D. & COLLEDGE, W. H. 2003. A comparison of linear and branched polyethylenimine (PEI) with DCChol/DOPE liposomes for gene delivery to epithelial cells in vitro and in vivo. *Gene Therapy,* 10**,** 1654.
WU, M. & YUAN, F. 2011. Membrane Binding of Plasmid DNA and Endocytic Pathways Are Involved in Electrotransfection of Mammalian Cells. *PLoS ONE,* 6**,** e20923.
WU, X. & GEHRING, W. 2014. Cellular uptake of the Antennapedia homeodomain polypeptide by macropinocytosis. *Biochemical and Biophysical Research Communications,* 443**,** 1136-1140.
XU, X., RAN, Q., DEY, P., NIKAM, R., HAAG, R., BALLAUFF, M. & DZUBIELLA, J. 2018. Counterion-Release Entropy Governs the Inhibition of Serum Proteins by Polyelectrolyte Drugs. *Biomacromolecules,* 19**,** 409-416.
XUE, F., WEN, Y., WEI, P., GAO, Y., ZHOU, Z., XIAO, S. & YI, T. 2017. A smart drug: a pH-responsive photothermal ablation agent for Golgi apparatus activated cancer therapy. *Chemical Communications,* 53**,** 6424-6427.
YANES, R. E., TARN, D., HWANG, A. A., FERRIS, D. P., SHERMAN, S. P., THOMAS, C. R., LU, J., PYLE, A. D., ZINK, J. I. & TAMANOI, F. 2013. Involvement of lysosomal exocytosis in the

excretion of mesoporous silica nanoparticles and enhancement of the drug delivery effect by exocytosis inhibition. *Small,* 9**,** 697-704.
YANG, F., ZHANG, Y. & LIANG, H. 2014. Interactive Association of Drugs Binding to Human Serum Albumin. *International Journal of Molecular Sciences,* 15**,** 3580-3595.
YARMUSH, M. L., GOLBERG, A., SERSA, G., KOTNIK, T. & MIKLAVCIC, D. 2014. Electroporation-based technologies for medicine: principles, applications, and challenges. *Annu Rev Biomed Eng,* 16**,** 295-320.
YESSINE, M.-A. & LEROUX, J.-C. 2004. Membrane-destabilizing polyanions: interaction with lipid bilayers and endosomal escape of biomacromolecules. *Advanced Drug Delivery Reviews,* 56**,** 999-1021.
YIM, N., RYU, S. W., CHOI, K., LEE, K. R., LEE, S., CHOI, H., KIM, J., SHAKER, M. R., SUN, W., PARK, J. H., KIM, D., HEO, W. D. & CHOI, C. 2016. Exosome engineering for efficient intracellular delivery of soluble proteins using optically reversible protein-protein interaction module. *Nat Commun,* 7**,** 12277.
YOO, J.-W., IRVINE, D. J., DISCHER, D. E. & MITRAGOTRI, S. 2011. Bio-inspired, bioengineered and biomimetic drug delivery carriers. *Nat Rev Drug Discov,* 10**,** 521-535.
YOUNG, J. L. & DEAN, D. A. 2015. Electroporation-mediated gene delivery. *Adv Genet,* 89**,** 49-88.
YOUNG, N. S., LEVIN, J. & PRENDERGAST, R. A. 1972. An invertebrate coagulation system activated by endotoxin: evidence for enzymatic mediation. *Journal of Clinical Investigation,* 51**,** 1790-1797.
YU, M. & ZHENG, J. 2015. Clearance Pathways and Tumor Targeting of Imaging Nanoparticles. *ACS Nano,* 9**,** 6655-6674.
ZAHND, C., KAWE, M., STUMPP, M. T., DE PASQUALE, C., TAMASKOVIC, R., NAGY-DAVIDESCU, G., DREIER, B., SCHIBLI, R., BINZ, H. K., WAIBEL, R. & PLUCKTHUN, A. 2010. Efficient tumor targeting with high-affinity designed ankyrin repeat proteins: effects of affinity and molecular size. *Cancer Res,* 70**,** 1595-605.
ZANONI, M., PICCININI, F., ARIENTI, C., ZAMAGNI, A., SANTI, S., POLICO, R., BEVILACQUA, A. & TESEI, A. 2016. 3D tumor spheroid models for in vitro therapeutic screening: a systematic approach to enhance the biological relevance of data obtained. *Sci Rep,* 6**,** 19103.
ZARRABI, K., FANG, C. & WU, S. 2017. New treatment options for metastatic renal cell carcinoma with prior anti-angiogenesis therapy. *Journal of Hematology & Oncology,* 10**,** 38.
ZHANG, J., YANG, P. L. & GRAY, N. S. 2009. Targeting cancer with small molecule kinase inhibitors. *Nat Rev Cancer,* 9**,** 28-39.
ZHANG, S., NELSON, A., COLDRICK, Z. & CHEN, R. 2011. The Effects of Substituent Grafting on the Interaction of pH-Responsive Polymers with Phospholipid Monolayers. *Langmuir,* 27**,** 8530-8539.
ZHANG, S., ZHAO, B., JIANG, H., WANG, B. & MA, B. 2007. Cationic lipids and polymers mediated vectors for delivery of siRNA. *J Control Release,* 123**,** 1-10.
ZHU, L., KATE, P. & TORCHILIN, V. P. 2012. Matrix metalloprotease 2-responsive multifunctional liposomal nanocarrier for enhanced tumor targeting. *ACS Nano,* 6**,** 3491-8.

Appendix

Appendix A

Structural characterisation of PLP synthesised in this work was performed by ^{1}H-Nuclear Magnetic Resonance (NMR). Polymer powder was dissolved in d_6-DMSO and its spectrum was obtained using 400 MHz NMR spectrometer (Bruker, Germany) at room temperature. The spectrum was compared to PLP spectrum which was reported by Eccleston et al. (1999) to confirm polymer identity.

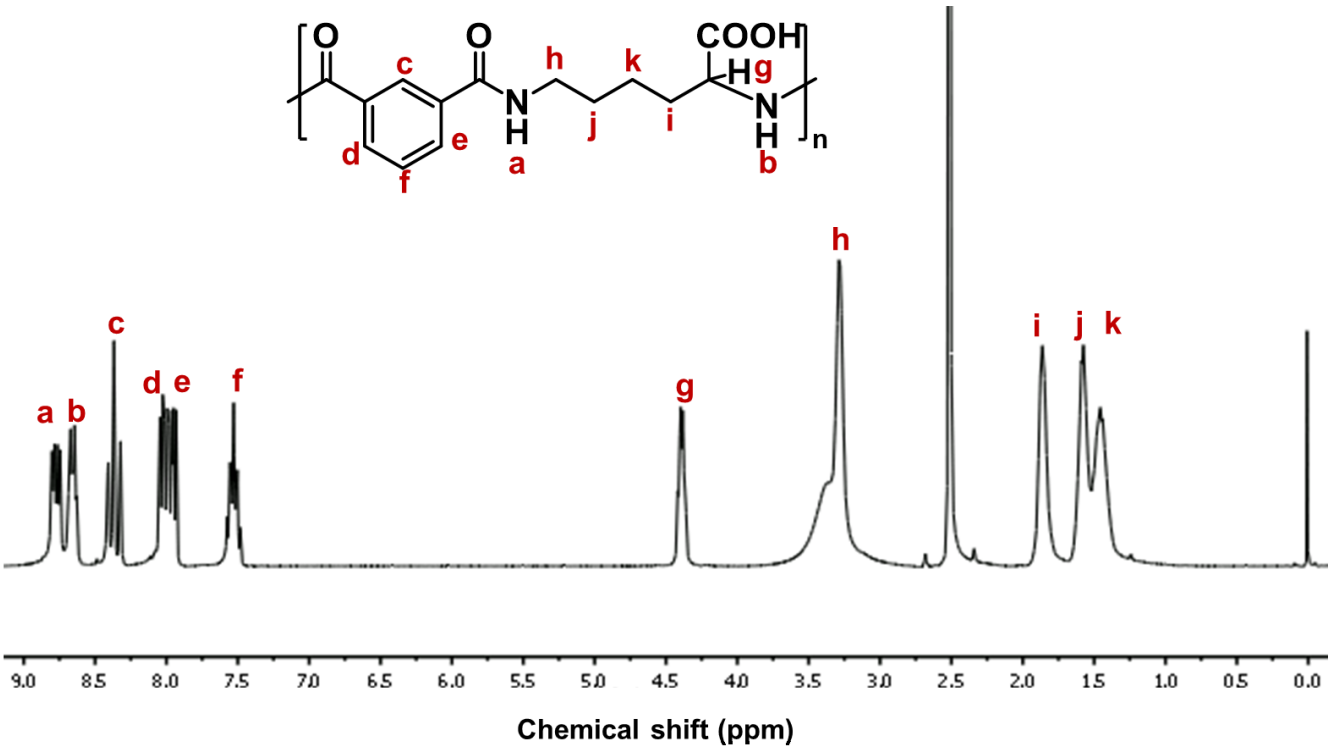


Figure A-1. ^{1}H-NMR spectrum of PLP methyl ester in DMSO-d6 at room temperature. Peaks were assigned according to chemical shifts.

Appendix B

Structural characterisation of PP50 synthesised in this work was performed by ^{1}H-NMR. Polymer powder was dissolved in d_6-DMSO and its spectrum was obtained using 400 MHz NMR spectrometer (Bruker, Germany) at room temperature. The degree of substitution with L-phenylalanine was determined by the ratio of the integral of 7.13-7.33 ppm to the integral of 7.45-7.64. The degree grafting with L-phenylalanine used herein was equal to 51%.

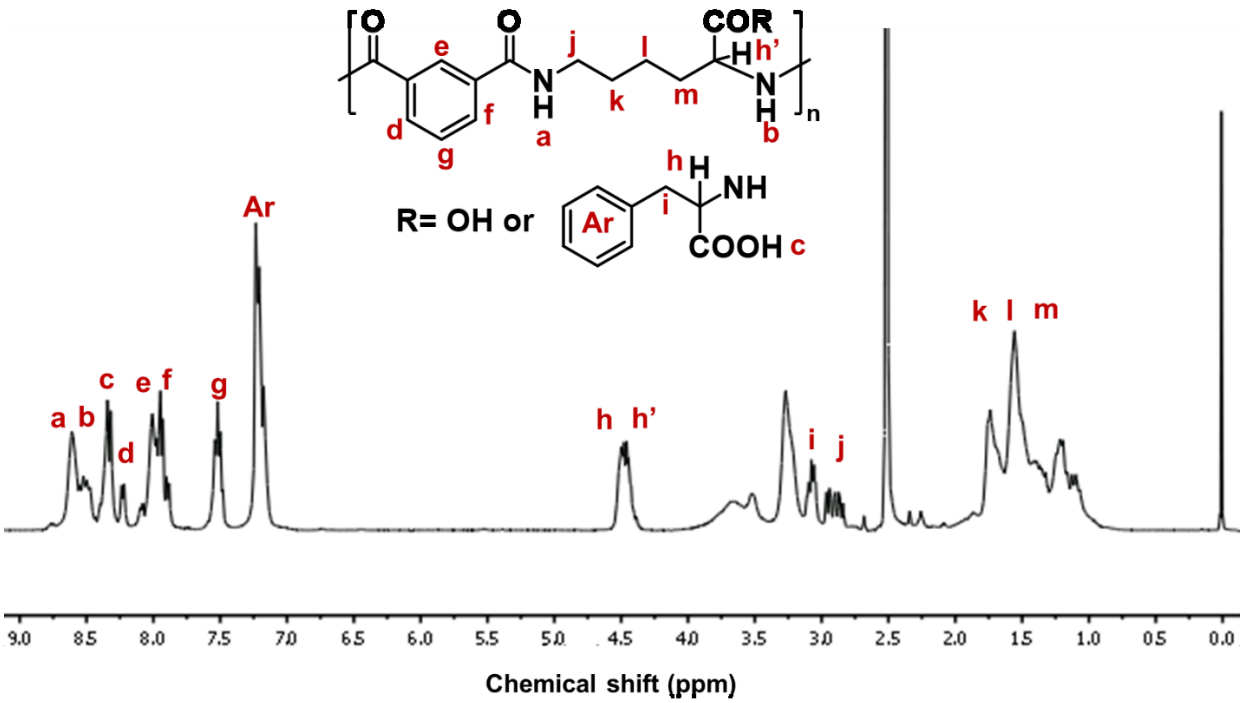


Figure A-2. ^{1}H-NMR spectrum of PP50 in DMSO-d6 at room temperature. Peaks were assigned according to chemical shifts.

Appendix C

Analysis of EVs subsequent to treatment with PP50 (1 mg mL^{-1}) and Bim-Cy7 (20 μM) or Bim-Cy7 alone was performed by flow cytometry. The scatter plots presented below illustrate the distribution of the EV population concentrated on CD9 magnetic beads (blue) as compared to the magnetic beads alone (red).

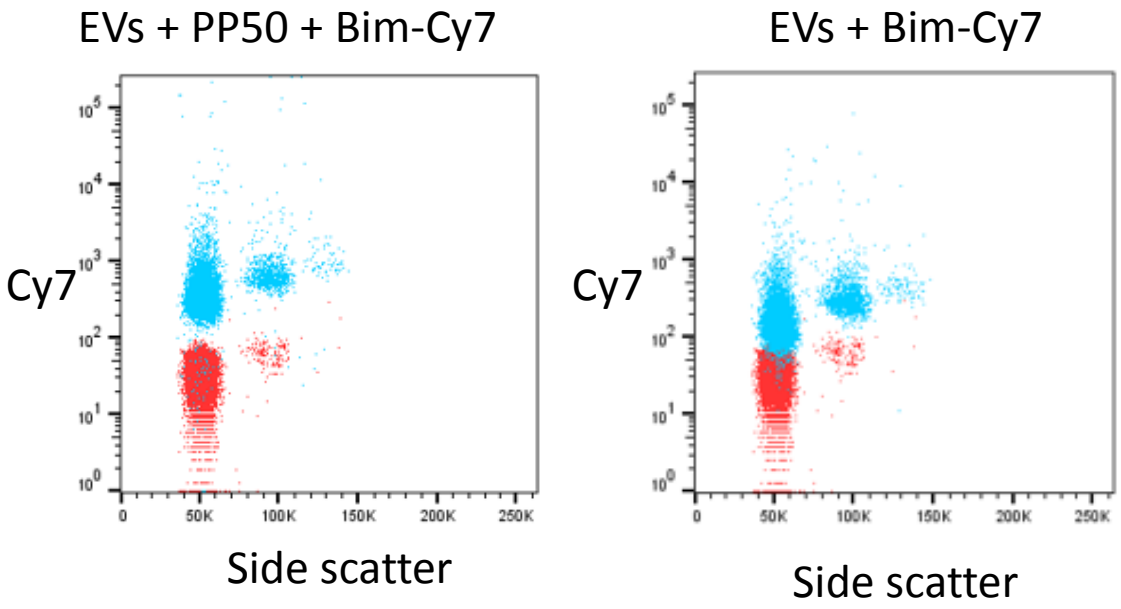


Figure A-3. Scatter plots of EVs concentrated on CD9 magnetic beads following treatment with of Bim-Cy7 (20 μM) by co-incubation with PP50 (1 mg mL^{-1}) at pH 6.5 for 1.5 h and EV isolation by ultracentrifugation, analysed by flow cytometry. The population of magnetic beads only is shown in red whereas the EV samples are shown in blue. Flow cytometry of EVs was performed by Christina Schindler (MedImmune).

Appendix D

Delivery of 150 kDa FITC-Dextran by co-incubation with PP50 was compared to delivery of the same payload using the commercially available delivery agent Pulsin™ and analysed using confocal microscopy. As illustrated by, PP50-mediated delivery resulted in a diffused intracellular green signal, whereas Pulsin™-mediated delivery produced a pattern of fluorescent spots, suggesting a high level of endosomal entrapment.

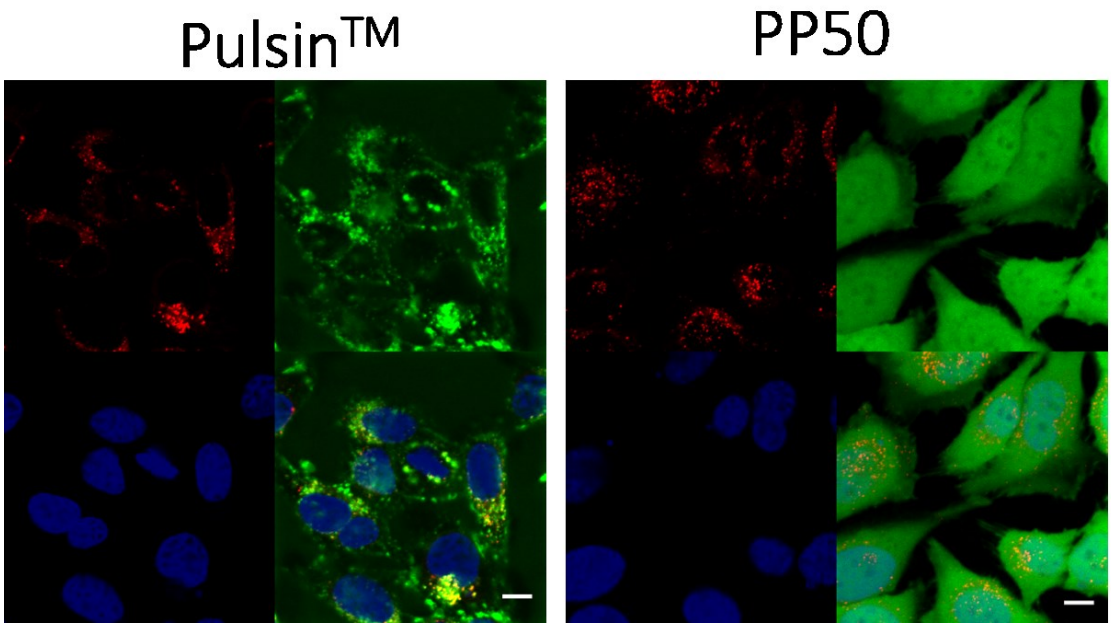


Figure A-4. Comparison of delivery of FITC-Dextran (150 kDa) using PP50 and Pulsin. For PP50 delivery, 0.5 mg mL^{-1} of polymer was used at pH 6.5. Pulsin preparation and concentration was as advised in the manufacturer's protocol. FITC-Dextran concentration was equal to 10 μM and the treatment time was 1 h. The presented channels are LysotrackerRed (red), FITC-Dextran (green) and Hoechst (blue) as well as a merged image. Scale bar = 10 μm.

Appendix E

A549 xenograft tumour bearing CD-1 nude (n = 2) were dosed with PP50-Bim-Cy7 and imaged using the IVIS Spectrum System 1 h post injection. The images present dorsal view.

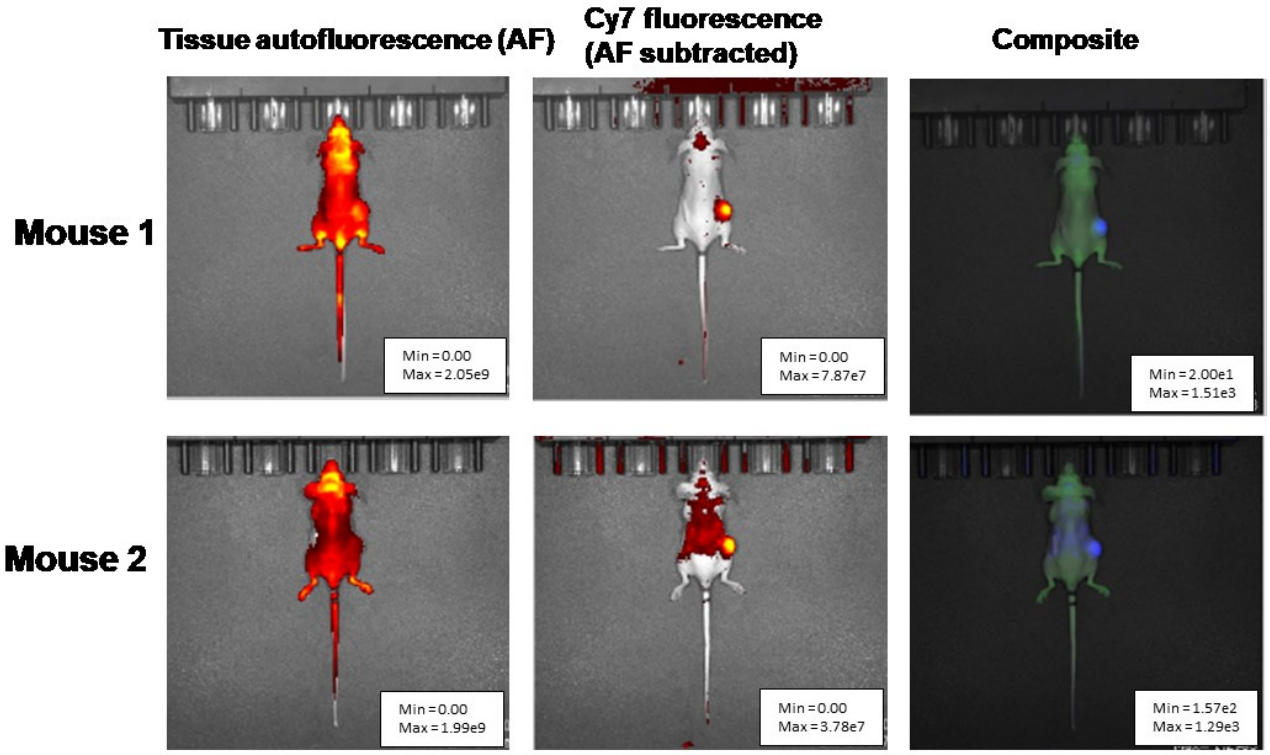


Figure A-5. Distribution of the Cy7 fluorescent signal in tumour-bearing CD-1 nude mice (dorsal view) 1 h after intravenous injection of PP50-Bim-Cy7 at 17.5 μM. The bright yellow and orange areas correspond to a stronger fluorescent signal. The compsote image shows the tissue autofluorescence in green and the Cy7 specific signal in blue, indicating preferential accumulation of the conjugate in the tumours. The minimum and maximum recorded fluorescence values are presented in the insets for each image.

Appendix F

Permissions summary table for third party copyright works

Name in this work	Source	Copyright holder	Permission required (yes/no)	Permission obtained (yes/no/NA)	Permission note
Figure 1-3	Endosomal Escape Pathways for Non-Viral Nucleic Acid Delivery Systems, DOI: 10.5772/46006	IntechOpen Limited	No (unrestricted use, distribution, and reproduction allowed)	NA	NA
Figure 1-2	Pathways of clathrin-independent endocytosis, Nature Reviews Molecular Cell Biology volume8, pages603–612 (2007)	© 2007 Springer Nature	Yes	Yes	License number 4425871096765
Tables 1-2 and 1-3	In vitro and ex vivo strategies for intracellular delivery, Nature volume538, pages183–192 (13 October 2016)	© 2016 Springer Nature	Yes	Yes	License number 4425880041973